Static and Dynamic Analysis of Hydrodynamic Flexible Oil Bearings using Micropolar Lubrication

A thesis submitted in fulfillment of the requirement for the award of the degree of

DOCTOR OF PHILOSPHY

Submitted by

PikeshBansal
Regn. No. 950908011

Under the supervision of

Dr. A.K. Chattopadhayay
Ex professor
Mechanical Engineering Department
Thapar University, Patiala
India.
Supervisor

Dr. V.P. Agrawal
Visiting Professor
Mechanical Engineering Department
Thapar University, Patiala
India.
Supervisor

DEPARTMENT OF MECHANICAL ENGINEERING
THAPAR UNIVERSITY
PATIALA-147004

June, 2016

CERTIFICATE

I, Pikesh Bansal hereby certify that the work presented in this thesis report entitled **"Static and Dynamic Analysis of Hydrodynamic Flexible Oil Bearings using Micropolar Lubrication"** in fulfillment of requirement for the award of degree of **Doctor of Philosophy** submitted in Mechanical Engineering Department, Thapar University, Patiala, is an authentic record of my own work carried out under the supervision of **Dr. A.K. Chattopadhayay** (Ex Professor, Mechanical Engineering Department, Thapar University, Patiala) and **Dr. V.P. Agrawal** (Visiting Professor, Mechanical Engineering Department, Thapar University, Patiala) from March 2010 to May 2016. The matter presented in this thesis has not been submitted either in part or full to any other University or Institution for the award of any other degree.

Pikesh Bansal

Date: May 30, 2016

Registration No.: 950908011

It is certified that the above statement made by the student is correct to the best of our knowledge and belief.

Dr. A.K. Chattopadhayay
Ex professor
Mechanical Engineering Department
Thapar University, Patiala
India.
Supervisor

Dr. V.P. Agrawal
Visiting Professor
Mechanical Engineering Department
Thapar University, Patiala
India.
Supervisor

ACKNOWLEDGEMENT

Pursuing Ph.D. is both painful and enjoyable experience as it requires continuous hard work, time management, and step by step detailed analysis of the problem which leads to enhancement in knowledge about the subject matter, augments writing skills and develops various skills of problem solving. During the course of my Ph.D. work I realized that it was, in fact, teamwork of supervisors, Doctoral committee, members of department, colleagues, family members and reviewers of published work. All those people have helped me, guided me, put me through bad times in order to motivate me to go in more depth of the subject and supported me through worse times their contribution is overwhelming. Though it will not be enough to express my gratitude in words to all these people, I would still like to give my many, many thanks to all these people.

First and foremost, I would like to express my sincere gratitude with deference towards my supervisor Dr. A.K. Chattopadhayay (Ex Professor, Mechanical Engineering Department, Thapar University, Patiala) and Dr. V.P. Singh (Visiting Professor, Mechanical Engineering Department, Thapar University, Patiala) for their valuable guidance and stimulation in pursuance of this work. Despite their busy schedule, they always spared time for me. I am highly obliged to Dr. A.K. Chattopadhayay for his valuable guidance, scholarly inputs and consistent encouragement that I received throughout the research work. He is kind of person who would keep pondering on the subject, until he is satisfied with the suggestion given to me during the course of research. This motivated me to work harder on my work. I would also like to thank Dr.V.P. Agrawal for his invaluable support and guidance during my research work. He is an amicable person with positive disposition and fervor to work day and night. He would go through my work thoroughly and give suggestions to improve my work. His positive attitude and useful suggestions helped me get out of the rough patch during my research work. I express my gratitude to both and wish for continuous guidance from both for future research accomplishments.

I am also indebted to members of Doctoral committee; Dr. D. Gangacharyulu and Dr. S.K. Mohapatra, for their invaluable comments and suggestions which diverted my attention towards weak aspects of my research and made me improve my work. It gives me great pleasure to thank members of doctoral committee for their selfless efforts and valuable time in improving my research work at each stage of doctoral program.

I would like extend my thanks to members of mechanical department at Thapar University for their constant support, guidance and encouragement every now and then whenever required during my doctoral program. I would like to thank Dr. Tarun Nanda for his meticulous approach in guiding me through the various procedures and important guidelines of Thapar University. I am thankful to Dr. Rahul Chibber for his support and encouragement during initial phase of my doctoral program. I am indebted to Dr. Ravinder Kr. Duvedi for his constant support and encouragement during the entire 6 years of my research work. I am grateful to Dr. Ajay Batish for his guidance and encouragement for giving me his precious time for discussions during my research work. I am thankful to Dr. Sandeep Sharma, Dr. J.S. Saini, Dr. A.S. Jawanda, Mr. Kishore Kumar and Dr. S.P. Nigam for their motivation, support and important suggestions at each every step of my work.

A good support system is required to sustain the pressure of working hard day and night during the course of research work which was duly provided by my colleagues and friends at Mody University, Lakshmangarh. I would like to extend my thanks to Mr. NitinBaroule, Mr. Vikrant Sharma, Mr. Atul Kumar, Mr. MukulPaliwal, Mr. Ajeet Kumar and Mr. Mukesh Kumar for their wonderful company, support, encouragement and suggestions during the course of my work. I would also like to thank Mr. Ravi Chomal for his support in running my computer program on laboratory PC's and helping me get the results in 2-3 weeks which would otherwise take months. I am also grateful to Dr. S.K. Lenka for his word of advice and constant encouragement. I am thankful to Mr. B.S. Sekhawat, Mr. B.L. Meel, Mr. Ramesh Kumar and Mr. Ramsaroop for their support and encouragement.

I am indebted to my father Sh. S.S. Bansal from whom I have learned the never to let go attitude and also his tremendous support in saying you do your work properly leave rest of the things on me. I am also thankful to my mother Smt. MeenaBansal for her constant support and encouragement right from my school days to this day. I am grateful to my wife Mrs. Uma Bansal for her helping hand in every situation of life. I owe special thanks to my kids ShravyaBansaland Rochelle Bansal for patiently waiting for this day and regret troubling them for not able to give my ample time during my research work.

Last but not the least I would like to thank all friends, colleagues, students and relatives who directly or indirectly pushed me to accomplish this task. I would also like to thanks reviewers

of my research papers who had given me directions to improve my work. I am thankful to those who had made the road on which I can travel researchers and scientists whose work is quoted or consulted in the present research.

PikeshBansal **Dated: 30 May, 2016**

ABSTRACT

Necessity to make more efficient mechanical system in order to sustain in competitive world there is demand for efficient bearing system which can carry high load at high speeds. Hydrodynamic journal bearings are best suited for rotating machinery applications which require carrying high load when machinery is working at high speeds. Hydrodynamic journal bearings have wide range of application due to their ability to carry high load at high speed of operation. Ever increasing demand to improve the design in order to increase quality and reliability has led to use of liner. In order to enhance performance of bearings additives are added to lubricating oil. These additives are long chained carbons when mixed in lubricating oil and also metal debris during operation fluid no longer behaves as Newtonian fluid. Many theories are presented by researchers for non-Newtonian behavior of fluids. But, theory of micropolar fluids is widely used in tribology to study performance characteristics of bearings. The above stated factors motivated authors to study effect of flexibility of bearing liner on hydrodynamic journal bearings under micropolar lubrication.

Steady state performance characteristics in terms of load carrying capacity, attitude angle, friction parameter and end flow are presented in the study. The effect of flexibility of liner on steady state parameters under micropolar lubrication is presented in terms of graphs. Modified Reynolds equation is derived incorporating the effect of micropolar fluids to general equations of lubrication. Modified Reynolds equation is solved using finite difference method and distortion of liner is calculated by applying theory of elasticity. Results are presented in form of graphs. Detailed parametric study is done taking deformation factor as independent variable and others as parameter.

Linear dynamic analysis is conducted using perturbation method to study stability of hydrodynamic journal bearings. Small order perturbations are provided to get stability characteristics in terms of critical mass parameter and whirl ratio. Modified Reynolds equation is solved along with equations of motion. Finite difference method along with successive over relaxation scheme is used to get perturbed pressures along line of centers and perpendicular to lines of centers. Results are presented in the form of graphs for detailed parametric study conducted. Detailed effect of flexibility of linear and micropolar parameters on stability characteristics is discussed in analysis.

Trajectory of journal centre is predicted by non-linear transient analysis. Modified Reynolds equation is solved with equations of motion to get state space variables applying fourth order Runge-Kutta method. Effect of flexibility of liner on non-linear transient characteristics of hydrodynamic journal bearings is studied by applying theory of elasticity. Critical mass parameter is predicted by hit and trial method. Mass parameter for which trajectory of journal bearing centre follows limit cycle gives us measure of critical mass parameter. Results of non-linear transient analysis are compared with results of linear dynamic analysis. Effect of flexibility of liner and micropolar parameters on limit cycle is studied.

CONTENTS

Steady State Analysis of Finite Flexible Oil Journal Bearings with Micropolar Fluids

LIST OF PUBLICATIONS

1. P. Bansal, A.K. Chattopadhayay & V.P. Agrawal "Linear Stability Analysis of Hydrodynamic Journal Bearings with a Flexible Liner and Micropolar Lubrication", TribologyTransaction, Vol.58,2015, pp.316-326.

2. P. Bansal, A.K. Chattopadhayay & V.P. Agrawal, “Steady State Performance Characteristics of Micropolar Lubricated Hydrodynamic Journal Bearings with Flexible Liner”, Journal of institution of engineers (India) Series C, Vol.97(2), 2016, pp.195-207.

LIST OF FIGURES

NOMENCLATURE

$a = r_0$	Inner radius of the bearing liner [m]
b	Outer radius of the bearing liner [m]
C	Radial clearance [m]
C'	$2+\lambda/G$
C_B	Body couple per unit mass
D	Journal diameter [m]
D_{ij}	Damping coefficient of micropolar fluid for i = R, ϕ and j = R, ϕ [Ns/m]
$d_{m,n}$	Distortion of m, n harmonic
e	Eccentricity [m]
e_0	Steady state eccentricity [m]
E	Young's modulus [N/m^2]
F	Deformation factor, $F = \frac{\mu\omega R^3}{Ec^3}$
f	Coefficient of friction, $f=F_S/W$
f(R/C)	Friction parameter
F_B	Body force per unit mass
F_S	Friction force on journal surface [N]
$\bar{F}_S$	Non-dimensional friction force
$\bar{F}_R$	Non-dimensional fluid film force along lines of centers
$\bar{F}_\phi$	Non-dimensional fluid film force perpendicular to lines of centers
$(\bar{F}_R)_0, (\bar{F}_\phi)_0$	Non-dimensional steady state fluid film forces
h	Oil film thickness [m]
h_0	Steady state oil film thickness [m]
h_{min}	Minimum oil film thickness
$\bar{h}_0$	Non-dimensional steady state oil film thickness
H	Thickness of bearing liner [m]
H/R	Bearing liner thickness to journal radius ratio
h_{cav}	Film thickness at point of Cavitation [m]
j	Microinertia constant
l_m	Non-dimensional characteristic length of micropolar fluid, $l_m=C/\Lambda$
L	Length of bearing

L/D	Slenderness ratio
L_R	Length ratio
m, n	Axial and circumferential harmonic
M	Mass of journal per bearing [kg]
$\bar{M}$	Non-dimensional mass parameter
$\bar{M}_C$	Critical mass parameter
N	Coupling number
p	Oil film pressure [pa]
p_0	Steady state film pressure
$\bar{p}$	Dimensionless pressure
$\bar{p}_1, \bar{p}_2$	Dimensionless perturbed pressures
Q_Z	End flow of oil [m^3/s]
$\bar{Q}_Z$	Non-dimensional end flow
R	Journal radius [m]
Re	Modified Reynolds equation
S	Sommerfeld number
S_{ij}	Stiffness coefficient of micropolar fluid for i = R, ϕ and j = R, ϕ (N/m)
$\bar{S}_{ij}$	Non-dimensional stiffness coefficient
t	Time [s]
$\bar{t}$	Non-dimensional time
U	Tangential velocity of the journal [m/s]
u_r, u_θ, u_z	Displacement components in r, θ and z directions
v	Microrotational velocity vector
V	Velocity vector
W_0	Steady state load [N]
$\bar{W}_0$	Non-dimensional steady state load
x, y, z	Circumferential, radial, axial coordinates
θ, $\bar{y}$, $\bar{z}$	Dimensionless coordinates, θ=x/R, $\bar{y} = y/a$, $\bar{z} = z/(L/2)$
u', v', w'	Radial, circumferential and axial displacements
ρ	Density
ε	Eccentricity ratio
ε_0	Steady state eccentricity ratio
ε_1	Small order perturbation of eccentricity ratio

ω	Angular velocity of journal
ω_p	Angular velocity of whirling motion of journal
ω_S	Threshold speed
μ	Viscosity of oil
μ_e	Effective viscosity
ν	Poisson's ratio
α, β, γ	Viscosity coefficient for micropolar fluid
χ	Spin viscosity
λ_R	Whirl ratio
τ_{ij}	Stress in i_{th} plane in j_{th} direction
τ_S	Shear stress along journal surface
λ, G	Lame's constant
δ_0	Steady state radial deformation at bearing liner surface
$\bar{\delta}_0$	Steady state non-dimensional radial deformation at bearing liner surface
ϕ	Attitude angle
ϕ_0	Steady state attitude angle
ϕ_1	Small order perturbation for attitude angle
θ	Angular coordinate of bearing
θ_1, θ_2	Angles of end and start of hydrodynamic film at each axial plane of bearing
Λ	Characteristic length of micropolar fluid

ABBREVIATIONS USED

1-D	One dimensional
2-D	Two dimensional
3-D	Three dimensional
EHD	Elastohydrodynamics
FEM	Finite element method
FDM	Finite difference method
JFO	Jacobson Floberg Olsson
NLTA	Non-linear transient analysis
ORF	Over relaxation factor
RKM	Runge-Kutta Method
SOR	Successive over relaxation

Chapter 1 Introduction

1.1 Introduction

Bearings are integral parts of support system of machine components. Tribology, science of friction, wear and lubrication is essential part of bearings design. Emphasis on study of this subject started about 100 years back with pioneer work of noted researchers like Petroff [2], Tower [3] and Reynolds [4]. Since then attempts were made to find an analytical solution whose results are close to experimental readings. Progress in field of computers, mathematics and numerical analysis techniques have led to progress in field of Tribology. Many authors have since then carried out experimental and theoretical research on study of hydrodynamic journal bearings in order to improve their design.

In this chapter, efforts are made to present brief review of available literature on hydrodynamic journal bearings.

1.2 Hydrodynamic journal bearings

Necessity to make more efficient mechanical system in order to sustain in competitive world there is demand for efficient bearing system which can carry high load at high speeds. Hydrodynamic journal bearings are best suited for rotating machinery applications which require carrying high load when machinery is working at high speeds. In order to design better and efficient bearing, knowledge of true or expected operating conditions is vital. Extensiveness of subject can be understood from fact that countless studies are presented on journal bearing and still research is going on in this area.

Although first formulation of a hypothesis regarding force necessary to overcome viscous resistance of a fluid was derived by **Newton [1]** in 1668, **Petroff [2]** made first significant contribution theoretically in 1883 with his consideration of effect of viscous force in fluid film lubrication.

Tower's **[3]** experiments for determination of suitable methods of lubricating railway axle bearings, which were partial bearings lubricated from an oil bath, were first significant experimental studies and developed pressure distribution in bearing clearance under loaded condition as measured through a number of pressure gauges at mid-plane in circumferential direction was found to exhibit a peak, which was several times higher than mean pressure

calculated on basis of projected area. Just after three years of **Tower**'s first experiments, **Reynolds [4]** presented a theoretical study to justify experimental results of **Tower.** Experiments of **Tower** and analysis of **Reynolds** may be considered as first ever concept of hydrodynamic lubrication and field of ***Tribology.***

Tower's [3] were pioneers in developing concept of hydrodynamic lubrication with their experiments along with **Reynolds [4]** with his theoretical study. Since then many notable scientists and researchers have presented theoretical, experimental and analytical studies on this area of research. A few of them considered as benchmark work are only briefly reported.

At age of infancy of Tribology experimental and theoretical analyses were based upon use of liquid lubrication, but almost within a decade science reached its maturity following experiments of **Kingsbury [5]**, which not only extended concept of hydrodynamic lubrication to gasses by using air as lubricant, but also developed experimental set up to study behaviors of gas bearings based on concept of electrical analogy.

First exact solution of Reynolds equation for pressure distribution for full journal bearing using full film boundary condition was presented by **Sommerfeld [6]** in 1904 along with load and friction characteristics in terms of eccentricity ratio.

Harrison [7] in 1913 enriched hydrodynamic lubrication through his experiments with special reference to air as lubricant. **Rayleigh [8]** first investigated effect of film shape on operating characteristics of a bearing using calculus of variations. **Christopherson [9]** pioneered in establishing suitability of Southwell's relaxation method for lubrication problems and using relaxation method **Cameron** and **Wood [10]** obtained solution of finite bearings and presented bearing characteristics for two slenderness ratios using realistic boundary conditions. During same time **Vogelpohl [11]** developed an approximate solution based on infinite series. **Ocvirk [12]** presented solution of Reynolds equation using narrow bearing approximation.

Harrison [13] initiated theoretical research on dynamic characteristics of impervious self-acting oil bearing. It was presented in this theoretical research that orbital motion of journal axis under constant load are satisfied by hydrodynamic equations of a light rigid rotor, which are supported by a pair of infinitely long bearing under full film lubrication.

However, derivation of Reynolds equation was based upon some specific assumptions relating to cavitation, fluid inertia forces and non-linear flow effects. Among studies of effect of convective inertia forces on hydrodynamic lubrication **Kahlert [14]** and **Osterle** and **Saibel [15]** are always cited for their pioneering studies. Investigations of cavitation in fluid film started with experiments of **Coles** and **Hughes [16]**, which showed that end of pressure curve was coinciding with position of zero pressure gradient, which however, conflicted with experimental results of **Jacobson** and **Floberg [17]**, which indicated that pressure cavitated somewhere beyond point observed.

In year 1958, Tribology achieved another important advancement with numerical solution of bearing characteristics using digital computers by **Pinkus [18]** and **Raimondi** and **Boyd [19].**

1.3 Hydrodynamic journal bearings with flexible liner

Hydrodynamic journal bearings are most effective at higher operating speeds but are susceptible to wear damages when working at lower speed (during starting and stopping of machinery). Journal bearings are imparted with liner in order to shield bearing from getting damaged during low speed operation. Flexibility of bearing liner material used affects operating characteristics of journal bearings. Elastic deformation of liner due to hydrodynamic fluid pressure modifies fluid film profile which, in turn, changes pressure distribution and hence performance characteristics of journal bearings.

Work in area of hydrodynamic journal bearings considering flexibility of bearing liner started by work of **Higginson [20]**.

Holmes [21] presented study on instability of circular bearing oil films. Stability of shaft showed improvement on reducing slenderness ratio. He predicted response calculation and stability should include damping coefficients. This led to increase in stability and reduction in forced vibration amplitudes. He also showed that measure of stability is provided by static locus.

O'Donoghue et al. [22] gave solution to problem of hydrodynamic lubrication of journal bearings taking into account elastic distortion of shaft. Exact solution to find elastic deformation for pressure distribution around a bearing was given. Iterative method to calculate pressure distribution satisfying hydrodynamic and elastic requirement of system

was presented. Theory predicts that for highly loaded bearings peak pressure for a given load decreases. Eccentricity ratio increases for particular load and bearing stiffness reduces.

Brighton et al. [23] described method of solution for finite bearings considering effect of elastic distortions. In this paper three displacement components were solved simultaneously satisfying boundary conditions by using an approximate method.

Benjamin and Castelli [24] investigated problem of compliant surface journal bearings. Mathematically problem was divided in to two parts elasticity and fluid problem. Raleigh Ritz and collocation method were used to solve elasticity problem. Fluid problem represented by Reynolds equation is coupled with solution of elasticity problem. Resulting set of equations are solved by Newton Raphson method.

Oh and Huebner [25] applied finite element technique to solve elastohydrodynamic finite journal bearing problem. Reynolds equation for fluid film and 3-D elasticity equations for bearing housing were solved simultaneously using a unique iteration scheme. Analysis yields pressure distribution and displacement distribution which satisfy elastohydrodynamic requirements of realistic three dimensional bearing geometries. From these distributions, important information such as stress in bearing material and minimum film thickness in lubricant may be calculated. In calculations it is assumed that bearing operated with a constant property lubricant and a linearly elastic bearing material.

An analysis was made by **Conway and Lee [26]** for effect of flexibility on performance characteristics of journal bearing. Results are shown in terms of graph for bearing characteristics.

Jain et al. [27] calculated effect of flexibility of bearing shell on bearing performance.FEM is used to solve governing Reynolds equation. Results are presented for various deformation coefficients.

Jain et al. [28] determined performance characteristics of compliant shell journal bearings having aspect ratio of 1.0 and eccentricity ratio up to 0.8. Modified fluid film pressure profile taking into consideration deformation in bearing shell is generated by using iterative

procedure. Results in study show a considerable change in performance characteristics considering deformation of bearing shell.

Majumdar et al. [29] conducted dynamic analysis for journal bearings considering flexibility of liner. Graphical results were presented for steady state and dynamic characteristics. He presented effect of flexibility of liner on bearings stability taking Newtonian fluids as lubricant. Linearization method using first order perturbation theory was used for stability analysis. It was concluded that region of stability decreased as bearing liner was made more flexible for high eccentricity ratio; as length to diameter ratio was increased, distortion effects were more prominent. This leads to decrease in stability. Increase in distortion of liner increases direct coupled radial stiffness coefficient. Reverse effect was noted for cross-coupled stiffness and damping coefficients. Flexibility of liner did not affect other coefficients. Hydrodynamic pressure and hence load capacity is decreased as bearing liner was made more flexible, especially at eccentricity ratios greater than 0.8.

A theoretical study on linear and non-linear transient motion analysis was presented by **Chandrawat and Sinhasan [30]** for a flexible shell journal bearing. In this study analysis is done using a computer aided program. Transient responses of system have been predicted by drawing trajectories of journal center motion. Higher stability is predicted by non-linear analysis as predicted by results of study.

Braun and Dougherty [31, 32] in two part paper have given a hybrid model for solution of compliant wall bearing problem. In first part of two part paper, they have introduced an iterative solution combining FEM and FDM to generate bearing pressure profile taking into consideration deformation of liner. Cylindrical 3-D FEM model is used for axisymmetric body which is subjected to non-axisymmetric loading and has been combined with FDM to get pressure profile by solving Reynolds equation. Second part of paper presents results of parametric study conducted on model presented in part 1. It can be predicted that wall compliance considerably influences performance characteristics of journal bearing taking angular velocity, liner material, shaft axial alignment and working fluids as parameters.

A realistic model for journal bearing was taken by **Lahmar [33]** for Elastohydrodynamic (EHD) analysis considering couple-stress effects for lubricants. Stokes theory of micro-continuum is applied to derive Modified Reynolds equation. Perturbation technique is applied

to calculate 8 coefficients of stiffness and damping to analyze bearing system. Load carrying capacity and hence stability is higher for couple stress lubricants. Lower values are predicted for attitude angle and friction parameter under couple-stress lubrication.

Boucherit et al. [34] analyzed misaligned complaint journal bearings. Couple stress effects were incorporated to get steady state and dynamic characteristics. Elastic thin liner model is implemented to calculate displacement of bearing liner interface. Misalignment and couple stress parameters effect on static and dynamic performance characteristics are depicted in graphs presented.

Lahmar et al. [35] investigated theoretically effect of static and dynamic deformation on stability characteristics for complaint journal bearing. It is predicted in analysis that surface coatings from soft materials effect stability of complaint journal bearings. Results are presented in term of graphs for static and dynamic deformations of liner against various performance characteristics.

Kuznetsov and glavatskih [36] have conducted dynamic analysis considering effect of mechanical and thermal deformation for complaint journal bearings. It found from analysis that bearing stability improves by using compliant lining.

1.4 Stability analysis for hydrodynamic journal bearing

As high speed is essential to generate fluid film pressure by self-action, hydrodynamic bearings have found applications mostly in high-speed machinery such as turbines, turbogenarators, turbopumps etc. Instability of rotor-bearing system is major problem in application of oil lubricated bearings. As threshold of instability is relatively low analysis of such bearings has gained importance. Many researchers over span of time have presented their work in field of stability analysis of journal bearings. Review of work of some researchers in field of stability analysis for hydrodynamic journal bearings is presented below.

Newkirk [37] and **Newkirk** and **Taylor [38]** first described oil whirl as lateral self-excited vibration of shaft due to dynamic oil film forces on bearing. **Hagg [39]** presented stability analysis including damping force terms. However, earliest attempt for prediction of half speed whirl was perhaps due to **Poritsky [40]** and **Hagg** and **Warner [41]**. Extensive

experimental investigations on short bearings were conducted by **Newkirk** and **Lewis [42]**. It was predicted that low viscosity oil, moderate bearing loads and larger clearances favored stable operation. Natural frequency of vibration of rotor was detected equal to whirl frequency. However, severe whirl was found to occur at frequency which is near to half of running speed, in some cases where bearing is operating with light loads.

Pinkus [43] showed through experiments whipping starts at half running speed of shaft. He predicted better stability at higher viscosity. Though, his findings were different from findings of **Newkirk** and **Lewis [42].**

First attempts to actually solve simultaneously equations of motion and gas lubrication equations were made by **Constantinescu [44]** and by **Sternlicht *et al* . [45]**.

Hori [46] associated whirl whip with dynamic stability of rotor. Reynolds equation was solved under dynamic condition considering long bearing approximation for 180° oil film bearing. Stiffness and damping coefficients were found to be related to incremental linearized journal forces and corresponding increments of displacement and velocity respectively.

Castelli and **Elrod [47]** used digital computers to solve numerically Reynolds equation and complete set of non-linear differential equations of motion for small perturbations from steady state position for infinitely long gas journal bearing.

Stability analysis of cylindrical journal bearings was carried out by **Rentzepis** and **Sternlicht [48]** and region of stability was analytically determined. Linear vibrational equation of motion was employed to obtain region of stability bounded by operating eccentricity curves and families of load carrying capacity. Results showed existence of a minimal value in stability curves and their prediction was supported by experimental evidence.

Gross [49] presented study on nature of whirl for hydrostatic journal bearing with air lubrication. This study included self-acting bearings as a special case. Synchronous whirl led by rotor unbalance were predicted at more than one critical speed. When rotational frequency would be two times lowest critical frequency it would result in self-excited whirl.

Pan and **Sternlicht [50]** worked on plain cylindrical gas journal bearings to get translatory motion of vertical rotor. To foretell theoretically dynamic characteristics of rotor/bearing system, it is essential to calculate accurately fluid film forces of bearing under dynamic condition. Motion of lubricant, with a small clearance ratio and a moderate speed is governed by generalized Reynolds equation. Reynolds equation gets complicated due to compressibility criterion if lubricant is gaseous. Finite approximations in case of vertical rotor which is operating in plain journal bearing were given by modified compressibility number and transformation of coordinate system, ignoring effects of temperature and viscosity changes. Attitude angle in presence of whirling motion is quite different from static one. On other hand, magnitudes of film forces are not too much different. They also showed that modified compressibility number was reduced to zero at half frequency. Reynolds equation for an isothermal gaseous film and with approximation of a small eccentricity ratio becomes similar to that of liquid film.

Vibration effects of single symmetrical rotor in short bearing were studied by **Morrison [51].** Stiffness and damping coefficients were found and these were verified with the experimental results.

Reynolds and **Gross [52]** presented method to experimentally identify cylindrical and conical modes of synchronous and self-excited whirl. They pointed out that both types of whirl, *viz.* cylindrical and conical, could exist simultaneously. In order to have stable operation of bearing, it is required to have large eccentricity ratio when bearing is working at speed which is above whirl threshold. Similarly, stable region in case of balanced rotors was established to be extended to small eccentricity ratios when bearing is operating at speed below threshold speed.

Large amplitude of self-excited whirl occurring beyond threshold speed depends upon performance characteristics and geometrical configuration. Threshold speed was found to exhibit almost linear relationship with unit load. Threshold eccentricity ratio enhances as clearance ratio increases. Whirl ratio was found to remain between 0.485 and 0.50.

General theoretical analysis presented by **Lund** and **Sternlicht [53]** provided a direct method to calculate force to be transmitted by two symmetrical bearing rotor to study dynamic analysis of rotating machinery.

In an experimental work of **Sternlicht** and **Winn [54]** for plain cylindrical gas journal bearings, considering phenomenon of half-frequency whirl instability, effects of load, mass, slenderness ratio and clearance on threshold of instability were established and compared with theory **[48].**

Experimental results indicated that for a given bearing load, speed reduced to minimum for a particular clearance and half frequency whirl was greater on either side of this clearance. Onset of cylindrical half-frequency whirl increased with increase in rotor mass and onset of half frequency whirl increased almost linearly with load. Eccentricity ratio at onset of instability remained constant for particular rotor mass and bearing clearance, although bearing load was varied.

Use of external damping against oil-whirl instability and its usefulness for achieving stability control were studied and discussed by **Holmes [55]** for rigid and flexible rotor systems. Results for flexible rotor-damping system in study showed that even small excitation of external damping augments instability onset speed and these effects were more prominent at higher eccentricity ratio.

Marsh [56] presented new theory for aerodynamic journal bearings assuming that pressure field generated by minute dynamic motions was applied with local linearization to calculate onset of half speed whirl. Translational and conical dynamic stiffness matrices were made to conduct dynamic analyses. Translational and conical modes of whirl for both single and double bearing systems were predicted to derive stability criterion.

Ausman [57] presented stability theory for translatory half-speed whirl for long self-acting gas journal bearing for time dependent Reynolds equation considering linearized 'ph' approximation. Theory showed that threshold speed at which half speed whirl is onset depends on three non-dimensional steady state parameters, eccentricity ratio, bearing stability parameter and bearing compressibility parameter. Bearings were found to be unstable below a minimum operating eccentricity ratio for a particular bearing compressibility parameter and bearing stability parameter. Whirl frequency was found equal to or a little less than half of rotor speed at this particular whirl threshold point. This finding supported results of **Reynolds *et al.* [52]**.

Holmes [58] calculated frequency response and stability limits for a symmetrical rigid rotor utilizing values of bearing coefficients given by **Smith [59]** for finite bearings. Time transient method of obtaining stability threshold speed of short, long and finite bearings was studied by **Badgley [60]** in his Ph. D. dissertation. Orbits of balanced horizontal rotor on rigid supports were examined with various methods of perturbation to determine influence on stability boundary. It was observed that threshold speed at high eccentricities was reduced by large initial velocities.

Badgley and **Booker [61]** simulated non-linear motion of rotor system using Runga-Kutta extrapolation procedure. Hydrodynamic film forces were obtained by solving Reynolds equation for short, long and finite bearings. It was found from observations that onset of instability was significantly affected by large initial velocity disturbances in comparison to smaller velocity disturbances.

In a time transient analysis by **Akers *et al.* [62]**, equations of motion for a finite journal bearing for various slenderness ratios were solved, which showed that stability was non-uniform with addition of out of balance loads, and improved with increase in viscosity of oil, but is found to be unaffected by initial disturbances imparted on shaft. Trajectories of motion of bearing center were obtained in both uncavitated and cavitated conditions.

Capone [63] studied theoretically oil whirl for unloaded journal bearing using half-Sommerfeld boundary conditions. He presented effect of operating parameters such as rotor mass, speed, geometrical configuration on whirling characteristics. Considering a long bearing approximation and with assumption that journal center traced a circular trajectory under unloaded condition, dynamic equilibrium equations were presented and results were compared experimentally.

Singh and **Sinhasan [64]** analyzed relative stability of porous journal bearing. Results showed porous journal bearing with axes skewed has smaller threshold speed in comparison to similar system with parallel axis. It was also noted that with increase in skew component corresponding non-dimensional mass of journal decreased.

Stability of conical whirl for a symmetric rotor bearing system was conducted theoretically by **Yoshihiro *et al.* [65]** with an infinitely short bearing approximation considering effect of moment of inertia of rotor. Stiffness and damping properties used to predict limit of variation in stability with an infinitely short bearing approximation, taking eccentricity ratio and moment of inertia ratio (0 to 0.49) as parameters. Theoretical study predicted an improvement in stability at higher moment of inertia ratio.

Guha [66] theoretically conducted stability analysis of porous oil journal bearings. Results in study showed that an increase in limit of stability with corresponding increase in any of the parameters namely permeability factor, bearing feeding parameter, clearance ratio, moment of inertia ratio and slenderness ratio when other parameters remained unaltered.

In 1986, **Guha [67]** extended previous theoretical investigation and result supported results obtained in previous study except that no appreciable effect on conical stability was found by altering values of non-dimensional speed parameter for a constant bearing feeding parameter. Study on conical stability for hydrodynamic porous gas journal bearing with tangential velocity slip was reported by **Guha [68]**, which shows that conical stability deteriorated with bearing number, velocity slip and bearing feeding parameter but increased with slenderness ratio. Thickness ratio, permeability and porosity parameter were found to have insignificant effects on stability.

Ramesh and Majumdar [69] presented stability analysis of rough journal bearings using nonlinear transient analysis. Results presented in the study show that there is marginal affect on stability as composite roughness increases. But, variation is noteworthy as shear flow factor is considered.

However, experimental evidences since early years of last century put forward realization of existence of a separate lubrication theory for fluid suspension and effort for establishing a theory was intensified since mid of last century. Early studies on such theories of fluid micro-continua have no concern with research work of bearings. Theory was later simplified to an acceptable fluid film lubrication theory, called micropolar lubrication theory and in subsequent years this simplified micropolar lubrication theory was introduced in analyses of bearings.

Hence, in what follows, an attempt has been made to present a brief review of available literature in following sequence:

(a) A review of theory of micropolar fluid,

(b) A review of bearings with micropolar lubrication,

1.5 Theory of micropolar fluid

Work of various researchers which led to development of theory of micropolar fluids is mentioned here under.

Kingsbury [70] observed such rheological abnormalities that varied from a small enhancement of viscosity to rigidity in adhering layer ranging from 10^{-3} mm to 10^{-7} mm and attributed this difference in behavior of molecules to possible enhanced viscosity in part of fluid. In 1909 **Cosserat** and **Cosserat [71]** developed theories of oriented media in which there exist three directors at each point. **Jeffery [72]** worked on study of effect on viscosity due to suspended ellipsoidal particles in fluids. Results indicated enhancement of viscosity of such fluid suspension than its base fluid. **Hardy** and **Nottage [73]** concluded that to be beyond range of surface influence, liquid film must be between 0.00762 to 0.01015 mm. in thickness. **Needs [74]**, experimentally calculated the effect of boundary lubrication on viscosity for two circular parallel plates. Through these sets of experiments it was found that there is increase in time lag in their time of approach for plates in comparison to classical Newtonian theory considering film thickness below 0.00127 mm. result indicated an effective viscosity increased up to 5 times in boundary film than that in bulk. He found evidences where effective viscosity in boundary film increased nearly five times than that in bulk. **Buckley**'s **[75]** experiment showed total loss of rigidity in clean liquid at a distance of 0.3 x 10^{-4} mm from a solid boundary. Unexpected behavior of fluid containing oblong molecules in a shear field was recognized by **Anzelius [76]** and this dependence of stress and moment at each point of fluid was expressed by him as a function of orientation of substructure and usual rate of strain tensor. **Henniker [77]** found an extensive enhancement in viscosity within 50000A of surface, during experimentation of Couette type flow performed on leuben oil containing additives of aluminum napthenate up to 2%. Later by squeeze film experiments of various fluids (*e.g.* solutions of pure fatty acids in pure hydrocarbon solvents) between two plates submerged in fluid and by measuring gap between plates as a function of time. **Fuks [78, 79]** found existence of a residual film between plates even after squeezing for a very

long time, similar to those obtained by **Needs [74]**. He observed that fatty acid concentration increased thickness of residual film.

A few more experiments by **Hoyt** and **Fabula [80]** and by **Vogel** and **Patterson [81]** showed that skin friction near rigid body reduced to an extent of 30-35% for small concentration of additives. Earlier additives were considered to be beneficial in boundary lubrication not in hydrodynamic lubrication, but experiments also had shown evidences of favorable effects in thin film hydrodynamic lubrication by their usages.

Two contemporary studies were presented in 1966. Using pure paraffines, mainly hexadecane as lubricants containing various long chained polar additives in a slow running four ball machine **Askwith *et al.* [82]** found positive influence of additives. As a part of his work on squeeze film studies using all fluids even pure cetane showed a plate gap of about 2 x 10-4 mm supporting findings of **Fuks [78, 79]**. **Cameron** and **Gohar [83]** studied lubricated point contacts using oils and showed existence of larger film thickness than that of theoretical one, particularly in low film thickness with a plausible explanation of existence of a thin layer with enhanced viscosity near surface.

For EHD lubrication, EHD film thickness was also found to be enhanced in different experiments of **Kannel *et al.* [84], Parker** and **Kannel [85]** and **Drauglis *et al.* [86]**, when organic phosphonate anti wear additives were used along with base fluids [di(2ethylhexyl)sebacate] in experiments for a pair of rolling contact crowned disks with smooth surfaces.

In context of above examples and a lot more during mid of previous century, it is to be noted that classical continuum theory cannot explain such phenomena as it does not contain any mechanism to include those micromotions. This motivated researchers to extend applicability of continuum mechanics. To figure macroscopic expression of microscopic events i.e. micromotions and deformations field theory approach was included in order to gradually develop theories of microcontinua.

Moreover, experimental evidences predicted increase in lubricating efficiency and few other qualities when Newtonian lubricants are added with little of long chain polymer solution. Practice of adding such additives to most engine oils started with such results. Further, it led

to advances in development of improved lubricants in a direction of these new additives. Classical continuum theory does not have any mechanism to explain such phenomena and thus paved way for development of theory of microcontinua.

First major development in modern continuum theories of non-Newtonian fluids may be attributed to **Ericksen** and **Truesdell [87]** who generalized and simplified theories of **Cosserat** and **Cosserat [71]** and to **Ericksen [88, 89]** who further explored work of **Jeffery [72]** and **Anzelius [76]**.

In order to account for presence of substructures in fluids, **Ericksen [88, 89]** linked substructure vector with each fluid point. Constitutive equations and stress tensor for motion of substructure vector were developed. Stress tensor resulted in coupling between fluid velocity field and orientation of substructure. Governing equations of motion of rigid particle associated with preferred single directional substructure vector were similar to those of **Jeffery [72],** ignoring gradient terms of substructure vector.

Slightly different approach of statistical treatment of structured continua for kinematical strain measures for a fluid with rigid structure was adopted by **Grad [90]** and by **Dahler** and **Scriven [91]** using concept of couple stress tensor, arising from flux of angular momentum of substructures and interactions of particles and concluded that statistical approach and continuum approach yield same macroscopic behavior. Work of **Ericksen [88, 89]** was extended by **Hand [92]** to study effects of deformation of substructures on apparent viscosity. A second order tensor was introduced to each particle in order to represent geometry of spherical particles. Under effect of shear field these spherical particles deformed into ellipsoids. Study put forward an explanation from continuum point of view for experimentally observed normal stress difference and shear rate dependence of apparent viscosity for polyisobutylene, but is restricted to dilute suspensions. Rheological behavior studies of complex microstructures offers great scope of application of microcontinuum theory **[93]**.

Search for consistent theory got another leap forward with presentation of polar fluid analogue of Navier-Stokes equations by **Condiff** and **Dahler [94]** for a linear isotropic fluid. This theory was able to describe interaction of internal spin with fluid flow with introduction

of continuous spin field. It was also able to describe viscous transport of internal angular momentum through couple stress.

A number of important contributions were also made by **Allen *et al.* [95]**, **Kaloni** and **DeSilva [96], Kline** and **Allen [97, 98]** in late sixties and early seventies of last millennium. Governing equations in form of mass balance, linear and angular momenta balance and canonical form of energy equation were presented for fluid with deforming microstructure by **Allen *et al.* [95]** by postulating energy balance and inequality of production of entropy. Constitutive equations for oriented fluid with deformable but non-interacting substructure were presented by **Kaloni** and **DeSilva [96]**. They applied theory of oriented fluids to study behavior of dilute suspensions by discussing case of dilute suspension of viscoelastic spheres in steady laminar flow. Effects of fluid microstructures were studied by **Kline** and **Allen [97]** for non-steady fluid flow containing microstructures for suddenly accelerated plane wall problem. Linear constitutive equations for fluid suspension of deformable particles was presented in study made by **Kline** and **Allen [98],** assuming particles to be spherical when undeformed and ellipsoidal when sheared. This theory qualitatively predicts behavior in steady shear flow of dilute solutions of random coiling macromolecules.

In spite of efforts put by various researchers in providing all these accountable studies **Eringen** and his co-investigators **[99 – 105]** were able to provide with a full consistent theory which can be applied to real life practical problems with acceptable simplifications.

During their stay at Purdue University at Indiana, U.S.A. **Eringen** and **Suhubi** presented two papers **[99, 100]** on non-linear theory of micro-elastic solids. In first **[99]** of study series, balance of momenta, theories of motion, conservation of energy, and entropy along with boundary conditions and lastly constitutive equations of "simple micro-elastic solids" were presented in tensorial forms.

Concept of inertial spin, stress moment, mechanism of surface tension and laws of motion were some other natural and obvious outcomes of theory. They presented mathematical model to define "simple micro-elastic materials" previously known as "micro-elastic materials". This mathematical model was defined by applying simplest continuum theory and methods of statistical mechanics without using molecular points of view.

Extension of previous work, in Part-II **[100] Suhubi** and **Eringen,** after introduction of strain measures, displacement vector and tensor, presented constitutive equations for isotropic micro-elastic solids, field equations of linear micro-elastic solids, linear theory of couple stress and application of theory to study of Rayleigh surface waves in micro-elasticity. Important points to be noted are that 18 material constants are required for complete description of micro-elastic properties of isotropic linear elastic solid and only possible initial stress is hydrostatic pressure in case of isotropic micro-elastic solid.

Subsequent to introduction of micro-elastic solids, **Eringen [101]** in 1964 proposed a similar theory— basic equations, jump conditions and constitutive equations of ***'simple microfluent'*** media. ***'Simple microfluids'*** are considered to be fluent medium and generalization of Stokesian fluids. As these fluids possess local inertia, Eringen extended continuum theory to consider: (a) conservation of micro-inertia moments, and (b) balance of first stress moments, and developed and discussed concepts of inertial spin, body moments, gyration tensors, stress moments, wherein stresses and stress moments were expressed in terms of deformation rate tensor and various microdeformation rate tensors. Simple microfluid in its simplest form has as many as twenty two viscosity coefficients and fluids in which gyrational effects are important, such as anistropic fluids, vortex fluids and fluid having surface tensions are guessed to fall in this group.

In 1965 **Eringen [102, 103]** presented theory of micromorphic material. As even linear theory was too complicated for engineering application, **Eringen [103]** simplified it with consideration of a subclass of micromorphic materials, named as micropolar media. Study however presented discussions on deformation and motion, laws of motion, constitutive equations, theory of micropolar media, micropolar viscoelasticity, micropolar materials with attenuating neighbourhood and problem of micropolar channel flow, with assumptions of linear constitutive equations, microisotropic medium and negligible heat conduction.

As an extension of above study, linear theory with basic equations, theory of micropolar elasticity, couple stress theory, non-negative internal energy and Uniqueness theorem of micropolar elasticity were presented by **Eringen [104]** in same year.
Finally, totality of microcontinuum theory was achieved by **Eringen [105]**, when he presented laws of motion, constitutive equations of microfluids, definition of micropolar

fluids— theories of its thermodynamics and field equations and study of such a fluid flow in a circular pipe.

1.6 Bearings with micropolar lubrication

First application of theory of micropolar fluids in field of lubrication was presented by **Eringen [105].** Steady motion in circular channel for micropolar fluids was presented. Graphs representing profiles for velocity, shear stress difference, microrotational velocity and couple stress on fluid surface adjacent to wall. Though shearing stress remained same as classical theory, surface shear reduced which was quantitatively equal to effect of distributed couples which are aroused in thin layer adjacent to surface of fluid. This indicated development of boundary layer phenomenon which could not be described using Navier-Stokes theory.

Couple stress and micropolar theories were first applied by **Ariman** and **Cakmak [106]** to Poiseuille and Couette types of flow problems for one-dimensional fully developed and steady flow of incompressible fluid between two parallel plates. In this study equations for velocity distribution and mass flux were presented. Results for velocity profiles for both types of flow and mass flux were shown in comparative graphical forms for couple stress and micropolar fluids.

Study was later extended by **Ariman *et al.* [107]** for micropolar fluid flow between two concentric cylinders for Poiseuille flow and Couette flow. Velocity, shear stress difference, microrotational velocity and couple stress profiles were discussed.

In 1971 **Allen** and **Kline [108]** gave an approximate analytical solution for two-dimensional slider bearing with micropolar lubrication containing rigid spherical substructure and using order-of magnitude arguments reduced governing equations by set of coupled, linear, ordinary differential equations. They observed that in presence of microstructure in fluid resultant pressure attained maximum value when value of ratio to exit gap width is 2.2. Effect of substructure also increased resultant force of fluid on guide surface from corresponding values computed from classical theories, compared with **Schlichting [146]**, but coefficient of friction was found to decrease.

In January 1972 **Datta [109]** presented theoretical study of pivoted slider bearing with convex pad surface under micropolar lubrication. Modified Reynolds equation was derived to show effect of micropolar fluids as lubricant. Effect of pad surface curvature was presented and discussed in parametric study on pressure, load capacity, center of pressure and friction coefficient. It was shown that micropolar fluid resulted in higher load carrying capacity than Newtonian fluid.

Contemporary numerical work of **Balaram** and **Sastri [110]** supported findings of Ref. **[108]**. They obtained solutions for velocity and spin fields, volume flow rate, resultant pressure, resultant force of fluid on guide surface and pressure distribution, using method of separation of variables and presented numerical results for various microstructure characteristics in their paper.

Theoretical study by **Agrawal *et al.* [111]** was presented on squeeze films on hydrostatic bearings with micropolar fluids as lubricant. Results in study showed that in micropolar lubricants squeeze film bearings exhibited larger time of approaches and for a given flow rate externally pressurized bearing under micropolar lubrication showed higher load carrying capacity.

Khader and **Vachon [112]** studied steady incompressible laminar flow of micropolar fluids between two circular parallel disks, geometry being limited to that of thrust bearing with lubricant being introduced from top and obtained relations of pressure, load capacity and wall shear stress as functions of ratio of half of clearance between disks to radius of gyration of microstructure and thus ratio of bearing clearance to particle size and fluid properties.

From graphs showing effect of ratio on pressure distribution and shear stress it was concluded that contaminated lubricant would improve load carrying capacity as well as shear stress from corresponding values in classical case when ratio tended to ∞.

An analytical study was made by **Maiti [113]** on non-dimensional pressures, load carrying capacity and frictional resistance for composite as well as step slider bearings considering two dimensional steady laminar flow of micropolar lubricant. Parametric studies showed that load carrying capacity was higher in micropolar lubricants than in Newtonian lubricants and in composite slider bearing than in plain slider bearing.

At end of same year theoretical investigation by **Indrasena [114]** on kinetic properties of slow motions and potential flow were presented. He considered steady, inviscid and incompressible micropolar fluid flow in absence of body couples.

Theoretical study presented by **Maiti [115]** on squeeze films between two circular plates with fixed lower plate and incompressible micropolar lubrication exhibited better performances in respect of time of approach and load carrying capacity when compared with Newtonian lubricants.

Shukla and **Isa [116]** presented optimum film thickness for maximum load capacity of externally pressurized bearing using micropolar lubricants. It was found that increase in step height ratio or parameters characterizing microstructure of suspension increased maximum load carrying capacity. Influence of these parameters on flow flux was also presented.

Balaram [117] calculated expressions for pressure, relationship of film thickness with time and load carrying capacity of squeeze film in an analysis of micropolar squeeze films between two rectangular plates of infinite length. It can be deciphered from results shown that as density of macromolecular volume increased load carrying capacity increased. But, an increase in substructure particle size load carrying capacity decreased. Squeeze film action was also found to increase in micropolar fluid.

Prakash and his co-workers presented a number of studies on different types of lubrications and for different configurations of bearings using micropolar lubricants during 1975. **Prakash** and **Christensen [118]** developed hydrodynamic theory for two-dimensional micropolar lubrication of rigid cylinder on plane surface in order to make critical analysis of micropolar effects revealed in results of **Fuks [78, 79]** and **Askwith *et al.* [82].** Expressions for non-dimensional forms of film pressure, load capacity, frictional drag, power loss, relative power loss and temperature rise were predicted. Results showed increase in effective viscosity and reduction in frictional drag with increase in micropolar effect.

Prakash and **Sinha [119]** presented a paper on journal bearing taking two-dimensional steady incompressible laminar flow between two eccentric cylinders in relative rotary motion considering lubricant to be micropolar fluid. Governing equations were reduced into coupled, ordinary differential equations. Parametric study of non-dimensional form of various bearing

performance characteristics (pressure distribution, velocity distributions, load capacity, flow flux, frictional drag and coefficient of friction) were presented under this type of lubrication. Micropolar effect on infinitely long journal bearing characteristics was presented graphically which confirmed an increase in effective viscosity as shown by experimental evidences **[74]** especially in thin films. Two parameters characterizing micropolarity in a combined manner were considered separately by them rather than to use their product as were considered by **Eringen [105]** and other authors.

Authors again published analytical study **[120]** to obtain Reynolds equation from field equations of micropolar fluids and presented non-dimensional forms of load and time for steady laminar incompressible micropolar squeeze flow for both parallel circular plates and parallel rectangular plates when upper plate was moving towards stationary lower plate without having any relative tangential velocity of plates. Results were found to have excellent qualitative agreement with **Needs' [74]** experimental results.

Prakash and **Sinha [121]** also presented theoretical analysis of squeeze films in both full and half journal bearings. He considered incompressible, steady and laminar flow between two eccentric cylinders. He calculated non-dimensional pressure distribution, response time and load capacity using modified Reynolds equation for micropolar fluids. Results supported experimental results **[74, 77]** of increase in effective viscosity in narrow passages.

In 1976, in another study, **Prakash** and **Sinha [122]** presented Reynolds equation and expressions for various bearing characteristics of squeeze films for dynamically loaded infinitely long journal bearing for steady incompressible two-dimensional micropolar fluid flow with no journal rotation under sinusoidal load. Graphical representation of results exhibited decreasing velocity of approach with increasing micropolar effect.

Mahanti and **Ramanaiah [123]** presented theoretical study of squeeze films of thrust bearing with micropolar fluids as lubricant. He considered effects of inertia and material constants of fluid. Micropolar lubrication exhibited higher time of approach in squeeze film bearing and higher load carrying capacity in thrust bearing, than those with Newtonian lubrication.

Application of theory of micropolar fluid as presented by **Prakash** and **Christensen [124]** in analysis of elastohydrodynamic inlet zone of line contact, assuming an infinitely long

cylinder in its axial direction under isothermal condition, showed good agreement with results and explanations of previous authors that micropolar fluid theory might offer possible explanation for film thickness enhancement caused by additives.

Isa and **Zaheeruddin [125]** presented analysis of hydrostatic step seal and hydrostatic conical step bearing under micropolar lubrication. Results presented in analysis showed that non-dimensional load carrying capacity and flow flux increase with increase in micropolar effect.

Analysis of 1-D journal bearings, both infinitely short and infinitely long, with micropolar lubrication, was presented by **Zaheeruddin** and **Isa [126]**. An increase in equivalent viscosity of micropolar fluid was shown in results presented which eventually increased time of approach and load carrying capacity, but decreased coefficient of friction.

Tipei [127] also obtained similar results in his analysis of short bearing problem with micropolar fluids as lubricant. For constant viscosity and other micropolar coefficients, he presented simplified generalized expressions for velocity field, friction torque and side flow. It was found from observations of results that fluid pressure was more when micropolar fluid theory is applied to analysis in comparison to Newtonian theory. General bearing characteristics except coefficient of friction, which showed lower values, were found to exhibit improved results than those in Newtonian lubricants.

Isa and **Zaheeruddin [128]** presented paper on squeeze film two dimensional infinitely long porous journal bearings with micropolar lubrication. They considered homogeneous and isotropic material for bearings in analysis. Generalized Reynolds equation for squeeze film porous journal bearing is derived for micropolar lubrication and also generalized form of Darcy's law for flow of micropolar fluid in porous channel. Analysis showed higher values of load carrying capacity and squeeze time in micropolar lubrication.

Analysis of porous journal bearings operating under cyclic load taking long bearing and short bearing approximation under micropolar lubrication is presented in another paper by **Zaheeruddin [129].** Analysis was to show bearing wall thickness, permeability of bearing material and effects of microstructures present in lubricants on operating eccentricity ratio.

3-D Reynolds equation was first presented by **Singh** and **Sinha [130]**, which authors solved to yield expressions for velocity distribution, microrotational velocities flow flux and frictional torques.

Huang *et al.* [131] presented study on finite width journal bearings in 3-D steady flow of incompressible micropolar fluid. Analysis showed that at high eccentricity ratio and lower width to diameter ratio effect of micropolar theory was more pronounced. Results in analysis showed favorable trends for load carrying capacity and friction coefficients using micropolar fluid theory. Volumetric side flow showed marginal difference using either type of theory.

Lubricating effectiveness of micropolar fluid was studied by **Khonsari** and **Brewe [132]** for a journal bearing of finite length and non-dimensional expressions were developed for load capacity, leakage flow rate and friction force. Results showed achievements of higher load carrying capacity, but, lower frictional parameter in comparison with those with Newtonian fluid.

Stability analysis of finite width journal bearing under micropolar lubrication was carried out by **Huang** and **Weng [133]**. Linear dynamic analysis was carried out for journal bearing under both Newtonian and micropolar lubrication and results were presented in form of graphs for stiffness, damping coefficients and critical stability parameter. Micropolar fluids exhibited narrower stability region of journal, larger normal stiffness coefficient and smaller normal damping coefficient. Stable operations were predicted at low Sommerfeld number through results. This is due to increase in effective viscosity and load carrying capacity under micropolar lubrication. Long journal was found to exhibit significant difference in values of critical mass parameter for Newtonian and micropolar fluids, whereas short bearing was found to be almost equally stable in both types of lubrication.

Chaturani and **Narasimman [134]** generated equations of motion for steady flow of micropolar fluid between two rotating disks of finite radius rotating at different/same speeds. These equations of motion were further linearized by quasi-linearization technique after being reduced to set of ordinary non-linear coupled differential equations. Numerical solutions were obtained using fourth order Runga-Kutta method via orthonormalisation.

Hogan [135] presented solution to steady laminar micropolar fluid flow by applying finite element method using variational approach. Simulated results were generated for fully developed flow through straight tube and in order to authenticate results these were compared with already existing analytical results. Comparison between results for this type of flow and Newtonian flow was made for flow through a constrained tube.

Bessonov [136] applied concept of boundary viscosity and ignored deformation of microelements as done by **Eringen [105]** in order to derive generalized Reynolds equation for application of concept of micropolar fluids in lubrication problem. This generalized Reynolds equation is applied in lubrication problem for calculating performance characteristics for plane slider bearing assuming long bearing approximation. Results presented in study show that friction coefficient is reduced significantly with a minor change in load carrying capacity when micropolar parameters are varied.

Eringen along with **Okada [137]** again enriched field by calculating rate of flowing out of thin film of liquid from two surfaces moving towards each other using non-linear lubrication theory of fluids. Exact solutions were presented for spread of thin films on rotating surface and for drainage curves and results generated were compared with results generated by experimental studies.

Lin [138] presented combined effect of 3-D irregularities and lubricant rheology on performance characteristics of hydrodynamic journal bearing. Elrod cavitation algorithm model is incorporated in equations derived in this study. JFO boundary conditions are implicitly incorporated at rupture and reformation boundaries in numerical procedure used this conserves mass throughout bearing. Results presented in study show that pressure distribution of bearing depends on micropolar parameters as well as on asperity size.

Conical whirl instability through linear dynamic analysis for unloaded rigid rotor supported on hydrodynamic journal bearing taking micropolar fluids theory to define lubrication regime has been presented by **Das et al. [139]**. Pressure profile is generated by solving modified Reynolds equation for micropolar fluids. Results in terms of graphs are used to show variation of conical stability parameters versus moment of inertia ratio for various bearing parameters. It is predicted from results that threshold speed for conical whirl instability is more in case of micropolar fluids.

Das et al. [140] presented steady state analysis of misaligned hydrodynamic journal bearings considering axial and twisting displacements considering micropolar lubrication theory. Modified Reynolds equation based on micropolar fluid theory for lubrication is solved by FDM technique in order to obtain steady state film pressure profile. Journal bearings under misaligned condition showed better load carrying capacity with micropolar lubricant regime in comparison to Newtonian flow regime. Beneficial effects were also noticed for friction parameter.

Parametric study on lubricating effect of micropolar fluids have been presented by **Wang and Zhu [141]** on dynamically loaded journal bearing. They derived a general modified Reynolds equation in comparison to classical Reynolds equation for dynamic load. Oil film pressure and oil film thickness is more for micropolar fluids for same dynamic loads in comparison to Newtonian fluids and side leakage flow was found to reduce.

Das et al. [142] presented comparison of linear dynamic analysis and non-linear dynamic analysis in terms of stability characteristics of hydrodynamic journal bearing under micropolar lubrication. Non-linear analysis shows better stability at higher eccentricity ratio. It is also deciphered from results that linear analysis gives conservative results for short and finite bearing configuration. Non-linear analysis and perturbation technique show agreement with each other qualitatively.

Linear dynamic analysis to theoretically calculate stability characteristics for hydrodynamic journal bearing under micropolar lubrication was discussed by **das et al. [143]**. Results presented in study predict that better threshold of stability is attained when journal bearing is running under micropolar fluid regime in comparison to Newtonian fluid regime. It can also be shown that as micropolar effect increases threshold of stability also improves and maximum effect is observed when non-dimensional characteristic length approaches around 10.0.

Theoretical analysis in terms of steady state performance characteristics for finite grooved hydrodynamic journal bearing considering thermal and cavitating effects under micropolar lubrication is studied by **Wang and Zhu [144]**. Same values of frictional film content are observed considering Newtonian and micropolar fluids in cavitated region, while non-dimensional density is higher in case of micropolar fluids in full film region.

Nair et al. [145] evaluated steady state performance characteristic and linear dynamic characteristics of elliptical elastohydrodynamic journal bearings under micropolar lubrication. Results of study show that enhancement in volume concentration of additives increases threshold speed. Damped frequency of whirl decreases when value of deformation coefficient is kept constant.

Verma et al. [146] investigated problem of four pocket hydrostatic journal bearing system considering micropolar fluids as lubricant. FEM is used to calculate steady state and dynamic characteristics. From results it is revealed that increase in micropolar effect leads to increase in pocket pressure, minimum film thickness. Results showed Stiffness and damping coefficients increased with enhanced micropolar effect.

Nicodemus and Sharma [147] presented a study to examine combined effect of wear, bearing configuration and behavior of micropolar lubricant on bearing performance for capillary compensated four pocket hydrostatic journal bearing. Micropolar fluids show better performance characteristics in comparison to Newtonian fluids neglecting wear but advantage is lost considering effect of wear.

Steady state performance characteristics for non-circular two, three and four lobed bearing under micropolar lubrication were presented in a paper by **Rahamtabadi et al. [148]**. Better performance characteristics are shown by micropolar fluids.

Naduvinamani and Santosh [149] had presented analytical evaluation of static and dynamic performance characteristics of squeeze film lubrication considering effect of micropolar fluids for finite porous journal bearing. Velocity of journal center reduces with effect of micropolar fluids when operated under cyclic load. Steady state load carrying capacity and maximum fluid pressure decrease and journal center velocity increases under effect of porous matrix.

Nicodemus and Sharma [150] studied effect of wear analytically using Dufrane's abrasive wear model for multi recess hybrid journal bearing under micropolar lubrication by calculating fluid film pressure solving modified Reynolds equation using FEM in conjunction with Newton-Raphson method. Performance characteristics of bearing are significantly

affected by wear and micropolar effect so it is imperative to consider effect of these two parameters for accurately designing bearings.

Lin et al. [151] obtained linear dynamic performance characteristic for parabolic-film slider bearings under micropolar lubrication. Improvement in performance was observed for bearings with larger fluid-gap interaction and coupling number taking bearing of smaller heights.

Analytical study on effect of various types of geometric irregularities of journal such as, bellmounth shape, barrel shape and circumferential undulation, under micropolar lubrication for 4-pocket hybrid journal bearing was presented by **Sharma and Rajput [152]**. Proper selection of lubricant and type of compensating device can reduce deterioration of journal bearing due to these geometric imperfections.

Dhawan and Verma [153] theoretically predicted dynamic and steady state characteristics of noncircular hybrid journal bearings under micropolar lubrications. Results of study predict reduction in bearing flow and film thickness for higher restrictor design parameter. Study predicts noncircular bearings offer better performance under micropolar fluids regime.

Mehrzadi et al. [154] computed stability of circular and noncircular journal bearings under micropolar lubrication. FEM was applied to solve modified Reynolds equation to obtain dynamic characteristics. Results of study illustrate that stability is increased by using noncircular bearings. Better performance characteristics were observed under micropolar lubrication. Effect of micropolar fluids is prominent at higher coupling numbers.

Dynamic analysis of noncircular hybrid Journal bearing was conducted by **Kumar and Verma [155]**. FEM was used to get dynamic solution by solving Modified Reynolds equation. Results in the form of graphs compare effect of micropolar fluids on circular and noncircular bearings. Micropolar fluid parameters affect bearing performance characteristics.

Quite recently **Khatak and Garg [156]** theoretically computed thermohydrostatic analysis of hybrid journal bearing. Modified Reynolds, 3-D energy and 3-D conduction equations are solved to get performance characteristics. It is concluded in the study that thermal effects can’t be neglected during journal bearing analysis.

1.7 Concluding remarks

From the above survey it seems that lot of study can still be done on hydrodynamic oil journal bearing performance with micropolar fluid as lubricant. Also the foregoing review shows that there is very little information available in the open literature regarding the effect of elastic deformation of bearing shell on the hydrodynamic characteristic of finite length self-acting oil journal bearing with micropolar fluid as lubricant. The steady state, dynamic characteristic including and stability of self acting journal bearings with elastic deformation of bearing liner have been studied using Newtonian fluids and the literature review above shows that micropolar characteristic effect on the rigid bearing performance, but no such literature is available which simultaneously incorporates the elastic deformation of bearing liner and effect of micropolar fluids as lubricant.

1.8 Objectives of the present work

The stepwise objectives for the present research activity are listed below:

1. Development of modified Reynolds equation for flexible oil bearing from the basic equations.
2. Development of steady state solution by using finite difference technique with successive over relaxation scheme.
3. To obtain dynamic pressure in the bearing by first solving the displacement equations to get distortion coefficient and then by simultaneous solution of modified Reynolds equation using finite difference technique with successive over relaxation.
4. To obtain the steady state characteristics viz. dimensionless load parameter, attitude angle, friction parameter and end flow for various design parameter viz. eccentricity ratio, slenderness ratio, Poisson's ratio, bearing liner thickness to radius ratio.
5. To obtain the dynamic characteristic viz. critical mass parameter, whirl ratio for various design parameter viz. eccentricity ratio, slenderness ratio, Poisson's ratio, bearing liner thickness to radius ratio.

Chapter 2 Basic Equations

2.1 Introduction

Micropolar fluids are fluids having substructure in addition to mass and velocity. Presence of microstructures in lubricating fluid, particularly in hydrodynamic lubrication, imparts microrotation and microdeformation of particles. Conservation of micro-inertia moments and balance of first stress moments are used in addition to basic principles of continuum to analyze such fluids. As such a micro-fluid in its simplest form contains 22 viscosity coefficients, and as micro-fluid theory is too complicated and difficult to apply to solution of non-trivial problems in lubrication, analysis has been limited to micropolar fluid, in which micro-deformation effects are ignored. Eringen [105] was first to develop theory of micropolar fluids which can be applied to field of lubrication. **Prakash** and **Sinha[119]** and later **Singh** and **Sinha[130]**

In this chapter, starting from basic field equation and using certain assumptions, modified Reynolds equation is derived and brief discussion of various non-dimensional parameters related to micropolar fluid has been made.

2.2 Field equations

Vectorial form of field equations for micropolar fluids are [119]:

Principle of conservation of mass:

$$\frac{\partial \rho}{\partial t} + \nabla.(\rho \boldsymbol{V}) = 0 \tag{2.1}$$

Conservation of linear momentum:

$$(\lambda + 2\mu)\nabla(\nabla.\boldsymbol{V}) - \frac{2\mu + \chi}{2}\nabla \times \nabla \times \boldsymbol{V} + \chi \nabla \times \boldsymbol{v} - \nabla \pi^* + \rho \boldsymbol{F_B} = \rho \frac{D\boldsymbol{V}}{Dt} \tag{2.2}$$

Conservation of angular momentum:

$$(\alpha + \beta + \gamma)\nabla(\nabla.\boldsymbol{v}) - \gamma \nabla \times \nabla \times \boldsymbol{v} + \chi \nabla \times \boldsymbol{V} - 2\chi \boldsymbol{v} + \rho \boldsymbol{C_B} = \rho j \frac{D\boldsymbol{v}}{Dt} \tag{2.3}$$

Equations for stress tensor $t_{k1}$and couple stress tensor m_{k1} are [119]:

$$t_{k1} = \left(-\pi^* + \lambda \boldsymbol{V}_{r,r}\right)\delta_{k1} + \left(\mu - \frac{1}{2}\chi\right)\left(\boldsymbol{V}_{k,1} + \boldsymbol{V}_{1,k}\right) + \chi(\boldsymbol{V}_{1,k} - \eta_{k1r}\boldsymbol{v}_r)$$
$$m_{k1} = \alpha \boldsymbol{v}_{r,r}\delta_{k1} + \beta \boldsymbol{v}_{k,1} + \gamma \boldsymbol{v}_{1,k} \tag{2.4}$$

η_{k1r} is alternating tensor. An index followed by comma represents partial differentiation with respect to space variable x_k.

2.3 Derivation of modified Reynolds equation

Above micropolar effects are then incorporated into lubrication problem for journal bearing to derive modified Reynolds equation with certain simplifications.

2.3.1 Basic assumptions

Basic assumptions in micropolar lubrication to journal bearing include usual lubrication assumptions **[144]** of lubrication and assumptions for micropolar fluids **[130]**:

(i) Flow is incompressible and steady, i.e. ρ=constant and $\frac{\partial \rho}{\partial t} = 0$.

(ii) Flow is laminar i.e. free of vortices and turbulence.

(iii) Body forces are negligible, i.e. F_B=0

(iv) Body couples are negligible, i.e. C_B=0.

(v) Film is very thin in comparison to length and span of bearing. Thus, curvature effect of fluid film may be ignored.

(vi) No slip occurs at bearing surfaces.

(vii) Bearing surfaces are smooth, non-porous and rigid i.e. no effects of surface roughness or porosity and surface can withstand infinite pressure and stress theoretically without having any deformation.

(viii) No fluid flow exists across fluid film, i.e. lubrication characteristics are independent of y-direction.

(ix) Micropolar properties are also independent of y-direction.

Velocity vector, microrotational velocity vector and fluid film pressure are given as:

$$\left.\begin{array}{c} \boldsymbol{V} = [\boldsymbol{V}_X(x,y,z), \boldsymbol{V}_Y(x,y,z), \boldsymbol{V}_Z(x,y,z)] \\ v = [\boldsymbol{v}_1(x,y,z), \boldsymbol{v}_2(x,y,z), \boldsymbol{v}_3(x,y,z)] \\ p = p(x,y,z) \end{array}\right\} \tag{2.5}$$

Note that for $\alpha = \beta = \gamma = \chi = 0$ and for negligible body couple per unit mass equation (2.3) yields $\boldsymbol{v} = 0$ and so, equation (2.2) reduces to classical Navier-Stokes equation. For $\chi = 0$ velocity vector and microrotational velocity vector are uncoupled and global motion of fluid becomes free of microrotational and their effects.

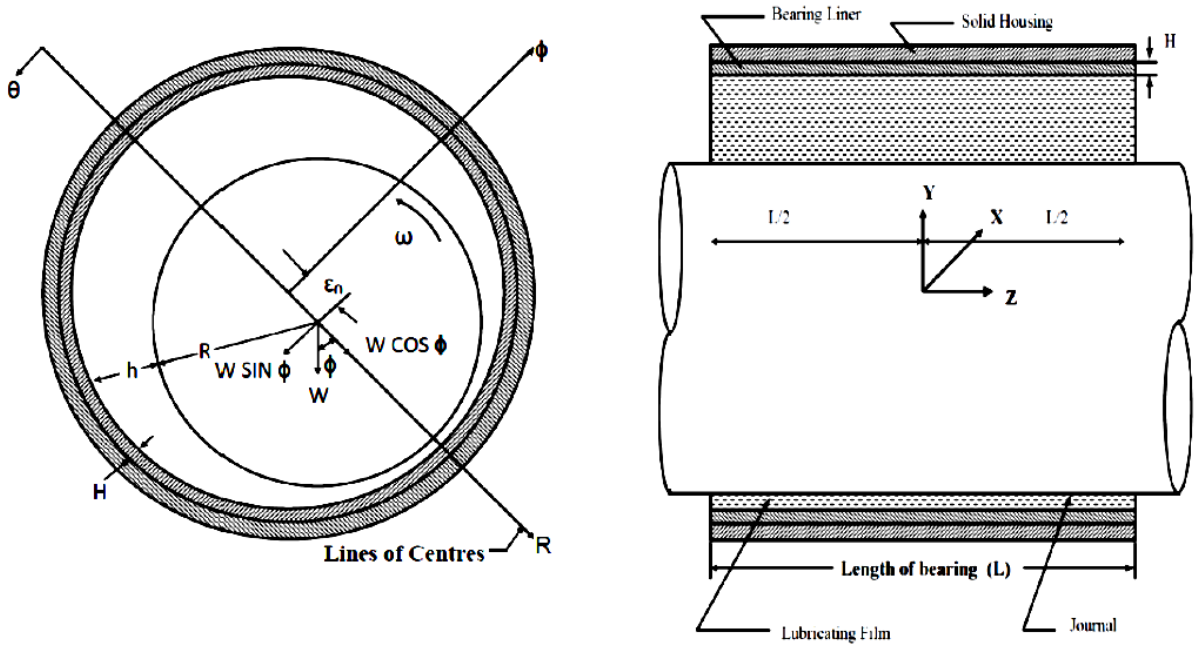

Figure 2.1 Schematic diagram of journal bearing with coordinate system for the derivation of Reynolds equation

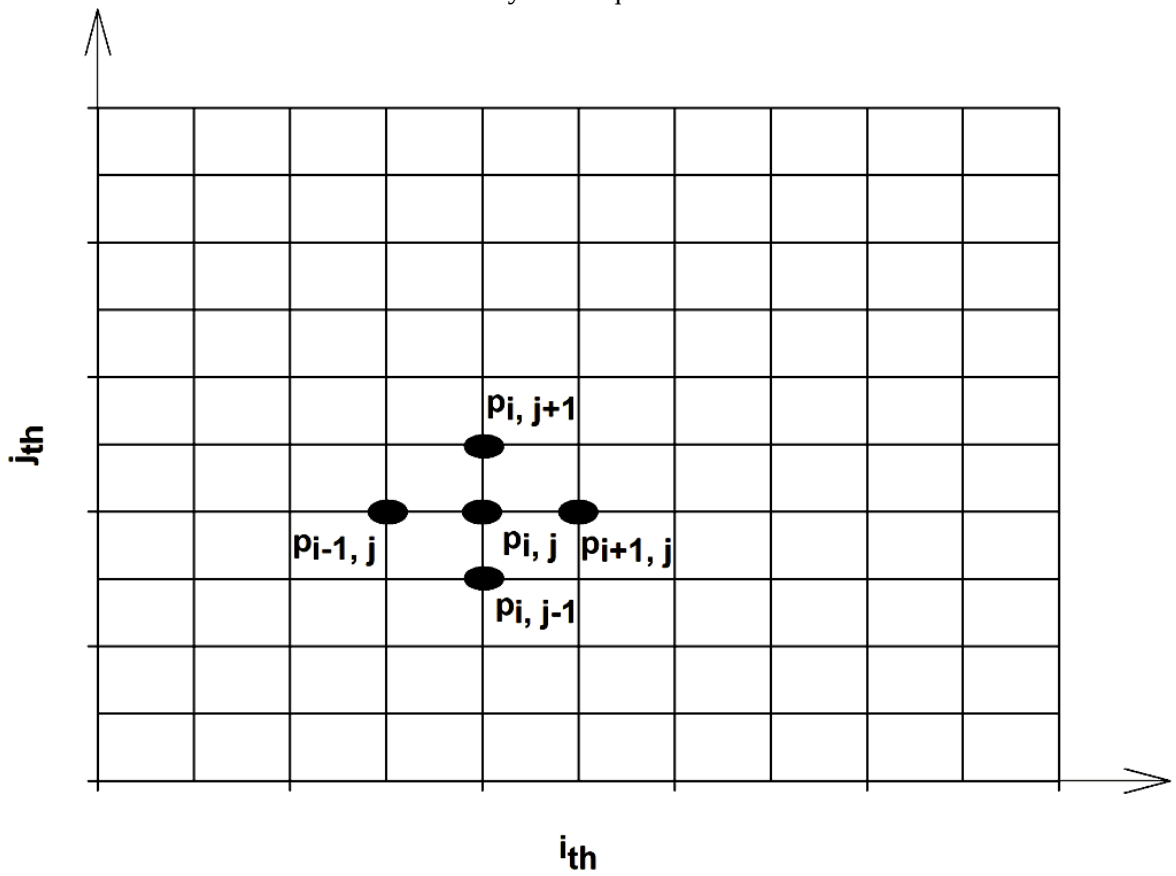

Figure 2.2 Grid used in the analysis for finite difference method

2.3.2 Directional flow equations

With above assumptions equation (2.1) reduces to

$$\left.\begin{aligned} \nabla.\boldsymbol{V} = 0 \\ i.e.\frac{\partial \boldsymbol{V}_X}{\partial x}+\frac{\partial \boldsymbol{V}_Y}{\partial y}+\frac{\partial \boldsymbol{V}_Z}{\partial z}=0 \end{aligned}\right\} \tag{2.6}$$

It can be considered that,

$$\nabla.\boldsymbol{v} = 0 \tag{2.7}$$

Explanation for equation (2.7) can be given following Tipei [127] as:

In case of flow in thin layers bounded by solid surfaces, as in lubrication problem, component of $\boldsymbol{v}$ perpendicular to boundaries becomes negligible with respect to other two components. Since derivatives with respect to normal *y*-direction are much larger than other derivatives, *i.e.*$\frac{\partial}{\partial x} \gg \frac{\partial}{\partial y}\ or\ \frac{\partial}{\partial z}$, hence $\nabla.(\nabla.\boldsymbol{v}) = \frac{\partial^2 \boldsymbol{v}_1}{\partial \mathrm{x}\,\partial \mathrm{y}} + \frac{\partial^2 \boldsymbol{v}_3}{\partial \mathrm{z}\,\partial \mathrm{y}}$ while other components are much smaller. Component of $(\nabla \times \boldsymbol{v})$ upon *y*-coordinate *i.e.* $\left[\frac{\partial \boldsymbol{v}_1}{\partial z} - \frac{\partial \boldsymbol{v}_3}{\partial x}\right]$ is also small and may be neglected and hence equation (2.3) as projected upon *y*-axis yields$\nabla(\nabla.\boldsymbol{v}) \approx 0$. This result can be obtained directly under usual approximations in lubrication theory **[145]** by considering$\nabla^2\boldsymbol{v} \gg \nabla(\nabla.\boldsymbol{v})$.

$$\nabla \times \nabla \times \boldsymbol{V} = \nabla(\nabla.\mathbf{V}) - \nabla^2\mathbf{V} \text{ and } \nabla \times \nabla \times \boldsymbol{v} = \nabla(\nabla.\boldsymbol{v}) - \nabla^2\boldsymbol{v} \tag{2.8}$$

With basic assumption and equation (2.8), equation (2.2) yields following three equations along x-, y- and z- direction respectively.

$$\frac{(2\mu+\chi)}{2}\left(\frac{\partial^2 V_X}{\partial x^2}+\frac{\partial^2 V_X}{\partial y^2}+\frac{\partial^2 V_X}{\partial z^2}\right)+\chi\left(\frac{\partial v_3}{\partial y}-\frac{\partial v_2}{\partial z}\right)-\frac{\partial p}{\partial x}=\rho\left(V_X\frac{\partial V_X}{\partial x}+V_Y\frac{\partial V_X}{\partial y}+V_Z\frac{\partial V_X}{\partial z}\right) \tag{2.9}$$

$$\frac{(2\mu+\chi)}{2}\left(\frac{\partial^2 V_Y}{\partial x^2}+\frac{\partial^2 V_Y}{\partial y^2}+\frac{\partial^2 V_Y}{\partial z^2}\right)+\chi\left(\frac{\partial v_1}{\partial y}-\frac{\partial v_3}{\partial z}\right)-\frac{\partial p}{\partial y}=\rho\left(V_X\frac{\partial V_Y}{\partial x}+V_Y\frac{\partial V_Y}{\partial y}+V_Z\frac{\partial V_Y}{\partial z}\right) \tag{2.10}$$

$$\frac{(2\mu+\chi)}{2}\left(\frac{\partial^2 V_Z}{\partial x^2}+\frac{\partial^2 V_Z}{\partial y^2}+\frac{\partial^2 V_Z}{\partial z^2}\right)+\chi\left(\frac{\partial v_2}{\partial y}-\frac{\partial v_1}{\partial z}\right)-\frac{\partial p}{\partial z}=\rho\left(V_X\frac{\partial V_Z}{\partial x}+V_Y\frac{\partial V_Z}{\partial y}+V_Z\frac{\partial V_Z}{\partial z}\right) \tag{2.11}$$

Similarly, with basic assumptions and equation (2.8), equation (2.3) yields following three equations along x-, y- and z- direction respectively.

$$\gamma\left(\frac{\partial^2 v_1}{\partial x^2}+\frac{\partial^2 v_1}{\partial y^2}+\frac{\partial^2 v_1}{\partial z^2}\right)+\chi\left(\frac{\partial V_X}{\partial y}-\frac{\partial V_Y}{\partial z}\right)-2\chi v_1=\rho j\left(V_X\frac{\partial v_1}{\partial x}+V_Y\frac{\partial v_1}{\partial y}+V_Z\frac{\partial v_1}{\partial z}\right) \tag{2.12}$$

$$\gamma\left(\frac{\partial^2 v_2}{\partial x^2}+\frac{\partial^2 v_2}{\partial y^2}+\frac{\partial^2 v_2}{\partial z^2}\right)+\chi\left(\frac{\partial V_X}{\partial z}-\frac{\partial V_Z}{\partial x}\right)-2\chi v_2=\rho j\left(V_X\frac{\partial v_2}{\partial x}+V_Y\frac{\partial v_2}{\partial y}+V_Z\frac{\partial v_2}{\partial z}\right) \tag{2.13}$$

$$\gamma\left(\frac{\partial^2 v_3}{\partial x^2}+\frac{\partial^2 v_3}{\partial y^2}+\frac{\partial^2 v_3}{\partial z^2}\right)+\chi\left(\frac{\partial V_Y}{\partial z}-\frac{\partial V_X}{\partial x}\right)-2\chi v_3=\rho j\left(V_X\frac{\partial v_3}{\partial x}+V_Y\frac{\partial v_3}{\partial y}+V_Z\frac{\partial v_3}{\partial z}\right) \tag{2.14}$$

2.3.3 Non-dimensional scheme

Equations (2.9) through (2.14) when non-dimensionalized with following substitutions

$$\left.\begin{gathered}\bar{x}=\frac{x}{R};\bar{y}=\frac{y}{C};z=\frac{z}{L/2};\ \delta_1=\frac{C}{R};\ \delta_2=\frac{C}{L/2};\delta_3=\frac{h_{min}}{R};\ \delta_4=\frac{L/2}{R};\\ \bar{V}_i=\frac{V_i}{U},\qquad \text{where i = x, y, z};\ \bar{v}_i=v_i\frac{C}{U},\qquad \text{where i = 1,2,3};\ \xi=\frac{h_{min}}{C};\\ \bar{p}=\frac{ph_{min}^2}{\left(\mu+\frac{\chi}{2}\right)UR};R_e=\frac{2\rho CU}{(2\mu+\chi)};R_R=\frac{\rho jUh}{2\mu\Lambda};N=\left(\frac{\chi}{2\mu+\chi}\right)^{1/2};\\ l_m=\frac{C}{\Lambda};L_R=\frac{h_{min}}{\Lambda};\ \text{where }\Lambda=\left(\frac{\gamma}{4\mu}\right)^{1/2}\text{ and is of dimension of length}\end{gathered}\right\} \tag{2.15}$$

following equations will result:

$$\left(\delta_1^2\frac{\partial^2\bar{V}_X}{\partial\bar{x}^2}+\frac{\partial^2\bar{V}_X}{\partial\bar{y}^2}+\delta_2^2\frac{\partial^2\bar{V}_X}{\partial\bar{z}^2}\right)+2N^2\left(\frac{\partial\bar{v}_3}{\partial\bar{y}}-\delta_2\frac{\partial\bar{v}_2}{\partial\bar{z}}\right)-\frac{1}{\xi^2}\frac{\partial\bar{p}}{\partial\bar{x}}=R_e\left(\delta_1\bar{V}_X\frac{\partial\bar{V}_X}{\partial\bar{x}}+\bar{V}_Y\frac{\partial\bar{V}_X}{\partial\bar{y}}+\delta_2\bar{V}_Z\frac{\partial\bar{V}_X}{\partial\bar{z}}\right) \tag{2.16}$$

$$\xi\delta_3\left(\delta_1^2\frac{\partial^2\bar{V}_Y}{\partial\bar{x}^2}+\frac{\partial^2\bar{V}_Y}{\partial\bar{y}^2}+\delta_2^2\frac{\partial^2\bar{V}_Y}{\partial\bar{z}^2}\right)+2\xi\delta_3N^2\left(\delta_2\frac{\partial\bar{v}_1}{\partial\bar{z}}-\delta_1\frac{\partial\bar{v}_3}{\partial\bar{x}}\right)-\frac{\partial\bar{p}}{\partial\bar{y}}=\xi\delta_3R_e\left(\delta_1\bar{V}_X\frac{\partial\bar{V}_Y}{\partial\bar{x}}+\bar{V}_Y\frac{\partial\bar{V}_Y}{\partial\bar{y}}+\delta_2\bar{V}_Z\frac{\partial\bar{V}_Y}{\partial\bar{z}}\right) \tag{2.17}$$

$$\xi^2\delta_4\left(\delta_1^2\frac{\partial^2\bar{V}_Z}{\partial\bar{x}^2}+\frac{\partial^2\bar{V}_Z}{\partial\bar{y}^2}+\delta_2^2\frac{\partial^2\bar{V}_Z}{\partial\bar{z}^2}\right)+2\xi^2\delta_4N^2\left(\delta_1\frac{\partial\bar{v}_2}{\partial\bar{x}}-\delta_1\frac{\partial\bar{v}_1}{\partial\bar{y}}\right)-\frac{\partial\bar{p}}{\partial\bar{z}}=\xi^2\delta_4R_e\left(\delta_1\bar{V}_X\frac{\partial\bar{V}_Z}{\partial\bar{x}}+\bar{V}_Y\frac{\partial\bar{V}_Z}{\partial\bar{y}}+\delta_2\bar{V}_Z\frac{\partial\bar{V}_Z}{\partial\bar{z}}\right) \tag{2.18}$$

$$\left(\delta_1^2\frac{\partial^2\bar{v}_1}{\partial\bar{x}^2}+\frac{\partial^2\bar{v}_1}{\partial\bar{y}^2}+\delta_2^2\frac{\partial^2\bar{v}_1}{\partial\bar{z}^2}\right)+\frac{N^2L_R^2}{2(1-N^2)\xi^2}\left(\frac{\partial\bar{V}_Z}{\partial\bar{y}}-\delta_2\frac{\partial\bar{V}_y}{\partial\bar{z}}\right)-\frac{N^2L_R^2}{(1-N^2)\xi^2}\bar{v}_1=R_R\left(\delta_1\bar{V}_X\frac{\partial\bar{v}_1}{\partial\bar{x}}+\bar{V}_Y\frac{\partial\bar{v}_1}{\partial\bar{y}}+\delta_2\bar{V}_Z\frac{\partial\bar{v}_1}{\partial\bar{z}}\right) \tag{2.19}$$

$$\left(\delta_1^2\frac{\partial^2\bar{v}_2}{\partial\bar{x}^2}+\frac{\partial^2\bar{v}_2}{\partial\bar{y}^2}+\delta_2^2\frac{\partial^2\bar{v}_2}{\partial\bar{z}^2}\right)+\frac{N^2L_R^2}{2(1-N^2)\xi^2}\left(\delta_2\frac{\partial\bar{V}_X}{\partial\bar{y}}-\delta_1\frac{\partial\bar{V}_Z}{\partial\bar{x}}\right)-\frac{N^2L_R^2}{(1-N^2)\xi^2}\bar{v}_2=R_R\left(\delta_1\bar{V}_X\frac{\partial\bar{v}_2}{\partial\bar{x}}+\bar{V}_Y\frac{\partial\bar{v}_2}{\partial\bar{y}}+\delta_2\bar{V}_Z\frac{\partial\bar{v}_2}{\partial\bar{z}}\right) \tag{2.20}$$

$$\left(\delta_1^2\frac{\partial^2\bar{v}_3}{\partial\bar{x}^2}+\frac{\partial^2\bar{v}_3}{\partial\bar{y}^2}+\delta_2^2\frac{\partial^2\bar{v}_3}{\partial\bar{z}^2}\right)+\frac{N^2L_R^2}{2(1-N^2)\xi^2}\left(\delta_1\frac{\partial\bar{V}_Y}{\partial\bar{x}}-\delta_1\frac{\partial\bar{V}_X}{\partial\bar{y}}\right)-\frac{N^2L_R^2}{(1-N^2)\xi^2}\,\bar{v}_3 = R_R\left(\delta_1\bar{V}_X\frac{\partial\bar{v}_3}{\partial\bar{x}}+\bar{V}_Y\frac{\partial\bar{v}_3}{\partial\bar{y}}+\delta_2\bar{V}_Z\frac{\partial\bar{v}_3}{\partial\bar{z}}\right) \quad (2.21)$$

2.3.4 Study of non-dimensional parameters

In this section interpretations of non-dimensional parameters are given briefly. As current analysis is aimed at showing micropolar effects on hydrodynamic journal bearings, separate importance is given in discussion of micropolar properties at end of this section.

- **Micropolar parameters**

  N and Λ are two parameters which characterize micropolar fluids. They distinguish micropolar fluids from Newtonian fluids. N is non-dimensional parameter called *coupling number*. N couples linear and angular momentum equations arising out of microrotational effect of suspended particles in fluid. Λ, dimensional parameter represents interaction between micropolar fluid and film gap. Λ is termed as *characteristic length* of micropolar fluid and has dimension of length. l_m is non-dimensional quantity and is known as *non-dimensional characteristic length* of micropolar fluid. For χ = 0, N = 0 equations representing linear and angular momentums are uncoupled. This reduces equation (2.2) to that of classical Navier-Stokes equation. On other hand strong micropolar effect is exhibited with increase in value of Λ or decrease in clearance in between journal and bearing *i.e.* when non-dimensional characteristic length l_m decreases. Second case is most likely here as C is usually very small in lubrication theory. Hence for $N \to 0$ or for $l_m \to 0$, micropolar characteristic is lost.

- **Other non-dimensional parameters and order analysis**

  L_R, a non-dimensional quantity, may be termed as *length ratio*. During initial stage of application of micropolar theory to lubrication flow problems, researchers**[105, 127]** used either NL_R or Nl_m as parameter in discussing micropolar fluid; but as these products characterize combinational effects, later N and l_m were considered separately to study their effects as can be found in **Prakash** and **Sinha[119]**. R_e may be considered as *modified Reynolds number*. R_e is always less than classical Reynolds number. Generally for lubrication problem, $R_e << 1$. It is usually of order of 10^{-3}. μ is

replaced by effective viscosity, μ_e, *i.e.* $\left(\mu + \frac{1}{2}\chi\right)$. As *j* is square of a length typically of microstructure as discussed earlier, it is reasonable to consider $R_R << 1$. Also with assumptions that δ_1, δ_2 and δ_3 are of order of 10^{-3} and δ_4, ξ, L_R are of order of 1, equations (2.16) to (2.21) will reduce to

$$\frac{\partial^2 \bar{V}_X}{\partial \bar{y}^2} + 2N^2 \frac{\partial \bar{v}_3}{\partial \bar{y}} - \frac{1}{\xi^2}\frac{\partial \bar{p}}{\partial \bar{x}} = 0 \tag{2.22}$$

$$\frac{\partial \bar{p}}{\partial \bar{y}} = 0 \tag{2.23}$$

$$\frac{\partial^2 \bar{V}_Z}{\partial \bar{y}^2} - 2N^2 \frac{\partial \bar{v}_1}{\partial \bar{y}} - \frac{1}{\xi^2 \delta_4}\frac{\partial \bar{p}}{\partial \bar{z}} = 0 \tag{2.24}$$

$$\frac{\partial^2 \bar{v}_1}{\partial \bar{y}^2} + \frac{N^2 L_R^2}{2(1-N^2)\xi^2}\frac{\partial \bar{V}_z}{\partial \bar{y}} - \frac{N^2 L_R^2}{(1-N^2)\xi^2}\bar{v}_1 = 0 \tag{2.25}$$

$$\frac{\partial^2 \bar{v}_2}{\partial \bar{y}^2} - \frac{N^2 L_R^2}{(1-N^2)\xi^2}\bar{v}_2 = 0 \tag{2.26}$$

$$\frac{\partial^2 \bar{v}_3}{\partial \bar{y}^2} - \frac{N^2 L_R^2}{2(1-N^2)\xi^2}\frac{\partial \bar{V}_X}{\partial \bar{y}} - \frac{N^2 L_R^2}{(1-N^2)\xi^2}\bar{v}_3 = 0 \tag{2.27}$$

2.3.5 Velocity and microrotational velocity vectors

Now to solve velocity components and microrotational velocity components equations (2.22) through (2.27) are returned to their dimensional forms as follows:

$$\frac{(2\mu + \chi)}{2}\frac{\partial^2 V_X}{\partial y^2} + \chi \frac{\partial v_3}{\partial y} - \frac{\partial p}{\partial x} = 0 \tag{2.28}$$

$$\frac{\partial p}{\partial y} = 0 \tag{2.29}$$

$$\frac{(2\mu + \chi)}{2}\frac{\partial^2 V_Z}{\partial y^2} + \chi \frac{\partial v_1}{\partial y} - \frac{\partial p}{\partial z} = 0 \tag{2.30}$$

$$\gamma \frac{\partial^2 v_1}{\partial y^2} + \chi \frac{\partial V_Z}{\partial y} - 2\chi v_1 = 0 \tag{2.31}$$

$$\gamma \frac{\partial^2 v_2}{\partial y^2} - 2\chi v_2 = 0 \tag{2.32}$$

$$\gamma \frac{\partial^2 v_3}{\partial y^2} + \chi \frac{\partial V_X}{\partial y} - 2\chi v_3 = 0 \tag{2.33}$$

As x = Rθ, equation (2.28) reduces to

$$\frac{(2\mu+\chi)}{2}\frac{\partial^2 V_X}{\partial y^2}+\chi\frac{\partial v_3}{\partial y}-\frac{1}{R}\frac{\partial p}{\partial \theta}=0 \tag{2.34}$$

Solving equations (2.30) and (2.31) expressions for v_1 and V_Z are evaluated as follows

$$v_1 = A_1 + A_2 e^{ay} + A_3 e^{-ay} + \left(\frac{1}{2\mu}\frac{\partial p}{\partial z}\right) y \tag{2.35}$$

$$V_Z = 2A_1 y + 2A_2\frac{N^2}{a}e^{ay} - 2A_3\frac{N^2}{a}e^{-ay} + A_4 + \left(\frac{1}{2\mu}\frac{\partial p}{\partial z}\right) y^2 \tag{2.36}$$

Where A_1, A_2, A_3, and A_4 are four constants to be evaluated from boundary conditions and a is non-dimensional quantity given by, $a = \frac{N}{\Lambda} = \sqrt{\frac{4\mu N^2}{\gamma}}$

Boundary conditions for v_1 and V_Z are:

(i) At y=0 v_1=0 and V_Z=0

(ii) At y=h v_1=0 and V_Z=0

Using above boundary conditions in equations (2.35) and (2.36) A_1, A_2, A_3, and A_4 are evolved as

$$\left.\begin{aligned} A_1 &= -\frac{h}{4\mu}\frac{\partial p}{\partial z}; & A_2 &= -\frac{h}{4\mu}\frac{\partial p}{\partial z}\frac{1}{(e^{ah}-1)};\\ A_3 &= \frac{h}{4\mu}\frac{\partial p}{\partial z}\frac{1}{(1-e^{-ah})}; & A_4 &= \frac{h\,N^2}{2\mu a}\frac{\partial p}{\partial z}\frac{(1+e^{-ah})}{(1-e^{-ah})}; \end{aligned}\right\} \tag{2.38}$$

With substitutions of A_1, A_2, A_3, and A_4 expressions for v_1 and V_Z become

$$v_1 = \frac{h}{4\mu}(\sinh ay)\left\{\frac{(\cosh ay-1)}{\sinh ay}-\frac{(\cosh ah+1)}{\sinh ah}\right\}\frac{\partial p}{\partial z}+\frac{y}{2\mu}\frac{\partial p}{\partial z} \tag{2.39}$$

$$V_Z = \frac{y(y-h)}{2\mu}\frac{\partial p}{\partial z}+\frac{h}{2\mu}\frac{N^2}{a}\left\{\sinh ay-\frac{(\cosh ay-1)(\cosh ah+1)}{\sinh ah}\right\}\frac{\partial p}{\partial z} \tag{2.40}$$

Similarly, solving equations (2.33) and (2.34) with following boundary conditions

(i) At y = 0 v_3 = 0 and V_X = 0

(ii) At y = h v_3 = 0 and V_X = U

(2.41)

Following equations will result:

$$v_3 = -\frac{h}{4\mu R}(\sinh ay)\left\{\frac{(\cosh ay-1)}{\sinh ay}-\frac{(\cosh ah+1)}{\sinh ah}\right\}\frac{\partial p}{\partial \theta}-\frac{y}{2\mu R}\frac{\partial p}{\partial \theta}$$

$$+\frac{U}{2\left[\frac{2N^2}{a}-h\frac{(\cosh ah+1)}{\sinh ah}\right]}\left\{\sinh ay-\frac{(\cosh ay-1)(\cosh ah+1)}{\sinh ah}\right\}\frac{\partial p}{\partial \theta}$$

(2.42)

$$V_X=\frac{y(y-h)}{2\mu R}\frac{\partial p}{\partial \theta}+\frac{h}{2\mu R}\frac{N^2}{a}\left\{\sinh ay-\frac{(\cosh ay-1)(\cosh ah-1)}{\sinh ah}\right\}\frac{\partial p}{\partial \theta}$$
$$-\frac{U}{2\left[\frac{2N^2}{a}-h\frac{(\cosh ah+1)}{\sinh ah}\right]}\left[\frac{2y(\cosh ah+1)}{\sinh ah}\right.$$
$$\left.+\frac{2N^2}{a}(\sinh ay)\left\{\frac{(\cosh ay-1)}{\sinh ay}-\frac{(\cosh ah-1)}{\sinh ah}\right\}\right]$$

(2.43)

Now, from principle of conservation of mass as stated in equation (2.1) it follows that

$$\frac{\partial(\rho V_Y)}{\partial y}=\frac{\partial \rho}{\partial t}-\frac{\partial(\rho V_X)}{\partial x}-\frac{\partial(\rho V_Z)}{\partial z}$$

(2.44)

Integrating both sides with respect to y within limit 0 and h, equation (2.43) becomes:

$$\rho(V_h-V_0)=-\int_0^h\frac{\partial \rho}{\partial t}dy-\int_0^h\frac{\partial(\rho V_X)}{\partial x}dy-\int_0^h\frac{\partial(\rho V_Z)}{\partial z}dy$$

(2.45)

Where, $\left(V_y\right)_{y=h}=V_h$ and $\left(V_y\right)_{y=0}=V_0$

As upper limit h is function of coordinates x,z integration before differentiation can be performed by using leibnitz's rule and using boundary conditions that

(i) At y = 0 $V_X = 0$ and $V_Z = 0$
(ii) At y = h V_X = U and $V_Z = 0$

(2.46)

And noting that $Vh = U\frac{\partial h}{\partial x}+\frac{\partial h}{\partial t}$ and $V_0 = 0$, following equation will result:

$$\frac{\partial}{\partial x}\left[\frac{\rho h}{12\mu}\left\{h^2+12\Lambda^2-6\mathrm{N}\Lambda h\coth\frac{\mathrm{Nh}}{2\Lambda}\right\}\frac{\partial p}{\partial x}\right]+\frac{\partial}{\partial z}\left[\frac{\rho h}{12\mu}\left\{h^2+12\Lambda^2-6\mathrm{N}\Lambda h\coth\frac{\mathrm{Nh}}{2\Lambda}\right\}\frac{\partial p}{\partial z}\right]$$
$$=\frac{\partial}{\partial x}\left(\frac{\rho U h}{2}\right)+\frac{\partial(\rho h)}{\partial t}$$

(2.47)

For incompressible fluid flow equation (2.47) reduces to give Reynolds equation for incompressible fluid flow in micropolar lubrication:

$$\frac{\partial}{\partial x}\left[\frac{h^3}{\mu}\boldsymbol{\Phi}(\Lambda,N,h)\frac{\partial p}{\partial x}\right]+\frac{\partial}{\partial z}\left[\frac{h^3}{\mu}\boldsymbol{\Phi}(\Lambda,N,h)\frac{\partial p}{\partial z}\right]=6\frac{\partial(Uh)}{\partial x}+12\frac{\partial h}{\partial t}$$

(2.48)

$$\boldsymbol{\Phi}(\Lambda,N,h)=\left\{1+12\frac{\Lambda^2}{h^2}-6\frac{N\Lambda}{h}\coth\frac{Nh}{2\Lambda}\right\}$$

(2.49)

Introducing rotating coordinate system and considering that journal center is rotating at angular velocity ω_p, equation (2.48) becomes [142]:

$$\frac{\partial}{\partial x}\left[\frac{h^3}{\mu}\mathbf{\Phi}(\Lambda, N, h)\frac{\partial p}{\partial x}\right] + \frac{\partial}{\partial z}\left[\frac{h^3}{\mu}\mathbf{\Phi}(\Lambda, N, h)\frac{\partial p}{\partial z}\right] = 6U\frac{\partial h}{\partial x} + 12\frac{\partial h}{\partial t} - 12\omega_p\frac{\partial h}{\partial \theta} \tag{2.50}$$

Equation (2.50) represents modified Reynolds equation for micropolar lubrication.

Chapter 3 Steady State Analysis of Finite Flexible Oil Journal Bearings with Micropolar Fluids

3.1. Introduction

Steady state analysis of bearings under micropolar lubrication has been discussed by many researchers. Prakash and Sinha[119] conducted steady state analysis of infinitely long journal bearing considering 2-D flow field. Huang *et al.* [131], Khonsari and Brewe [132] conducted steady state analysis of journal bearing considering incompressible micropolar lubricant. Authors have reported [20-33] that effect of deformation of liner can't be neglected while design of bearings. But, all these studies have taken Newtonian fluids as lubricant. Combined effect of deformation of liner and micropolar parameters is not reported in literature. This motivated the authors to work in this field.

This chapter deals with theoretical analysis of steady state characteristics of hydrodynamic journal bearings taking into consideration effect of elasticity of bearing liner and assuming micropolar fluids as lubricants. Deformation equations for bearing surface are solved simultaneously with modified Reynolds equation to theoretically predict fluid film pressure distribution.

3.2 Theoretical analysis

Figure 3.1 shows schematically journal bearing of length 'L' and diameter 'D' consisting of bearing liner of wall thickness 'H' surrounded by a relatively rigid housing rotating with angular velocity 'ω' and uniform tangential velocity 'U' within bearing liner, force fitted in solid metal sleeve.

Modified Reynolds equation derived in section 2.3.5 equation (2.50) for steady state conditions is reduced to

$$\frac{\partial}{\partial x}\left[\frac{h_0^3}{\mu}\boldsymbol{\Phi}(\Lambda,N,h_0)\frac{\partial p_0}{\partial x}\right]+\frac{\partial}{\partial z}\left[\frac{h_0^3}{\mu}\boldsymbol{\Phi}(\Lambda,N,h_0)\frac{\partial p_0}{\partial z}\right]=6\frac{\partial h_0}{\partial x}$$

$$\boldsymbol{\Phi}(\Lambda,N,h)=\left\{1+12\frac{\Lambda^2}{h^2}-6\frac{N\Lambda}{h}\coth\frac{Nh}{2\Lambda}\right\},\Lambda=\left(\frac{\gamma}{4\mu}\right)^{1/2},N=\left(\frac{\chi}{2\mu+\chi}\right)^{1/2} \tag{3.1}$$

Equation 3.1 when non-dimensionalised with following substitutions,

$$\theta = \frac{x}{R}, \bar{z} = \frac{2z}{L}, \bar{h}_0 = \frac{h_0}{C}, \bar{p}_0 = \frac{p_0 C^2}{\mu \omega R^2}, l_m = \frac{C}{\Lambda}$$

following equation is obtained in non-dimensional form:

$$\frac{\partial}{\partial \theta}\left[\bar{g}\left(l_m, N, \bar{h}_0\right)\frac{\partial \bar{p}_0}{\partial \theta}\right] + \left(\frac{D}{L}\right)^2 \frac{\partial}{\partial \bar{z}}\left[\bar{g}\left(l_m, N, \bar{h}_0\right)\frac{\partial \bar{p}_0}{\partial \bar{z}}\right] = \frac{1}{2}\frac{\partial \bar{h}_0}{\partial \theta}$$
$$\bar{g}\left(l_m, N, \bar{h}_0\right) = \frac{\bar{h}_0^3}{12} + \frac{\bar{h}_0}{l_m^2} - \frac{N\bar{h}_0^2}{2l_m}\coth\frac{Nl_m\bar{h}_0}{2} \quad (3.2)$$

Boundary conditions for equation (3.2) are as follows:

1. Steady state pressures at ends of bearing are zero.

$$\bar{p}_0(\theta, \pm 1) = 0$$

2. Pressure distribution is symmetrical about mid-plane for steady state pressures of bearing.

$$\frac{\partial \bar{p}_0(\theta, 0)}{\partial \bar{z}} = 0$$

3. Cavitation boundary conditions:

$$\bar{p}_0(\theta_2, \bar{z}) = \frac{\partial \bar{p}_0(\theta_2, 0)}{\partial \bar{z}} = 0$$
$$\bar{p}_0(\theta, \bar{z}) = 0, \text{for } \theta_2 \le \theta \le \theta_1$$

Where θ_1 and θ_2 represents angles at end and start of hydrodynamic film at each axial plane of bearing. During computation all negative pressure are set to be zero in order to implement Reynolds cavitation boundary conditions.

4. Periodic boundary conditions

$$\bar{p}_0(\theta, \bar{z}) = \bar{p}_0(\theta + 2\pi, \bar{z})$$

Steady state fluid film thickness, h_0, for flexible bearing can be written as,

$$h_0 = C + e_0 \cos\theta + \delta_0 \quad (3.3)$$

δ_0 is steady state radial deformation of bearing liner surface. δ_0 dependant on both θ and z. Equation (3.3) when non-dimensionalised with following substitutions,

$$\bar{h}_0 = \frac{h_0}{C}, \varepsilon_0 = \frac{e_0}{C} \; and \; \bar{\delta}_0 = \frac{\delta_0}{C}$$
$$\bar{h}_0 = 1 + \varepsilon_0 \cos\theta + \bar{\delta}_0 \quad (3.4)$$

Non-dimensional steady state pressure distribution for flexible bearing is calculated by solving 2-D steady state modified Reynolds equation (3.2) assuming bearing to be rigid.

This pressure distribution is then expressed as double Fourier series as expressed in equation (A 1.13) of appendix-I.

$$\bar{p} = \frac{\bar{p}_{0,0}}{2} + \sum_{\substack{m=0 \\ (m,n) \neq (0,0)}}^{\infty} \sum_{n=0}^{\infty} \bar{p}_{m,n} \cos\left(\frac{2m\pi\bar{z}}{L}\right) \cos\left(n\theta + \beta_{m,n}\right) \tag{3.5}$$

Values of $\bar{p}_{m,n}, \beta_{m,n}$ and $\bar{p}_{0,0}$ can be obtained from relations (appendix) of appendix-I.

Now, in order to calculate steady state radial deformation this steady state non-dimensional pressure distribution is put in relations (A 1.10, A1.11 and A1.12). $\bar{p}_{m,n}$ and $\beta_{m,n}$ are calculated by applying Simpson's 1/3rd rule. Displacement components in r, θ and z directions, represented in form of harmonic functions are found from $\bar{p}_{m,n}$ and $\beta_{m,n}$. These displacement components are used to get six components of stress, which are substituted in three basic equations of equilibrium from fundamentals of elasticity. These equilibrium equations (A 2.21, A 2.22 and A 2.23) satisfying boundary conditions (A 2.24, A 2.25, A 2.26 and A2.27) are solved for unit pressure by FDM with a successive over relaxation (SOR) factor to get displacement components.

Displacement components in r, θ and z directions are found from pressure distribution, which has been expressed as Fourier series. Displacement components are expressed in displacement equations (appendix) of appendix-II and boundary conditions are given in equations (A 2.24) through (A 2.27) of appendix-II. These displacement components are used to calculate six components of stress as given by stress displacement relationships given by equations (2.4) through (2.9) of appendix-II. Then these six components of stress are used in equilibrium equations to obtain three displacement equations (A 2.10) through (A 2.12). These displacement equations are solved for unit pressure, μ and values of distortion coefficient $d_{m,n}$ are obtained from relation (A 2.62) of appendix-II and are stored in computer memory. Radial deformation $\bar{\delta}_0$ of bearing surface at any (θ, $\bar{z}$) is computed with help of equation (A 2.63) and using relation (A 1.10), (A 1.11) and (A 1.12) with $d_{m,n}$ and is given by,

$$\bar{\delta}_0 = 2(1+\nu)F\left[\bar{p}_{0,0}d_{0,0} + \sum_{m=0}^{\infty}\sum_{n=0}^{\infty} \bar{p}_{m,n}d_{m,n}\cos(m\pi\bar{z})\cos\left(n\theta + \beta_{m,n}\right)\right] \tag{3.6}$$

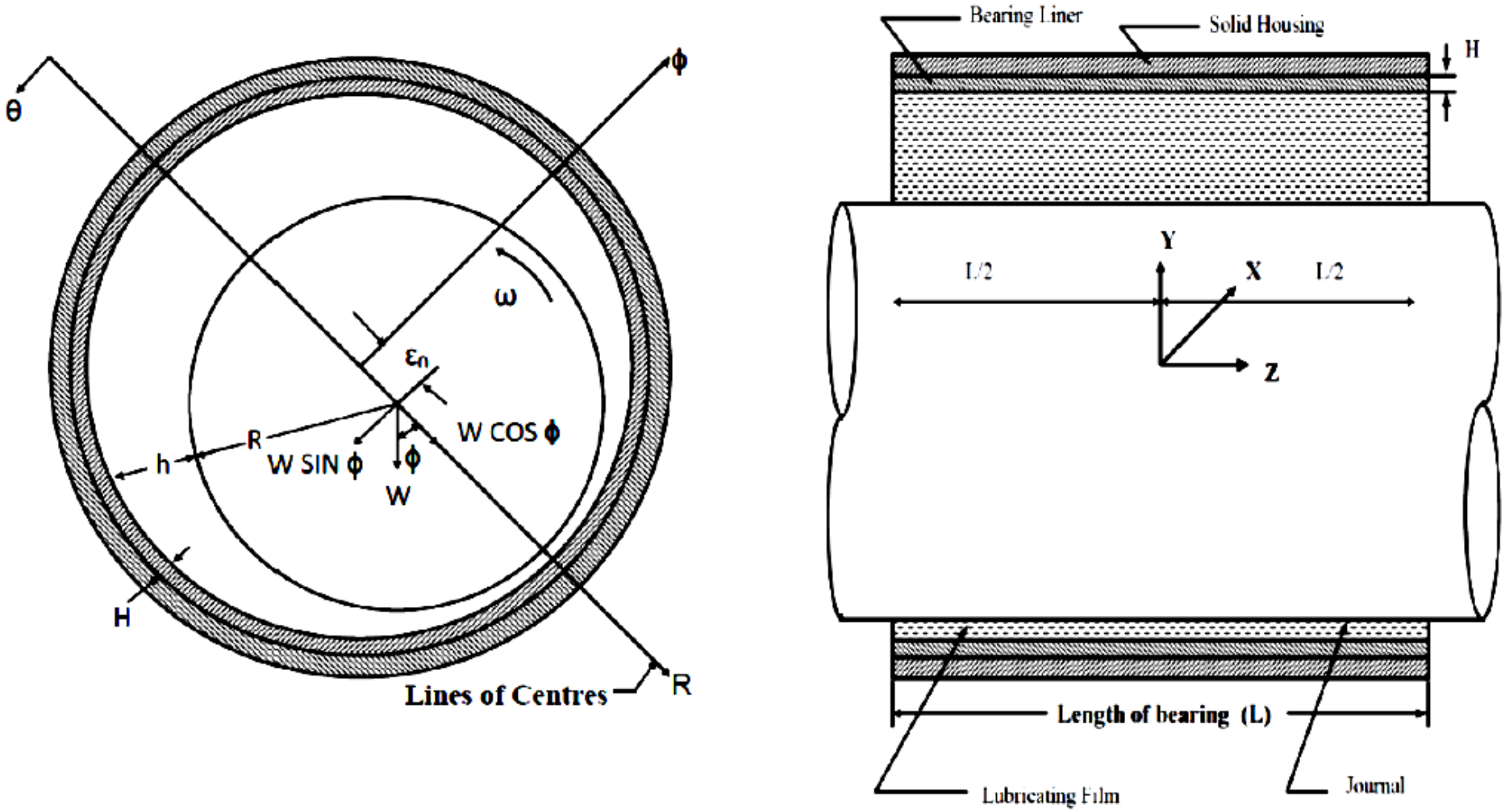

Figure 3.1 Schematic diagram of journal bearing with coordinate system used in analysis.

3.3 Method of solution

Modified Reynolds equation (3.2) is solved considering boundary conditions to get steady state pressure. Modified Reynolds equation (3.2) is solved using FDM approach and numerical solution is obtained by using SOR scheme. Orthogonal grid is used in analysis as variation of pressure across film is negligible. In this representation grid point is designated as (i, j) where i and j represent coordinates along x(θ) and z($\bar{z}$) directions respectively.

Expanding equation (3.2) we get

$$C_B\left[\frac{\partial^2\bar{p}_0}{\partial\theta^2}+\left(\frac{D}{L}\right)^2\frac{\partial^2\bar{p}_0}{\partial\bar{z}^2}\right]+C_A\left[\frac{\partial\bar{h}_0}{\partial\theta}\frac{\partial\bar{p}_0}{\partial\theta}+\left(\frac{D}{L}\right)^2\frac{\partial\bar{h}_0}{\partial\bar{z}}\frac{\partial\bar{p}_0}{\partial\bar{z}}\right]=\frac{1}{2}\frac{\partial\bar{h}_0}{\partial\theta} \tag{3.7}$$

$$\left.\begin{aligned} C_A &= \frac{\bar{h}_0^2}{4}+\frac{1}{l_m^2}-\frac{N\bar{h}_0}{l_m}\coth\left(\frac{Nl_m\bar{h}_0}{2}\right)+\frac{N^2h_0^2}{4}\operatorname{cosech}^2\left(\frac{Nl_m\bar{h}_0}{2}\right)\\ C_B &= \frac{\bar{h}_0^3}{12}+\frac{\bar{h}_0}{l_m^2}-\frac{N\bar{h}_0^2}{2l_m}\coth\left(\frac{Nl_m\bar{h}_0}{2}\right)\end{aligned}\right\} \tag{3.8}$$

Since $\bar{\delta}_0$ is dependent on both θ and z. $\bar{h}_0$ will be dependent on both θ and z. Differentiating equation 3.4 with respect to θ and z we get,

$$\frac{\partial\bar{h}_0}{\partial\theta}=-\varepsilon_0\sin\theta+\frac{\partial\bar{\delta}_0}{\partial\theta}$$

$$\frac{\partial\bar{h}_0}{\partial\bar{z}}=\frac{\partial\bar{\delta}_0}{\partial\bar{z}}$$

Substituting above relation into equation (3.7) we get,

$$C_B\left[\frac{\partial^2\bar{p}_0}{\partial\theta^2}+\left(\frac{D}{L}\right)^2\frac{\partial^2\bar{p}_0}{\partial\bar{z}^2}\right]-C_A\varepsilon_0\sin\theta\frac{\partial\bar{p}_0}{\partial\theta}+C_A\frac{\partial\bar{\delta}_0}{\partial\theta}\frac{\partial\bar{p}_0}{\partial\theta}+C_A\left(\frac{D}{L}\right)^2\frac{\partial\bar{\delta}_0}{\partial\bar{z}}\frac{\partial\bar{p}_0}{\partial\bar{z}}$$
$$=\frac{1}{2}\frac{\partial\bar{\delta}_0}{\partial\theta}-\frac{1}{2}\varepsilon_0\sin\theta \tag{3.9}$$

Equation (3.8) is then written in finite difference form. Second order and first order derivatives of pressure are approximated by central differences as:

$$\frac{\partial^2\bar{p}_0}{\partial\theta^2}=\frac{(\bar{p}_0)_{i+1,j}-2(\bar{p}_0)_{i,j}+(\bar{p}_0)_{i-1,j}}{(\Delta\theta)^2}$$

$$\frac{\partial^2\bar{p}_0}{\partial\bar{z}^2}=\frac{(\bar{p}_0)_{i,j+1}-2(\bar{p}_0)_{i,j}+(\bar{p}_0)_{i,j-1}}{(\Delta\bar{z})^2}$$

$$\frac{\partial \bar{p}_0}{\partial \theta} = \frac{(\bar{p}_0)_{i+1,j} - (\bar{p}_0)_{i-1,j}}{2(\Delta\theta)}$$
$$\frac{\partial \bar{p}_0}{\partial \bar{z}} = \frac{(\bar{p}_0)_{i,j+1} - (\bar{p}_0)_{i,j-1}}{2(\Delta\bar{z})}$$
$$\frac{\partial \bar{\delta}_0}{\partial \theta} = \frac{(\bar{\delta}_0)_{i+1,j} - (\bar{\delta}_0)_{i-1,j}}{2(\Delta\theta)}$$
$$\frac{\partial \bar{\delta}_0}{\partial \bar{z}} = \frac{(\bar{\delta}_0)_{i,j+1} - (\bar{\delta}_0)_{i,j-1}}{2(\Delta\bar{z})}$$

Using above representations equation (3.7) can be expressed in finite difference form as:

$$(\bar{p}_0)_{i,j} = C_1(\bar{p}_0)_{i+1,j} + C_2(\bar{p}_0)_{i-1,j} + C_3(\bar{p}_0)_{i,j+1} + C_4(\bar{p}_0)_{i,j-1} + C_n \tag{3.10}$$

$$\left.\begin{aligned}
Z_1 &= (\bar{\delta}_0)_{i+1,j} - (\bar{\delta}_0)_{i-1,j} \\
Z_2 &= (\bar{\delta}_0)_{i,j+1} - (\bar{\delta}_0)_{i,j-1} \\
C_0 &= 2\left[1 + \left(\frac{D}{L}\right)^2 \left(\frac{\Delta\theta}{\Delta\bar{z}}\right)^2\right] \\
C_1 &= \frac{1}{C_0}\left[1 - \frac{(C_A)_{i,j}}{2(C_B)_{i,j}}\varepsilon_0(\Delta\theta)\sin\theta_i + \frac{(C_A)_{i,j}}{4(C_B)_{i,j}}Z_1\right] \\
C_2 &= \frac{1}{C_0}\left[1 + \frac{(C_A)_{i,j}}{2(C_B)_{i,j}}\varepsilon_0(\Delta\theta)\sin\theta_i - \frac{(C_A)_{i,j}}{4(C_B)_{i,j}}Z_1\right] \\
C_3 &= \frac{1}{C_0}\left(\frac{D}{L}\right)^2 \left(\frac{\Delta\theta}{\Delta\bar{z}}\right)^2 \left[1 + \frac{(C_A)_{i,j}}{4(C_B)_{i,j}}Z_2\right] \\
C_4 &= \frac{1}{C_0}\left(\frac{D}{L}\right)^2 \left(\frac{\Delta\theta}{\Delta\bar{z}}\right)^2 \left[1 - \frac{(C_A)_{i,j}}{4(C_B)_{i,j}}Z_2\right] \\
C_n &= \left[\frac{1}{2C_0(C_B)_{i,j}}\varepsilon_0(\Delta\theta)^2\sin\theta_i - \frac{\Delta\theta}{4C_0(C_B)_{i,j}}Z_1\right]
\end{aligned}\right\} \tag{3.11}$$

Where $(C_A)_{i,j}$ and $(C_B)_{i,j}$ are calculated by equation (3.8), in which $\bar{h}_0$ is calculated for each θ_i and $\bar{z}_j$.

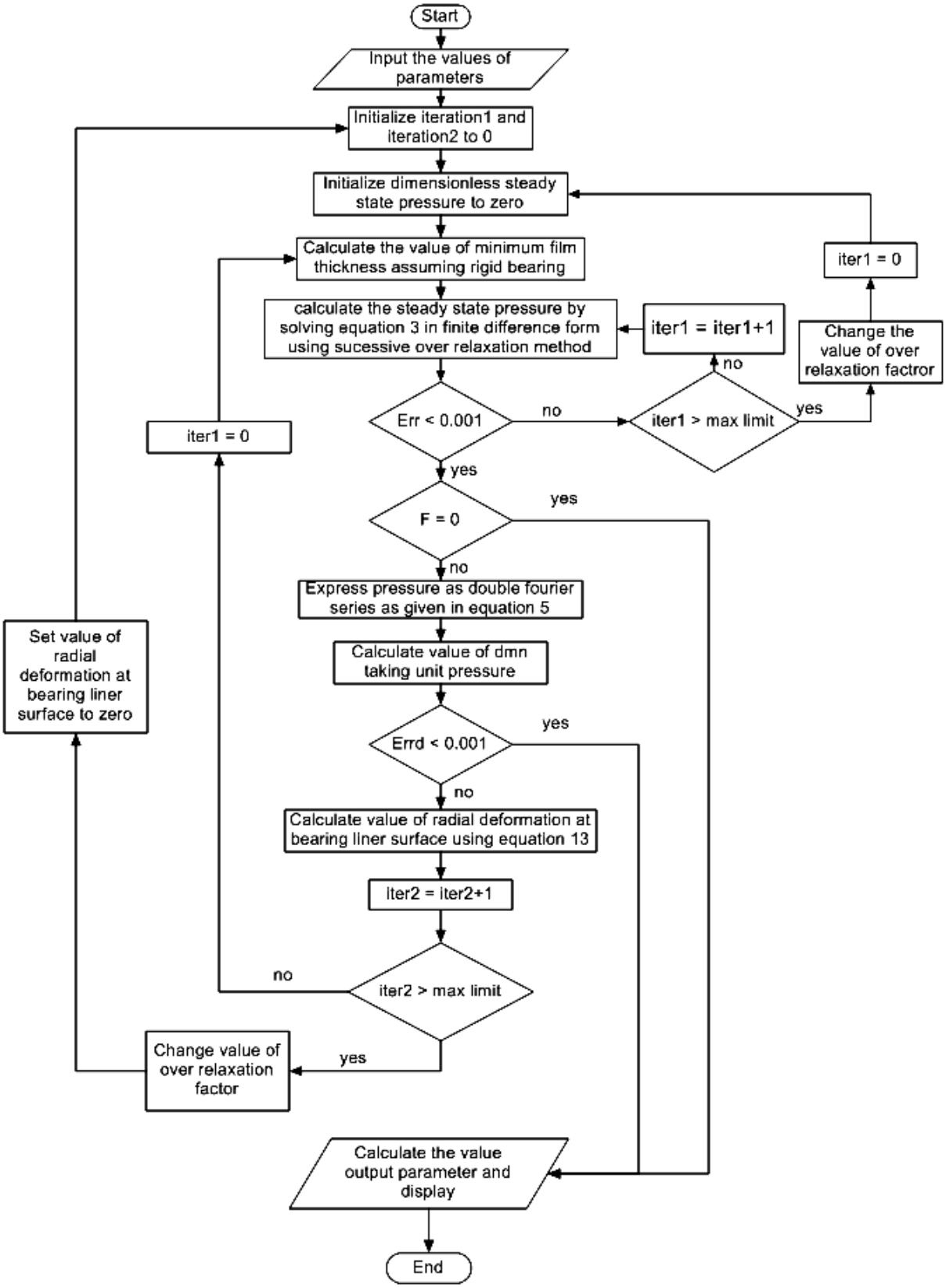

Figure 3.2 Flow chart for solution procedure

To compute pressure numerically division along θ (along bearing circumference) and $\bar{z}$ (bearing length) directions are taken to be 178 and 18 respectively. Since pressure distribution is symmetrical about mid plane, pressure distribution in one-half of bearing need to be calculated. To compute pressure distribution numerically, pressure at each grid point is assumed equal to zero initially. Pressure distribution calculated after iteration is multiplied by over relaxation factor (ORF). Iterative procedure is repeated until convergence is achieved where convergence criterion for iteration is $\left|\frac{\sum \bar{p}_0^{n+1} - \sum \bar{p}_0^{n}}{\sum \bar{p}_0^{n+1}}\right| \leq 0.001$, where n represents number of iterations. It is found that rate of convergence depends on value of ORF. Value of ORF is chosen on hit and trial basis. However, for this analysis ORF is taken to be 1.03.

Following steady state performance parameters of flexible journal bearing can be calculated once steady-state film pressure field is obtained.

3.3.1. Bearing with flexible liner

Pressure is first calculated by assuming rigid bearing i.e. assuming steady state radial deformation to be zero and assuming pressure at each grid point to be zero. Pressure is calculated by solving equation (3.9) in finite difference form satisfying all boundary conditions. In order to make calculations easier cavitation boundary conditions are replaced by method of constraints as suggested by christopherson [9]. This steady state non-dimensional pressure distribution is used to calculate steady state radial deformation of bearing liner surface using method explained above in section 3.2. This steady state deformation is used to calculate new minimum film thickness which is further used to generate next iteration of steady state pressure. Process is repeated until convergence is achieved. Thus steady state non-dimensional pressure distribution is achieved for Journal bearings with flexible liner. steady state pressure distribution is thus calculated for various eccentricity ratios (0.2, 0.4, 0.6, 0.8), slenderness ratios (0.5, 1.0, 1.5), deformation factor (0.1, 0.2, 0.3, 0.4, 0.5, 0.6), Poisson's ratio (0.2, 0.3, 0.4), liner thickness to journal radius ratio (0.3, 0.4, 0.5), characteristic length (1.0, 10.0, 20.0, 30.0, 40.0, 50.0, 60.0) and coupling number (0.1, 0.3, 0.5, 0.7, 0.9). This pressure distribution is further used to calculate journal bearing characteristic parameters.

3.4 Bearing characterisitcs

3.4.1. Load capacity, attitude angle and Sommerfeld number

Steady state fluid film force components along line of center and perpendicular to lines of centers are given respectively by:

$$\left.\begin{aligned}(F_R)_0 &= \int_{-L/2}^{L/2}\int_{\theta_1}^{\theta_2} p_0 \cos\theta d\theta dz \\ (F_\phi)_0 &= \int_{-L/2}^{L/2}\int_{\theta_1}^{\theta_2} p_0 \sin\theta d\theta dz\end{aligned}\right\} \tag{3.12}$$

$$\bar{p}_0 = \frac{p_0 C^2}{\mu\omega R^2}, \bar{z} = \frac{2z}{L}, (\bar{F}_R)_0 = \frac{2(F_R)_0 C^2}{\mu\omega R^3 L} \; and \; (\bar{F}_R)_0 = \frac{2(F_R)_0 C^2}{\mu\omega R^3 L}$$

Using above relations components of fluid film force in non-dimensional forms along line of centres and perpendicular to line of centres respectively are given as follows:

$$\left.\begin{aligned}(\bar{F}_R)_0 &= \int_{0}^{1}\int_{\theta_1}^{\theta_2} \bar{p}_0 \cos\theta d\theta d\bar{z} \\ (\bar{F}_\phi)_0 &= \int_{0}^{1}\int_{\theta_1}^{\theta_2} \bar{p}_0 \sin\theta d\theta d\bar{z}\end{aligned}\right\} \tag{3.13}$$

Utilizing above non-dimensional fluid film force components, non-dimensional steady state load, attitude angle and Sommerfeld number can be obtained as follows:

$$\left.\begin{aligned}\bar{W}_0 &= \left[\{(\bar{F}_R)_0\}^2 + \left\{(\bar{F}_\phi)_0\right\}^2\right]^{1/2} \\ \phi_0 &= tan^{-1}\left[-\frac{(\bar{F}_\phi)_0}{(\bar{F}_R)_0}\right] \\ S &= \frac{1}{\pi\bar{W}_0}\end{aligned}\right\} \tag{3.14}$$

Where

$$\bar{W}_0 = \frac{2W_0 C^2}{\mu\omega R^3 L}$$

3.4.2. Frictional force, coefficient of friction and friction parameter

Shear stress along journal surface can be calculated using shear stress equation (2.4) and boundary conditions as stated in equation (2.37 (i) and 2.41(i)).

$$\tau_s = \frac{(2\eta + \chi)}{2}\left(\frac{\partial V_X}{\partial y}\right)_{y=0}$$

(3.15)

Frictional force can be obtained by integrating shear stress over moving frictional force.

$$F_S = \int_{-L/2}^{L/2}\int_{0}^{2\pi} \tau_s R d\theta dz$$

(3.16)

Non-dimensional friction force can be determined by substituting value of τ_s and taking into account Floberg [17] correction factor for cavitated zone is as follows:

$$\bar{F}_S = 2\left[\int_0^1\int_{\theta_1}^{\theta_2} A d\theta d\bar{z} + \int_0^1\int_{\theta_2}^{2\pi+\theta_1} A\frac{(\bar{h}_0)_{cav}}{\bar{h}_0} d\theta d\bar{z}\right]$$

(3.17)

where

$$A = \frac{\bar{h}_0}{2}\frac{\partial \bar{p}_0}{\partial \theta} + \frac{1}{\left\{\bar{h}_0 - \frac{2N}{l_m}\right\}}\tanh\left(\frac{N l_m \bar{h}_0}{2}\right) \; and \; \bar{F}_S = \frac{2F_S C}{\mu\omega R^2 L}$$

$(\bar{h}_0)_{cav}$ represents fluid film thickness corresponding to cavitation zone. Coefficient of friction is given by

$$f = \frac{F_S}{W_0}$$

(3.18)

friction parameter is given by

$$f\left({}^{R}/_{C}\right) = \frac{\bar{F}_S}{\bar{W}_0}$$

(3.19)

3.4.3. End flow rate

Volume flow rate from clearance space is given by

$$Q_Z = 2\int_0^{2\pi}\int_0^{h_0} (V_Z)_{Z=L/2} dy R d\theta \tag{3.20}$$

Substituting $V_Z$using equation (2.40) and performing integration with respect to y and non-dimensionalising with substitutions below:

$$\bar{Q}_Z = \frac{Q_Z L}{2C\omega R^3} \tag{3.21}$$

End flow rate in non-dimensional form for bearing can be calculated using formula given below:

$$\bar{Q}_z = -2\int_0^{2\pi} \bar{g}\,(l_m, N, \bar{h}_0)\left(\frac{\partial \bar{p}_0}{\partial \bar{z}}\right)_{\bar{z}=\pm 1} d\theta \tag{3.22}$$

Non-dimensional end flow can be determined by calculating numerically $\left(\frac{\partial \bar{p}_0}{\partial \bar{z}}\right)_{\bar{z}=\pm 1}$ following backward difference formula of order $[(\Delta z)^2]$ and then by numerical integration using Simpson's 1/3-rd formula.

3.5 Result and discussion

Schematic diagram of bearing is shown in figure 3.1. It is evident from above equations that steady state characteristics viz. load carrying capacity ($\bar{W}_0$), attitude angle (ϕ_0), friction parameter ($f\left({}^{R}/_{C}\right)$) and end flow rate ($\bar{Q}_z$) depend upon steady state oil film pressure ($\bar{p}_0$). Steady state oil film pressure depends on eccentricity ratio (ε_0), slenderness ratio ($\frac{L}{D}$), characteristic length (l_m), coupling number (N) and steady state radial deformation of bearing liner surface $\left(\bar{\delta}_0\right)$ as is evident from equation (3.4) and equation (3.9). Steady state radial deformation of bearing liner surface $\left(\bar{\delta}_0\right)$ depends upon Poisson's ratio (ν), deformation factor (F) and bearing liner thickness to journal radius ratio ($\frac{H}{R}$). For parametric study deformation factor is chosen as independent variable and others as parameter. Detailed parametric study have been conducted to show effects of these parameters on steady state

pressure profiles, steady state load, attitude angle, friction parameter and end flow rate in respective non-dimensional form.

Validity of computer program is validated by comparing results with already published results. Figure 3.3 presents results of rigid bearing under micropolar lubrication. Results in graph show comparison of present results with Rahamatabadi et al. [148]. Hydrodynamic journal bearings considering deformation of liner taking Newtonian fluids are presented in figure 3.4. Figure shows comparison of Majumdar et al. [29] with results generated by present program. Present results are within 3-4% of published results. Difference in results is due to change of approximation scheme in different software.

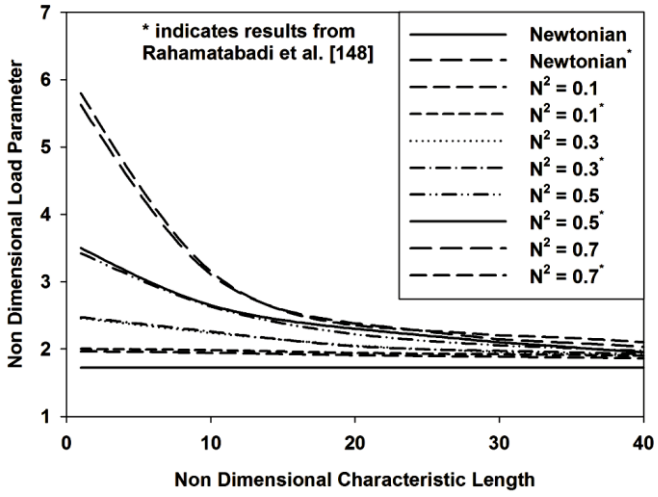

Figure 3.3 $\bar{W}_0$Vs. l_m various N^2 for rigid bearing at $\frac{L}{D} = 1.0, \varepsilon_0 = 0.5$

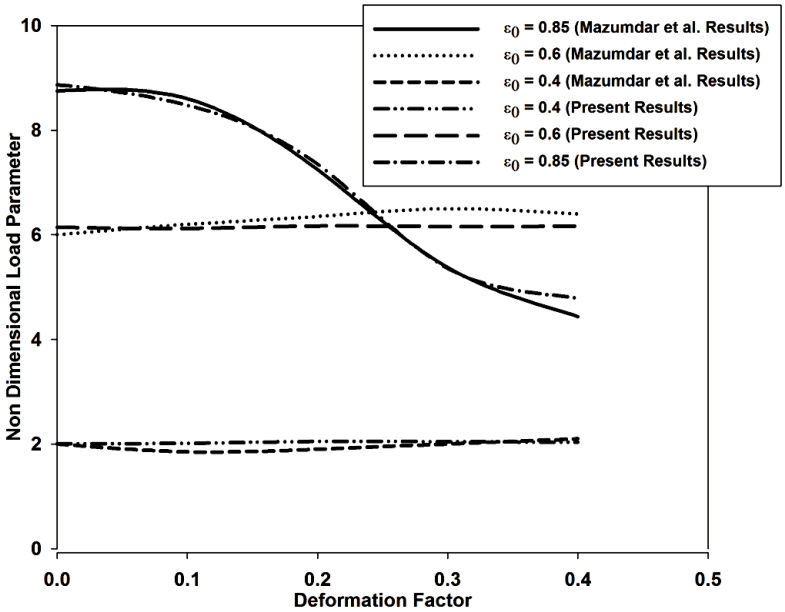

Figure 3.4 $\bar{W}_0$Vs. F various ε_0 for bearing with liner taking Newtonian fluid as lubricant at $\frac{L}{D} = 1.0. \sigma = 0.4, \frac{H}{R} = 0.3$

3.5.1 Load carrying capacity

3.5.1.1 Effect of eccentricity ratio (ε_0):

$\bar{W}_0$ as function of F for various ε_0 at $\frac{L}{D} = 1.0, N^2 = 0.5, l_m = 40.0, \frac{H}{R} = 0.3, \nu = 0.4$ is shown in Figure 3.5. It can be observed from graph that steady state load decreases with increase in deformation factor. As eccentricity ratio increases beyond 0.8 decrease in load is sharper. This is due to fact that increase in eccentricity ratio increases $\bar{\delta}$, which in turn increases $\bar{h}$ and eventually decreasing true eccentricity of bearing. Steady state load increases with increase in eccentricity ratio but as value goes above 0.85 load decreases due to effect of flexibility of liner. Conway and Lee [26] made similar observation while analysing flexible bearings using short bearing approximation. Results presented in graph predict that effect of flexibility of bearing liner can't be neglected at higher when bearing is working under conditions with high eccentricity ratio.

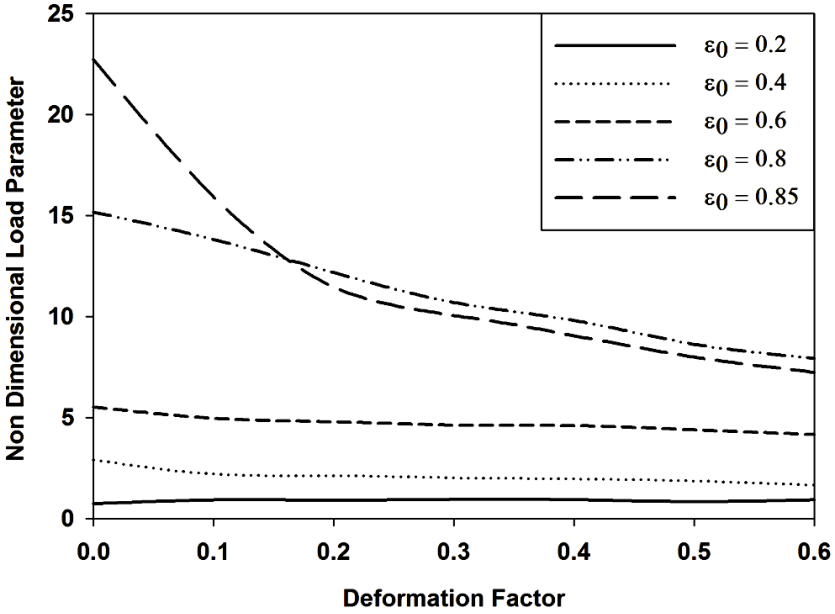

Figure 3.5 $\bar{W}_0$ Vs. F for various ε_0 at $\frac{L}{D} = 1.0, N^2 = 0.5, l_m = 40.0, \frac{H}{R} = 0.3, \nu = 0.4$.

3.5.1.2 Effect of slenderness ratio ($\frac{L}{D}$):

Variation of steady state non-dimensional load parameter against deformation factor for various values of slenderness ratio at $\varepsilon_0 = 0.8, N^2 = 0.5, l_m = 40.0, \frac{H}{R} = 0.3, \nu = 0.4$ is shown in figure 3.6. It is found that when other factors are unaltered non-dimensional load parameter increases with increase in slenderness ratio. Also it can be interpreted that l_m decreases with increase in deformation factor.

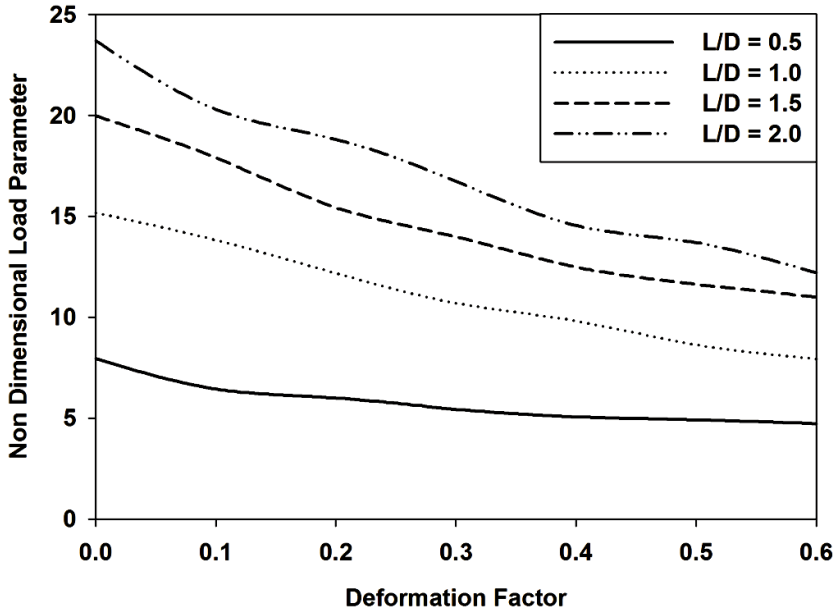

Figure 3.6 $\overline{W}_0$ Vs. F for various $\frac{L}{D}$ at $\varepsilon_0 = 0.8, N^2 = 0.5, l_m = 40.0, \frac{H}{R} = 0.3, \nu = 0.4$.

3.5.1.3 Effect of Poisson's ratio (ν):

Variation of steady state load parameter with respect to deformation factor for various Poisson's ratio at $\varepsilon_0 = 0.8, \frac{L}{D} = 1.0, N^2 = 0.5, l_m = 40.0, \frac{H}{R} = 0.3$ is shown in figure 3.7. From variation in graph it can be observed that steady state load decreases with increase in Poisson's ratio of material of bearing liner. Further as is evident from other graphs also that steady state load decreases with increase in deformation factor.

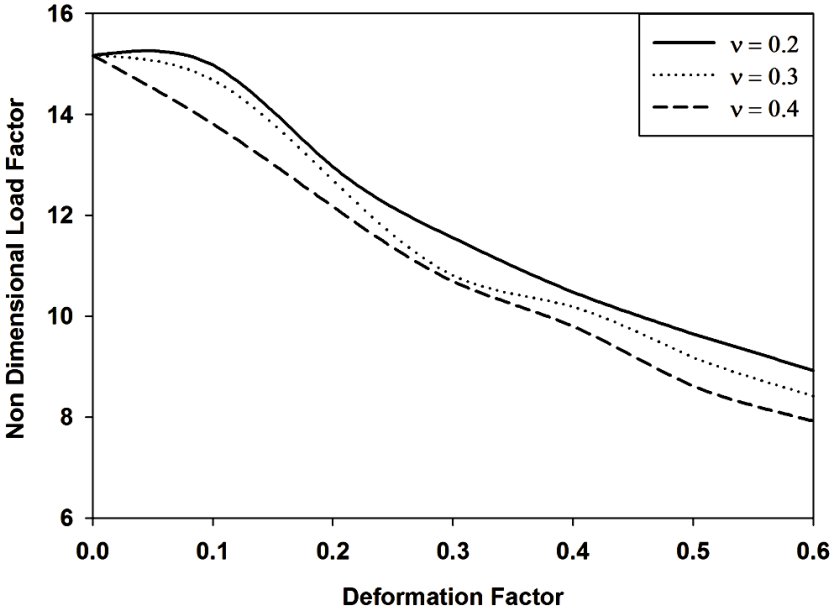

Figure 3.7 $\overline{W}_0$ Vs. F for various ν at $\varepsilon_0 = 0.8, \frac{L}{D} = 1.0, N^2 = 0.5, l_m = 40.0, \frac{H}{R} = 0.3$.

3.5.1.4 Effect of $\frac{H}{R}$ ratio:

Variation of steady state load parameter versus deformation factor for various values of $\frac{H}{R}$ ratio at $\varepsilon_0 = 0.8, \frac{L}{D} = 1.0, N^2 = 0.5, l_m = 40.0, \nu = 0.4$ is shown in figure 3.8. It is observed from variation in graph that steady state load decreases with increase in $\frac{H}{R}$ ratio.

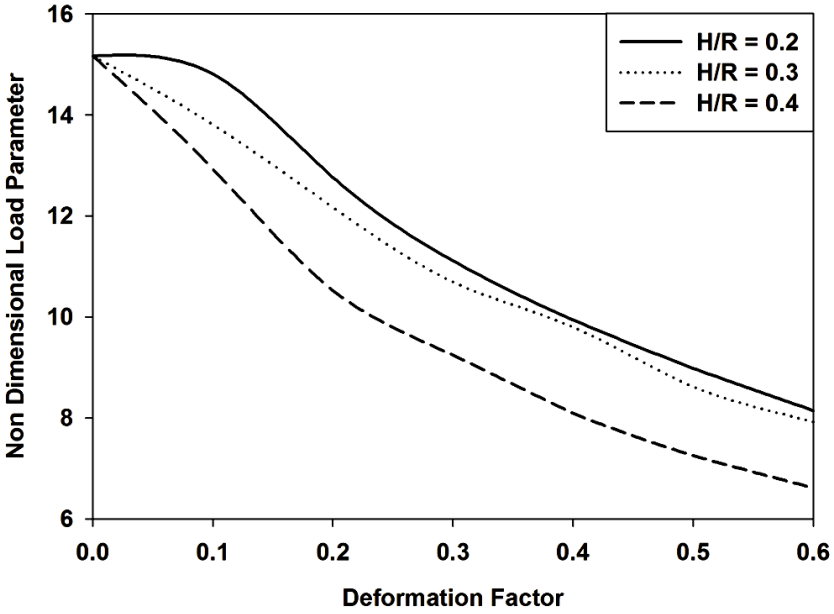

Figure 3.8 $\bar{W}_0$ Vs. F for various $\frac{H}{R}$ ratio at $\varepsilon_0 = 0.8, \frac{L}{D} = 1.0, N^2 = 0.5, l_m = 40.0, \nu = 0.4$.

3.5.1.5 Effect of characteristic length (l_m):

Figure 3.9 shows effect of variation of deformation factor and characteristic length on steady state load for $\varepsilon_0 = 0.8, \frac{L}{D} = 1.0, N^2 = 0.5, \frac{H}{R} = 0.3, \nu = 0.4$. Steady state load decrease with increase in deformation factor. Steady state load decreases with increase in l_m which is due to decrease in steady state pressure. This happens due to decrease in characteristic length of substructure, which will vanish as $l_m \to \infty$. Fluid will behave as Newtonian fluid when $l_m \to \infty$. Results in graph also show similar trends steady state load reaches near load in case of Newtonian fluid as l_m increases.

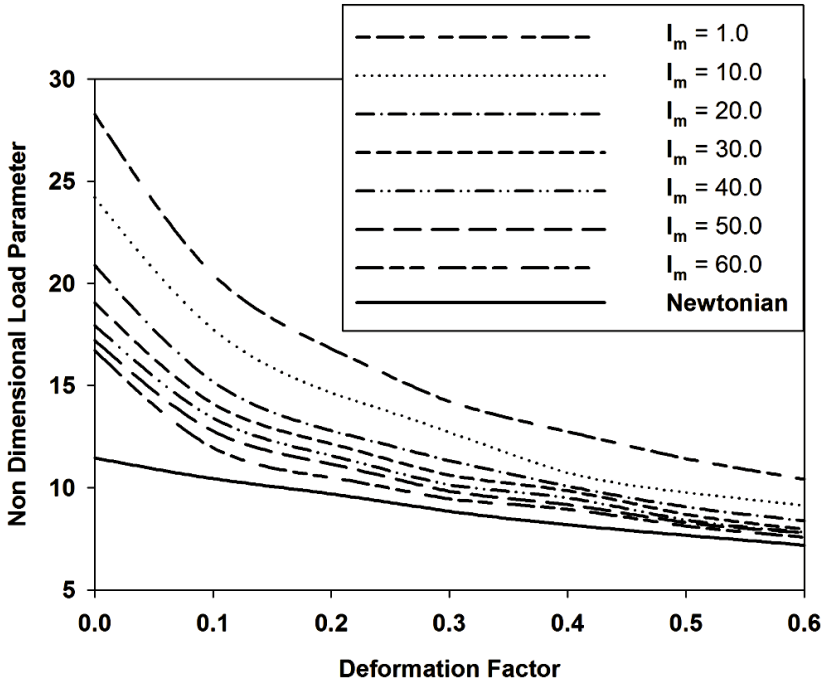

Figure 3.9 $\bar{W}_0$ Vs. F for various l_m at $\varepsilon_0 = 0.8, \frac{L}{D} = 1.0, N^2 = 0.5, \frac{H}{R} = 0.3, \nu = 0.4$.

3.5.1.6 Effect of coupling number (N):

Steady state load as function of deformation factor for various N^2 at $\varepsilon_0 = 0.8, \frac{L}{D} = 1.0, \frac{H}{R} = 0.3, l_m = 40.0, \nu = 0.4$ is shown in figure 3.10. It can be deciphered from graph that steady state load increases with increase in value of N^2. At finite value of l_m and at $N^2 \neq 0$ effect of angular momentum equation will modify Reynold's equation through coupling number. Similar observations were made by Khonsari and Brewe [132] while analysing hydrodynamic journal bearing under micropolar lubrication.

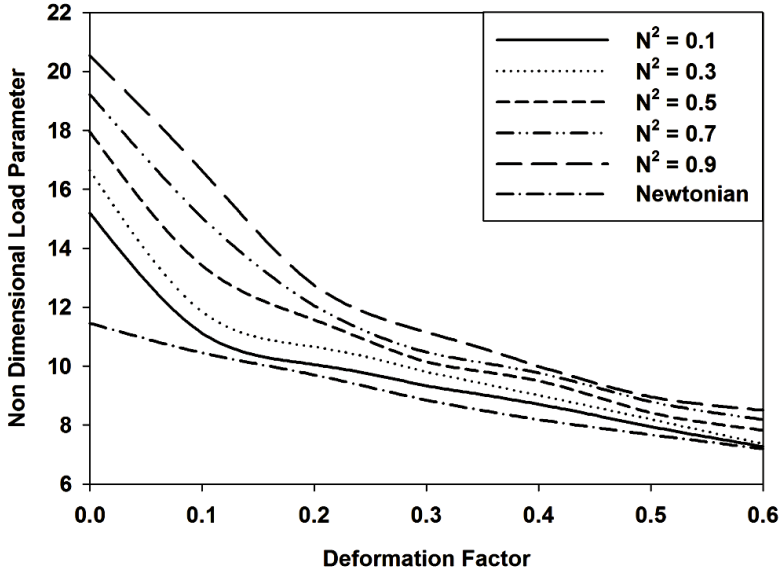

Figure 3.10 $\bar{W}_0$ Vs. F for various N^2 at $\varepsilon_0 = 0.8, \frac{L}{D} = 1.0, \frac{H}{R} = 0.3, l_m = 40.0, \nu = 0.4$.

3.5.2 Attitude angle

3.5.2.1 Effect of eccentricity ratio (ε_0):

Variation of attitude angle with respect to deformation factor for various eccentricity ratio's at $\frac{L}{D} = 1.0, N^2 = 0.5, l_m = 40.0, \frac{H}{R} = 0.3, \nu = 0.4$ is shown in figure 3.11. It can be observed while analyzing graph that attitude angle is small at greater eccentricity ratio. However, this is not case when eccentricity ratio is increased beyond 0.8. Reasons for this fact are same as described in case of steady state load. Attitude angle increases with increase in deformation factor as is clear from nature of graph.

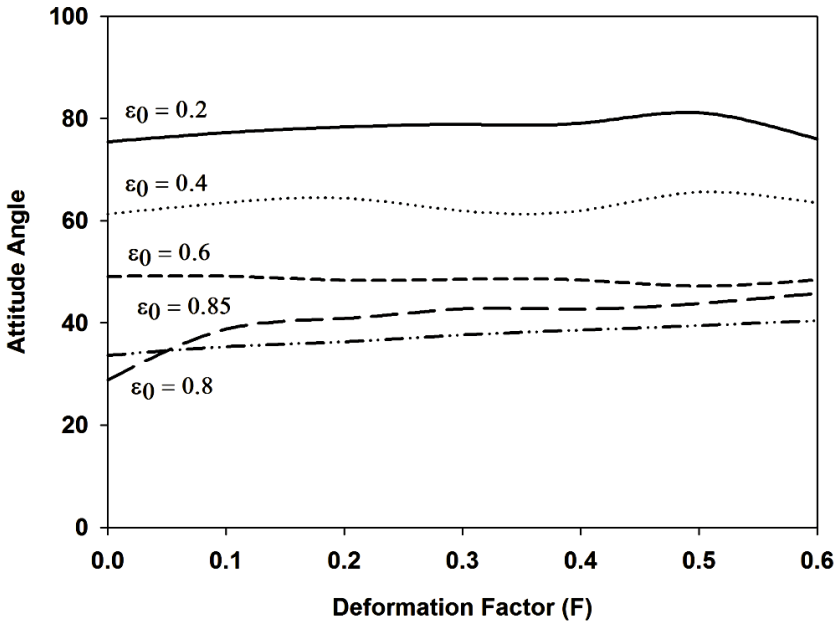

Figure 3.11 ϕ_0 Vs. F for various ε_0 at $\frac{L}{D} = 1.0, N^2 = 0.5, l_m = 40.0, \frac{H}{R} = 0.3, \nu = 0.4$.

3.5.2.2 Effect of slenderness ratio ($\frac{L}{D}$):

Figure 3.12 shows attitude angle versus deformation factor for various slenderness ratio's at $\varepsilon_0 = 0.8, N^2 = 0.5, l_m = 40.0, \frac{H}{R} = 0.3, \nu = 0.4$. It is evident from nature of curves as shown in graph that there is higher value of attitude angle when slenderness ratio is increased. Also from family of curves it can be predicted that more value of deformation factor greater is value of attitude angle.

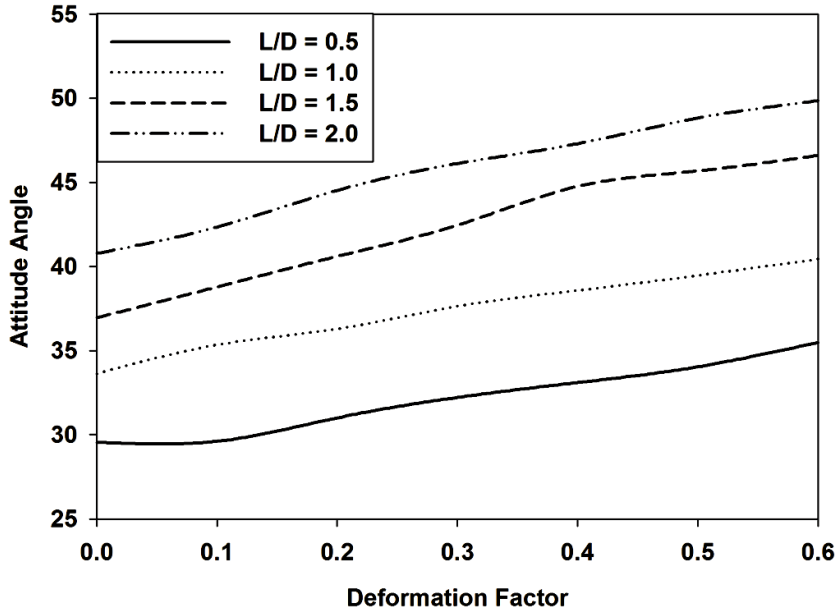

Figure 3.12 ϕ_0 Vs. F for various $\frac{L}{D}$ at $\varepsilon_0 = 0.8, N^2 = 0.5, l_m = 40.0, \frac{H}{R} = 0.3, \nu = 0.4$.

3.5.2.3 Effect of Poisson's ratio (ν):

Effect of Poisson's ratio on attitude angle considering deformation of liner in micropolar regime is shown in figure 3.13. Figure depicts graphically variation of attitude angle versus deformation factor for various values of Poisson's ratio at $\varepsilon_0 = 0.8, \frac{L}{D} = 1.0, N^2 = 0.5, l_m = 40.0, \frac{H}{R} = 0.3$. Scrutiny of figure reveals that attitude angle increases with increase in Poisson's ratio. It is also observed that attitude angle increases with increase in deformation factor.

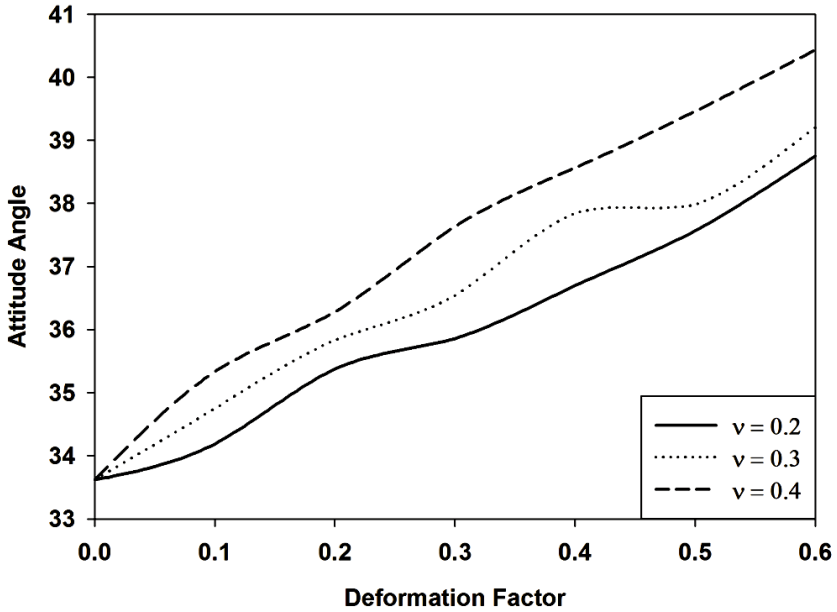

Figure 3.13 ϕ_0 Vs. F for various ν at $\varepsilon_0 = 0.8, \frac{L}{D} = 1.0, N^2 = 0.5, l_m = 40.0, \frac{H}{R} = 0.3$.

3.5.2.4 Effect of $\frac{H}{R}$ ratio:

Attitude angle versus deformation factor for various values of liner thickness to journal radius at $\varepsilon_0 = 0.8, \frac{L}{D} = 1.0, N^2 = 0.5, l_m = 40.0, \nu = 0.4$ is shown in figure 3.14. It is observed from graph that attitude angle increases with increase in deformation factor. Also, it is clearly visible that greater $\frac{H}{R}$ ratio more is value of attitude angle.

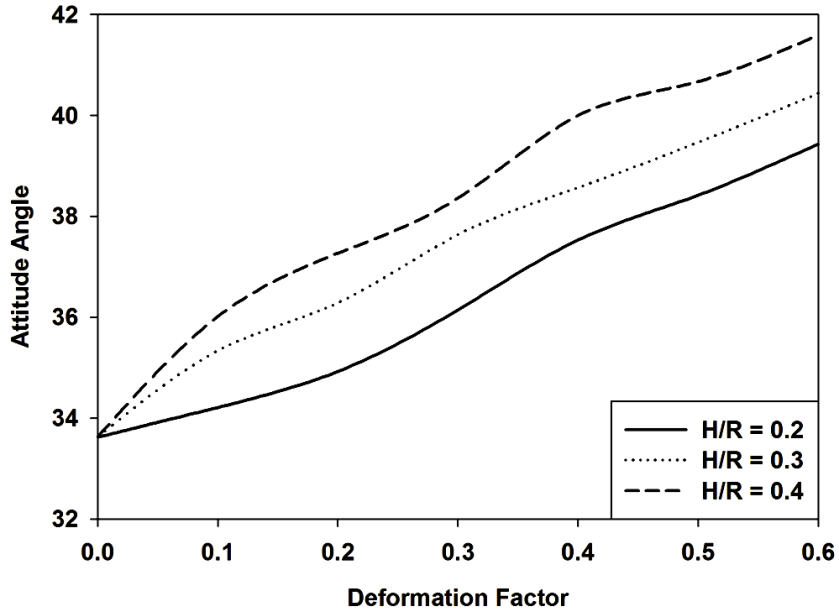

Figure 3.14 ϕ_0 Vs. F for various $\frac{H}{R}$ ratio at $\varepsilon_0 = 0.8, \frac{L}{D} = 1.0, N^2 = 0.5, l_m = 40.0, \nu = 0.4$.

3.5.2.5 Effect of characteristic length (l_m):

Figure 3.15 shows variation of attitude angle versus l_m for various values of F and results are compared with change in attitude angle for Newtonian fluid as lubricant ($\varepsilon_0 = 0.8, \frac{L}{D} = 1.0, N^2 = 0.5, \frac{H}{R} = 0.3, \nu = 0.4$). Increase in deformation factor leads to greater attitude angle. Initially, attitude angle decrease with increase in l_m reaches minimum values at $l_m \to 10.0$. Further, attitude angle increases with increase in l_m. Attitude angle at $l_m \to 0.0$ is same as for Newtonian fluids. This observation is due to fact that attitude angle being ratio of two components of fluid film forces and both increase by same amount.

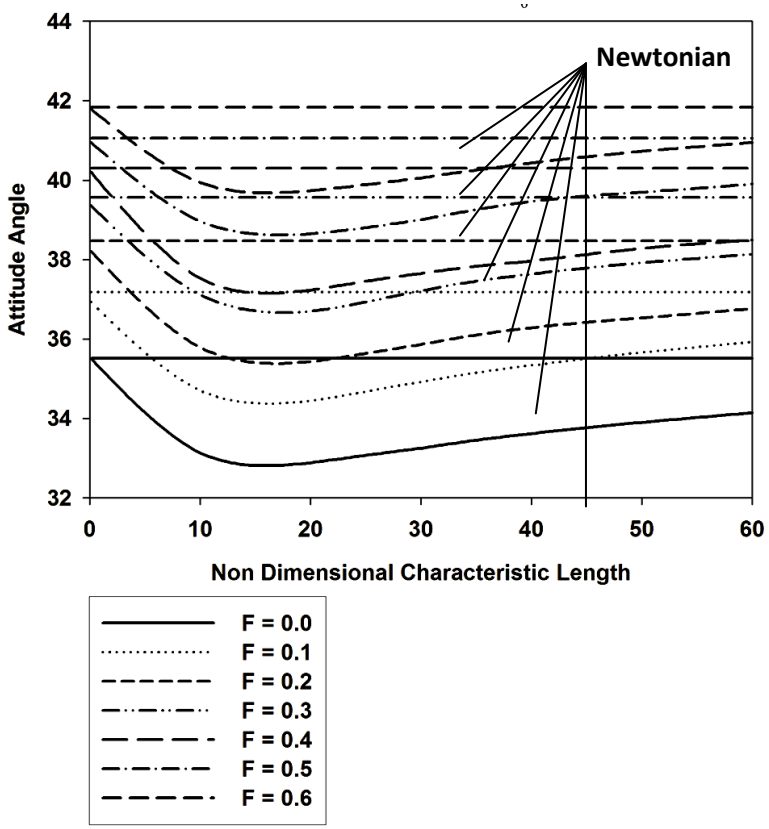

Figure 3.15 ϕ_0 Vs. l_m for various F at $\varepsilon_0 = 0.8, \frac{L}{D} = 1.0, N^2 = 0.5, \frac{H}{R} = 0.3, \nu = 0.4$.

3.5.2.6 Effect of coupling number (*N*):

Figure 3.16 gives us variation of attitude angle versus F for various values of coupling number at $\varepsilon_0 = 0.8, \frac{L}{D} = 1.0, \frac{H}{R} = 0.3, l_m = 40.0, \nu = 0.4$. It can be observed while analyzing graph that lower values of attitude angle are encountered at higher coupling number. Das et al. [140] predicted similar result while analyzing misaligned hydrodynamic journal bearing.

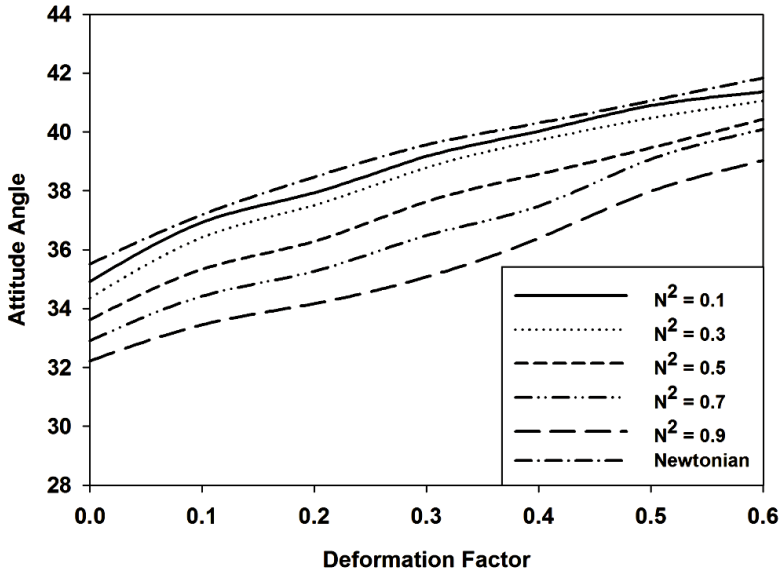

Figure 3.16 ϕ_0 Vs. F for various N^2 at $\varepsilon_0 = 0.8, \frac{L}{D} = 1.0, \frac{H}{R} = 0.3, l_m = 40.0, \nu = 0.4$.

3.5.3 Friction parameter

3.5.3.1 Effect of eccentricity ratio (ε_0):

Friction parameter is plotted as a function of deformation factor F for various values of eccentricity ratio at $\frac{L}{D} = 1.0, N^2 = 0.5, l_m = 40.0, \frac{H}{R} = 0.3, \nu = 0.4$ in figure 3.17. Lower values of friction parameter were observed at high deformation factor at low eccentricity ratio. But, trends are reversed at higher values of eccentricity ratio. Friction parameter being ratio of friction force and load, load decreases sharply at higher eccentricity ratio causes such reversal of trends.

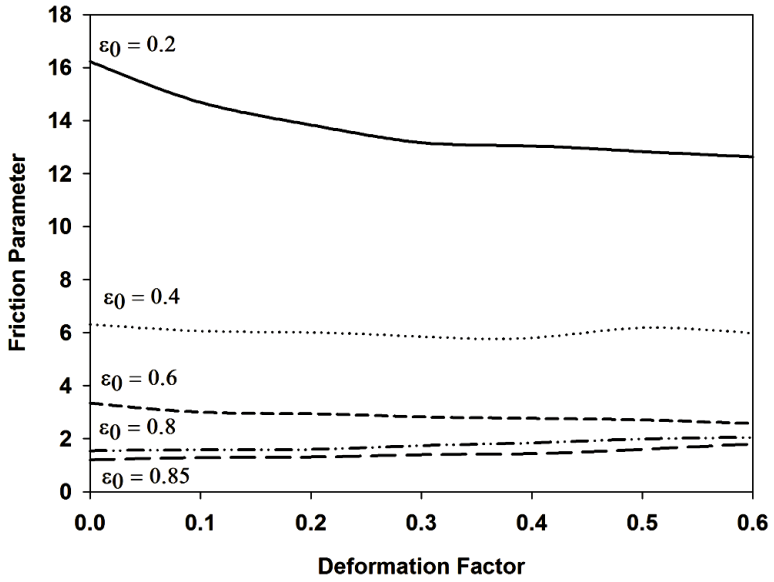

Figure 3.17 $f\left({}^{R}/_{C}\right)$ Vs. F for various ε_0 at $\frac{L}{D} = 1.0, N^2 = 0.5, l_m = 40.0, \frac{H}{R} = 0.3, \nu = 0.4$.

3.5.3.2 Effect of slenderness ratio ($\frac{L}{D}$):

Effect of variation of slenderness ratio on value of non-dimensional friction parameter considering deformation of bearing liner surface under micropolar regime is shown in figure 3.18. Graph in figure gives us variation of friction parameter versus deformation factor for various values of $\frac{L}{D}$ at $\varepsilon_0 = 0.8, N^2 = 0.5, l_m = 40.0, \frac{H}{R} = 0.3, \nu = 0.4$. Scrutiny of graph reveals that non-dimensional friction parameter decreases with increases $\frac{L}{D}$ value. It is also revealed that non-dimensional friction parameter decreases sharply as value of $\frac{L}{D}$ changes from 0.5 to 1.0 but variation in friction parameter is small as value of $\frac{L}{D}$ increases beyond 1.0.

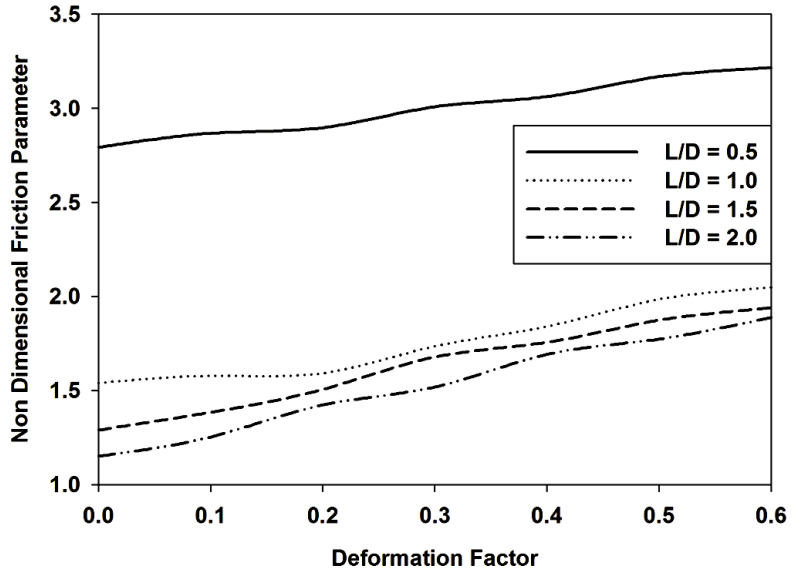

Figure 3.18 $f\left({}^{R}/_{C}\right)$ Vs. F for various $\frac{L}{D}$ at $\varepsilon_0 = 0.8, N^2 = 0.5, l_m = 40.0, \frac{H}{R} = 0.3, \nu = 0.4$.

3.5.3.3 Effect of Poisson's ratio (ν):

Non-dimensional friction parameter versus of deformation factor for various values of Poisson's ratio is shown in figure 3.19 for $\varepsilon_0 = 0.8, \frac{L}{D} = 1.0, N^2 = 0.5, l_m = 40.0, \frac{H}{R} = 0.3$. Nature of graph predicts that friction parameter shows better results at higher Poisson's ratio. Friction parameter increases with increase in deformation factor as is evident from family of curves. It is also evident that increase in friction parameter is sharp as F is increased beyond 0.2.

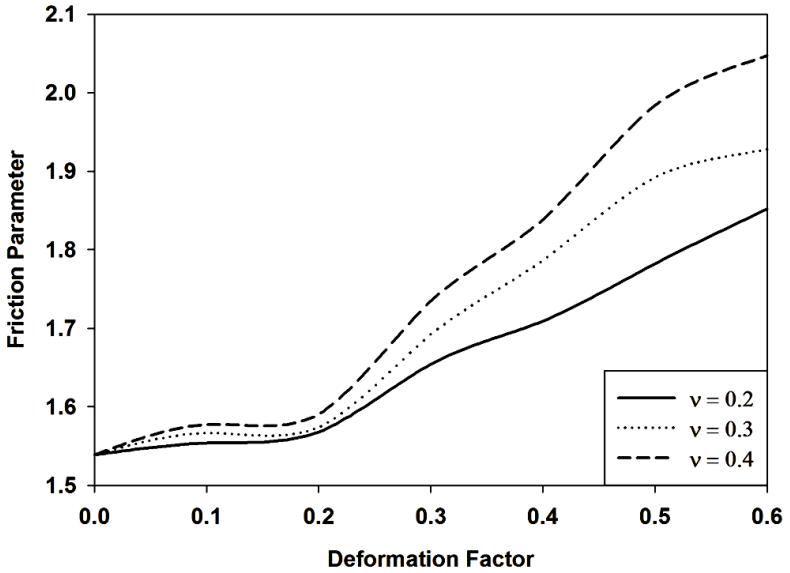

Figure 3.19 $f\left({}^{R}/_{C}\right)$ Vs. F for various ν at $\varepsilon_0 = 0.8, \frac{L}{D} = 1.0, N^2 = 0.5, l_m = 40.0, \frac{H}{R} = 0.3$.

3.5.3.4 Effect of $\frac{H}{R}$ ratio:

Figure 3.20 shows variation of non-dimensional friction parameter with deformation factor for various values of liner thickness to journal radius, when $\varepsilon_0 = 0.8, \frac{L}{D} = 1.0, N^2 = 0.5, l_m = 40.0, \nu = 0.4$. Scrutiny of graph reveals that value of non-dimensional friction parameter decreases with increase in $\frac{H}{R}$ ratio. It can also be observed that $f\left({}^{R}/_{C}\right)$ increases with increase in F.

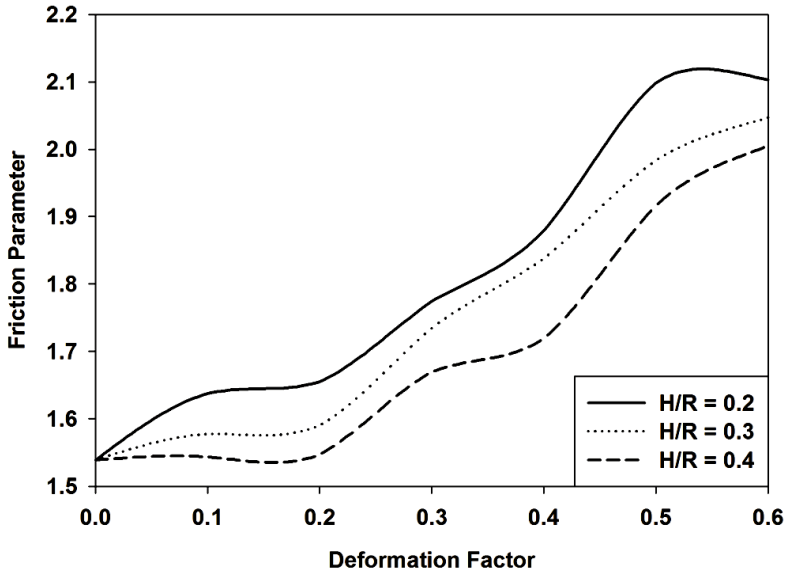

Figure 3.20 $f\left({}^{R}/_{C}\right)$ Vs. F for various $\frac{H}{R}$ ratio at $\varepsilon_0 = 0.8, \frac{L}{D} = 1.0, N^2 = 0.5, l_m = 40.0, \nu = 0.4$.

3.5.3.5 Effect of characteristic length (l_m):

Figure 3.21 shows variation of friction parameter against characteristic length for various values of deformation factor at $\varepsilon_0 = 0.8, \frac{L}{D} = 1.0, N^2 = 0.5, \frac{H}{R} = 0.3, \nu = 0.4$. It can be observed that higher values of friction parameter are predicted at higher values of deformation of factor. Initially, friction parameter decreases as characteristic length increases. Trends are reversed as $l_m \to 20.0$ as friction parameter is ratio of friction force and load.

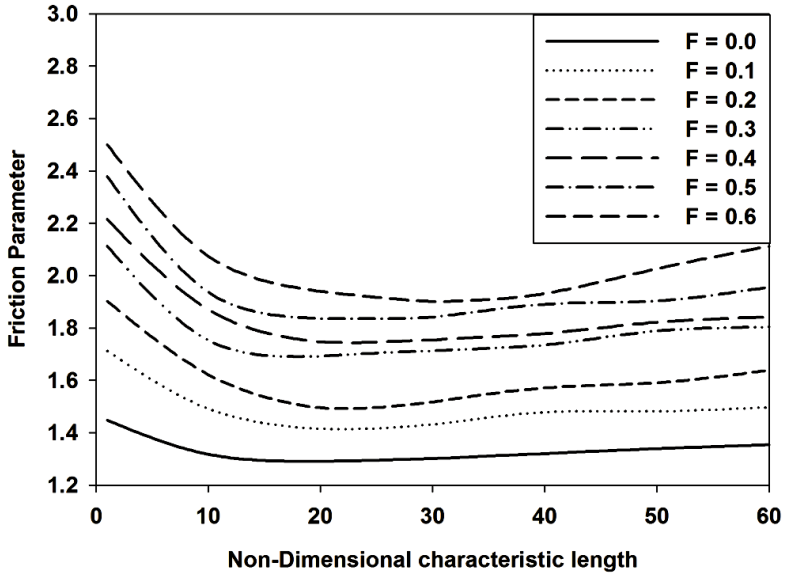

Figure 3.21 $f\left({}^{R}/_{C}\right)\, l_m$ for various F at $\varepsilon_0 = 0.8, \frac{L}{D} = 1.0, N^2 = 0.5, \frac{H}{R} = 0.3, \nu = 0.4$.

3.5.3.6 Effect of coupling number (*N*):

Family of curves in figure 3.22 shows variation of friction parameter against deformation factor for various values of coupling number at $\varepsilon_0 = 0.8, \frac{L}{D} = 1.0, \frac{H}{R} = 0.3, l_m = 40.0, \nu = 0.4$. While analyzing graph it's observed that higher values of friction parameter are encountered at higher coupling number. Lower friction values are seen when bearing is running under micropolar regime in comparison to Newtonian fluids regime. This is a beneficial trend from design point of view. Higher deformation factor higher is value of friction parameter keeping coupling number unchanged.

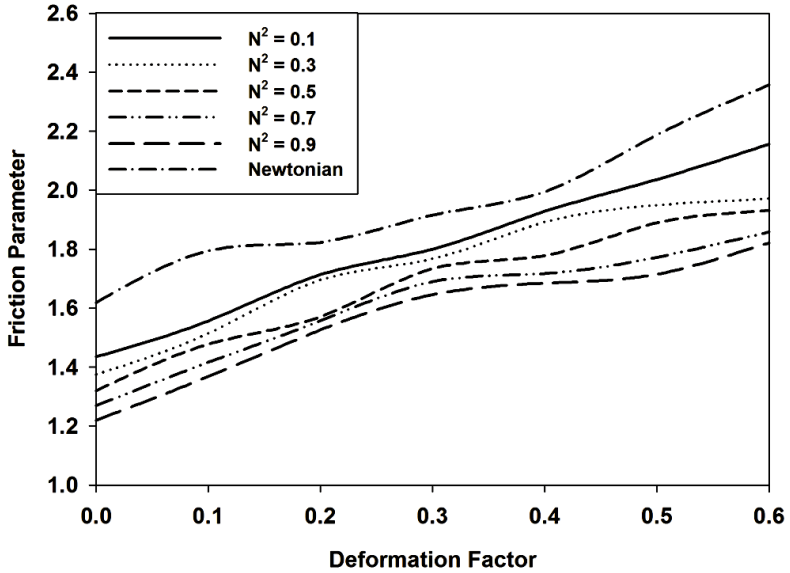

Figure 3.22 $f\left({}^{R}/_{C}\right)$ Vs. F for various N^2 at $\varepsilon_0 = 0.8, \frac{L}{D} = 1.0, \frac{H}{R} = 0.3, l_m = 40.0, \nu = 0.4$.

3.5.4 End flow

3.5.4.1 Effect of eccentricity ratio (ε_0):

Figure 3.23 shows variation of steady state end flow versus deformation factor for various values of eccentricity at $\frac{L}{D} = 1.0, N^2 = 0.5, l_m = 40.0, \frac{H}{R} = 0.3, \nu = 0.4$. End flow rate is more for larger values of deformation factor at higher eccentricity ratio. Variation of end flow is negligible at lower eccentricity ratio. End flow rate is higher as deformation factor increases. Value of end flow remains almost constant at low eccentricity ratio, but at $\varepsilon_0 \geq 0.7$ non-dimensional end flow increases with increase in value of deformation factor.

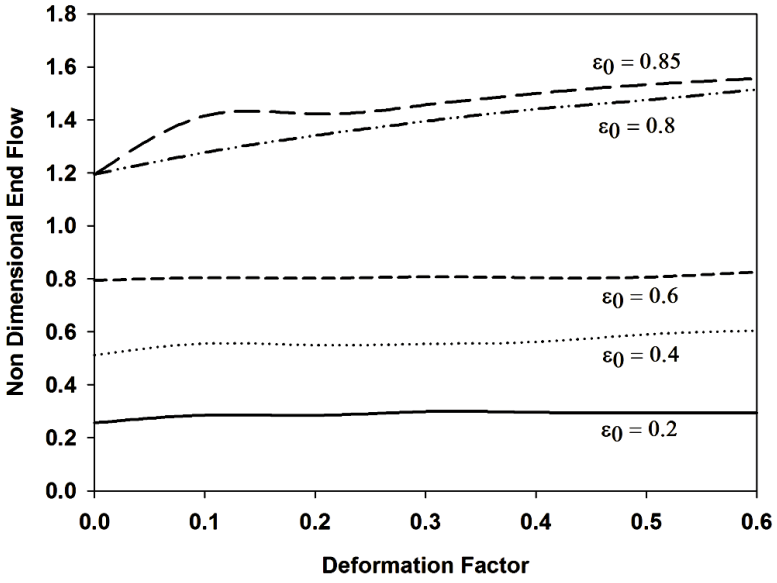

Figure 3.23 $\bar{Q}_Z$ Vs. F for various ε_0 at $\frac{L}{D} = 1.0, N^2 = 0.5, l_m = 40.0, \frac{H}{R} = 0.3, \nu = 0.4$.

3.5.4.2 Effect of slenderness ratio ($\frac{L}{D}$):

Effect of variation of $\frac{L}{D}$ on $\bar{Q}_Z$ considering deformation of bearing liner surface for micropolar regime is shown in Figure 3.24. Graph in figure gives variation of end flow rate with respect to deformation factor for various slenderness ratios', when $\varepsilon_0 = 0.8, N^2 = 0.5, l_m = 40.0, \frac{H}{R} = 0.3, \nu = 0.4$. Observations from family of curves in graph predict that end flow increases with increase in slenderness ratio. It can also be predicted that end flow increases with increase in value of deformation factor. This increase is less in case of lower values of $\frac{L}{D}$ whereas, value of non-dimensional end flow increases sharply for $\frac{L}{D}$=2.0.

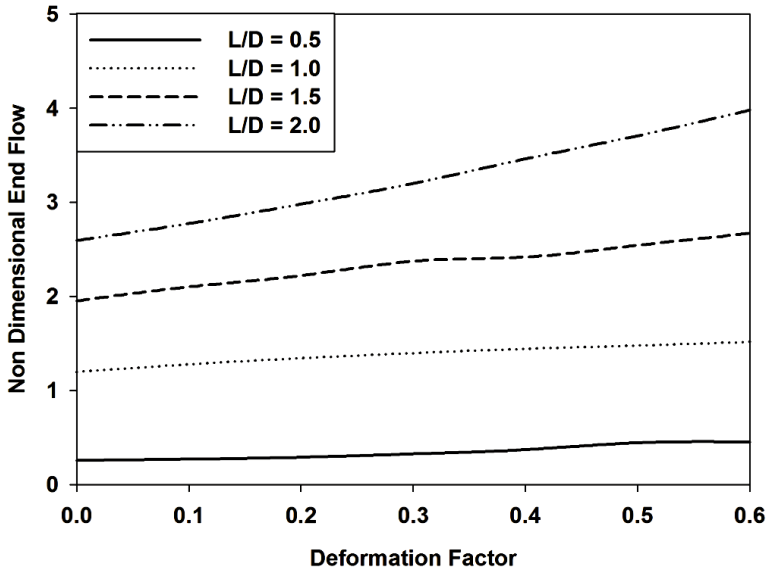

Figure 3.24 $\bar{Q}_Z$ Vs. F for various $\frac{L}{D}$ at $\varepsilon_0 = 0.8, N^2 = 0.5, l_m = 40.0, \frac{H}{R} = 0.3, \nu = 0.4$.

3.5.4.3 Effect of Poisson's ratio (ν):

$\bar{Q}_Z$ as a function of F for various values of Poisson's ratio is shown in figure 3.25 for $\varepsilon_0 = 0.8, \frac{L}{D} = 1.0, N^2 = 0.5, l_m = 40.0, \frac{H}{R} = 0.3$. While analyzing graph it can be observed that value of $\bar{Q}_Z$ decreases with increase in Poisson's ratio. From nature of plot it is also evident that non-dimensional end flow increases with increase in deformation factor.

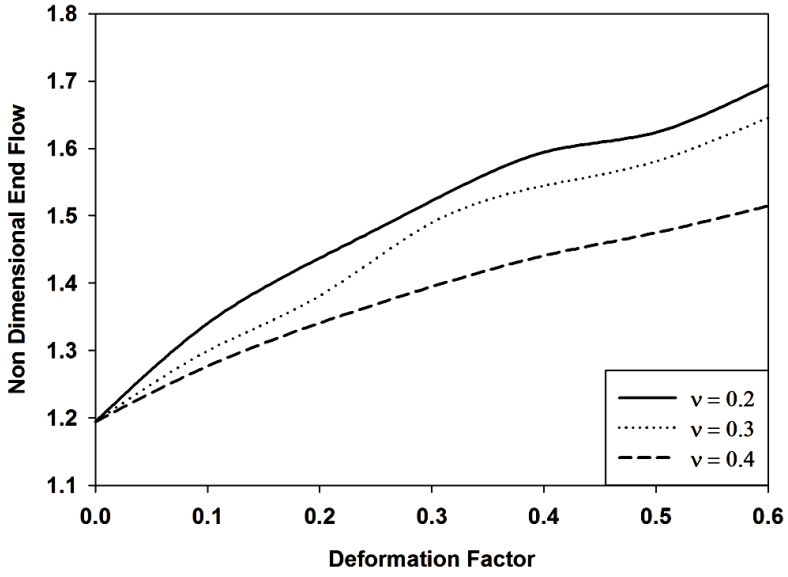

Figure 3.25 $\bar{Q}_Z$ Vs. F for various ν at $\varepsilon_0 = 0.8, \frac{L}{D} = 1.0, N^2 = 0.5, l_m = 40.0, \frac{H}{R} = 0.3$.

3.5.4.4 Effect of $\frac{H}{R}$ ratio:

Figure 3.26 shows variation of $\bar{Q}_Z$ with F for various values of liner thickness to journal radius, when $\varepsilon_0 = 0.8, \frac{L}{D} = 1.0, N^2 = 0.5, l_m = 40.0, \nu = 0.4$. Scrutiny of graphs reveals that $\bar{Q}_Z$ increases with increase in $\frac{H}{R}$ ratio. It is observed from nature of graph that end flow rate is higher deformation factor increases.

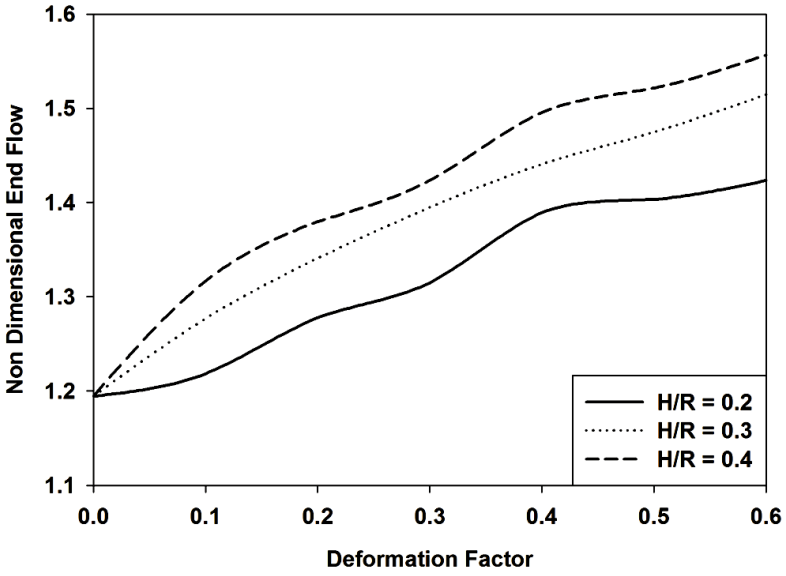

Figure 3.26 $\bar{Q}_Z$ Vs. F for various $\frac{H}{R}$ ratio at $\varepsilon_0 = 0.8, \frac{L}{D} = 1.0, N^2 = 0.5, l_m = 40.0, \nu = 0.4$.

3.5.4.5 Effect of characteristic length (l_m):

Family of curves in Figure 3.27 shows variation of $\bar{Q}_Z$ versus l_m for various values of F at $\varepsilon_0 = 0.8, \frac{L}{D} = 1.0, N^2 = 0.5, \frac{H}{R} = 0.3, \nu = 0.4$. It can be observed that end flow reduces as l_m increases reach a minimum value as $l_m \rightarrow 10.0$ and then increases further. At a particular value of l_m end flow is higher at higher values of deformation factor.

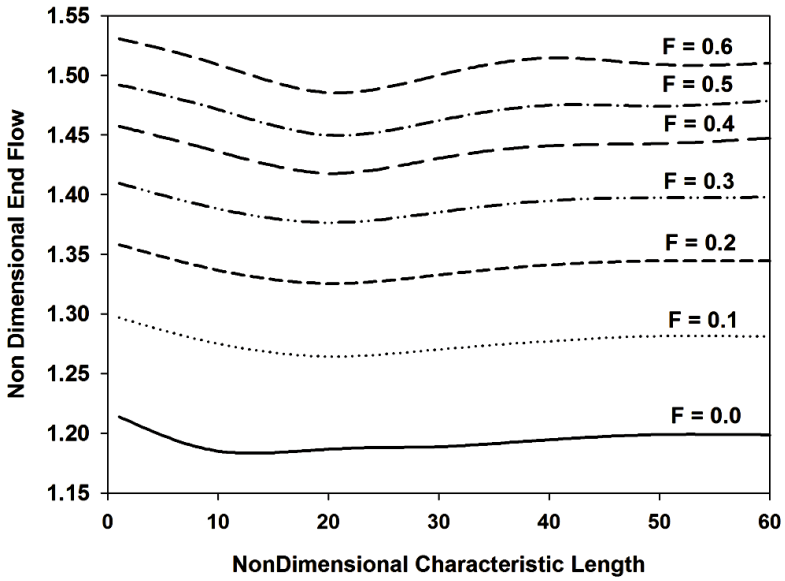

Figure 3.27 $\bar{Q}_Z$ Vs. l_m for various F at $\varepsilon_0 = 0.8, \frac{L}{D} = 1.0, N^2 = 0.5, \frac{H}{R} = 0.3, \nu = 0.4$.

3.5.4.6 Effect of coupling number (N):

Figure 3.28 shows variation of $\bar{Q}_Z$ versus F for various N^2 at $\varepsilon_0 = 0.8, \frac{L}{D} = 1.0, \frac{H}{R} = 0.3, l_m = 40.0, \nu = 0.4$. End flow is predicted to be more for higher values of deformation factor as is clear from graph.

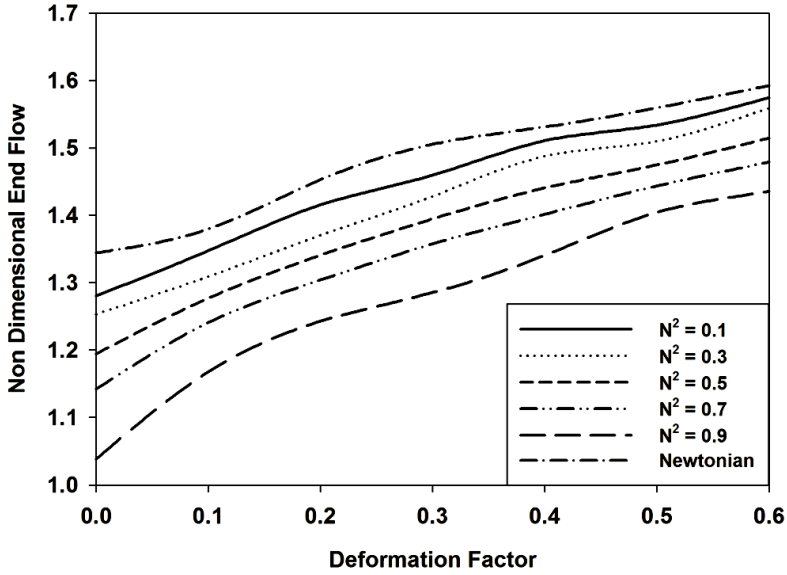

Figure 3.28 $\bar{Q}_Z$ Vs. F for various N^2 at $\varepsilon_0 = 0.8, \frac{L}{D} = 1.0, \frac{H}{R} = 0.3, l_m = 40.0, \nu = 0.4$.

Chapter 4 Linear Dynamic Analysis of Finite Flexible Oil Journal Bearings with Micropolar Fluids

4.1 Introduction

Present chapter deals with dynamic analysis of hydrodynamic journal bearings of finite width in micropolar lubrication regime taking into consideration effect of elastic distortion of bearing liner. Dynamic pressures are calculated using Perturbation technique. In this method equations of motion are linearized by using form of small order perturbations of eccentricity ratio and attitude angle. Deformation equations for bearing surface are simultaneously solved with modified Reynolds equation, equations of motion of journal to predict theoretically fluid film pressure distribution. Four components of stiffness and damping coefficients of bearings are calculated once perturbed pressures are known by numerical integration of perturbed pressure fields along line of centers and perpendicular to line of centers. Later it will be shown that real parts of these integrals will give to some scale components of stiffness and imaginary parts components of damping coefficients.

Threshold of oil whirl stability which is an important phenomenon exhibited by rotor/bearing system is also calculated apart from stiffness and damping coefficients. Study of oil whirl instability is important in bearing design as due to oil whirl, shaft shifts away from static equilibrium position. Due to this shaft whirls in an orbit and may come in contact with bearing surface and eventually may fail due to seizure.

In this analysis, threshold for oil whirl stability for rigid rotor in hydrodynamic journal bearings lubricated with micropolar fluid has been analyzed theoretically taking into consideration flexibility of bearing liner. Journal is also assumed to execute small harmonic oscillation about equilibrium position in this analysis, such that first order perturbation can be applied without serious error. Equations of motion of journal have been written using oil stiffness and damping coefficients, and resulting equations have been investigated for critical mass parameter and oil whirl stability. Effect of eccentricity ratio, L/D, ν and micropolar parameters on critical mass parameter and oil whirl stability have been investigated and results have been presented with help graphs.

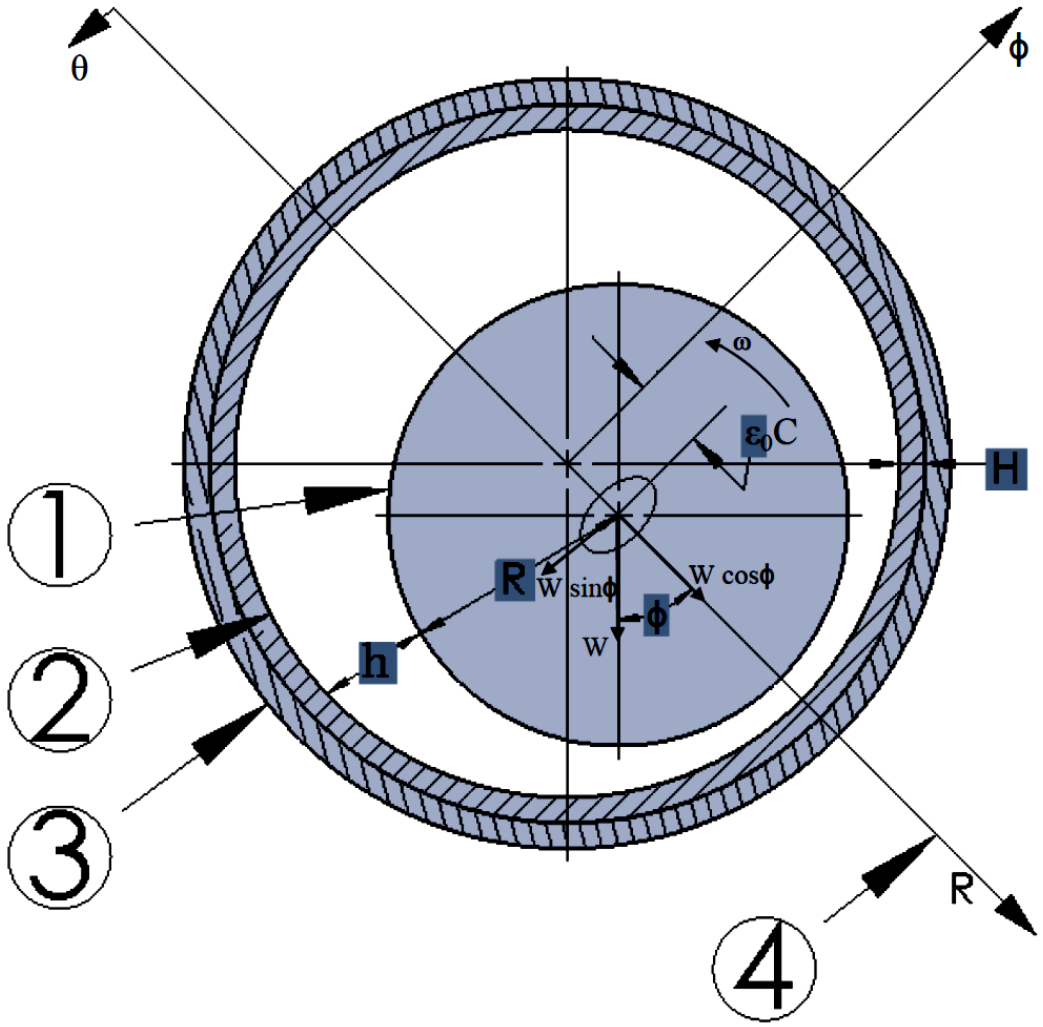

1. Journal 2. Flexible Liner 3. Solid Housing 4. Lines of centers
Figure 4.1 Schematic diagram of Journal Bearing.

4.2 Theoretical analysis

4.2.1 Governing equation

The schematic diagram of the journal bearing used in the analysis is shown in figure 4.1. Governing modified Reynolds equation for 2-D flow of micropolar lubricant is as follows [119, 130]

$$\frac{\partial}{\partial x}\left[\frac{h^3}{\mu}\boldsymbol{\Phi}(\Lambda,N,h)\frac{\partial p}{\partial x}\right]+\frac{\partial}{\partial z}\left[\frac{h^3}{\mu}\boldsymbol{\Phi}(\Lambda,N,h)\frac{\partial p}{\partial z}\right]=6U\left(1-\frac{2}{\omega}\frac{\partial \phi}{\partial t}\right)\frac{\partial h}{\partial x}+12\frac{\partial h}{\partial t} \tag{4.1}$$

$$\boldsymbol{\Phi}(\Lambda,N,h)=\left\{1+12\frac{\Lambda^2}{h^2}-6\frac{N\Lambda}{h}\coth\frac{Nh}{2\Lambda}\right\},\Lambda=\left(\frac{\gamma}{4\mu}\right)^{1/2},N=\left(\frac{\chi}{2\mu+\chi}\right)^{1/2}$$

Equation 4.1 applying following substitutions

$$\theta = \frac{x}{R}, \bar{z} = \frac{2z}{L}, \bar{h} = \frac{h}{C}, \bar{p} = \frac{pC^2}{\mu\omega R^2}, l_m = \frac{C}{\Lambda}, \bar{t} = \omega t$$

following equation is obtained in non-dimensional form:

$$\frac{\partial}{\partial\theta}\left[\bar{g}\left(l_m, N, \bar{h}\right)\frac{\partial\bar{p}}{\partial\theta}\right] + \left(\frac{D}{L}\right)^2 \frac{\partial}{\partial\bar{z}}\left[\bar{g}\left(l_m, N, \bar{h}\right)\frac{\partial\bar{p}}{\partial\bar{z}}\right] = \frac{1}{2}(1 - 2\phi')\frac{\partial\bar{h}}{\partial\theta} + \frac{\partial\bar{h}}{\partial\bar{t}} \tag{4.2}$$

$$\bar{g}\left(l_m, N, \bar{h}\right) = \frac{\bar{h}^3}{12} + \frac{\bar{h}}{l_m^2} - \frac{N\bar{h}^2}{2l_m}\coth\frac{Nl_m\bar{h}}{2}$$

$$\phi' = \frac{\partial\phi}{\partial\bar{t}}$$

4.2.2 Perturbation technique

Perturbation techniques provides small order perturbations to eccentricity ratio and attitude angle such as journal executes small harmonic oscillation about its equilibrium position, in order to eliminate time dependent terms without much errors. First order perturbation method is utilized for non-dimensional pressure and local film thickness with assumption that journal whirls about its mean steady state position given by eccentricity ratio ε_0 with amplitudes $Re\left(\varepsilon_1 e^{i\lambda_R\bar{t}}\right)$ and $Re\left(\varepsilon_0\phi_1 e^{i\lambda_R\bar{t}}\right)$ along line of centers and perpendicular to line of centers respectively for which non-dimensional pressure and local film thickness will be as follows:

$$\left.\begin{aligned}\bar{p} &= \bar{p}_0 + \bar{p}_1\varepsilon_1 e^{i\lambda_R\bar{t}} + \bar{p}_2\varepsilon_0\phi_1 e^{i\lambda_R\bar{t}} \\ \bar{h} &= \bar{h}_0 + \varepsilon_1 e^{i\lambda_R\bar{t}}\cos\theta + \varepsilon_0\phi_1 e^{i\lambda_R\bar{t}} sin\theta\end{aligned}\right\} \tag{4.3}$$

Where

$$\bar{h}_0 = 1 + \varepsilon_0\cos\theta + \bar{\delta}, \varepsilon = \varepsilon_0 + \varepsilon_1 e^{i\lambda_R\bar{t}}, \phi = \phi_0 + \phi_1 e^{i\lambda_R\bar{t}} \text{ and } \lambda_R = \frac{\omega_p}{\omega}$$

ε_1 and ϕ_1 are small order perturbations of eccentricity ratio and attitude angle respectively. Subscripts i=0, 1, 2 represents pressures for steady state and first order perturbations in equation (4.3), respectively. $\bar{\delta}$ is calculated in similar manner as described in steady state solution.

Substituting equation (4.3) into equation (4.2) and collecting first order terms of $\varepsilon_1$and $\varepsilon_0\phi_1$ following three equations are obtained

$$C_B\left[\frac{\partial^2\bar{p}_0}{\partial\theta^2}+\left(\frac{D}{L}\right)^2\frac{\partial^2\bar{p}_0}{\partial\bar{z}^2}\right]+C_A\left[\frac{\partial\bar{h}_0}{\partial\theta}\frac{\partial\bar{p}_0}{\partial\theta}+\left(\frac{D}{L}\right)^2\frac{\partial\bar{h}_0}{\partial\bar{z}}\frac{\partial\bar{p}_0}{\partial\bar{z}}\right]=\frac{1}{2}\frac{\partial\bar{h}_0}{\partial\theta} \tag{4.4}$$

$$\begin{aligned}C_B\left[\frac{\partial^2\bar{p}_1}{\partial\theta^2}+\left(\frac{D}{L}\right)^2\frac{\partial^2\bar{p}_1}{\partial\bar{z}^2}\right]+C_A cos\theta\left[\frac{\partial^2\bar{p}_0}{\partial\theta^2}+\left(\frac{D}{L}\right)^2\frac{\partial^2\bar{p}_0}{\partial\bar{z}^2}\right]+C_A\left[\frac{\partial\bar{h}_0}{\partial\theta}\frac{\partial\bar{p}_1}{\partial\theta}+\left(\frac{D}{L}\right)^2\frac{\partial\bar{h}_0}{\partial\bar{z}}\frac{\partial\bar{p}_1}{\partial\bar{z}}\right]\\+C_C cos\theta\left[\frac{\partial\bar{h}_0}{\partial\theta}\frac{\partial\bar{p}_1}{\partial\theta}+\left(\frac{D}{L}\right)^2\frac{\partial\bar{h}_0}{\partial\bar{z}}\frac{\partial\bar{p}_1}{\partial\bar{z}}\right]+C_A\left[-sin\theta\frac{\partial\bar{p}_0}{\partial\theta}+\left(\frac{D}{L}\right)^2 cos\theta\frac{\partial\bar{p}}{\partial\bar{z}}\right]\\=-\frac{1}{2}sin\theta+i\lambda_R cos\theta\end{aligned} \tag{4.5}$$

$$\begin{aligned}C_B\left[\frac{\partial^2\bar{p}_2}{\partial\theta^2}+\left(\frac{D}{L}\right)^2\frac{\partial^2\bar{p}_2}{\partial\bar{z}^2}\right]+C_A sin\theta\left[\frac{\partial^2\bar{p}_0}{\partial\theta^2}+\left(\frac{D}{L}\right)^2\frac{\partial^2\bar{p}_0}{\partial\bar{z}^2}\right]+C_A\left[\frac{\partial\bar{h}_0}{\partial\theta}\frac{\partial\bar{p}_2}{\partial\theta}+\left(\frac{D}{L}\right)^2\frac{\partial\bar{h}_0}{\partial\bar{z}}\frac{\partial\bar{p}_2}{\partial\bar{z}}\right]\\+C_C sin\theta\left[\frac{\partial\bar{h}_0}{\partial\theta}\frac{\partial\bar{p}_2}{\partial\theta}+\left(\frac{D}{L}\right)^2\frac{\partial\bar{h}_0}{\partial\bar{z}}\frac{\partial\bar{p}_2}{\partial\bar{z}}\right]+C_A\left[cos\theta\frac{\partial\bar{p}_0}{\partial\theta}+\left(\frac{D}{L}\right)^2 sin\theta\frac{\partial\bar{p}}{\partial\bar{z}}\right]\\=\frac{1}{2}cos\theta+i\lambda_R sin\theta-\frac{i\lambda_R}{\varepsilon_0}\frac{\partial\bar{h}_0}{\partial\theta}\end{aligned} \tag{4.6}$$

where

$$\left.\begin{aligned}C_A=\frac{\bar{h}_0^2}{4}+\frac{1}{l_m^2}-\frac{N\bar{h}_0}{l_m}\coth\left(\frac{Nl_m\bar{h}_0}{2}\right)+\frac{N^2\bar{h}_0^2}{4}\operatorname{cosech}^2\left(\frac{Nl_m\bar{h}_0}{2}\right)\\C_B=\frac{\bar{h}_0^3}{12}+\frac{\bar{h}_0}{l_m^2}-\frac{N\bar{h}_0^2}{2l_m}\coth\left(\frac{Nl_m\bar{h}_0}{2}\right)\\C_C=\frac{\bar{h}_0}{2}+N^2\bar{h}_0 cosech^2\left(\frac{Nl_m\bar{h}_0}{2}\right)-\frac{N}{l_m}coth\left(\frac{Nl_m\bar{h}_0}{2}\right)-\frac{N^3l_m\bar{h}_0^2}{4}cosech^2\left(\frac{Nl_m\bar{h}_0}{2}\right)coth\left(\frac{Nl_m\bar{h}_0}{2}\right)\end{aligned}\right\} \tag{4.7}$$

Equations (4.4), (4.5) and (4.6) represent governing differential equations for perturbed pressure.

Boundary conditions for perturbed pressures are:

1. Steady state pressures and perturbed pressures at ends of bearing are zero.

$$\bar{p}_i(\theta,\bar{z})=0,\qquad i=0,1,2\ at\ \bar{z}=\pm1\} \tag{4.8 a}$$

2. Pressure distribution is symmetrical about mid-plane for steady state pressures and perturbed pressures of bearing.

$$\left.\frac{\partial \bar{p}_i(\theta,\bar{z})}{\partial \bar{z}} = 0, \qquad i = 0,1,2 \; at \; \bar{z} = 0\right\}$$

(4.8 b)

3. Cavitation boundary conditions:

$$\left.\begin{gathered}\bar{p}_0(\theta_2,\bar{z}) = \frac{\partial \bar{p}_0(\theta_2,\bar{z})}{\partial \bar{z}} = 0 \\ \bar{p}_i(\theta,\bar{z}) = 0, \qquad i = 0,1,2 \quad for \quad \theta_2 \le \theta \le \theta_1\end{gathered}\right\}$$

(4.8 c)

Where θ_1 and θ_2 represents angles at end and start of hydrodynamic film at each axial plane of bearing. During computation all negative pressure are set to be zero in order to implement Reynolds cavitation boundary conditions.

4. Periodic boundary conditions:

$$\bar{p}_i(\theta,\bar{z}) = \bar{p}_i(\theta + 2\pi,\bar{z}), \quad i = 0,1,2\}$$

(4.8 d)

4.2.3 Numerical solution for pressures

4.2.3.1 Finite difference method (FDM)

Equations (4.5) and (4.6) are solved by using FDM with SOR scheme as discussed by Castelli et al. [47] to obtain perturbed pressure distributions $\bar{p}_1$and $\bar{p}_2$, satisfying boundary conditions as given in equation (4.8).

Following geometrical and operational symmetry of bearing over mid-plane, half of bearing length is considered and bearing surface area is divided into rectangular mesh of size($\Delta\theta \times \Delta\bar{z}$). First and second order derivatives of pressures are approximated by central difference method.

$$\left.\begin{gathered}\frac{\partial \bar{p}_n}{\partial \theta} = \frac{(\bar{p}_n)_{i+1,j} - (\bar{p}_n)_{i-1,j}}{2(\Delta\theta)} \\ \frac{\partial^2 \bar{p}_n}{\partial \theta^2} = \frac{(\bar{p}_n)_{i+1,j} - 2(\bar{p}_n)_{i,j} + (\bar{p}_n)_{i-1,j}}{(\Delta\theta)^2} \\ \frac{\partial^2 \bar{p}_n}{\partial \bar{z}^2} = \frac{(\bar{p}_n)_{i,j+1} - 2(\bar{p}_n)_{i,j} + (\bar{p}_n)_{i,j-1}}{(\Delta\bar{z})^2}\end{gathered}\right\}$$

Where n=1, 2

(4.9)

4.2.3.2 Perturbed pressure equations

With help of finite difference technique as stated in equation (4.9) and boundary condition in equation (4.8), equation (4.5) and (4.6) are reduced to give following pressure equations

$$(\bar{p}_1)_{i,j} = C_1(\bar{p}_1)_{i+1,j} + C_2(\bar{p}_1)_{i-1,j} + C_3(\bar{p}_1)_{i,j+1} + C_4(\bar{p}_1)_{i,j-1} + C_5(\bar{p}_0)_{i,j} + C_6(\bar{p}_0)_{i+1,j} + C_7(\bar{p}_0)_{i-1,j} + C_8(\bar{p}_0)_{i,j-1} + C_9(\bar{p}_0)_{i,j+1} + C_{10} \quad (4.10)$$

$$(\bar{p}_2)_{i,j} = C_1(\bar{p}_2)_{i+1,j} + C_2(\bar{p}_2)_{i-1,j} + C_3(\bar{p}_2)_{i,j+1} + C_4(\bar{p}_2)_{i,j-1} + C_{11}(\bar{p}_0)_{i,j} + C_{12}(\bar{p}_0)_{i+1,j} + C_{13}(\bar{p}_0)_{i-1,j} + C_{14}(\bar{p}_0)_{i,j-1} + C_{15}(\bar{p}_0)_{i,j+1} + C_{16} \quad (4.11)$$

Where $C_0, C_1, C_2, C_3 \; and \; C_4$ are as stated in equation (3.11) of chapter 3 and

$$C_5 = -\frac{(C_A)_{i,j}}{(C_B)_{i,j}} cos\theta_i;$$

$$C_6 = \frac{1}{C_0}\left[\frac{(C_A)_{i,j}}{(C_B)_{i,j}}\left\{\cos\theta_i - \frac{\Delta\theta}{2}sin\theta_i\right\} - \frac{(C_C)_{i,j}}{2(C_B)_{i,j}}\varepsilon_0(\Delta\theta)sin\theta_i cos\theta_i + \frac{(C_C)_{i,j}}{(C_B)_{i,j}}cos\theta_i\frac{Z_1}{4}\right]$$

$$C_7 = \frac{1}{C_0}\left[\frac{(C_A)_{i,j}}{(C_B)_{i,j}}\left\{\cos\theta_i + \frac{\Delta\theta}{2}sin\theta_i\right\} + \frac{(C_C)_{i,j}}{2(C_B)_{i,j}}\varepsilon_0(\Delta\theta)sin\theta_i cos\theta_i - \frac{(C_C)_{i,j}}{(C_B)_{i,j}}cos\theta_i\frac{Z_1}{4}\right]$$

$$C_8 = \left(\frac{D}{L}\right)^2\left(\frac{\Delta\theta}{\Delta\bar{z}}\right)^2\frac{1}{C_0}\left[\frac{(C_A)_{i,j}}{(C_B)_{i,j}}\left\{1 + \frac{\Delta\bar{z}}{2}\right\} + \frac{(C_C)_{i,j}}{(C_B)_{i,j}}\frac{Z_2}{4}\right]\cos\theta_i$$

$$C_9 = \left(\frac{D}{L}\right)^2\left(\frac{\Delta\theta}{\Delta\bar{z}}\right)^2\frac{1}{C_0}\left[\frac{(C_A)_{i,j}}{(C_B)_{i,j}}\left\{1 - \frac{\Delta\bar{z}}{2}\right\} - \frac{(C_C)_{i,j}}{(C_B)_{i,j}}\frac{Z_2}{4}\right]\cos\theta_i$$

$$C_{10} = \frac{(\Delta\theta)^2}{2C_0(C_B)_{i,j}}[\sin\theta_i - 2i\lambda_R\cos\theta_i]$$

$$C_{11} = -\frac{(C_A)_{i,j}}{(C_B)_{i,j}}sin\theta_i$$

$$C_{12} = \frac{1}{C_0}\left[\frac{(C_A)_{i,j}}{(C_B)_{i,j}}\left\{\sin\theta_i + \frac{\Delta\theta}{2}cos\theta_i\right\} - \frac{(C_C)_{i,j}}{2(C_B)_{i,j}}\varepsilon_0(\Delta\theta)sin^2\theta_i c + \frac{(C_C)_{i,j}}{(C_B)_{i,j}}sin\theta_i\frac{Z_1}{4}\right]$$

$$C_{13} = \frac{1}{C_0}\left[\frac{(C_A)_{i,j}}{(C_B)_{i,j}}\left\{\sin\theta_i - \frac{\Delta\theta}{2}cos\theta_i\right\} + \frac{(C_C)_{i,j}}{2(C_B)_{i,j}}\varepsilon_0(\Delta\theta)sin^2\theta_i c - \frac{(C_C)_{i,j}}{(C_B)_{i,j}}sin\theta_i\frac{Z_1}{4}\right]$$

$$C_{14} = \left(\frac{D}{L}\right)^2\left(\frac{\Delta\theta}{\Delta\bar{z}}\right)^2\frac{1}{C_0}\left[\frac{(C_A)_{i,j}}{(C_B)_{i,j}}\left\{1 + \frac{\Delta\bar{z}}{2}\right\} + \frac{(C_C)_{i,j}}{(C_B)_{i,j}}\frac{Z_2}{4}\right]\sin\theta_i$$

$$C_{15} = \left(\frac{D}{L}\right)^2\left(\frac{\Delta\theta}{\Delta\bar{z}}\right)^2\frac{1}{C_0}\left[\frac{(C_A)_{i,j}}{(C_B)_{i,j}}\left\{1 - \frac{\Delta\bar{z}}{2}\right\} - \frac{(C_C)_{i,j}}{(C_B)_{i,j}}\frac{Z_2}{4}\right]\sin\theta_i$$

$$C_{16} = -\frac{(\Delta\theta)^2}{2C_0(C_B)_{i,j}}\left[\cos\theta_i + 4i\lambda_R\sin\theta_i - \frac{i\lambda_R Z_1}{\varepsilon_0\Delta\theta}\right]$$

$$\theta_i = i(\Delta\theta)$$

(4.12)

Where, $(C_A)_{i,j}$, $(C_B)_{i,j}$ and $(C_C)_{i,j}$ are to be calculated by using equation (4.7), in which $\bar{h}_0 = \left(\bar{h}_0\right)_{i,j}$, $\frac{\partial \bar{h}_0}{\partial \bar{z}} = \left(\frac{\partial \bar{h}_0}{\partial \bar{z}}\right)_{i,j}$ and $\frac{\partial \bar{h}_0}{\partial \theta} = \left(\frac{\partial \bar{h}_0}{\partial \theta}\right)_{i,j}$ are to be calculated corresponding to each θ_i and $\bar{z}_j$. $\bar{h}_0$ is calculated in same manner as described in chapter 3.

To compute non-dimensional pressures numerically number of divisions along θ_i and $\bar{z}$ axes i.e. along bearing circumference and bearing length, considering half of bearing length, are taken as 178 and 18 respectively. Since perturbed pressure distributions are also symmetrical over mid-plane of bearing, half of bearing length is taken only. Iteration is started considering initial pressures at all mesh points as zeros and computed grid pressures are modified through SOR scheme. Iteration is terminated with convergence criterion for every pressure as $\left|\frac{\sum \bar{p}_i^{n+1} - \sum \bar{p}_i^{n}}{\sum \bar{p}_i^{n+1}}\right| \leq 0.001$ where, i = 1, 2.

4.2.4 Stiffness and damping coefficients

Components of dynamic load along line of centers and perpendicular to line of centers corresponding to perturbed pressure $\left(p_1 \varepsilon_1 e^{i\lambda_R \bar{t}}\right)$ in R-direction can be written as under

$$(W_d)_R e^{i\lambda_R \bar{t}} = -2 \int_0^{L/2} \int_{\theta_1}^{\theta_2} p_1 \cos\theta \, \varepsilon_1 e^{i\lambda_R \bar{t}} R d\theta dz \tag{4.13}$$

$$(W_d)_\phi e^{i\lambda_R \bar{t}} = -2 \int_0^{L/2} \int_{\theta_1}^{\theta_2} p_1 \sin\theta \, \varepsilon_1 e^{i\lambda_R \bar{t}} R d\theta dz \tag{4.14}$$

Journal executes small harmonic oscillation about its steady state position in an elliptic orbit. So, components of dynamic load can be expressed as a spring load and viscous damping load.

$$(W_d)_R e^{i\lambda_R \bar{t}} = S_{RR} C \varepsilon_R + D_{RR} \frac{d}{dt}(C \varepsilon_R) \tag{4.15}$$

$$(W_d)_\phi e^{i\lambda_R \bar{t}} = S_{\phi R} C \varepsilon_R + D_{\phi R} \frac{d}{dt}(C \varepsilon_R) \tag{4.16}$$

Combining equation (4.13) through (4.16), non-dimensionalising and noting that $\varepsilon_R = \varepsilon_1 e^{i\lambda_R \bar{t}}$, following components of stiffness and damping coefficient in non-dimensional form result

$$\left.\begin{aligned} \bar{S}_{RR} &= -Re\left[2\int_0^1\int_{\theta_1}^{\theta_2} \bar{p}_1 \cos\theta \, d\theta d\bar{z}\right] \\ \bar{S}_{\phi R} &= -Re\left[2\int_0^1\int_{\theta_1}^{\theta_2} \bar{p}_1 \sin\theta \, d\theta d\bar{z}\right] \\ \bar{D}_{RR} &= -Im\left[2\int_0^1\int_{\theta_1}^{\theta_2} \bar{p}_1 \cos\theta \, d\theta d\bar{z}\right]\Big/\lambda_R \\ \bar{D}_{\phi R} &= -Im\left[2\int_0^1\int_{\theta_1}^{\theta_2} \bar{p}_1 \sin\theta \, d\theta d\bar{z}\right]\Big/\lambda_R \end{aligned}\right\} \tag{4.17}$$

Similarly, considering dynamic displacement of journal along ϕ-direction, it can be shown that

$$\left.\begin{aligned} \bar{S}_{R\phi} &= -Re\left[2\int_0^1\int_{\theta_1}^{\theta_2} \bar{p}_2 \cos\theta \, d\theta d\bar{z}\right] \\ \bar{S}_{\phi\phi} &= -Re\left[2\int_0^1\int_{\theta_1}^{\theta_2} \bar{p}_2 \sin\theta \, d\theta d\bar{z}\right] \\ \bar{D}_{R\phi} &= -Im\left[2\int_0^1\int_{\theta_1}^{\theta_2} \bar{p}_2 \cos\theta \, d\theta d\bar{z}\right]\Big/\lambda_R \\ \bar{D}_{\phi\phi} &= -Im\left[2\int_0^1\int_{\theta_1}^{\theta_2} \bar{p}_2 \sin\theta \, d\theta d\bar{z}\right]\Big/\lambda_R \end{aligned}\right\} \tag{4.18}$$

$$\bar{S}_{ij} = \frac{2C^3 S_{ij}}{\mu\omega R^3 L} \; and \; \bar{D}_{ij} = \frac{2C^3 D_{ij}}{\mu\omega R^3 L}, i = R, \phi \; and \; j = R, \phi.$$

dynamic pressure distributions $\bar{p}_1$ and $\bar{p}_2$ have been obtained by FDM, above components of stiffness and damping coefficients can be easily obtained by numerical integration applying Simpson's 1/3rd rule.

4.2.5 Stability analysis of rigid rotor

Stability of bearing is studied through critical value of mass parameter and corresponding whirl ratio. Assuming journal to be rigid and of mass *M* per bearing. Equations of motion of journal can be written as

$$MC\left[\frac{d^2\varepsilon}{dt^2} - \varepsilon\left(\frac{d\phi}{dt}\right)^2\right] = F_R + Wcos\phi \tag{4.19}$$

$$MC\left[\varepsilon\frac{d^2\phi}{dt^2} + 2\frac{d\phi}{dt}\frac{d\varepsilon}{dt}\right] = F_\phi - Wsin\phi \tag{4.20}$$

To test stability, journal center motion is assumed to be such that

$$\varepsilon = \varepsilon_0 + \varepsilon_1 e^{i\lambda_R \bar{t}} \; and \; \phi = \phi_0 + \phi_1 e^{i\lambda_R \bar{t}} \tag{4.21}$$

For steady state following relationship exists

$$\left.\begin{aligned}(F_R)_0 + W_0 cos\phi_0 = 0\\ \left(F_\phi\right)_0 - W_0 sin\phi_0 = 0\end{aligned}\right\} \tag{4.22}$$

$(F_R)_0 \; and \; \left(F_\phi\right)_0$ are steady state components of lubricating film forces along R- and ϕ-directions respectively.

Substituting equations (4.21) and (4.22) into equation (4.19) and (4.20) and neglecting second order terms in ε_1 and $\varepsilon_0\phi_1$, equations of motion in non-dimensional forms are obtained as follows

$$(-\bar{M}\bar{W}_0\lambda_R^2 + \bar{S}_{RR} + i\lambda_R\bar{D}_{RR})\varepsilon_1 + \left(\varepsilon_0\bar{S}_{R\phi} + i\varepsilon_0\lambda_R\bar{D}_{R\phi} + \bar{W}_0 sin\phi_0\right)\phi_1 = 0 \tag{4.23}$$

$$\left(\bar{S}_{\phi R} + i\lambda_R\bar{D}_{\phi R}\right)\varepsilon_1 + \left(-\bar{M}\bar{W}_0\varepsilon_0\lambda_R^2 + \varepsilon_0\bar{S}_{\phi\phi} + i\varepsilon_0\lambda_R\bar{D}_{\phi\phi}\bar{W}_0 cos\phi_0\right)\phi_1 = 0 \tag{4.24}$$

For non-trivial solution of ε_1 and ϕ_1, determinant of equations (4.23) and (4.24) must vanish and thus

$$\begin{vmatrix}(-\bar{M}\bar{W}_0\lambda_R^2 + \bar{S}_{RR} + i\lambda_R\bar{D}_{RR}) & \left(\varepsilon_0\bar{S}_{R\phi} + i\varepsilon_0\lambda_R\bar{D}_{R\phi} + \bar{W}_0 sin\phi_0\right)\\ \left(\bar{S}_{\phi R} + i\lambda_R\bar{D}_{\phi R}\right) & \left(-\bar{M}\bar{W}_0\varepsilon_0\lambda_R^2 + \varepsilon_0\bar{S}_{\phi\phi} + i\varepsilon_0\lambda_R\bar{D}_{\phi\phi}\bar{W}_0 cos\phi_0\right)\end{vmatrix} = 0 \tag{4.25}$$

Equating imaginary and real terms of equation (4.24) separately to zero, following two equations result

$$\bar{M}\bar{W}_0 = \frac{\left[\left(\bar{S}_{\phi\phi}\bar{D}_{RR} + \bar{S}_{RR}\bar{D}_{\phi\phi}\right) - \left(\bar{S}_{\phi R}\bar{D}_{R\phi} + \bar{S}_{R\phi}\bar{D}_{\phi R}\right) - \frac{\bar{W}_0}{\varepsilon_0}\left(\bar{D}_{\phi R}\sin\phi_0 - \bar{D}_{RR}\,cos\phi_0\right)\right]}{\lambda_R^2\left(\bar{D}_{RR} + \bar{D}_{\phi\phi}\right)} \tag{4.26}$$

$$(\bar{M}\bar{W}_0)^2\lambda_R^4 - \left[\bar{M}\bar{W}_0\left(\bar{S}_{RR} + \bar{S}_{\phi\phi} + \frac{\bar{W}_0 cos\phi_0}{\varepsilon_0}\right) + \left(\bar{D}_{RR}\bar{D}_{\phi\phi} - \bar{D}_{R\phi}\bar{D}_{\phi R}\right)\right]\lambda_R^2 + \left(\bar{S}_{RR}\bar{S}_{\phi\phi} - \bar{S}_{R\phi}\bar{S}_{\phi R}\right) + \frac{\bar{W}_0}{\varepsilon_0}\left(\bar{S}_{RR}\cos\phi_0 - \bar{S}_{\phi R}sin\phi_0\right) = 0 \tag{4.27}$$

From equation (4.26) and (4.27), $\bar{M}$ and λ_R can be calculated. $\bar{M}$, thus calculated, represents critical mass parameter ($\bar{M}_C$), threshold value of $\bar{M}$ above which bearing will be unstable and λ_R represents corresponding whirl ratio. Journal speed corresponding to critical mass parameter is threshold speed ω_s.

4.3 Result and discussion

Dynamic characteristics in terms of critical mass parameter ($\bar{M}_C$) and whirl ratio (λ_R) are calculated using components of stiffness and damping coefficients. λ_R and $\bar{M}_C$ are dependent on steady state and perturbed film pressures $\bar{p}_0, \bar{p}_1$ and $\bar{p}_2$, and thus, in turn, depend upon eccentricity ratio (ε_0), slenderness ratio ($\frac{L}{D}$), characteristic length (l_m), coupling number (N) and radial deformation of bearing liner surface $\left(\bar{\delta}\right)$. Radial deformation of bearing liner surface$\left(\bar{\delta}\right)$ depends upon Poisson's ratio (ν), deformation factor (F) and bearing liner thickness to journal radius ratio ($\frac{H}{R}$). For parametric study, deformation factor (F) has been chosen as independent variable and others as parameters.

In order to validate authenticity of program, result generated by current program (assuming parameters values as per majumdar et al. [29] and Das et al. [143]) are compared with published results. Figure 4.2 shows variation of mass parameter with F for various ε_0. In this graph, values generated by current program are shown in comparison to values which are already published by majumdar et al. [29]. Figure 4.3 presents variation of mass parameter in comparison with l_m. Results in form of graph show comparison between results generated by current program and results already published by Das et al. [143]. Comparison of figure 4.2

and 4.3 shows that results generated by current program are within 4-7% of published result which is a good margin to believe authenticity of current program, taking into consideration that results are generated using different programs and assuming different round off criterion.

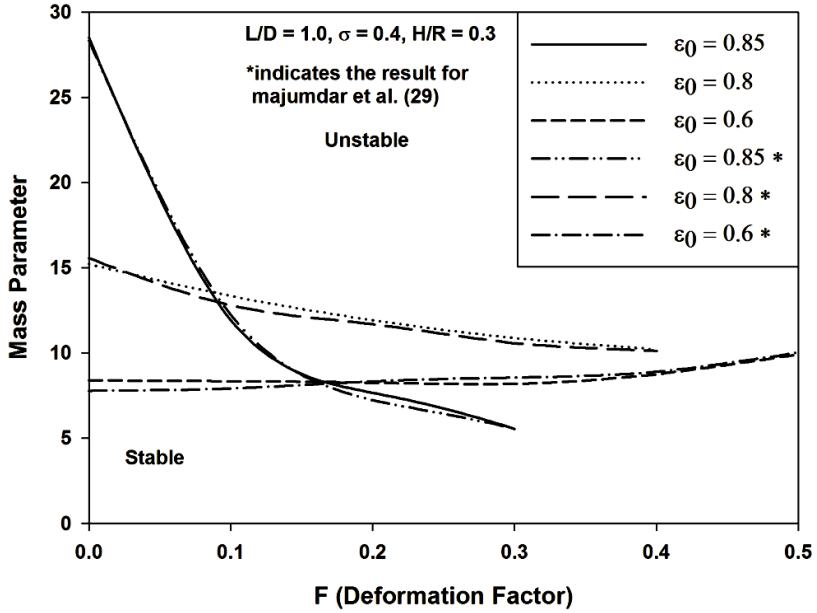

Figure 4.2 $\bar{M}_C$ Vs. F (Newtonian fluid).

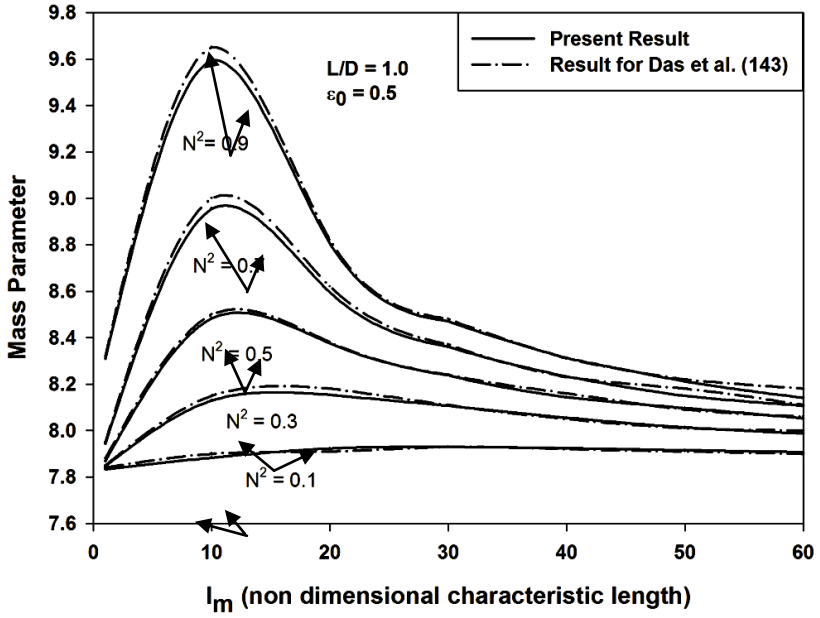

Figure 4.3 $\bar{M}_C$ Vs. l_m for various N^2 at $\varepsilon_0 = 0.5$ and $\frac{L}{D} = 1.0$ (Rigid Bearing under micropolar lubrication).

4.3.1 Non-dimensional Components of Stiffness and Damping Coefficients

4.3.1.1 Effect of eccentricity ratio (ε_0):

Figures 4.4 through 4.11 show variation of non-dimensional components of damping and stiffness coefficients as a function of deformation factor (F) when eccentricity ratio is

considered as parameter, keeping $\frac{L}{D}, N^2, l_m, \frac{H}{R}, \nu$ fixed at 1.0, 0.5, 40.0, 0.3 and 0.4 respectively.

It can be observed from graphs 4.5 and 4.7 that values of direct components of stiffness coefficients $\bar{S}_{RR}$ and $\bar{S}_{\phi\phi}$ decrease as deformation factor increases. It can also be seen clearly that direct components of stiffness increases as eccentricity increases. However, it is found that at higher eccentricity ratio decrease in direct components of stiffness is quite sharp as deformation factor increases. Trends are similar to trends shown by non-dimensional mass parameter. Variation of cross coupled components of stiffness $-\bar{S}_{\phi R}$ and $\bar{S}_{R\phi}$ can be seen in graphs shown in figure 4.4 and 4.6. Trends of curves in graph show similar trends as shown by direct components of stiffness.

Effect of eccentricity ratio on direct and cross coupled damping components can be seen in figures 4.8 through 4.11. Trend in graphs show that damping components decreases with increase in F and increases with increase in ε_0.

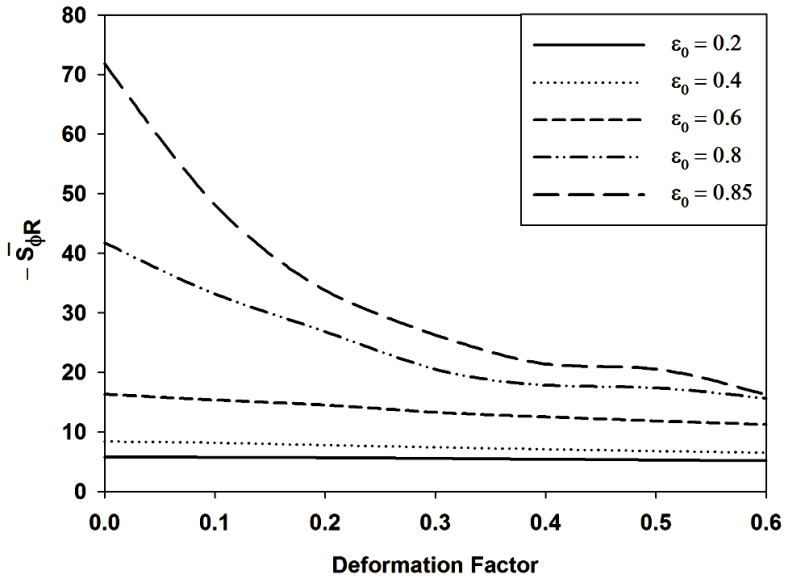

Figure 4.4 $-\bar{S}_{\phi R}$ Vs. F for various ε_0 at L/D=1.0, N^2=0.5, l_m=40.0, H/R=0.3, ν=0.4.

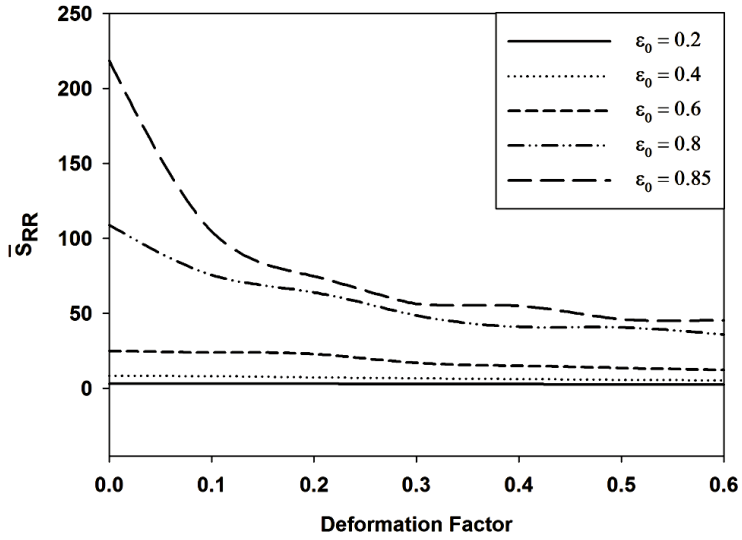

Figure 4.5 $\bar{S}_{RR}$ Vs. F for various ε_0 at $\frac{L}{D} = 1.0, N^2 = 0.5, l_m = 40.0, \frac{H}{R} = 0.3, \nu = 0.4$.

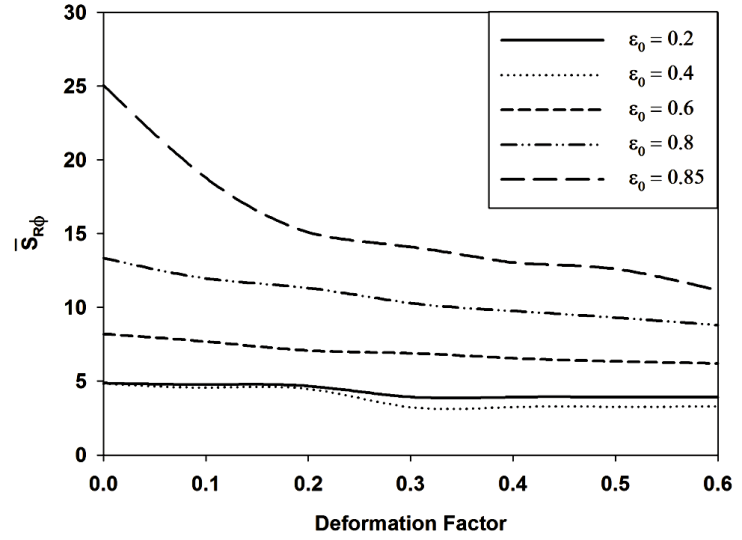

Figure 4.6 $\bar{S}_{R\phi}$ Vs. F for various ε_0 at $\frac{L}{D} = 1.0, N^2 = 0.5, l_m = 40.0, \frac{H}{R} = 0.3, \nu = 0.4$.

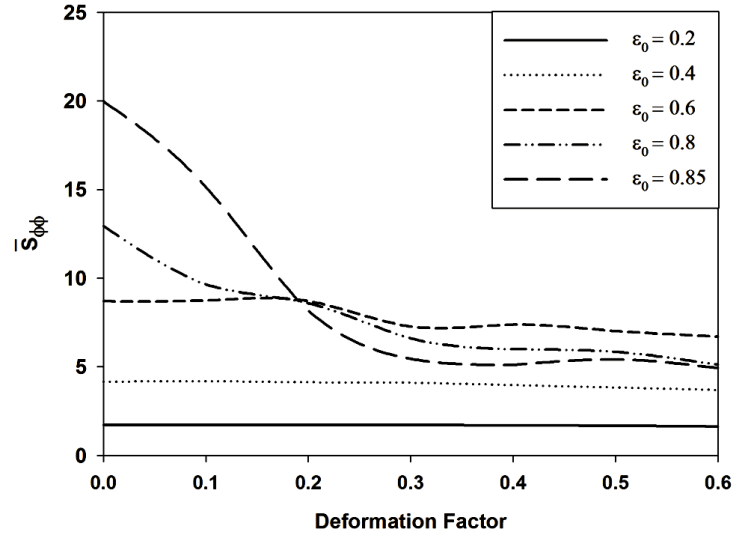

Figure 4.7 $\bar{S}_{\phi\phi}$ Vs. F for various ε_0 at $\frac{L}{D} = 1.0, N^2 = 0.5, l_m = 40.0, \frac{H}{R} = 0.3, \nu = 0.4$.

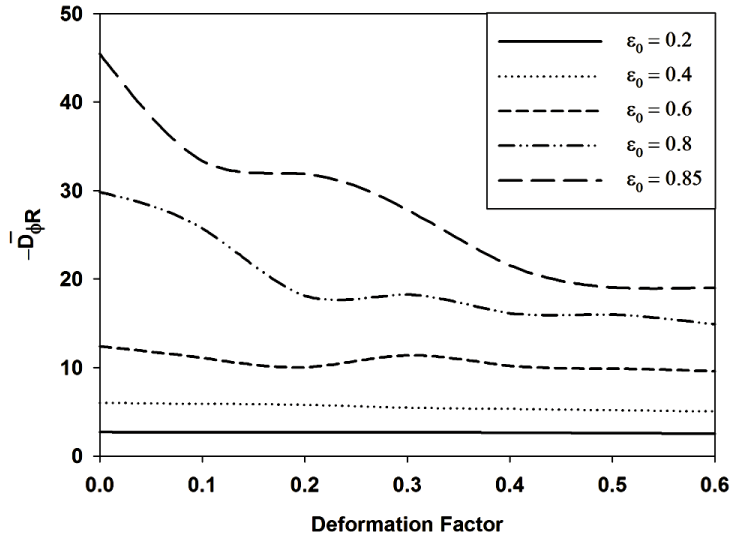

Figure 4.8 $-\bar{D}_{\phi R}$ Vs. F for various ε_0 at $\frac{L}{D} = 1.0, N^2 = 0.5, l_m = 40.0, \frac{H}{R} = 0.3, \nu = 0.4$.

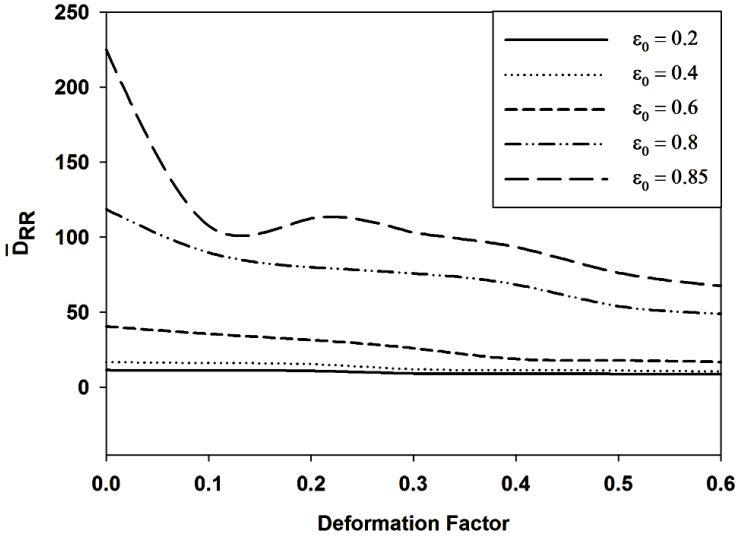

Figure 4.9 $\bar{D}_{RR}$ Vs. F for various ε_0 at $\frac{L}{D} = 1.0, N^2 = 0.5, l_m = 40.0, \frac{H}{R} = 0.3, \nu = 0.4$.

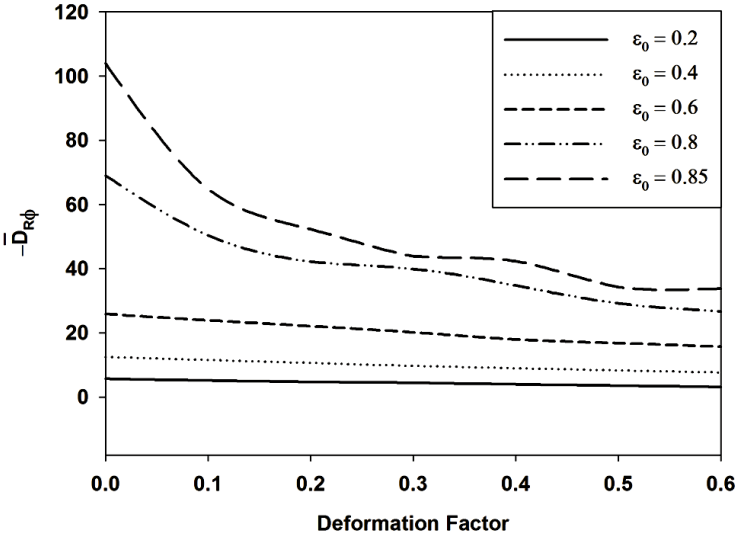

Figure 4.10 $-\bar{D}_{R\phi}$ Vs. F for various ε_0 at $\frac{L}{D} = 1.0, N^2 = 0.5, l_m = 40.0, \frac{H}{R} = 0.3, \nu = 0.4$.

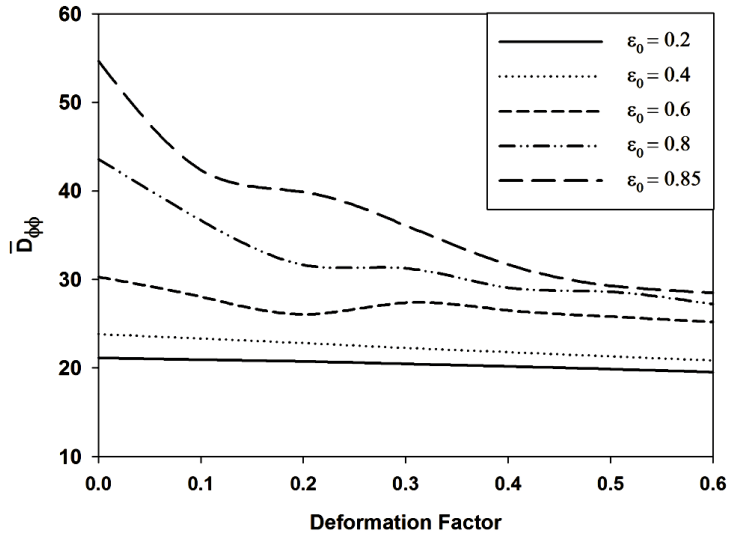

Figure 4.11 $\overline{D}_{\phi\phi}$ Vs. F for various ε_0 at $\frac{L}{D} = 1.0, N^2 = 0.5, l_m = 40.0, \frac{H}{R} = 0.3, \nu = 0.4$.

4.3.1.2 Effect of slenderness ratio ($\frac{L}{D}$):

Variation of components of damping and stiffness coefficients as function of F for various $\frac{L}{D}$ is shown in figures 4.12 through 4.19 at $\nu = 0.4, \frac{H}{R} = 0.3, N^2 = 0.5, l_m = 40.0$ and $\varepsilon_0 = 0.5$. Variation in graphs shows that components of stiffness and damping coefficients show higher trends with increase in slenderness ratio.

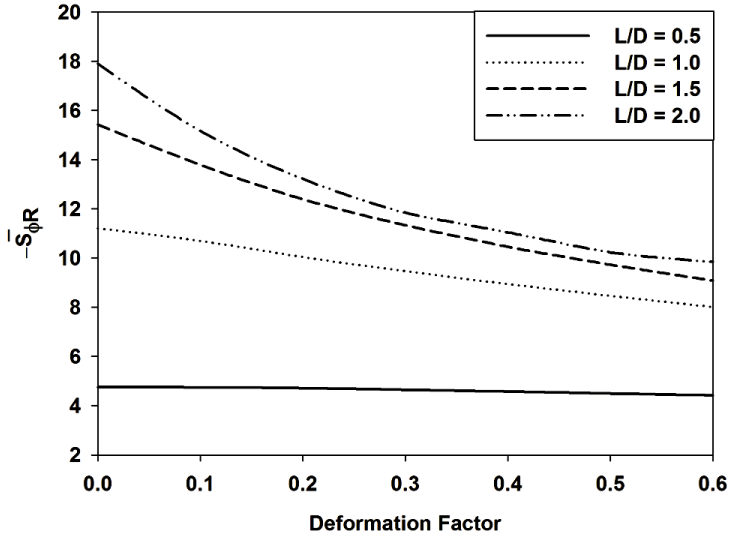

Figure 4.12 $-\bar{S}_{\phi R}$ Vs. F for various $\frac{L}{D}$ at $\varepsilon_0 = 0.5, N^2 = 0.5, l_m = 40.0, \frac{H}{R} = 0.3, \nu = 0.4$.

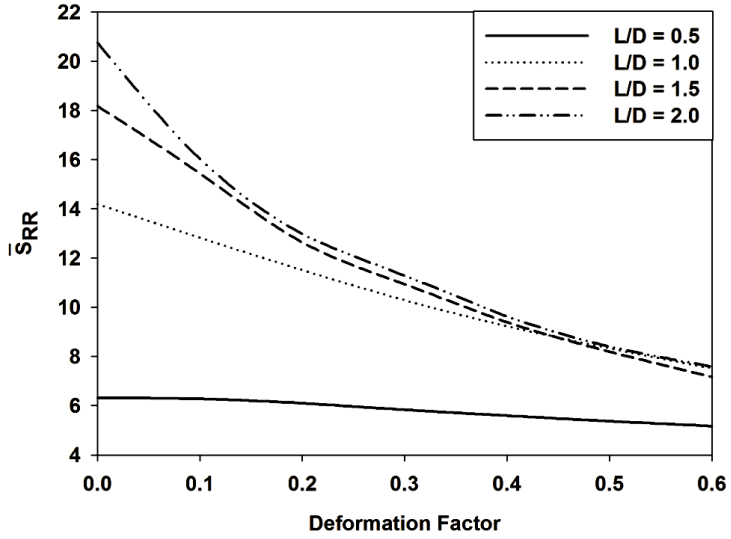

Figure 4.13 $\bar{S}_{RR}$ Vs. F for various $\frac{L}{D}$ at $\varepsilon_0 = 0.5, N^2 = 0.5, l_m = 40.0, \frac{H}{R} = 0.3, \nu = 0.4$.

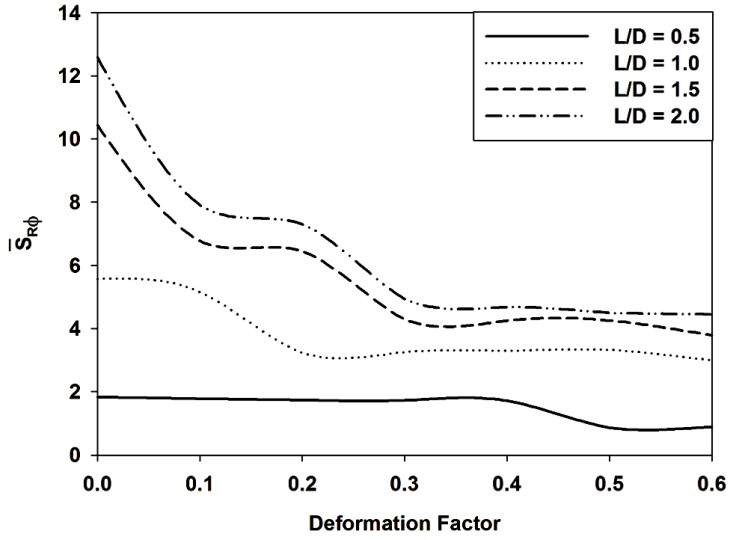

Figure 4.14 $\bar{S}_{R\phi}$ Vs. F for various $\frac{L}{D}$ at $\varepsilon_0 = 0.5, N^2 = 0.5, l_m = 40.0, \frac{H}{R} = 0.3, \nu = 0.4$.

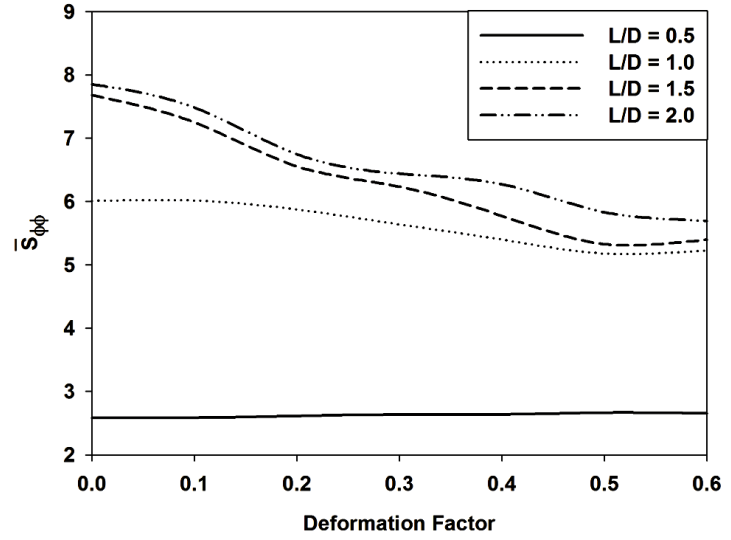

Figure 4.15 $\bar{S}_{\phi\phi}$ Vs. F for various $\frac{L}{D}$ at $\varepsilon_0 = 0.5, N^2 = 0.5, l_m = 40.0, \frac{H}{R} = 0.3, \nu = 0.4$.

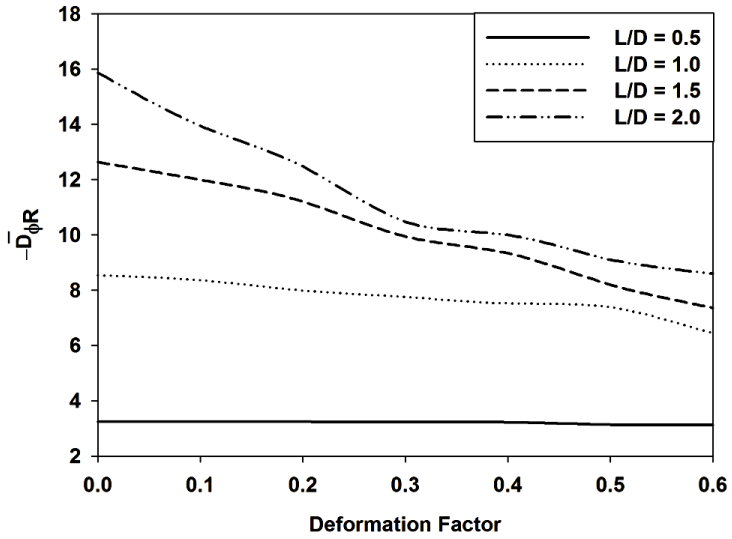

Figure 4.16 $-\bar{D}_{\phi R}$ Vs. F for various $\frac{L}{D}$ at $\varepsilon_0 = 0.5, N^2 = 0.5, l_m = 40.0, \frac{H}{R} = 0.3, \nu = 0.4$.

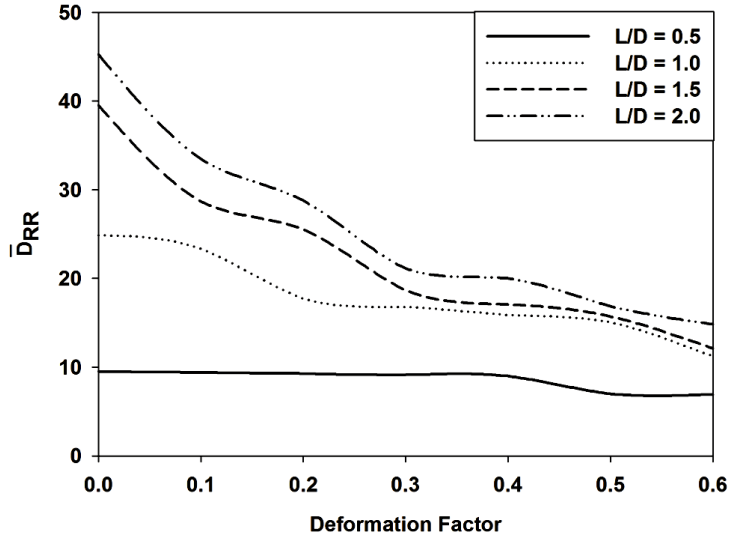

Figure 4.17 $\bar{D}_{RR}$ Vs. F for various $\frac{L}{D}$ at $\varepsilon_0 = 0.5, N^2 = 0.5, l_m = 40.0, \frac{H}{R} = 0.3, \nu = 0.4$.

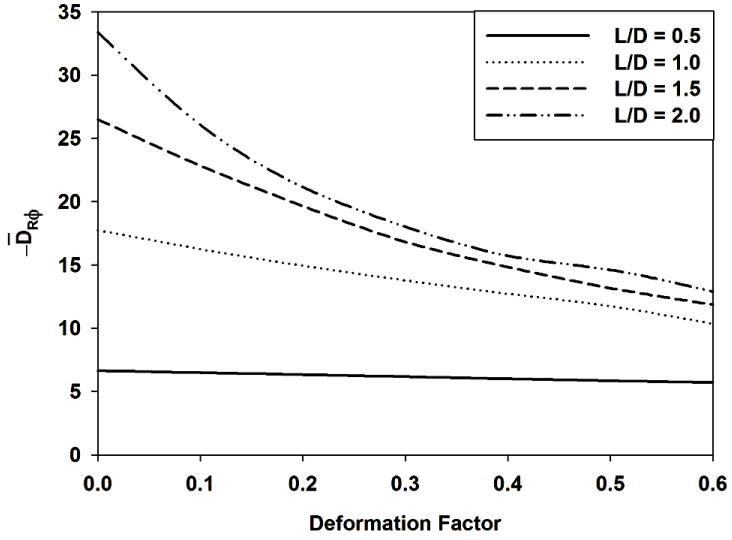

Figure 4.18 $-\bar{D}_{R\phi}$ Vs. F for various $\frac{L}{D}$ at $\varepsilon_0 = 0.5, N^2 = 0.5, l_m = 40.0, \frac{H}{R} = 0.3, \nu = 0.4$.

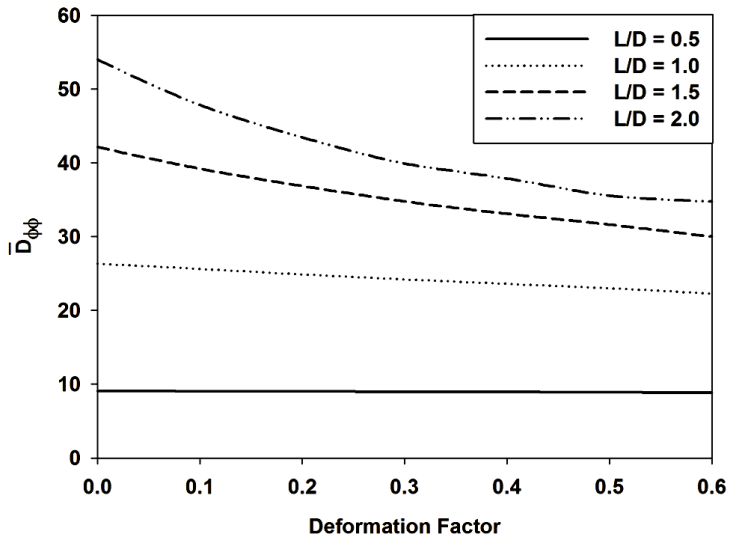

Figure 4.19 $\overline{D}_{\phi\phi}$ Vs. F for various $\frac{L}{D}$ at $\varepsilon_0 = 0.5, N^2 = 0.5, l_m = 40.0, \frac{H}{R} = 0.3, \nu = 0.4$.

4.3.1.3 Effect of Poisson's ratio (ν):

Effect of variation of ν on components of damping and stiffness coefficients can be seen in graphs shown in figures 4.20 through 4.27. Graphs in referred figure show trend of damping and stiffness components versus deformation factor (F) for various ν at $\frac{L}{D} = 1.0, \frac{H}{R} = 0.3, N^2 = 0.5, l_m = 40.0$ and $\varepsilon_0 = 0.5$. Trends in referred graphs show that damping and stiffness coefficients increases as Poisson's ratio is higher.

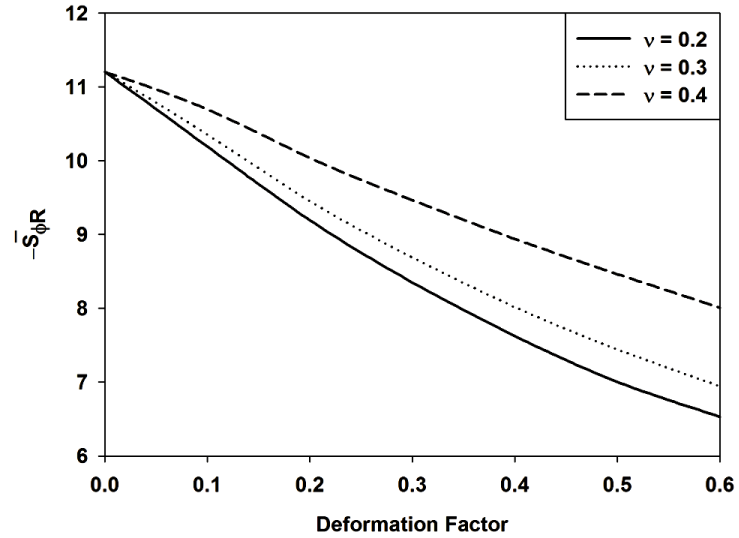

Figure 4.20 $-\bar{S}_{\phi R}$ Vs. F for various ν at $\frac{L}{D} = 1.0, \varepsilon_0 = 0.5, N^2 = 0.5, l_m = 40.0, \frac{H}{R} = 0.3$.

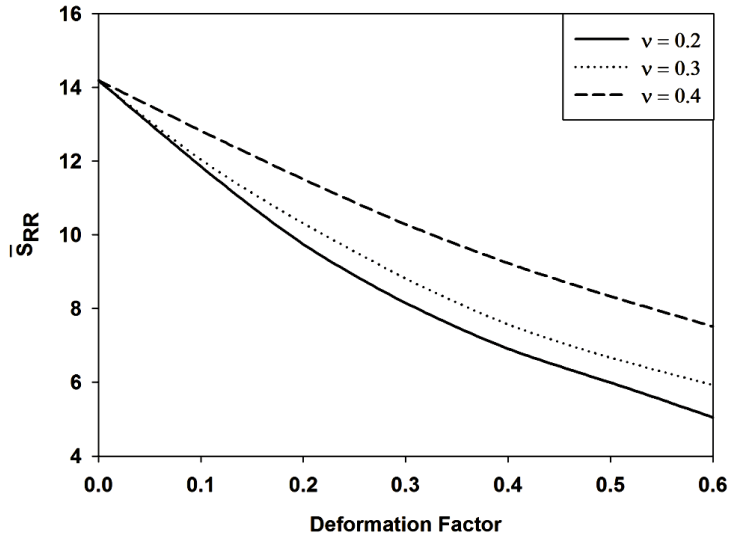

Figure 4.21 $\bar{S}_{RR}$ Vs. F for various ν at $\frac{L}{D} = 1.0, \varepsilon_0 = 0.5, N^2 = 0.5, l_m = 40.0, \frac{H}{R} = 0.3$.

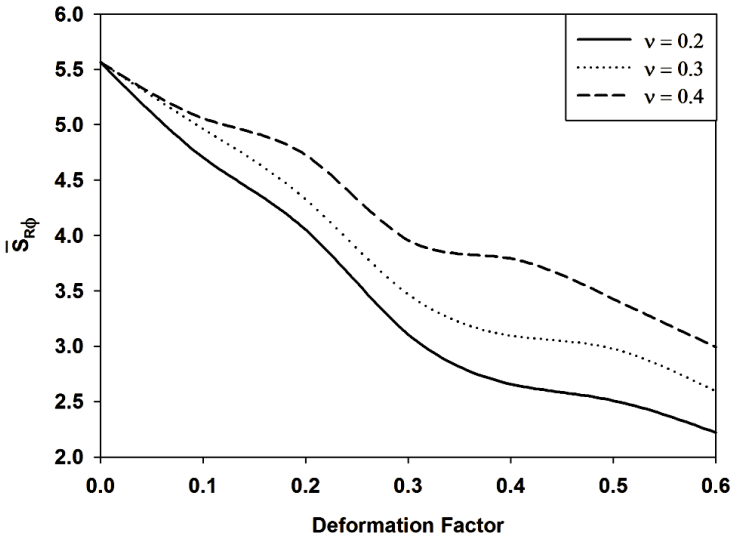

Figure 4.22 $\bar{S}_{R\phi}$ Vs. F for various ν at $\frac{L}{D} = 1.0, \varepsilon_0 = 0.5, N^2 = 0.5, l_m = 40.0, \frac{H}{R} = 0.3$.

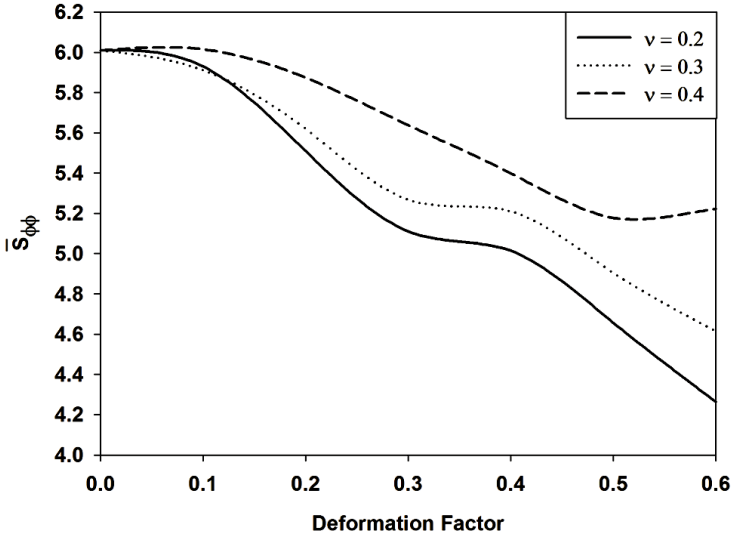

Figure 4.23 $\bar{S}_{\phi\phi}$ Vs. F for various ν at $\frac{L}{D} = 1.0, \varepsilon_0 = 0.5, N^2 = 0.5, l_m = 40.0, \frac{H}{R} = 0.3$.

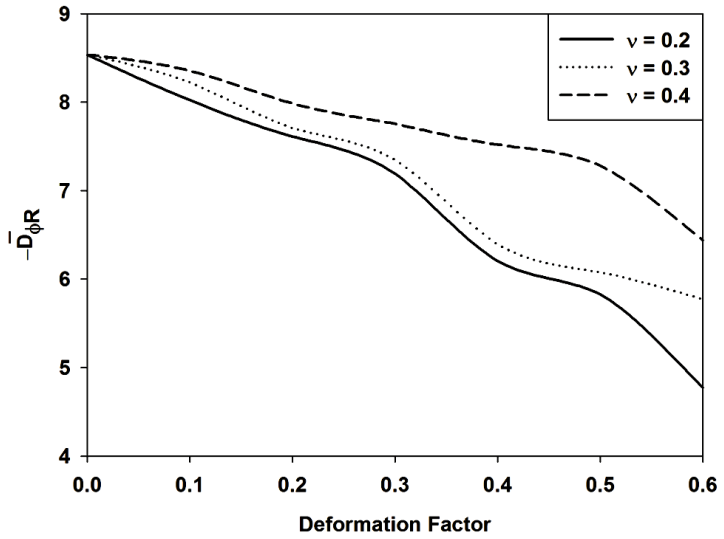

Figure 4.24 $-\bar{D}_{\phi R}$ Vs. F for various ν at $\frac{L}{D} = 1.0, \varepsilon_0 = 0.5, N^2 = 0.5, l_m = 40.0, \frac{H}{R} = 0.3$.

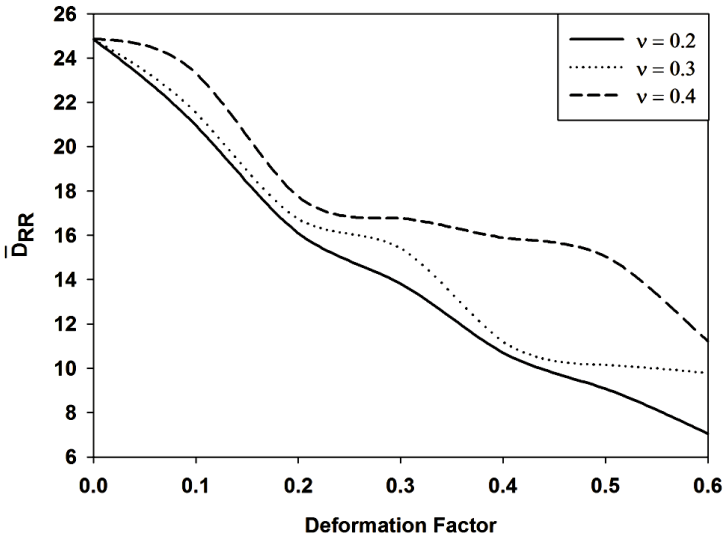

Figure 4.25 $\bar{D}_{RR}$ Vs. F for various ν at $\frac{L}{D} = 1.0, \varepsilon_0 = 0.5, N^2 = 0.5, l_m = 40.0, \frac{H}{R} = 0.3$.

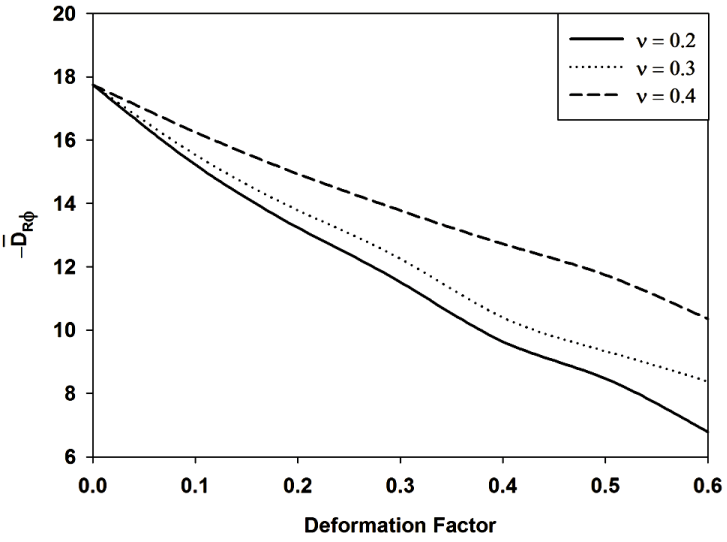

Figure 4.26 $-\bar{D}_{R\phi}$ Vs. F for various ν at $\frac{L}{D} = 1.0, \varepsilon_0 = 0.5, N^2 = 0.5, l_m = 40.0, \frac{H}{R} = 0.3$.

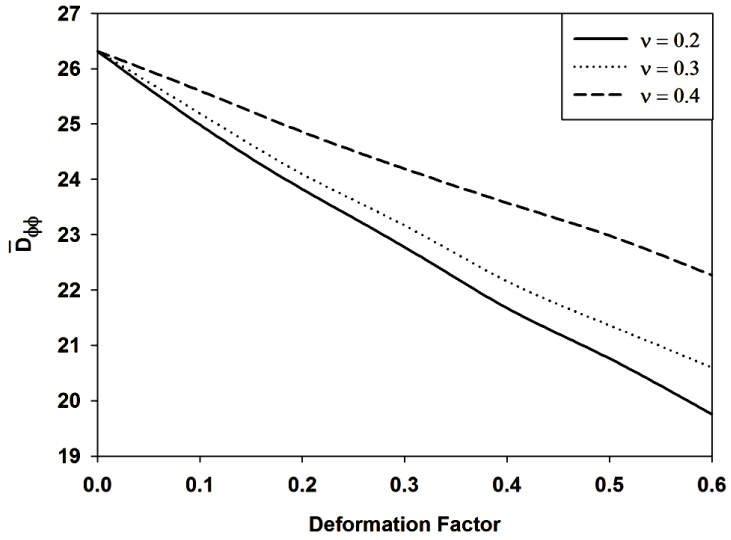

Figure 4.27 $\bar{D}_{\phi\phi}$ Vs. F for various ν at $\frac{L}{D} = 1.0, \varepsilon_0 = 0.5, N^2 = 0.5, l_m = 40.0, \frac{H}{R} = 0.3$.

4.3.1.4 Effect of $\frac{H}{R}$ ratio:

Figures 4.28 through 4.35 show variation of components of stiffness and damping coefficients versus deformation factor (F) for various $\frac{H}{R}$ ratio at $\frac{L}{D} = 1.0, \varepsilon_0 = 0.5, N^2 = 0.5, l_m = 40.0$ and $\nu = 0.4$. Graphs in figures show that values of damping and stiffness coefficients decreases as $\frac{H}{R}$ ratio is increased.

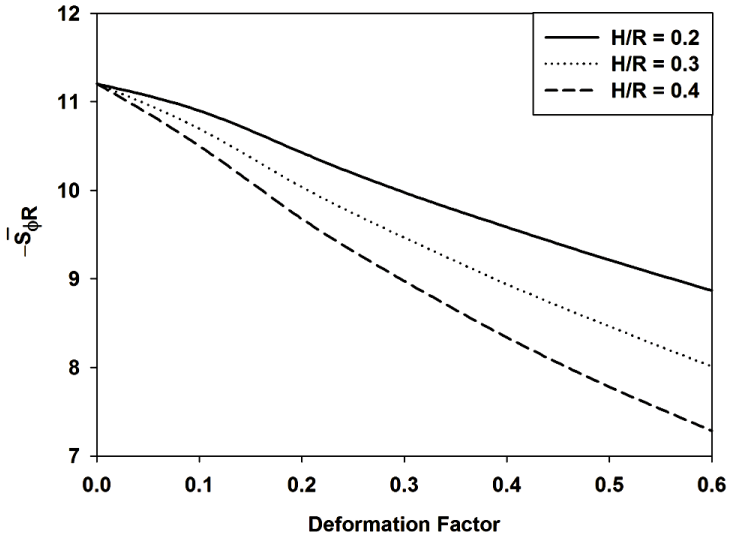

Figure 4.28 $-\bar{S}_{\phi R}$ Vs. F for various $\frac{H}{R}$ ratio at $\frac{L}{D} = 1.0, \varepsilon_0 = 0.5, N^2 = 0.5, l_m = 40.0, \nu = 0.4$.

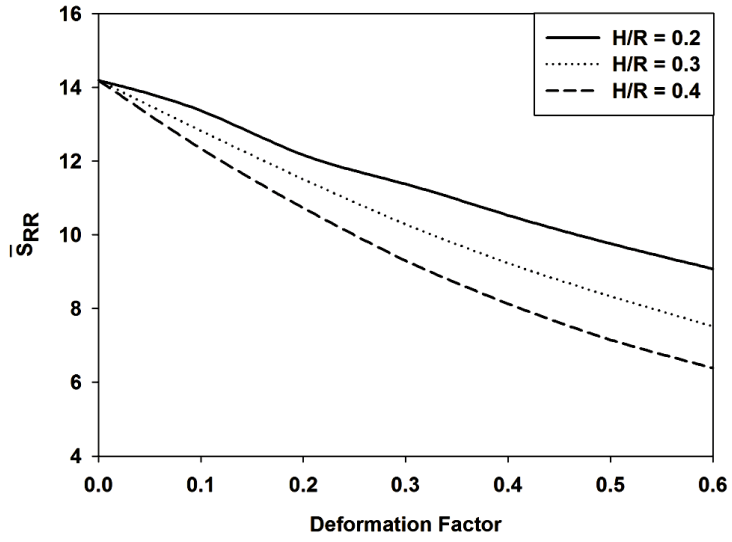

Figure 4.29 $\bar{S}_{RR}$ Vs. F for various $\frac{H}{R}$ ratio at $\frac{L}{D} = 1.0, \varepsilon_0 = 0.5, N^2 = 0.5, l_m = 40.0, \nu = 0.4$.

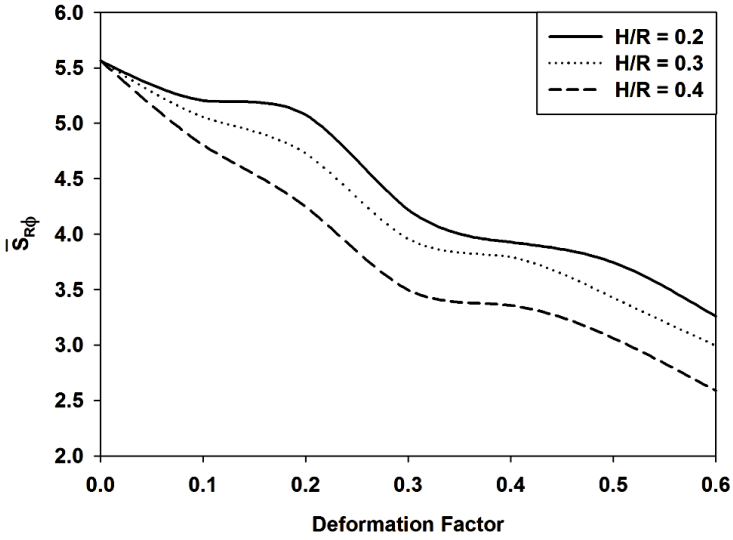

Figure 4.30 $\bar{S}_{R\phi}$ Vs. F for various $\frac{H}{R}$ ratio at $\frac{L}{D} = 1.0, \varepsilon_0 = 0.5, N^2 = 0.5, l_m = 40.0, \nu = 0.4$.

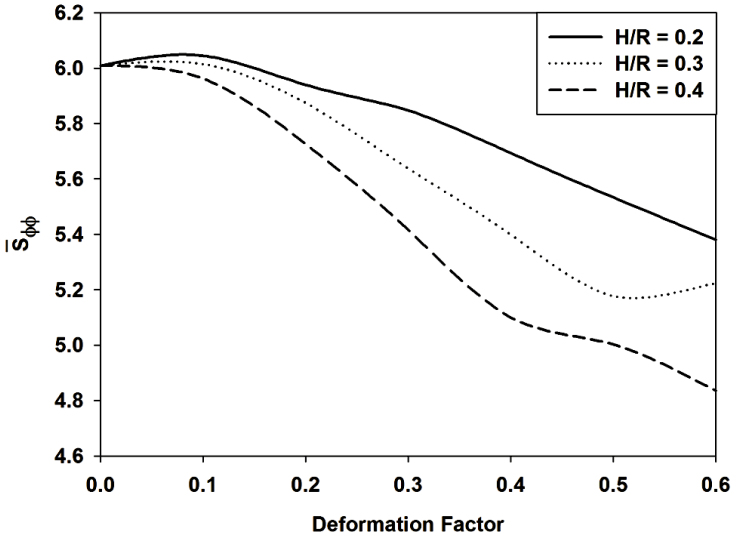

Figure 4.31 $\bar{S}_{\phi\phi}$ Vs. F for various $\frac{H}{R}$ ratio at $\frac{L}{D} = 1.0, \varepsilon_0 = 0.5, N^2 = 0.5, l_m = 40.0, \nu = 0.4$.

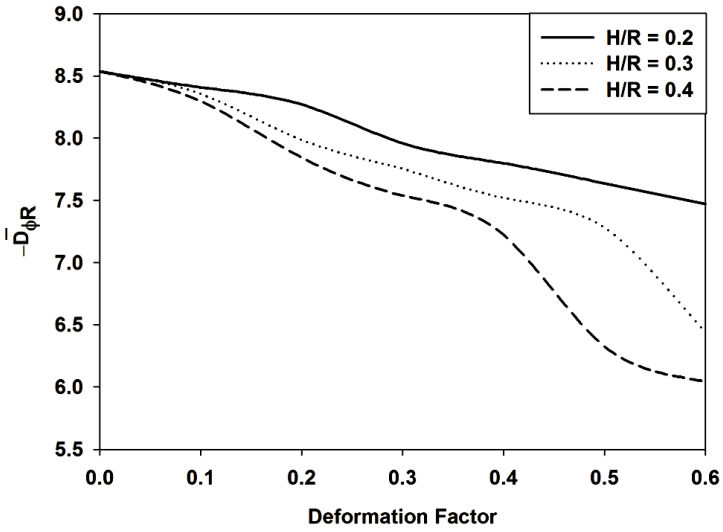

Figure 4.32 – $\overline{D}_{\phi R}$ Vs. F for various $\frac{H}{R}$ ratio at $\frac{L}{D} = 1.0, \varepsilon_0 = 0.5, N^2 = 0.5, l_m = 40.0, \nu = 0.4$.

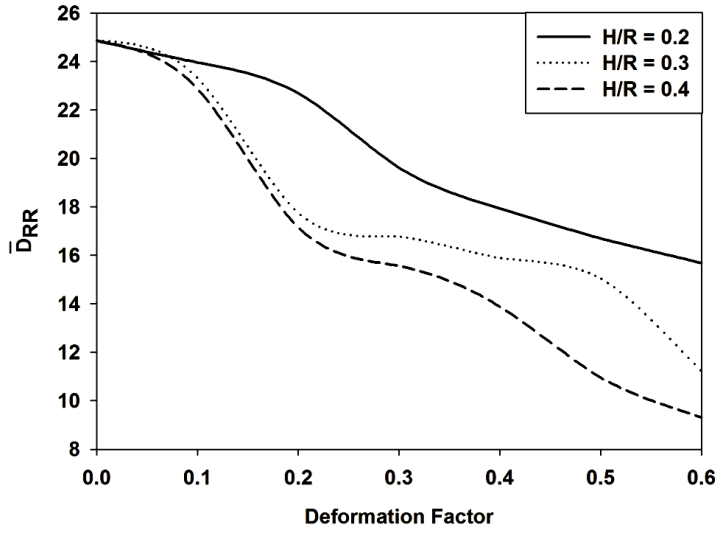

Figure 4.33 $\overline{D}_{RR}$ Vs. F for various $\frac{H}{R}$ ratio at $\frac{L}{D} = 1.0, \varepsilon_0 = 0.5, N^2 = 0.5, l_m = 40.0, \nu = 0.4$.

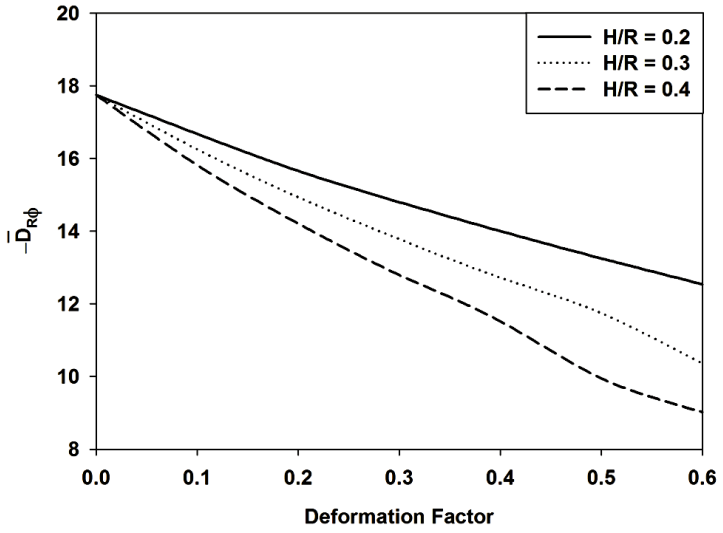

Figure 4.34 – $\overline{D}_{R\phi}$ Vs. F for various $\frac{H}{R}$ ratio at $\frac{L}{D} = 1.0, \varepsilon_0 = 0.5, N^2 = 0.5, l_m = 40.0, \nu = 0.4$.

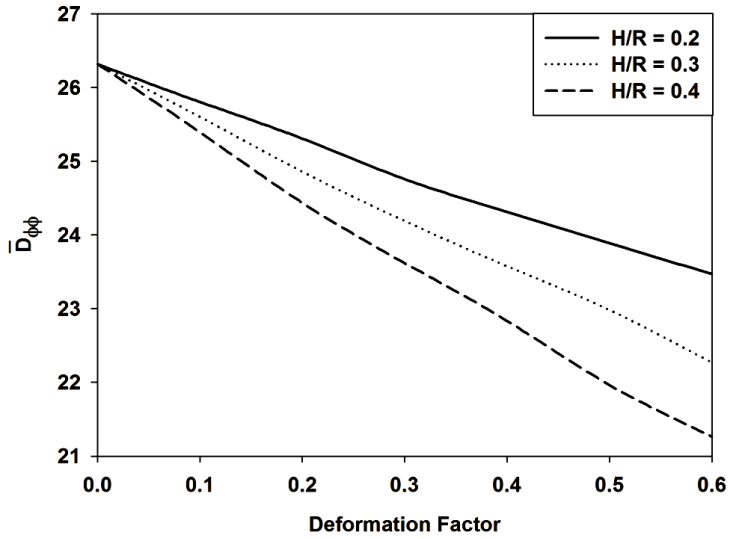

Figure 4.35 $\bar{D}_{\phi\phi}$ Vs. F for various $\frac{H}{R}$ ratio at $\frac{L}{D} = 1.0, \varepsilon_0 = 0.5, N^2 = 0.5, l_m = 40.0, \nu = 0.4$.

4.3.1.5 Effect of characteristic length (l_m):

Effect of non-dimensional characteristic length on stiffness and damping coefficients is shown in figures 4.36 through 4.43. Referred figures show variation of stiffness and damping coefficients versus deformation factor (F) for various of non-dimensional length (l_m) at $\frac{L}{D} = 1.0, \varepsilon_0 = 0.5, N^2 = 0.5, \frac{H}{R} = 0.3$ and $\nu = 0.4$. Variations in graphs show that stiffness and damping coefficients decrease as l_m increases.

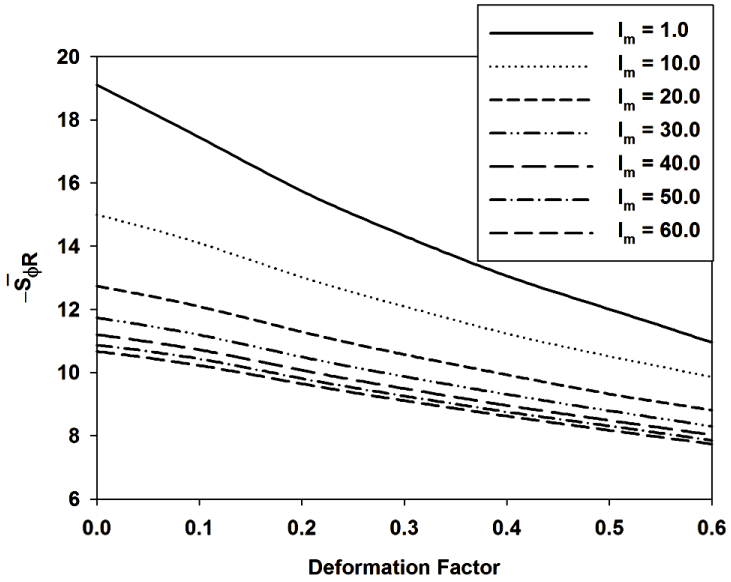

Figure 4.36 $-\bar{S}_{\phi R}$ Vs. F for various l_m at $\frac{L}{D} = 1.0, \varepsilon_0 = 0.5, N^2 = 0.5, \frac{H}{R} = 0.3, \nu = 0.4$.

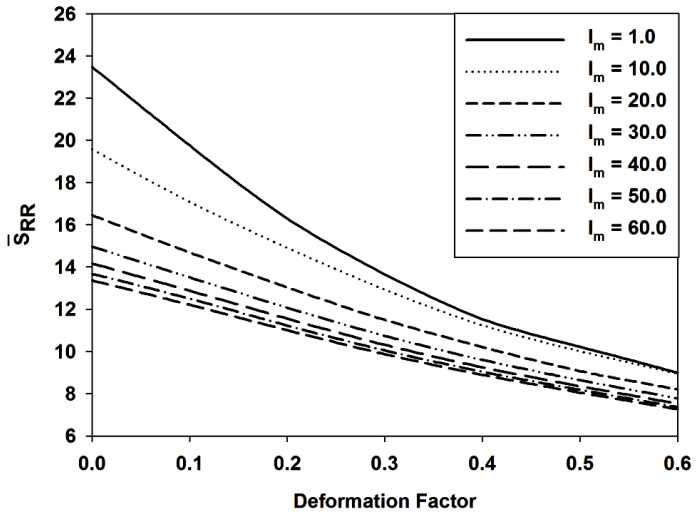

Figure 4.37 $\bar{S}_{RR}$ Vs. F for various l_m at $\frac{L}{D} = 1.0, \varepsilon_0 = 0.5, N^2 = 0.5, \frac{H}{R} = 0.3, \nu = 0.4$.

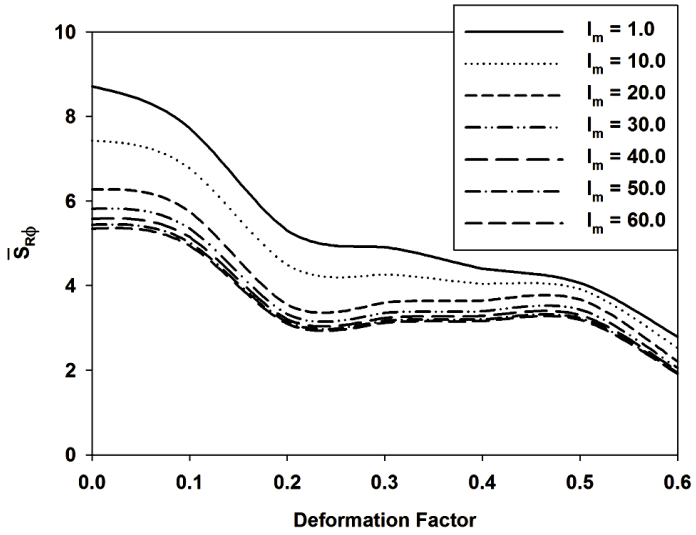

Figure 4.38 $\bar{S}_{R\phi}$ Vs. F for various l_m at $\frac{L}{D} = 1.0, \varepsilon_0 = 0.5, N^2 = 0.5, \frac{H}{R} = 0.3, \nu = 0.4$.

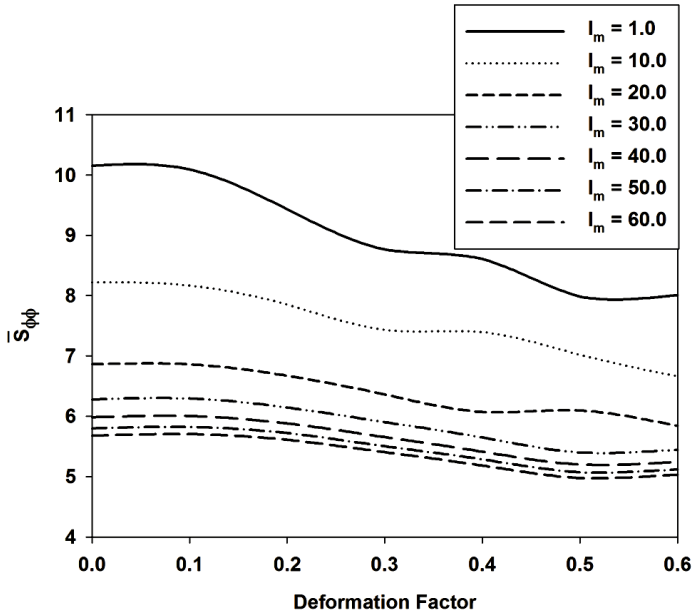

Figure 4.39 $\bar{S}_{\phi\phi}$ Vs. F for various l_m at $\frac{L}{D} = 1.0, \varepsilon_0 = 0.5, N^2 = 0.5, \frac{H}{R} = 0.3, \nu = 0.4$.

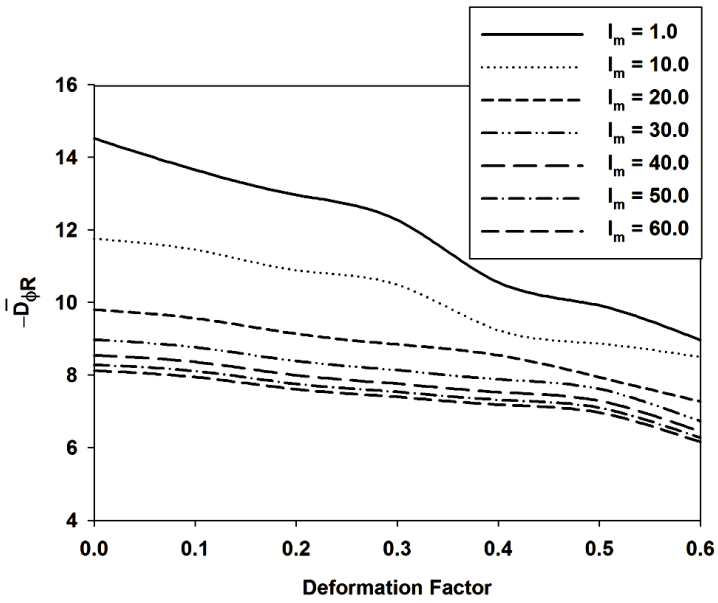

Figure 4.40 $-\bar{D}_{\phi R}$ Vs. F for various l_m at $\frac{L}{D} = 1.0, \varepsilon_0 = 0.5, N^2 = 0.5, \frac{H}{R} = 0.3, \nu = 0.4$.

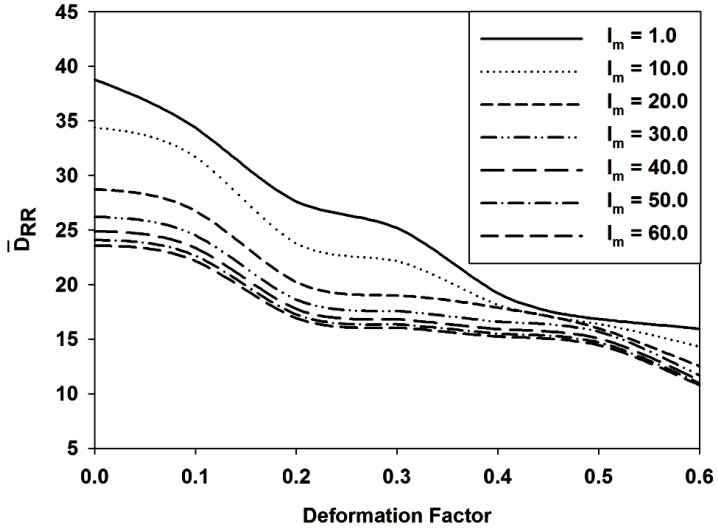

Figure 4.41 $\bar{D}_{RR}$ Vs. F for various l_m at $\frac{L}{D} = 1.0, \varepsilon_0 = 0.5, N^2 = 0.5, \frac{H}{R} = 0.3, \nu = 0.4$.

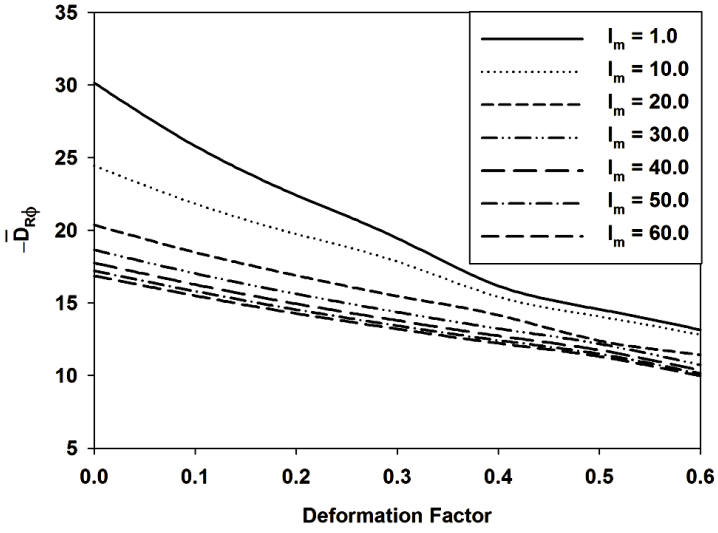

Figure 4.42 $-\bar{D}_{R\phi}$ Vs. F for various l_m at $\frac{L}{D} = 1.0, \varepsilon_0 = 0.5, N^2 = 0.5, \frac{H}{R} = 0.3, \nu = 0.4$.

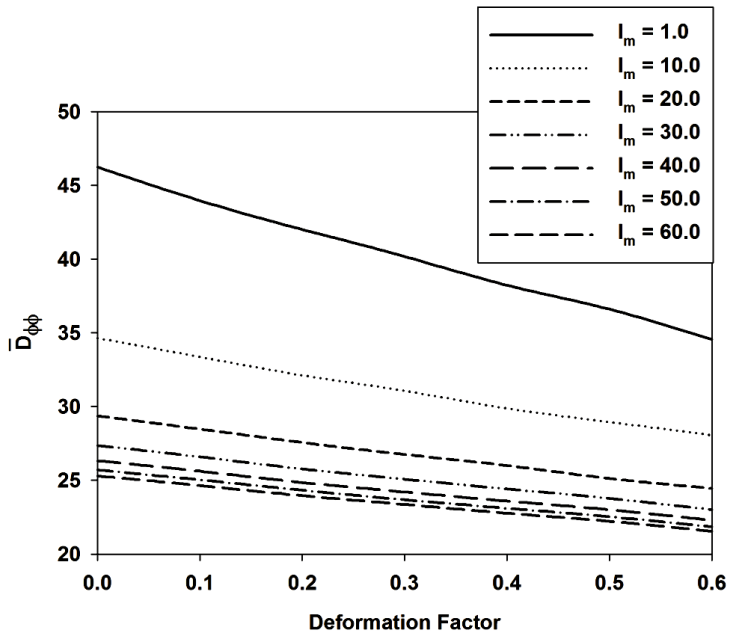

Figure 4.43 $\bar{D}_{\phi\phi}$ Vs. F for various l_m at $\frac{L}{D} = 1.0, \varepsilon_0 = 0.5, N^2 = 0.5, \frac{H}{R} = 0.3, \nu = 0.4$.

4.3.1.6 Effect of coupling number (*N*):

Figures 4.44 through 4.51 show variation of stiffness and damping coefficients versus deformation factor for various values of N^2at $\frac{L}{D} = 1.0, \varepsilon_0 = 0.5, l_m = 40.0, \frac{H}{R} = 0.3$ and $\nu = 0.4$. It can be observed from graphs shown in referred figures that value of damping and stiffness coefficients increases as coupling number increases.

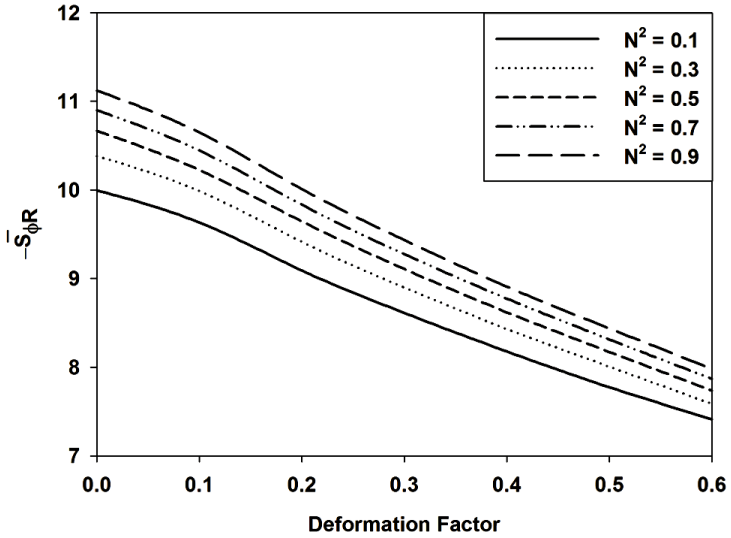

Figure 4.44 $-\bar{S}_{\phi R}$ Vs. F for various N^2 at $\frac{L}{D} = 1.0, \varepsilon_0 = 0.5, l_m = 40.0, \frac{H}{R} = 0.3, \nu = 0.4$.

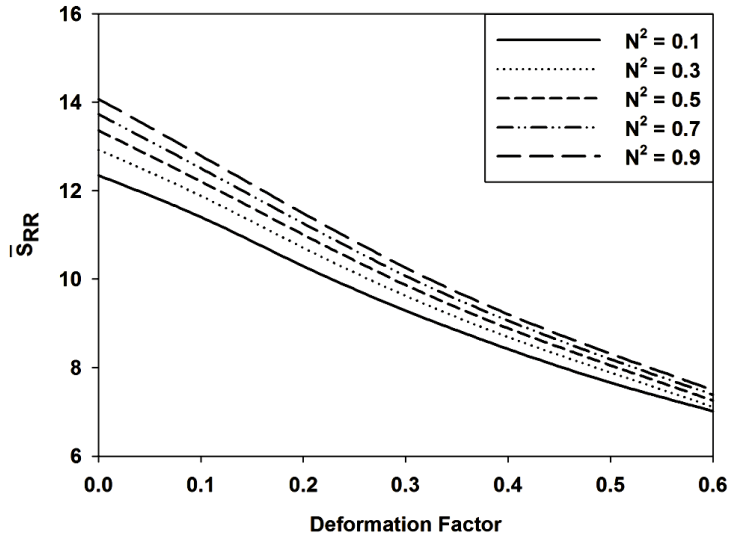

Figure 4.45 $\bar{S}_{RR}$ Vs. F for various N^2 at $\frac{L}{D} = 1.0, \varepsilon_0 = 0.5, l_m = 40.0, \frac{H}{R} = 0.3, \nu = 0.4$.

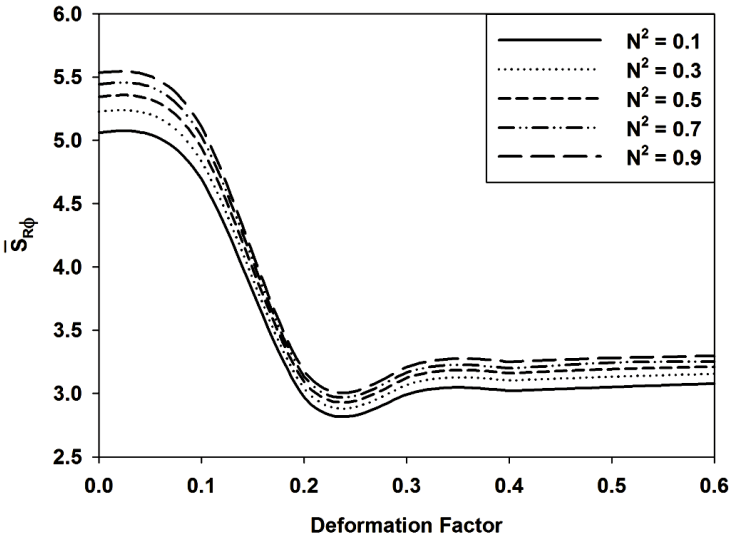

Figure 4.46 $\bar{S}_{R\phi}$ Vs. F for various N^2 at $\frac{L}{D} = 1.0, \varepsilon_0 = 0.5, l_m = 40.0, \frac{H}{R} = 0.3, \nu = 0.4$.

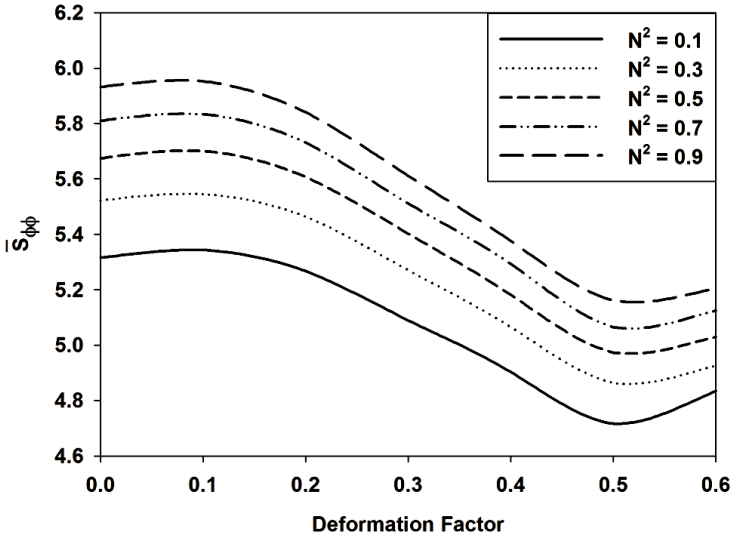

Figure 4.47 $\bar{S}_{\phi\phi}$ Vs. F for various N^2 at $\frac{L}{D} = 1.0, \varepsilon_0 = 0.5, l_m = 40.0, \frac{H}{R} = 0.3, \nu = 0.4$.

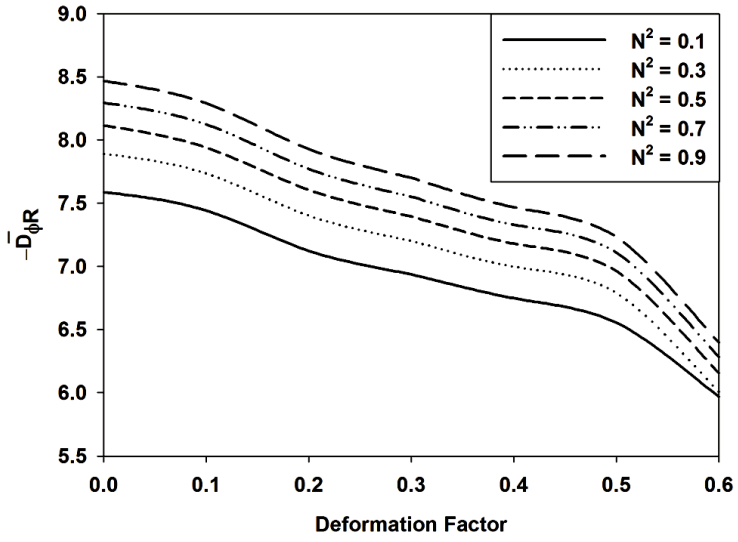

Figure 4.48 $-\overline{D}_{\phi R}$ Vs. F for various N^2 at $\frac{L}{D} = 1.0, \varepsilon_0 = 0.5, l_m = 40.0, \frac{H}{R} = 0.3, \nu = 0.4$.

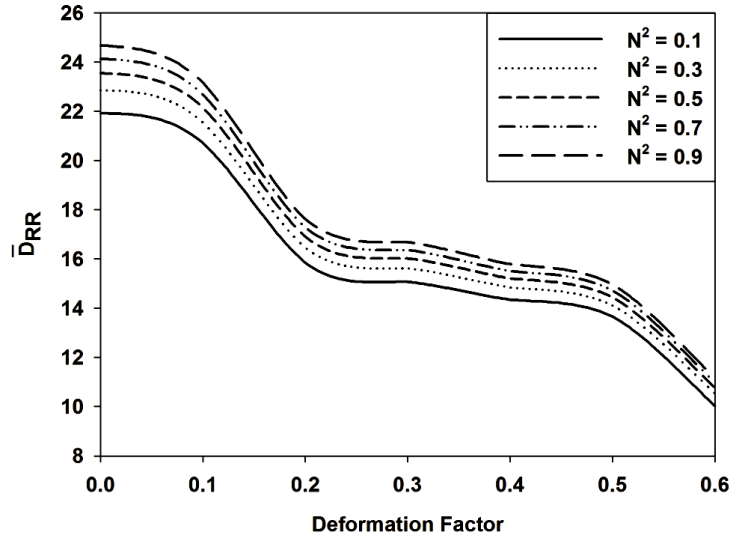

Figure 4.49 $\overline{D}_{RR}$ Vs. F for various N^2 at $\frac{L}{D} = 1.0, \varepsilon_0 = 0.5, l_m = 40.0, \frac{H}{R} = 0.3, \nu = 0.4$.

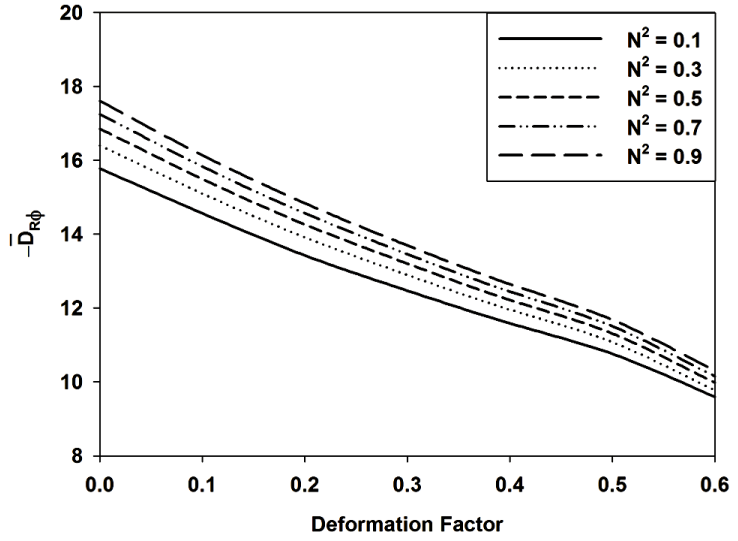

Figure 4.50 $-\overline{D}_{R\phi}$ Vs. F for various N^2 at $\frac{L}{D} = 1.0, \varepsilon_0 = 0.5, l_m = 40.0, \frac{H}{R} = 0.3, \nu = 0.4$.

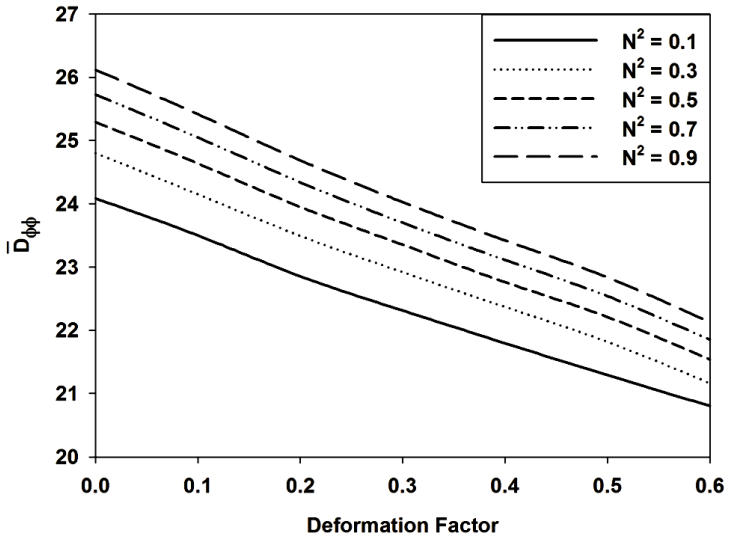

Figure 4.51 $\bar{D}_{\phi\phi}$ Vs. F for various N^2 at $\frac{L}{D} = 1.0, \varepsilon_0 = 0.5, l_m = 40.0, \frac{H}{R} = 0.3, \nu = 0.4$.

4.3.2 Critical Mass Parameter $(\bar{M}_C)$

4.3.2.1 Effect of eccentricity ratio (ε_0):

Figure 4.52 shows variation of mass parameter versus deformation factor for various eccentricity ratio at $\frac{L}{D} = 1.0, l_m = 40.0, N^2 = 0.5, \frac{H}{R} = 0.3$ and $\nu = 0.4$. On scrutiny of graph shown in figure it is evident that non-dimensional mass parameter reduces as deformation factor increases. It can be predicted by observing graph that mass parameter is high for higher eccentricity at $F = 0$. As F increases non-dimensional mass parameter decreases and it decreases sharply for curves with higher eccentricity ratio such that curve with ε_0=0.85 comes below curve with ε_0=0.8. This nature of graph is due to fact that as ε_0 increases it also increases $\bar{\delta}$. Increase in $\bar{\delta}$ increases $\bar{h}$ which results in decrease of pressure. Further it can be noticed from nature of curves that this decrease mass parameter is sharp as deformation factor increases from 0.0 to 0.1. As deformation factor is increased further critical mass parameter remains almost constant. Conway and Lee [26] using short bearing approximation and Majumdar et al. [29] using a finite bearing made similar observations for bearing with flexible liner taking into consideration Newtonian fluids as lubricant.

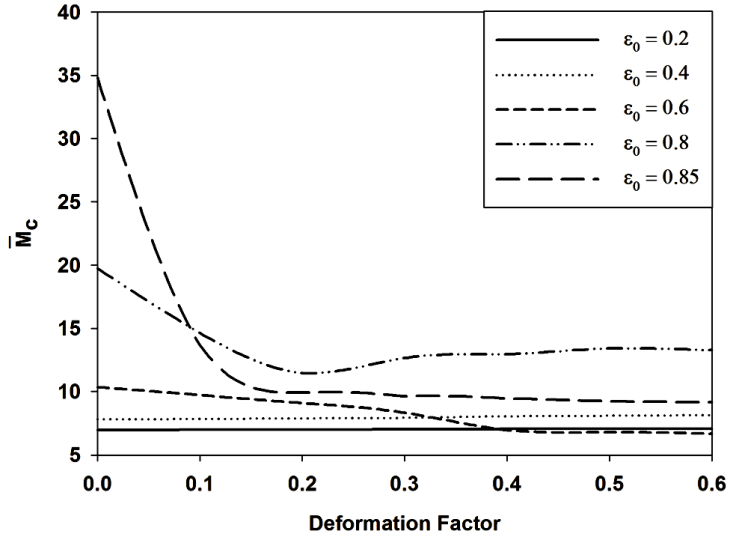

Figure 4.52 $\bar{M}_C$ Vs. F for various ε_0 at $\frac{L}{D} = 1.0, N^2 = 0.5, l_m = 40.0, \frac{H}{R} = 0.3, \nu = 0.4$.

4.3.2.2 Effect of slenderness ratio ($\frac{L}{D}$):

Non-dimensional mass parameter as function of deformation factor for various values of slenderness ratio at $\nu = 0.4, \varepsilon_0 = 0.5, N^2 = 0.5, \frac{H}{R} = 0.3$ and $l_m = 40.0$ is shown in figure 4.53. It can be observed from nature of graph in figure that non-dimensional critical mass parameter decreases with increase in slenderness ratio. It can also be observed that non-dimensional mass parameter decreases with increase in deformation factor.

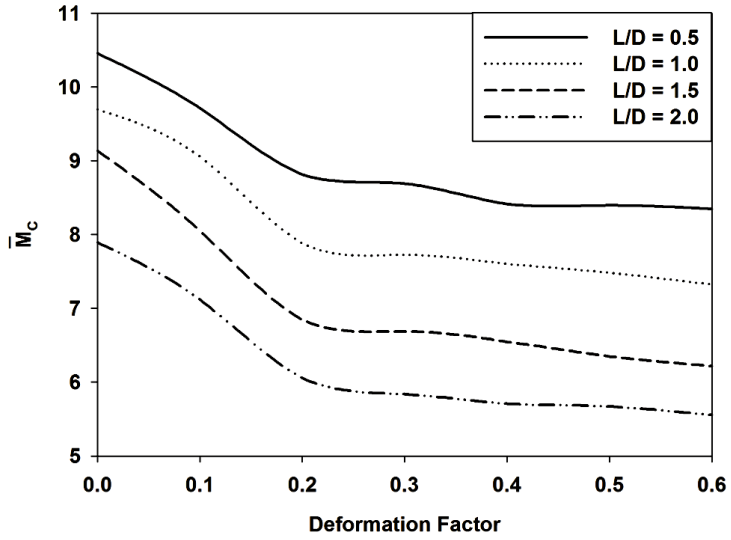

Figure 4.53 $\bar{M}_C$ Vs. F for various $\frac{L}{D}$ at $\varepsilon_0 = 0.5, N^2 = 0.5, l_m = 40.0, \frac{H}{R} = 0.3, \nu = 0.4$.

4.3.2.3 Effect of Poisson's ratio (ν):

Figure 4.54 shows graphically $\bar{M}_C$ as function of deformation factor (F) for $\frac{L}{D} = 1.0, \varepsilon_0 = 0.5, N^2 = 0.5, \frac{H}{R} = 0.3$ and $l_m = 40.0$ when Poisson's ratio is considered as parameter. It is observed from figure that $\bar{M}_C$ increases with increase in Poisson's ratio.

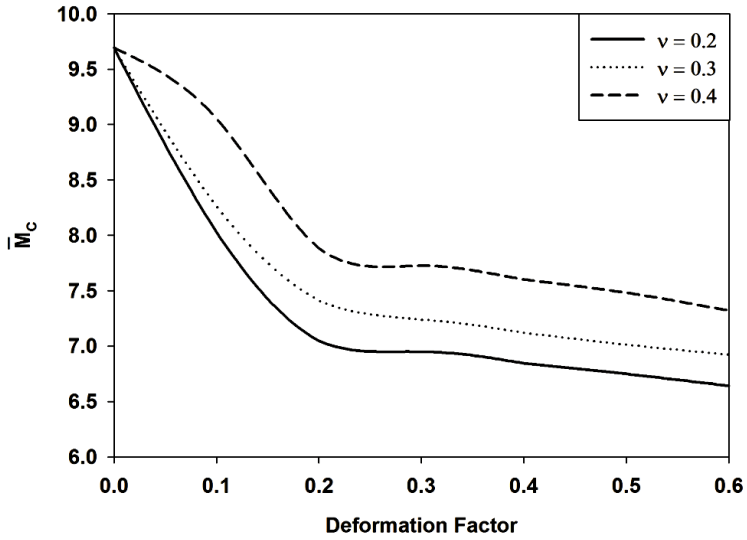

Figure 4.54 $\bar{M}_C$ Vs. F for various ν at $\frac{L}{D} = 1.0, \varepsilon_0 = 0.5, N^2 = 0.5, l_m = 40.0, \frac{H}{R} = 0.3$.

4.3.2.4 Effect of $\frac{H}{R}$ ratio:

Variation of $\bar{M}_C$ with liner thickness to journal radius ratio ($\frac{H}{R}$) is presented in figure 4.55. Critical mass parameter is found to be decreasing with increase in $\frac{H}{R}$ ratio. Further it is observed that critical mass parameter decreases with increase in deformation factor (F).

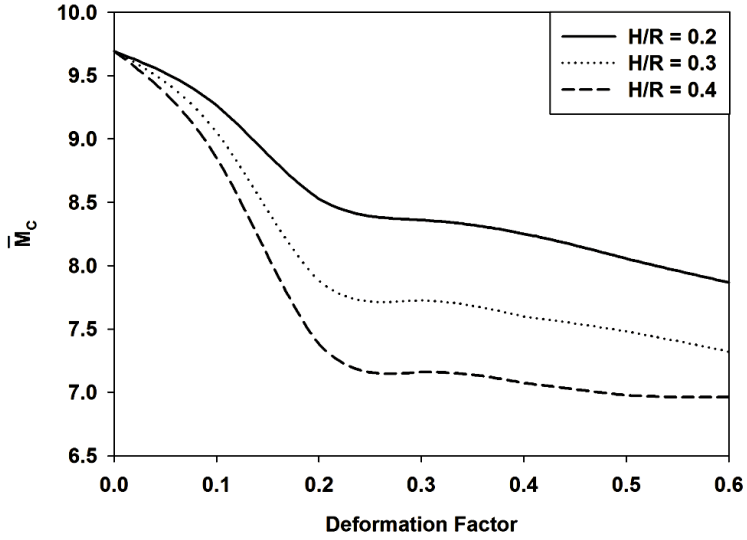

Figure 4.55 $\bar{M}_C$ Vs. F for various $\frac{H}{R}$ ratio at $\frac{L}{D} = 1.0, \varepsilon_0 = 0.5, N^2 = 0.5, l_m = 40.0, \nu = 0.4$.

4.3.2.5 Effect of characteristic length (l_m):

Critical mass parameter $\bar{M}_C$ is shown as a function of l_m for various values of deformation factor (F) at $\frac{L}{D} = 1.0, \varepsilon_0 = 0.5, N^2 = 0.5, \frac{H}{R} = 0.3$ and $\nu = 0.4$ in figure 4.56. From variations in curves shown in graph it is observed that critical mass parameter increases with increase in l_m and reaches a maximum value at $l_m = 10.0$. As l_m increases beyond 10.0 $\bar{M}_C$ does not vary much.

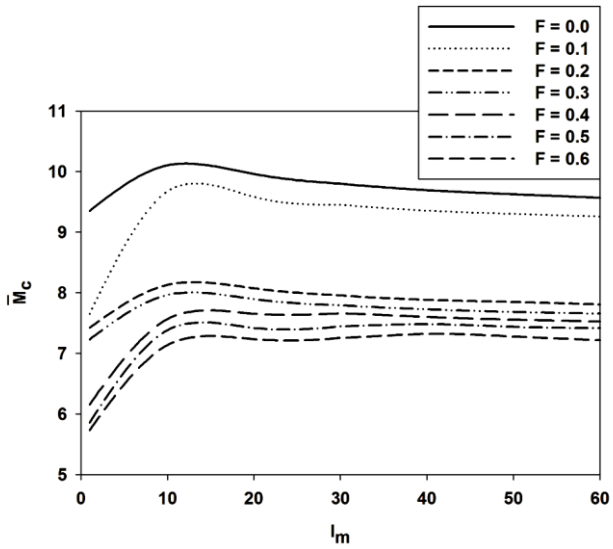

Figure 4.56 $\bar{M}_C$ Vs. l_m for various F at $\frac{L}{D} = 1.0, \varepsilon_0 = 0.5, N^2 = 0.5, \frac{H}{R} = 0.3, \nu = 0.4$.

4.3.2.6 Effect of coupling number (N):

Effect of coupling number on critical mass parameter for various values of deformation factor at $\frac{L}{D} = 1.0, \varepsilon_0 = 0.5, l_m = 40.0, \frac{H}{R} = 0.3$ and $\nu = 0.4$ is shown in figure 4.57. From family of curves shown in graph it can be observed that critical mass parameter increases with increase in coupling number. Further it can also be observed that critical mass parameter decreases with increase in deformation factor.

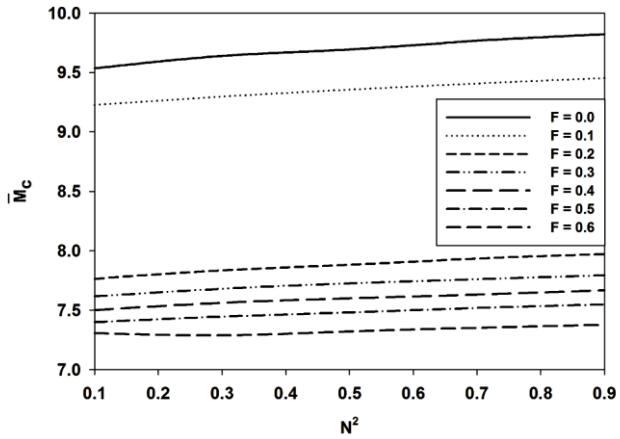

Figure 4.57 $\bar{M}_C$ Vs. N^2 for various F at $\frac{L}{D} = 1.0, \varepsilon_0 = 0.5, l_m = 40.0, \frac{H}{R} = 0.3, \nu = 0.4$.

4.3.3 Whirl Ratio (λ_R)

4.3.3.1 Effect of eccentricity ratio (ε_0):

Graph shown in figure 4.58 shows variation of whirl ratio versus deformation factor for various values of eccentricity ratio at $\frac{L}{D} = 1.0, N^2 = 0.5, l_m = 40.0, \frac{H}{R} = 0.3$ and $\nu = 0.4$. Variation in graph predicts that whirl ratio remains relatively constant with respect to deformation factor at lower eccentricity ratio. As eccentricity ratio increases beyond 0.6 whirl ratio increases with increase in deformation factor and this increase is sharp when deformation factor increases from 0.0 to 0.2. Whirl ratio decreases with increase in eccentricity ratio but as eccentricity ratio increases beyond 0.8 and at higher deformation factor reversed trends are observed in graph. This is due to fact that for a bearing with flexible liner as eccentricity ratio increases it also increases radial deformation of bearing surface which makes bearing to behave as working under lower eccentricity ratio.

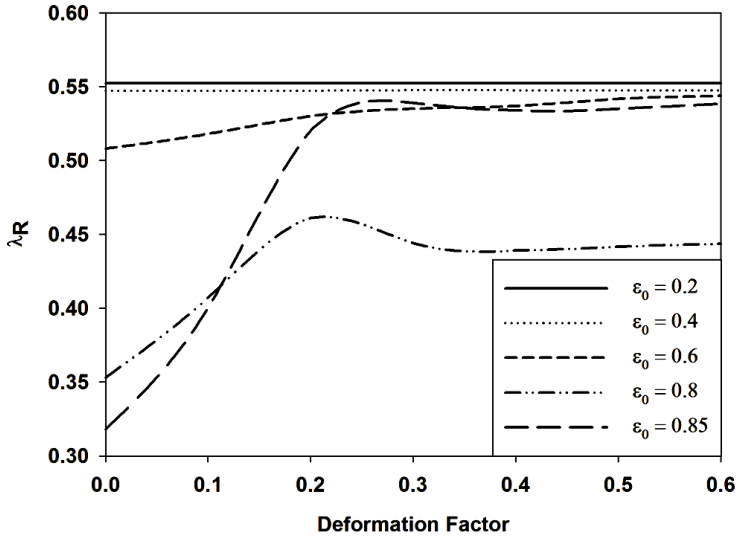

Figure 4.58 λ_R Vs. F for various ε_0 at $\frac{L}{D} = 1.0, N^2 = 0.5, l_m = 40.0, \frac{H}{R} = 0.3, \nu = 0.4$.

4.3.3.2 Effect of slenderness ratio $(\frac{L}{D})$

Whirl ratio decreases with increase in slenderness ratio as can be seen in figure 4.59 at $\varepsilon_0 = 0.5, N^2 = 0.5, l_m = 40.0, \frac{H}{R} = 0.3$ and $\nu = 0.4$. For particular $\frac{L}{D}$, whirl ratio increases as deformation factor increases when other parameters remain unaltered.

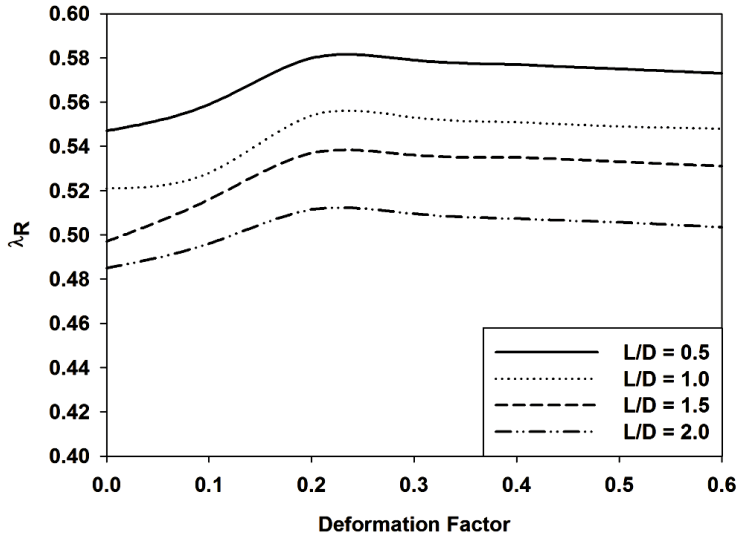

Figure 4.59 λ_R Vs. F for various $\frac{L}{D}$ at $\varepsilon_0 = 0.5, N^2 = 0.5, l_m = 40.0, \frac{H}{R} = 0.3, \nu = 0.4$.

4.3.3.3 Effect of Poisson's ratio (ν):

Figure 4.60 shows whirl ratio as a function of deformation factor at $\frac{L}{D} = 1.0, N^2 = 0.5, l_m = 40.0, \frac{H}{R} = 0.3$ and $\varepsilon_0 = 0.5$ when Poisson's ratio is considered as parameter. Study of figure shows that whirl ratio decreases as Poisson's ratio increases when other parameters are kept constant.

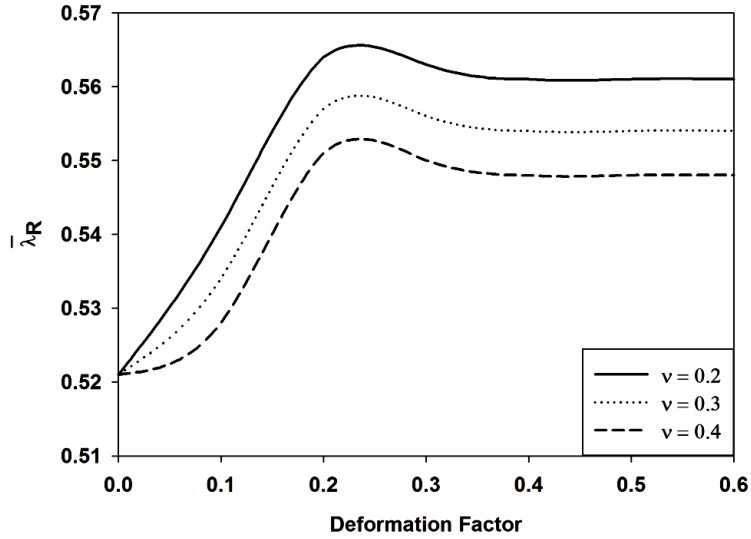

Figure 4.60 λ_R Vs. F for various ν at $\frac{L}{D} = 1.0, \varepsilon_0 = 0.5, N^2 = 0.5, l_m = 40.0, \frac{H}{R} = 0.3$.

4.3.3.4 Effect of $\frac{H}{R}$ ratio:

Graph of whirl ratio versus deformation factor for various values of $\frac{H}{R}$ ratio at $\frac{L}{D} = 1.0, N^2 = 0.5, l_m = 40.0, \nu = 0.4$ and $\varepsilon_0 = 0.5$ is shown in figure 4.61. From variation of family of curves it can be predicted that as liner thickness to journal radius increases whirl ratio also increases.

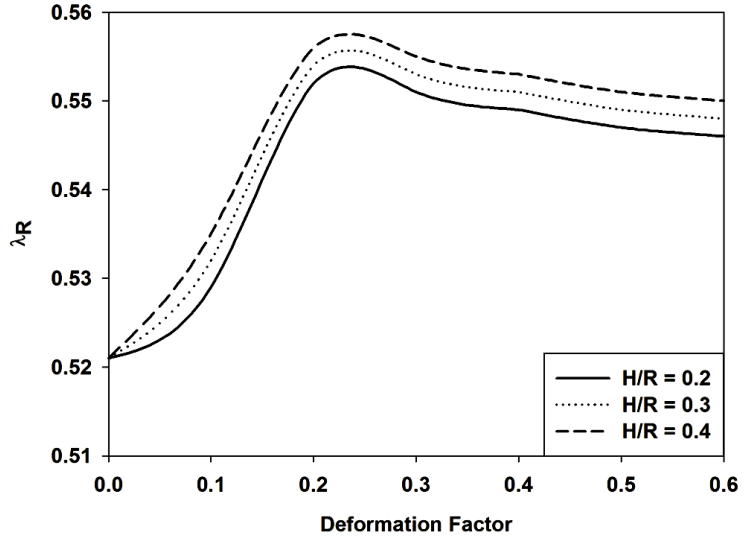

Figure 4.61 λ_R Vs. F for various $\frac{H}{R}$ ratio at $\frac{L}{D} = 1.0, \varepsilon_0 = 0.5, N^2 = 0.5, l_m = 40.0, \nu = 0.4$.

4.3.3.5 Effect of characteristic length (l_m):

Variation of whirl ratio with respect to l_m for various values of deformation factor at $\frac{L}{D} = 1.0$, $N^2 = 0.5, \varepsilon_0 = 0.5, \frac{H}{R} = 0.3$ and $\nu = 0.4$ is shown in figure 4.62. It can be discerned from figure that whirl ratio decreases as l_m increases and this decrease is sharp as l_m increases from 01 to 10.0.

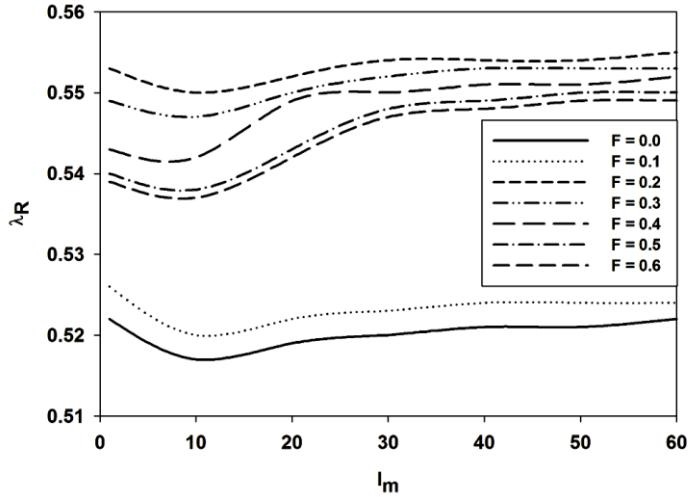

Figure 4.62 λ_R Vs. l_m for various F at $\frac{L}{D} = 1.0, \varepsilon_0 = 0.5, N^2 = 0.5, \frac{H}{R} = 0.3, \nu = 0.4$.

4.3.3.6 Effect of coupling number (N):

Figure 4.63 depicts whirl ratio as a function of coupling number for various values of deformation factor at $\frac{L}{D} = 1.0, \nu = 0.4, \frac{H}{R} = 0.3, l_m = 40.0$ and $\varepsilon_0 = 0.5$. Here, it is found that whirl ratio decreases as coupling number increases, but this decrease is very small. Further, for particular coupling number whirl ratio increases as deformation factor increases when other parameters are unaltered.

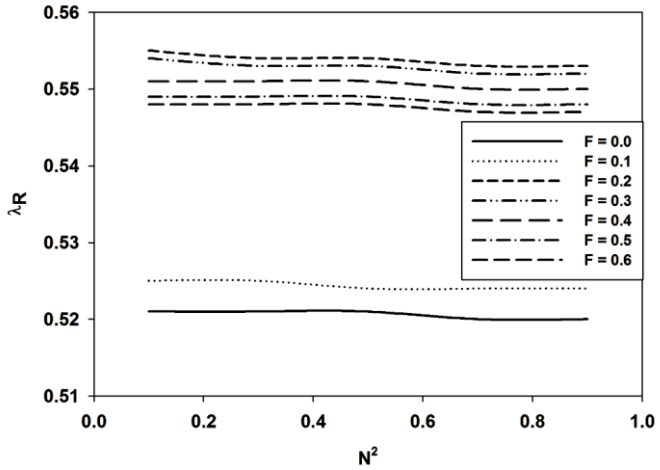

Figure 4.63 λ_R Vs. N^2 for various F at $\frac{L}{D} = 1.0, \varepsilon_0 = 0.5, l_m = 40.0, \frac{H}{R} = 0.3, \nu = 0.4$

4.3.4 Critical mass parameter versus Sommerfeld number

4.3.4.1 Effect of deformation factor

Figure 4.64 shows variation of critical mass parameter versus Sommerfeld number for various deformation factor at $\frac{L}{D} = 1.0, \nu = 0.4, \frac{H}{R} = 0.3, l_m = 40.0$ and $N^2 = 0.5$. Scrutiny of figure reveals that critical mass parameter decreases as Sommerfeld number increases. Further, it can be discerned that stability of bearing decreases as deformation factor increases.

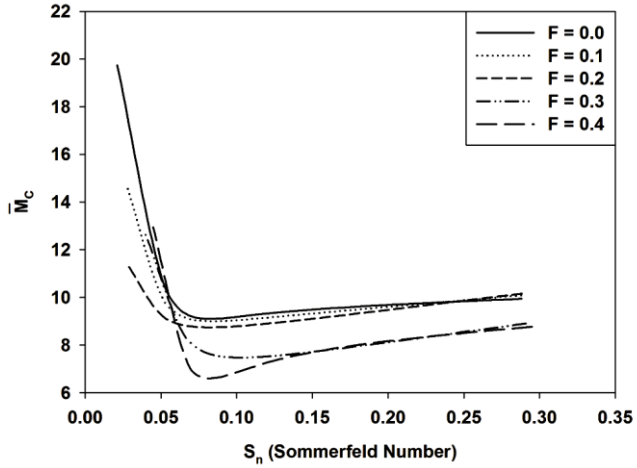

Figure 4.64 $\bar{M}_C$ Vs. Sommerfeld number for various F at $\frac{L}{D} = 1.0, N^2 = 0.5, l_m = 40.0, \frac{H}{R} = 0.3, \nu = 0.4.$

4.3.4.2 Effect of non-dimensional characteristic length

Graph shown in figure 4.65 depicts critical mass parameter as a function of Sommerfeld number for various values of non-dimensional characteristic length at $\frac{L}{D} = 1.0, \nu = 0.4, \frac{H}{R} = 0.3, F = 0.2$ and $N^2 = 0.5$. Variation in trends of graph show that stability of bearing increases with decreases in non-dimensional characteristic length. As l_m increases micropolar effect decreases hence stability threshold shifts towards Newtonian fluids.

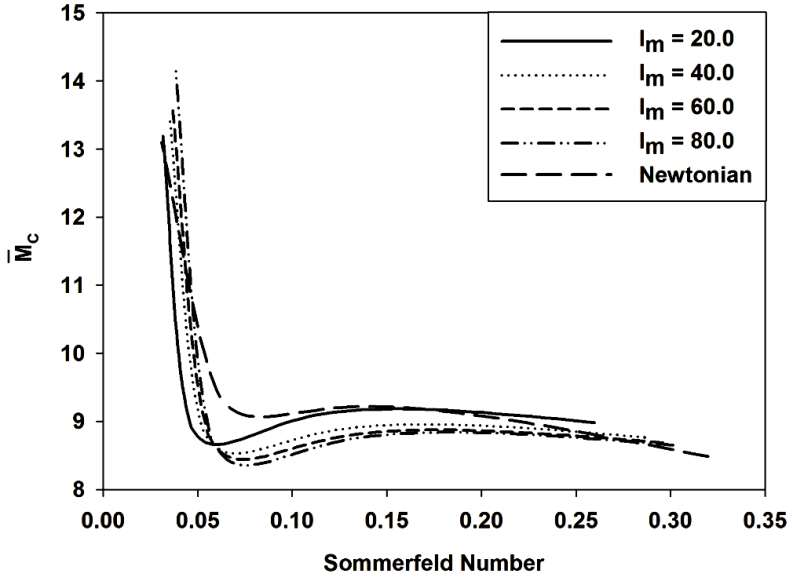

Figure 4.65 $\bar{M}_C$ Vs. Sommerfeld number for various l_m at $\frac{L}{D} = 1.0, N^2 = 0.5, F = 0.2, \frac{H}{R} = 0.3, \nu = 0.4$.

Chapter 5 Non-Linear Transient Analysis of Finite Flexible Oil Journal Bearings under Micropolar Lubrication

5.1 Introduction

Stability characteristics are determined using non-linear transient analysis (NLTA) for hydrodynamic journal bearing considering flexibility of liner an under micropolar lubrication. Effect of flexibility of liner in tandem with effect of micropolar parameters on dynamic performance characteristics in terms of critical mass parameter is shown.

Although considerable amount of work has been reported on stability and dynamic characteristics, but, studies dealing with non linear transient effect are quite rare. In this chapter NLTA is used to generate locus of journal for provided operating conditions taking into consideration flexibility of liner and under micropolar lubrication. Deformation equation for bearing surface are solved simultaneously with modified Reynolds equation considering time dependent terms to predict theoretically fluid film pressure and journal orbit under dynamic conditions. Locus of journal is plotted on polar plot for various values of mass parameter and threshold of stability in terms of critical mass parameter and whirl ratio is predicted by formation of limit cycle.

In this chapter deformation at bearing liner surface is calculated using theory of elasticity as described in Appendix-II. Dynamic pressure is obtained by solving modified Reynolds equation using FDM technique considering micropolar fluids as lubricant and effect of deformation of bearing liner surface. Locus of journal centre which shifts under effect of dynamic forces is obtained by solving equations of motion using fourth order Runge-Kutta method (RKM). Locus of journal centre trajectory which results in limit cycle gives us measure of critical mass parameter. In absence of experimental data, theoretical results from present work have been compared with already published theoretical results for bearing without considering flexibility of liner.

Effect of slenderness ratio, deformation factor, Poisson's ratio, H/R ratio, characteristic length and coupling number on limit cycle has been presented in this chapter in form of

graphs. Comparison of results from linear dynamic analysis and non-linear dynamic analysis is also conducted in this chapter.

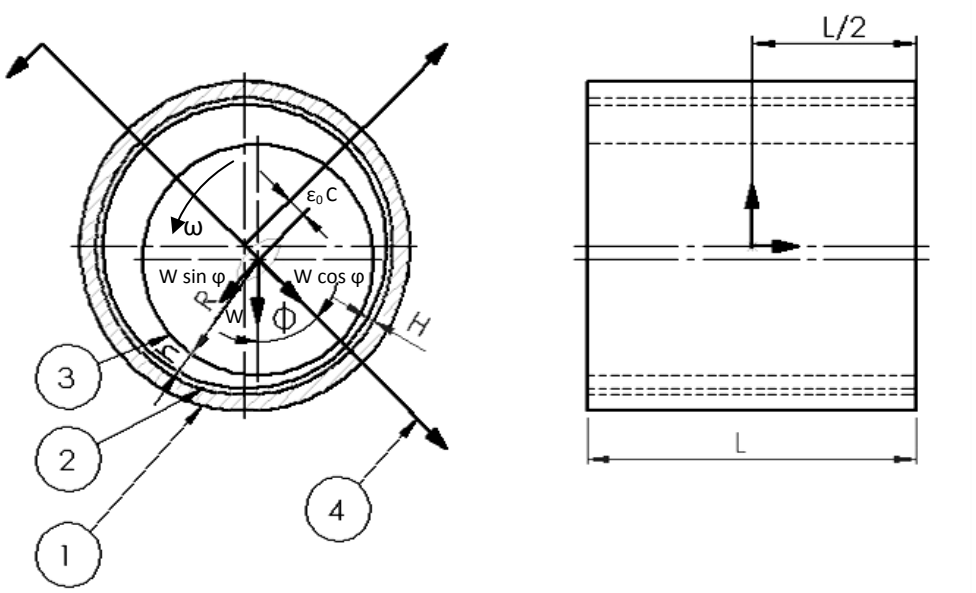

1. Solid Housing 2. Flexible Liner 3. Journal 4. Lines of centers
Figure 5.1 Schematic diagram of Journal Bearing used in analysis.

5.2 Theoretical analysis

5.2.1 Governing Equation

Hydrodynamic journal bearing with flexible liner under micropolar lubrication used in analysis is shown in figure 5.1. Modified Reynolds equation for non-linear dynamic analysis for micropolar fluids as lubricant can be written as follows

$$\frac{\partial}{\partial x}\left[\frac{h^3}{\mu}\boldsymbol{\Phi}(\Lambda,N,h)\frac{\partial p}{\partial x}\right]+\frac{\partial}{\partial z}\left[\frac{h^3}{\mu}\boldsymbol{\Phi}(\Lambda,N,h)\frac{\partial p}{\partial z}\right]=6U\left(1-\frac{2}{\omega}\frac{\partial \phi}{\partial t}\right)\frac{\partial h}{\partial x}+12\frac{\partial h}{\partial t} \tag{5.1}$$

$$\boldsymbol{\Phi}(\Lambda,N,h)=\left\{1+12\frac{\Lambda^2}{h^2}-6\frac{N\Lambda}{h}\coth\frac{Nh}{2\Lambda}\right\},\Lambda=\left(\frac{\gamma}{4\mu}\right)^{1/2},N=\left(\frac{\chi}{2\mu+\chi}\right)^{1/2}$$

Equation 5.1 with following substitutions

$$\theta=\frac{x}{R},\bar{z}=\frac{2z}{L},\bar{h}=\frac{h}{C},\bar{p}=\frac{pC^2}{\mu\omega R^2},l_m=\frac{C}{\Lambda},\bar{t}=\omega t$$

following equation is obtained in non-dimensional form:

$$\frac{\partial}{\partial\theta}\left[\bar{g}\left(l_m,N,\bar{h}\right)\frac{\partial\bar{p}}{\partial\theta}\right]+\left(\frac{D}{L}\right)^2\frac{\partial}{\partial\bar{z}}\left[\bar{g}\left(l_m,N,\bar{h}\right)\frac{\partial\bar{p}}{\partial\bar{z}}\right]=\frac{1}{2}(1-2\phi')\frac{\partial\bar{h}}{\partial\theta}+\frac{\partial\bar{h}}{\partial\bar{t}} \tag{5.2}$$

$$\bar{g}\left(l_m, N, \bar{h}\right) = \frac{\bar{h}^3}{12} + \frac{\bar{h}}{l_m^2} - \frac{N\bar{h}^2}{2l_m}\coth\frac{Nl_m\bar{h}}{2}$$

$$\phi' = \frac{\partial\phi}{\partial\bar{t}}$$

Boundary conditions for equation (5.2) are as follows:

1. Pressures at ends of bearing are zero

$$\bar{p}(\theta, \pm 1) = 0\}$$

(5.3 a)

2. Pressure distribution is symmetrical about mid-plane

$$\left.\frac{\partial\bar{p}(\theta, 0)}{\partial\bar{z}} = 0\right\}$$

(5.3 b)

Cavitation boundary conditions

$$\left.\begin{aligned}\bar{p}(\theta_2, \bar{z}) = \frac{\partial\bar{p}(\theta_2, \bar{z})}{\partial\bar{z}} = 0 \\ \bar{p}(\theta, \bar{z}) = 0, \quad for \quad \theta_2 \le \theta \le \theta_1\end{aligned}\right\}$$

(5.3 c)

Where θ_1 and θ_2 represents angles at end and start of hydrodynamic film at each axial plane of bearing. During computation all negative pressure are set to be zero in order to implement Reynolds cavitation boundary conditions.

3. Periodic boundary conditions

$$\bar{p}(\theta, \bar{z}) = \bar{p}(\theta + 2\pi, \bar{z})\}$$

(5.3 d)

Expression for film thickness for hydrodynamic journal bearing considering flexibility of bearing liner is as follows:

$$\bar{h} = 1 + \varepsilon\cos\theta + \bar{\delta}$$

(5.4)

$$\bar{h} = \frac{h}{C}, \varepsilon = \frac{e}{C}, \bar{\delta} = \frac{\delta}{C}$$

In order to obtain non-dimensional pressure distribution equation (5.2) is solved for first initial guess taking assuming pressure to be zero and $\delta = 0$. Pressure profile thus obtained is used first guess in order to obtain values of $\bar{\delta}$ by iterative procedure described in Appendix- I & II.

Pressure profile is expressed as follows (A 1.13):

$$\bar{p} = \frac{\bar{p}_{0,0}}{2} + \sum_{\substack{m=0 \\ (m,n) \neq (0,0)}}^{\infty} \sum_{n=0}^{\infty} \bar{p}_{m,n} \cos\left(\frac{2m\pi\bar{z}}{L}\right) \cos\left(n\theta + \beta_{m,n}\right) \tag{5.5}$$

Values of $\bar{p}_{m,n}$, $\beta_{m,n}$ and $\bar{p}_{0,0}$ can be obtained from relations (A 1.10, A1.11 and A 1.12) of appendix-I.

Displacement components namely from expressions (A2.1, A2.2 and A2.3) in r, θ and z directions are found from pressure distribution calculated above. Displacement components are expressed in displacement equations (A 2.1, A 2.2 and A 2.3) of appendix-II and boundary conditions are given in equations (A 2.24) through (A 2.27) of appendix-II. These displacement components are used to calculate six components of stress as given by stress displacement relationships given by equations (A 2.4) through (A 2.9) of appendix-II. Further these six components are used get 3 equilibrium equations (A 2.10) through (A 2.12).

These displacement equations are solved for unit pressure, μ and values of distortion coefficient $d_{m,n}$ are obtained from relation (A 2.62) of appendix-II and are stored in computer memory. Radial deformation $\bar{\delta}$ of bearing surface at any (θ, $\bar{z}$) is computed with help of equation (A 2.63) and using relation (A 1.10), (A 1.11) and (A 1.12) with $d_{m,n}$ and is given by,

$$\bar{\delta} = 2(1+\nu)F\left[\bar{p}_{0,0}d_{0,0} + \sum_{m=0}^{\infty}\sum_{n=0}^{\infty} \bar{p}_{m,n}d_{m,n}\cos(m\pi\bar{z})\cos\left(n\theta + \beta_{m,n}\right)\right] \tag{5.6}$$

5.2.2 Fluid film forces

At any point on journal, film pressure is p and corresponding film force is ($p\ R\ d\theta\ dz$). ($R\ d\theta\ dz$) is an elementary area at an angle θ with line of centers and on which pressure p is acting. This force will have components ($p\ R\ d\theta\ dz \cos\theta$) along line of centers and ($p\ R\ d\theta\ dz \sin\theta$) perpendicular to line of centers.

Components of fluid film forces along line of centers $(F_R)$and perpendicular to line of centers (F_ϕ) are given by

$$\left.\begin{aligned} F_R &= \int_{-L/2}^{L/2}\int_{\theta_1}^{\theta_2} p\cos\theta\ (R\ d\theta)\ dz \\ F_\phi &= \int_{-L/2}^{L/2}\int_{\theta_1}^{\theta_2} p\sin\theta\ (R\ d\theta)\ dz \end{aligned}\right\} \tag{5.7}$$

Non-dimensional fluid film force components $\bar{F}_R$ along line of centers and $\bar{F}_\phi$ perpendicular to line of centers are given by

$$\left.\begin{aligned} \bar{F}_R &= 2\int_{0}^{1}\int_{\theta_1}^{\theta_2} \bar{p}\cos\theta\ (R\ d\theta)\ d\bar{z} \\ \bar{F}_\phi &= 2\int_{0}^{1}\int_{\theta_1}^{\theta_2} \bar{p}\sin\theta\ (R\ d\theta)\ d\bar{z} \end{aligned}\right\} \tag{5.8}$$

With following substitutions

$$\bar{p} = \frac{pC^2}{\mu\omega R^2}, \bar{F}_R = \frac{F_R C^2}{\mu\omega R^2 L}, \bar{F}_\phi = \frac{F_\phi C^2}{\mu\omega R^2 L}\ and\ \bar{z} = \frac{2z}{L}$$

5.2.3 Steady state load

Expression for steady state load and attitude angle are as follows:

$$\bar{W}_0 = \left[\{(\bar{F}_R)_0\}^2 + \left\{\left(\bar{F}_\phi\right)_0\right\}^2\right]^{1/2} \tag{5.9}$$

$$\phi_0 = tan^{-1}\left[-\frac{\left(\bar{F}_\phi\right)_0}{(\bar{F}_R)_0}\right] \tag{5.10}$$

$$\bar{W}_0 = \frac{W_0 C^2}{\mu\omega R^3 L}$$

Where, $(\bar{F}_R)_0$ and $\left(\bar{F}_\phi\right)_0$are components of fluid film forces in *R*- and ϕ- directions respectively.

5.2.4 Equation of motion

Equation of motion of journal can be written as under:

$$MC\left[\frac{d^2\varepsilon}{dt^2}-\varepsilon\left(\frac{d\phi}{dt}\right)^2\right]=F_R+W_0cos\phi \tag{5.11}$$

$$MC\left[\varepsilon\frac{d^2\phi}{dt^2}+2\frac{d\phi}{dt}\frac{d\varepsilon}{dt}\right]=F_\phi-W_0sin\phi \tag{5.12}$$

(Assuming journal to be rigid and mass M per bearing)

Equations (5.11 and 5.12) in non-dimensional form can be written as

$$\bar{M}\bar{W}_0\left[\frac{d^2\varepsilon}{d\bar{t}^2}-\varepsilon\left(\frac{d\phi}{d\bar{t}}\right)^2\right]=\bar{F}_R+\bar{W}_0cos\phi \tag{5.13}$$

$$\bar{M}\bar{W}_0\left[\varepsilon\frac{d^2\phi}{d\bar{t}^2}+2\frac{d\phi}{d\bar{t}}\frac{d\varepsilon}{d\bar{t}}\right]=\bar{F}_\phi-\bar{W}_0sin\phi \tag{5.14}$$

$$\bar{M}=\frac{M\ C\ \omega^2}{W_0}$$

5.2.5 Method of solution

Using finite difference method we get equation of pressure from modified Reynolds equation (5.2) which is as follows:

$$\bar{p}_{i,j}=C_{1A}\bar{p}_{i+1,j}+C_{2A}\bar{p}_{i-1,j}+C_{3A}\bar{p}_{i,j+1}+C_{4A}\bar{p}_{i,j-1}+C_{5A} \tag{5.15}$$

$$\left.\begin{aligned}
C_{1A}&=\frac{1}{C_0}\left[1-\frac{(C_A)_{i,j}}{2(C_B)_{i,j}}\varepsilon(\Delta\theta)(\sin\theta)+\frac{(C_A)_{i,j}}{4(C_B)_{i,j}}\left(\bar{\delta}_{i+1,j}-\bar{\delta}_{i-1,j}\right)\right]\\
C_{2A}&=\frac{1}{C_0}\left[1+\frac{(C_A)_{i,j}}{2(C_B)_{i,j}}\varepsilon(\Delta\theta)(\sin\theta)-\frac{(C_A)_{i,j}}{4(C_B)_{i,j}}\left(\bar{\delta}_{i+1,j}-\bar{\delta}_{i-1,j}\right)\right]\\
C_{3A}&=\frac{1}{C_0}\left(\frac{\Delta\theta}{\Delta\bar{z}}\right)^2\left(\frac{D}{L}\right)^2\left[1+\frac{(C_A)_{i,j}}{4(C_B)_{i,j}}\left(\bar{\delta}_{i,j+1}-\bar{\delta}_{i,j-1}\right)\right]\\
C_{4A}&=\frac{1}{C_0}\left(\frac{\Delta\theta}{\Delta\bar{z}}\right)^2\left(\frac{D}{L}\right)^2\left[1-\frac{(C_A)_{i,j}}{4(C_B)_{i,j}}\left(\bar{\delta}_{i,j+1}-\bar{\delta}_{i,j-1}\right)\right]\\
C_{5A}&=\frac{\Delta\theta^2}{4(C_B)_{i,j}C_0}\left[2(1-2\phi')\varepsilon(\sin\theta)-(1-2\phi')\left(\frac{\bar{\delta}_{i+1,j}-\bar{\delta}_{i-1,j}}{\Delta\theta}\right)-4\varepsilon'\cos\theta\right]\\
C_0&=2\left[1+\left(\frac{\Delta\theta}{\Delta\bar{z}}\right)^2\left(\frac{D}{L}\right)^2\right]
\end{aligned}\right\} \tag{5.16}$$

$(C_A)_{i,j}$ and $(C_B)_{i,j}$ can be calculated by using equation given below and substituting value of $\bar{h}_{i,j}$, corresponding to each θ_i and $\bar{z}_j$

$$\left.\begin{aligned}(C_A)_{i,j} &= \frac{\bar{h}_{i,j}^2}{4} + \frac{1}{l_m^2} - \frac{N\bar{h}_{i,j}}{l_m}\coth\left(\frac{Nl_m\bar{h}_{i,j}}{2}\right) + \frac{N^2h_{i,j}^2}{4}\operatorname{cosech}^2\left(\frac{Nl_m\bar{h}_{i,j}}{2}\right)\\ (C_B)_{i,j} &= \frac{\bar{h}_{i,j}^3}{12} + \frac{\bar{h}_{i,j}}{l_m^2} - \frac{N\bar{h}_{i,j}^2}{2l_m}\coth\left(\frac{Nl_m\bar{h}_{i,j}}{2}\right)\\ \bar{h}_{i,j} &= 1 + \varepsilon\cos\theta_i,\ \ \theta_i = i\theta,\ \ \varepsilon' = \frac{d\varepsilon}{d\bar{t}},\ \ \phi' = \frac{d\phi}{d\bar{t}}\end{aligned}\right\} \tag{5.17}$$

Four first order differential equations can be obtained from 2 second order differential equations (5.13) and (5.14)

$$\left.\begin{aligned}\frac{d\varepsilon}{d\bar{t}} &= \varepsilon'\\ \frac{d\phi}{d\bar{t}} &= \phi'\\ \frac{d\varepsilon'}{d\bar{t}} &= \frac{1}{\bar{M}\bar{W}_0}(\bar{F}_R + \bar{W}_0 cos\phi) + \varepsilon\phi'^2\\ \frac{d\phi'}{d\bar{t}} &= \frac{1}{\bar{M}\bar{W}_0\varepsilon}(\bar{F}_R - \bar{W}_0 sin\phi) - \frac{2\varepsilon'\phi'}{\varepsilon}\end{aligned}\right\} \tag{5.18}$$

Set of equations (5.18) can be solved for state space variables $(\varepsilon,\ \phi,\ \varepsilon',\ \phi')$ by fourth order Runge-Kutta method. To calculate initial pressure for journal bearings considering elastic distortion on surface of bearing liner equation (5.15) is solved using FDM technique satisfying boundary conditions, considering starting oil pressure and deformation of bearing liner surface to be zero. This initial pressure distribution is used to calculate new pressure distribution in subsequent iterations until convergence is achieved. To accommodate effect of deformation of bearing surface liner, calculated steady state pressure is then put in relations (A 1.10), (A 1.11) and (A 1.12) to get $\bar{p}_{m,n}$ and $\beta_{m,n}$ by numerical integration process by applying Simpson's 1/3rd rule, and using values of $\bar{p}_{m,n}$ and $\beta_{m,n}$ displacement components in r, θ and z directions are calculated in terms of u', v' and w'. Using stress displacement relationships and by method described in Appendix II value of non-dimensional radial deformation $\bar{\delta}$ is calculated. New values of non-dimensional radial deformation are used to get new values of film thickness at every node point thus getting new pressure distribution. This procedure is repeated through iteration method until convergence is attained.

Once pressure profile is obtained, components of film forces are calculated along lines of centers and perpendicular to line of centers respectively using equation (5.8). Steady state load and attitude angle are further obtained by using equation (5.9) and (5.10).

Equations of motion as given in set of equations (5.18) are solved by fourth order RKM for time step $\Delta t = \frac{5\pi}{180}$ to obtain state space variables $(\varepsilon,\ \phi,\ \varepsilon',\ \phi')$. These variables are then used in equation (5.15) to find new dynamic pressure distribution and subsequently used in equations (5.18) to get new state space variables $(\varepsilon,\ \phi,\ \varepsilon',\ \phi')$. This problem is initial value problem so initial guess value of mass parameter is provided in order to study stability. Various values of mass parameter are tried and value of mass parameter corresponding to limit cycle gives us critical mass parameter.

Whirl ratio at threshold of stability is obtained by method described by Akers et al. [62]. Time taken to get same point on limit cycle by adding time step is calculated within accuracy of three significant digits. Thus whirl ratio is given by

$$\lambda_R = \frac{2\pi}{\bar{t}_C} \tag{5.19}$$

5.3 Result and discussion

Observations from equations (5.2) and (5.4) reveal that pressure distribution in film region will depend on independent parameters viz. slenderness ration (L/D), eccentricity ratio (ε), characteristic length (l_m), coupling number (N) and radial deformation (δ). From equation (5.6) it is evident that radial deformation will depend on deformation factor (F), Poisson's ratio (ν) and H/R ratio.

Figure 5.2 shows results by present method are compared with published results of Das et al. [142] for rigid bearing under similar conditions, in order to check validity of computer code. Comparison shows that errors between simulated results generated by current program and those already published are within 3-4 %.

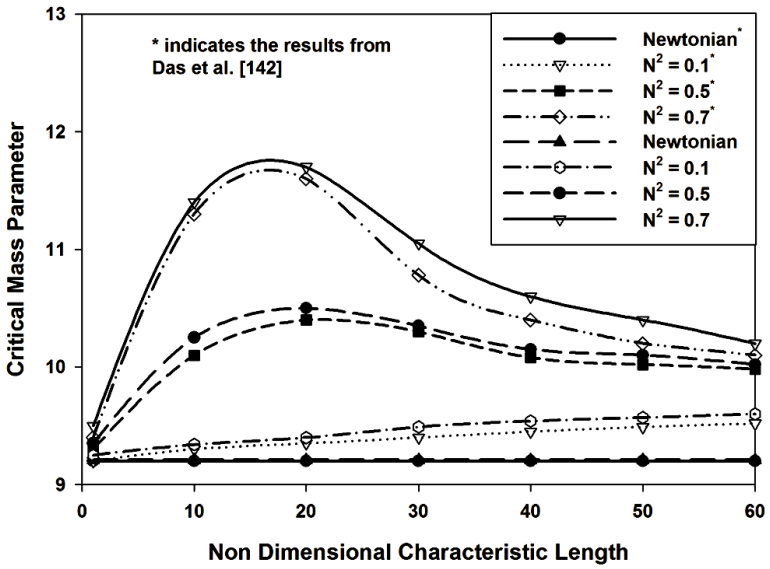

Figure 5.2 $\bar{M}_C$ Vs. l_m for various N^2 at $\varepsilon_0 = 0.5$ and $\frac{L}{D} = 1.0$ assuming rigid bearing.

Journal center trajectories for various values of parameters (F, l_m, N, ε, ν, $\frac{L}{D}$ and $\frac{H}{R}$ ratio) used in analysis are presented in figures 5.3 through 5.24. Three cases are presented for journal center trajectory:

1. $\bar{M} = 1.2\,\bar{M}_C$ locus of journal center diverges and orbit of journal center grows with time.
2. $\bar{M} = \bar{M}_C$ locus of journal center neither converges nor diverges and journal center moves along same trajectory. Value of mass parameter corresponding to this situation is termed as critical mass parameter.
3. $\bar{M} = 0.8\,\bar{M}_C$ locus of journal center converges and journal center settles down in to stable point with time.

Journal centre trajectories for $\bar{M} = 1.2\,\bar{M}_C$, $\bar{M} = \bar{M}_C$ and $\bar{M} = 0.8\,\bar{M}_C$ are presented in figures 5.3 through 5.24. Figure 5.3 & 5.4 represents journal centre trajectories for $\frac{L}{D} = 1.0, \frac{H}{R} = 0.3, \nu = 0.4, F = 0.2, l_m = 40.0, N^2 = 0.5$ and $\varepsilon_0 = 0.2, 0.3$ respectively. Journal centre trajectories for $\varepsilon_0 = 0.1, \frac{H}{R} = 0.3, \nu = 0.4, F = 0.3, l_m = 30.0, N^2 = 0.5$ and $\frac{L}{D} = 0.5, 1.0, 1.5$ are presented in figures 5.5, 5.6 and 5.7. Trajectories for journal centre motion for $\frac{L}{D} = 1.0, \varepsilon_0 = 0.1, \frac{H}{R} = 0.3, \nu = 0.4, l_m = 30.0, N^2 = 0.5$ and $F = 0.1, 0.2, 0.4, 0.5$ are presented in figures 5.8, 5.9, 5.10 & 5.11. Figure 5.12 and 5.13 represents journal centre trajectories for $\frac{L}{D} = 1.0, \frac{H}{R} = 0.3, F = 0.3, \varepsilon_0 = 0.1, l_m = 30.0, N^2 = 0.5$ and $\nu = 0.2, 0.3$. Trajectories for journal centre motion for $\frac{L}{D} = 1.0, \nu = 0.2, F = 0.3, \varepsilon_0 = 0.1, l_m =$

$30.0, N^2 = 0.5$ and $\frac{H}{R} = 0.2, 0.4$ are presented in the figures 5.14, 5.15. Figures 5.16 through 5.20 represents journal centre trajectories for $\frac{L}{D} = 1.0, \nu = 0.2, F = 0.3, \varepsilon_0 = 0.1, N^2 = 0.5, \frac{H}{R} = 0.3$ and $l_m = 1.0,\ 10,\ 20,\ 40,\ 50$. Journal centre trajectories for $\frac{L}{D} = 1.0, \nu = 0.2, F = 0.3, \varepsilon_0 = 0.1, l_m = 1.0, \frac{H}{R} = 0.3$ and $N^2 = 0.1, 0.3, 0.7, .9$ are shown in figures 5.21 through 5.24 respectively.

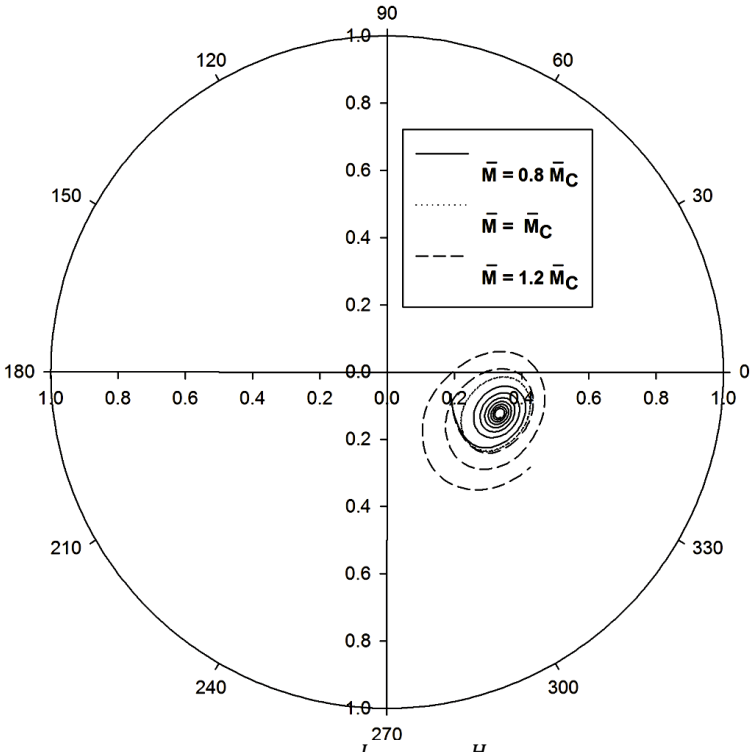

Figure 5.3 Trajectory of Journal center at $\frac{L}{D} = 1.0, \frac{H}{R} = 0.3, \nu = 0.4, F = 0.2, \varepsilon_0 = 0.2, l_m = 40.0, N^2 = 0.5$.

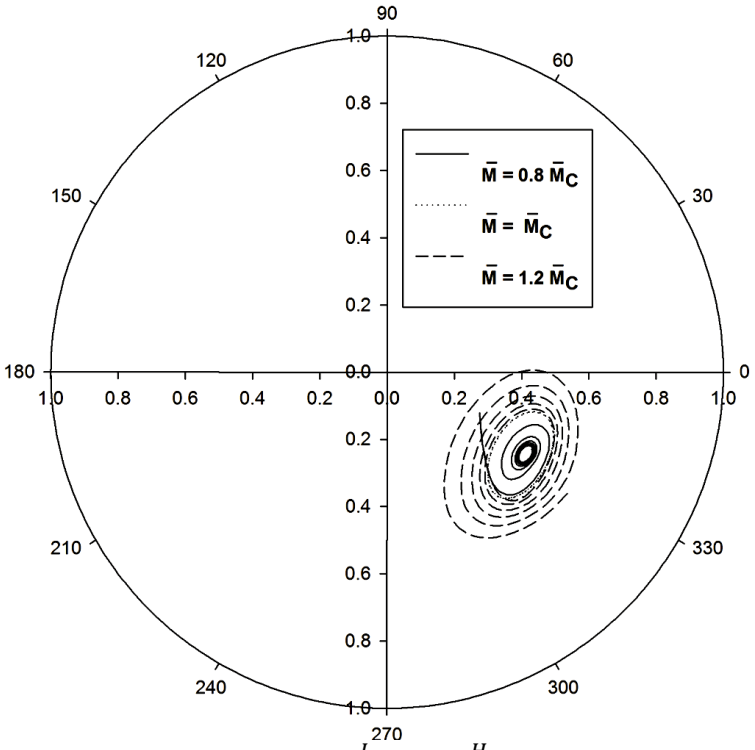

Figure 5.4 Trajectory of Journal center at $\frac{L}{D} = 1.0, \frac{H}{R} = 0.3, \nu = 0.4, F = 0.2, \varepsilon_0 = 0.3,$ $l_m = 40.0, N^2 = 0.5.$

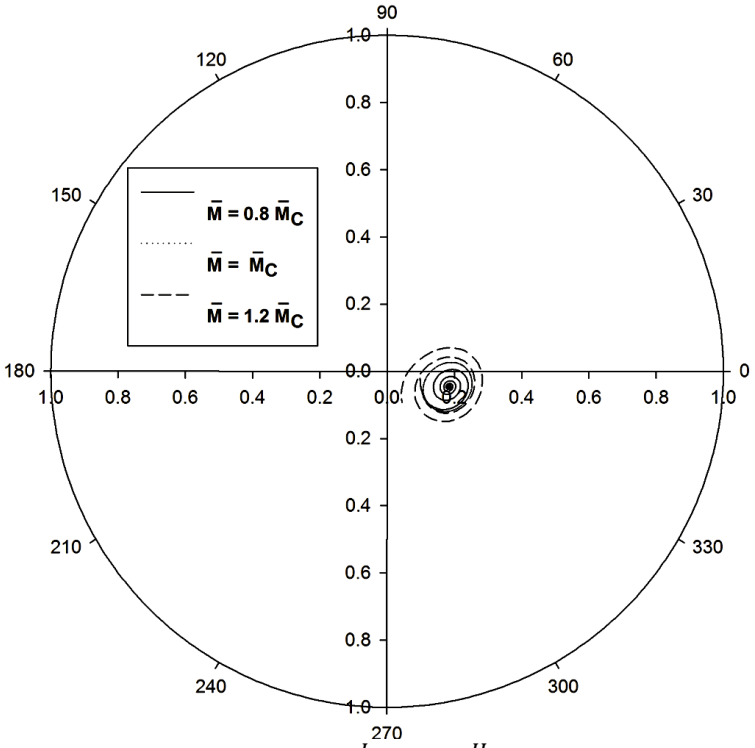

Figure 5.5 Trajectory of Journal center at $\frac{L}{D} = 0.5, \frac{H}{R} = 0.3, \nu = 0.4, F = 0.3, \varepsilon_0 = 0.1,$ $l_m = 30.0, N^2 = 0.5.$

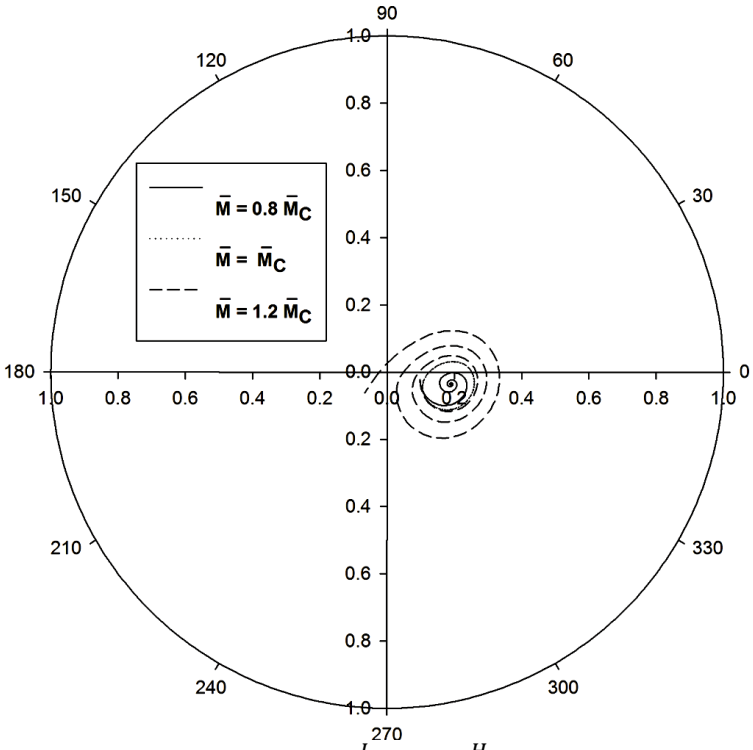

Figure 5.6 Trajectory of Journal center at $\frac{L}{D} = 1.0, \frac{H}{R} = 0.3, \nu = 0.4, F = 0.3, \varepsilon_0 = 0.1,$ $l_m = 30.0, N^2 = 0.5.$

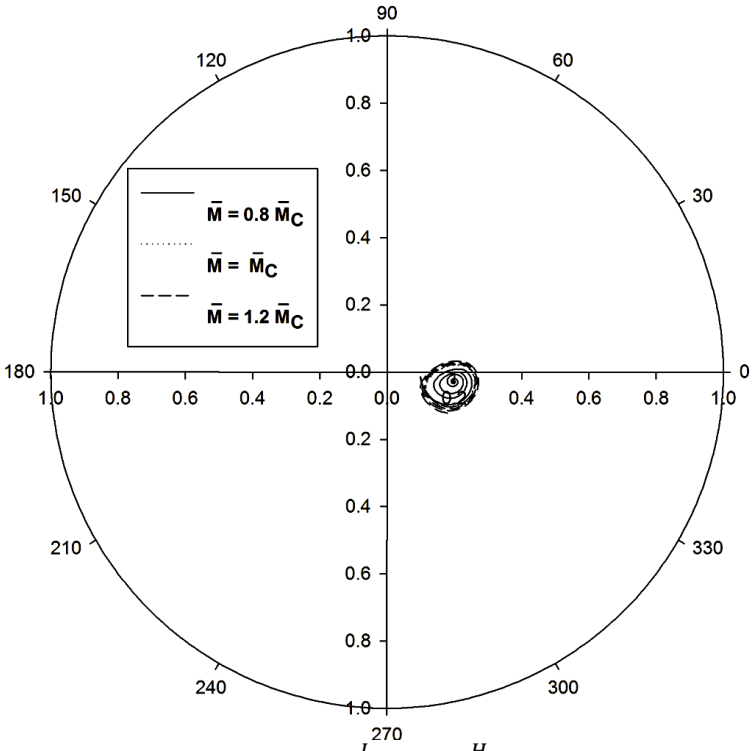

Figure 5.7 Trajectory of Journal center at $\frac{L}{D} = 1.5, \frac{H}{R} = 0.3, \nu = 0.4, F = 0.3, \varepsilon_0 = 0.1,$ $l_m = 30.0, N^2 = 0.5.$

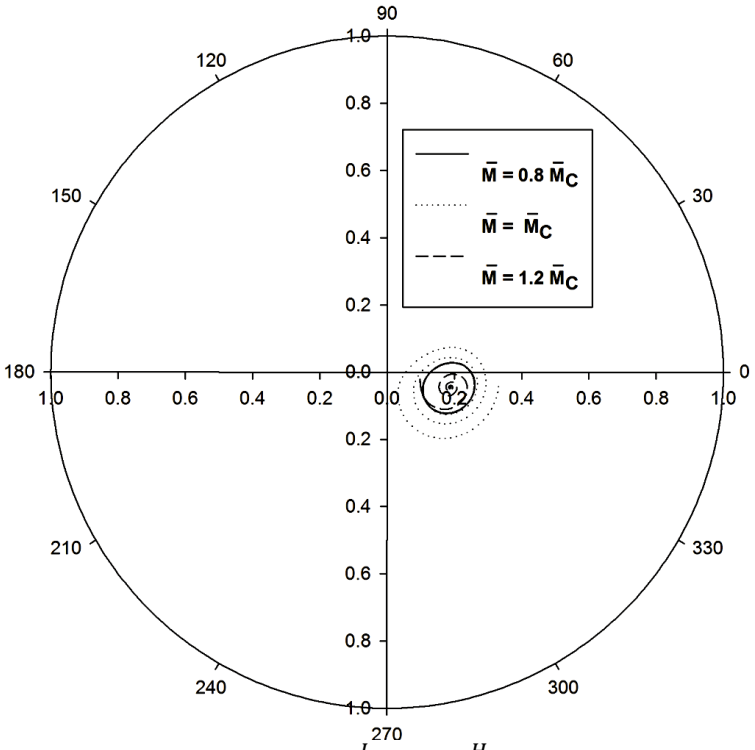

Figure 5.8 Trajectory of Journal center at $\frac{L}{D} = 1.0, \frac{H}{R} = 0.3, \nu = 0.4, F = 0.1, \varepsilon_0 = 0.1,$ $l_m = 30.0, N^2 = 0.5.$

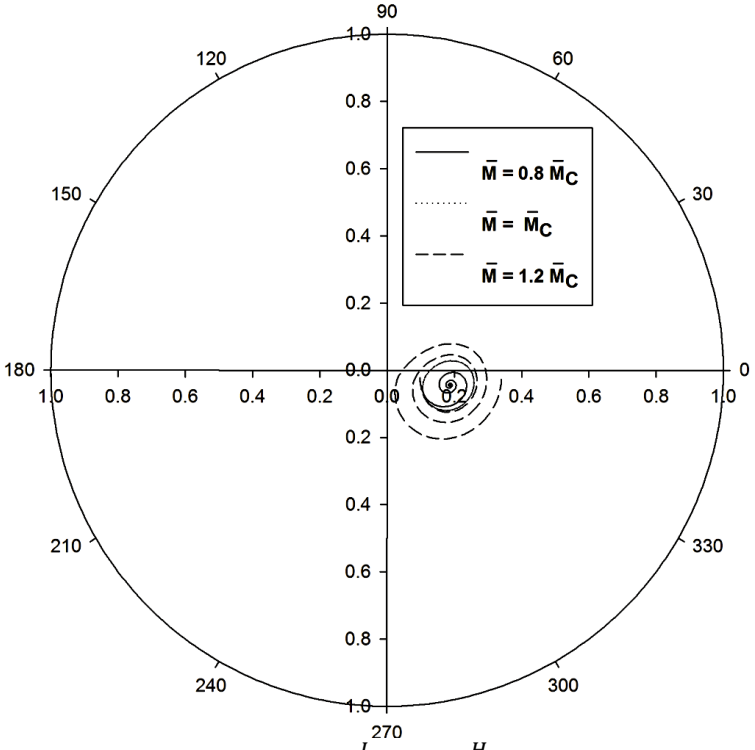

Figure 5.9 Trajectory of Journal center at $\frac{L}{D} = 1.0, \frac{H}{R} = 0.3, \nu = 0.4, F = 0.2, \varepsilon_0 = 0.1,$ $l_m = 30.0, N^2 = 0.5.$

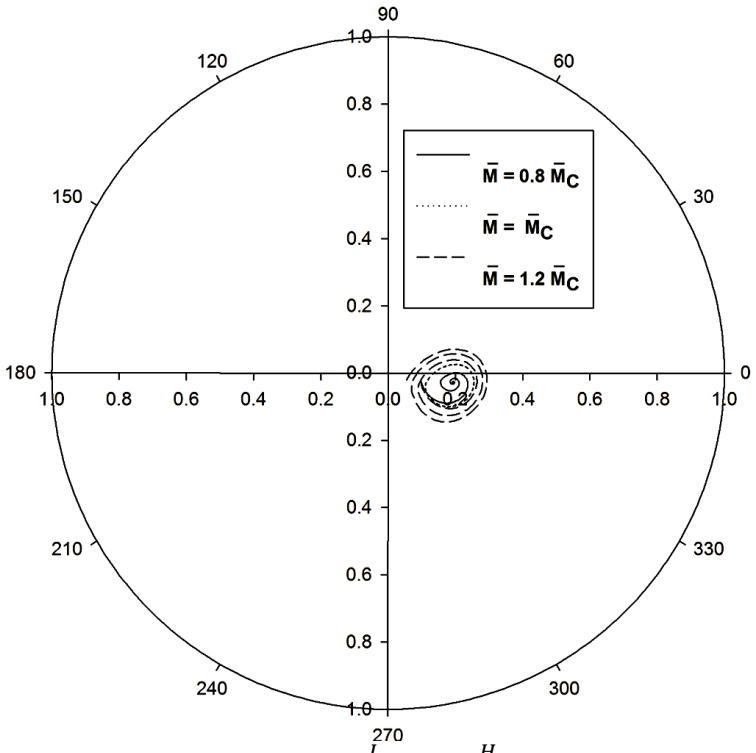

Figure 5.10 Trajectory of Journal center at $\frac{L}{D} = 1.0, \frac{H}{R} = 0.3, \nu = 0.4, F = 0.4, \varepsilon_0 = 0.1,$ $l_m = 30.0, N^2 = 0.5.$

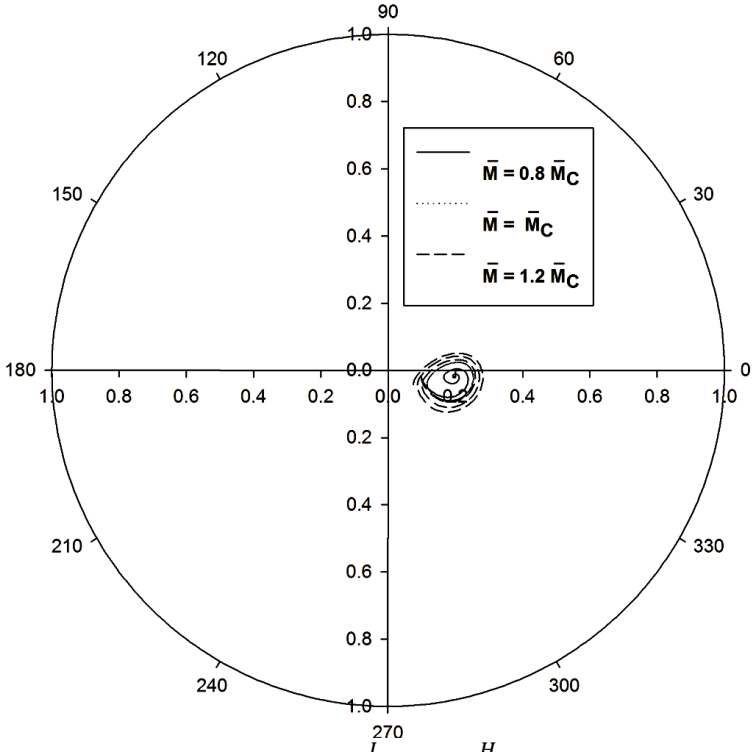

Figure 5.11 Trajectory of Journal center at $\frac{L}{D} = 1.0, \frac{H}{R} = 0.3, \nu = 0.4, F = 0.5, \varepsilon_0 = 0.1,$ $l_m = 30.0, N^2 = 0.5.$

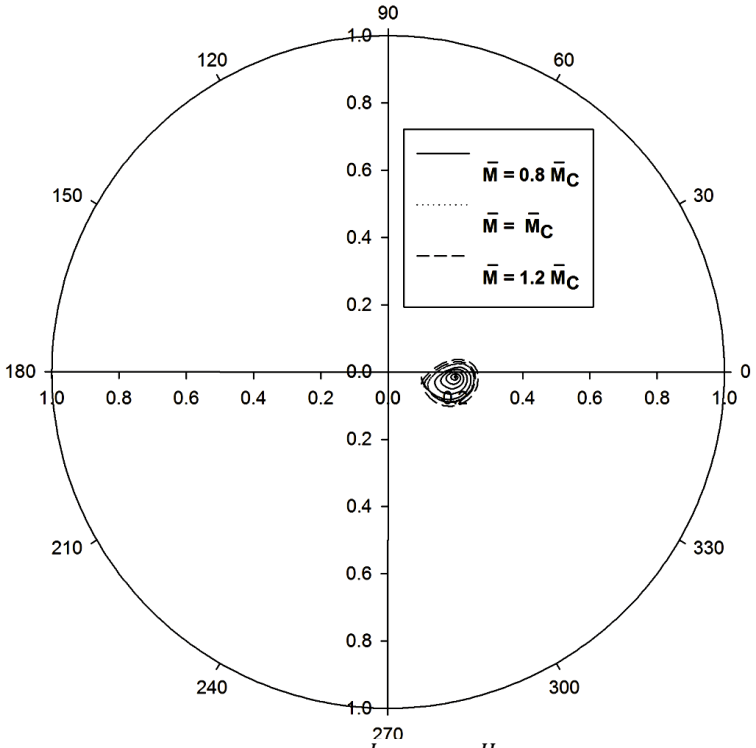

Figure 5.12 Trajectory of Journal center at $\frac{L}{D} = 1.0, \frac{H}{R} = 0.3, \nu = 0.2, F = 0.3, \varepsilon_0 = 0.1,$ $l_m = 30.0, N^2 = 0.5.$

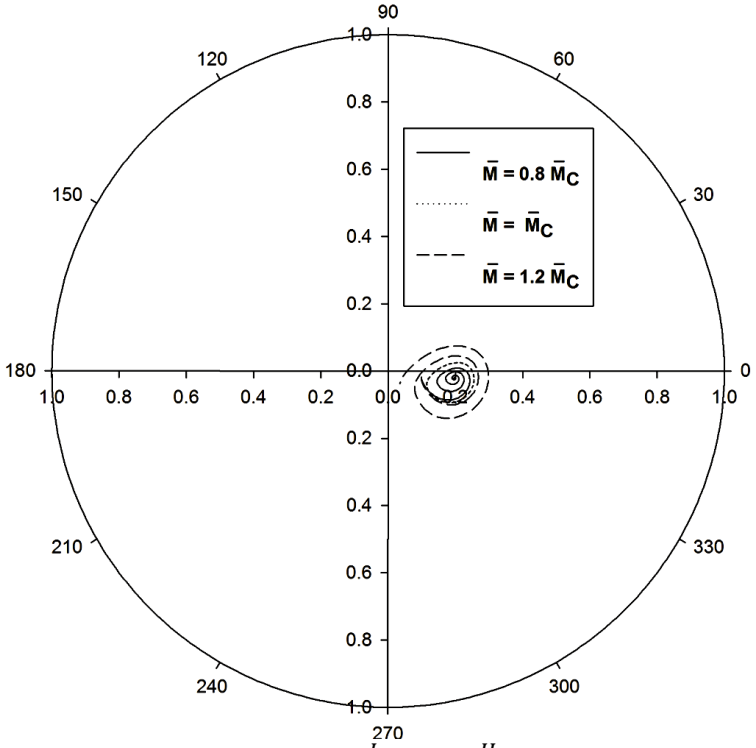

Figure 5.13 Trajectory of Journal center at $\frac{L}{D} = 1.0, \frac{H}{R} = 0.3, \nu = 0.3, F = 0.3, \varepsilon_0 = 0.1,$ $l_m = 30.0, N^2 = 0.5.$

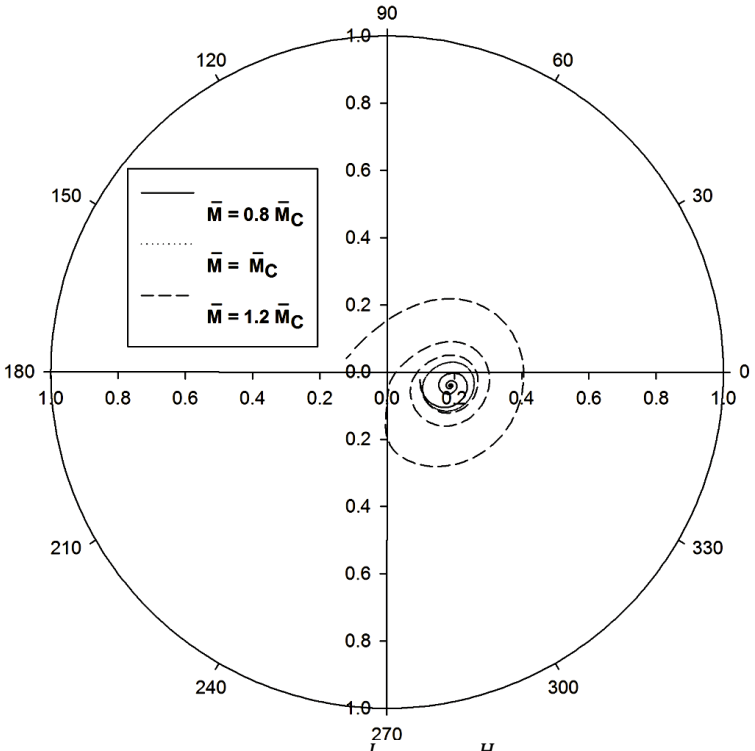

Figure 5.14 Trajectory of Journal center at $\frac{L}{D} = 1.0, \frac{H}{R} = 0.2, \nu = 0.4, F = 0.3, \varepsilon_0 = 0.1,$ $l_m = 30.0, N^2 = 0.5.$

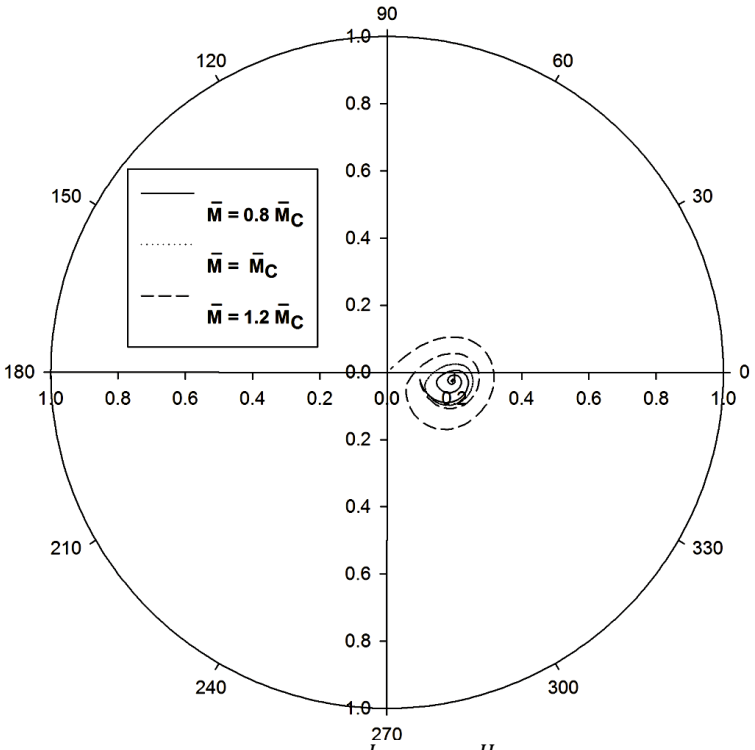

Figure 5.15 Trajectory of Journal center at $\frac{L}{D} = 1.0, \frac{H}{R} = 0.4, \nu = 0.4, F = 0.3, \varepsilon_0 = 0.1,$ $l_m = 30.0, N^2 = 0.5.$

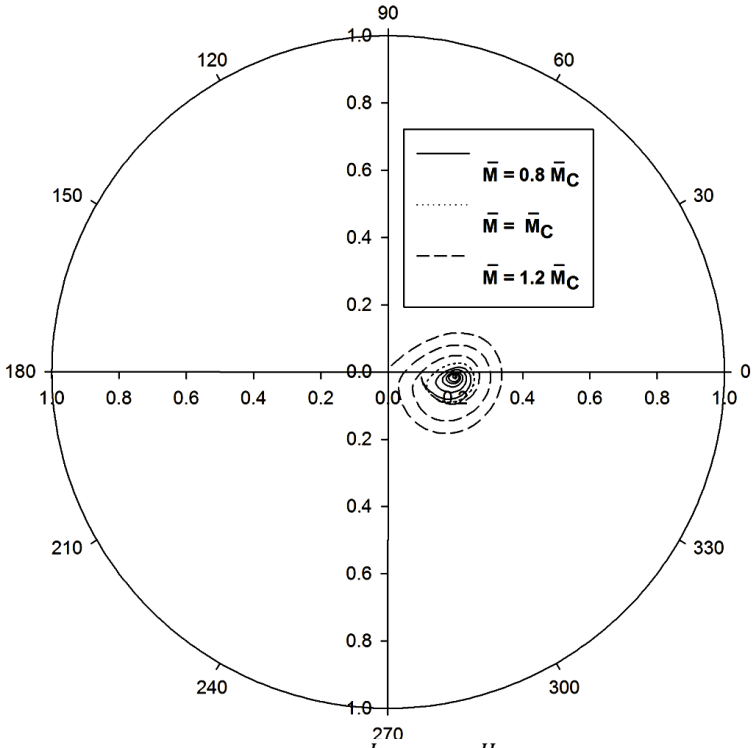

Figure 5.16 Trajectory of Journal center at $\frac{L}{D} = 1.0, \frac{H}{R} = 0.3, \nu = 0.4, F = 0.3, \varepsilon_0 = 0.1,$ $l_m = 1.0, N^2 = 0.5.$

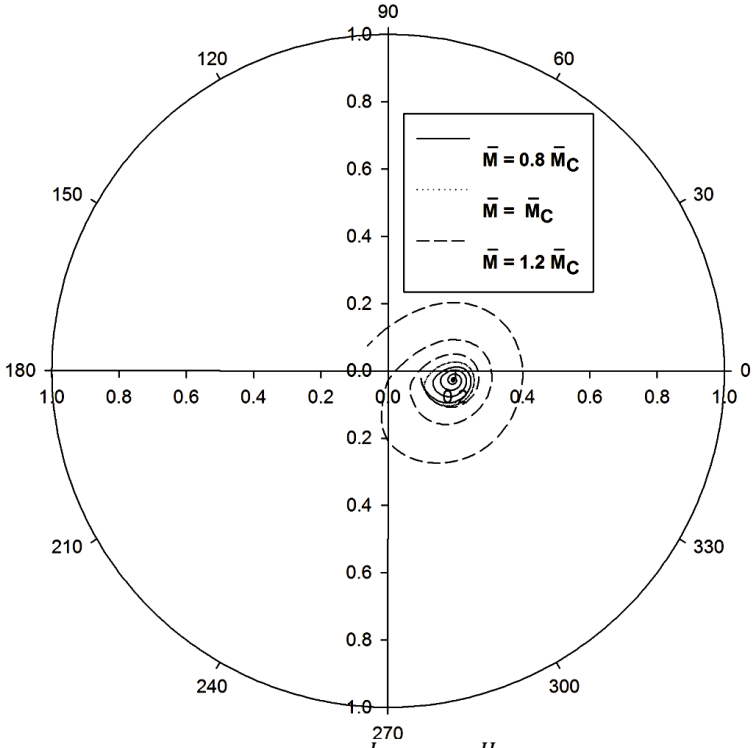

Figure 5.17 Trajectory of Journal center at $\frac{L}{D} = 1.0, \frac{H}{R} = 0.3, \nu = 0.4, F = 0.3, \varepsilon_0 = 0.1,$ $l_m = 10.0, N^2 = 0.5.$

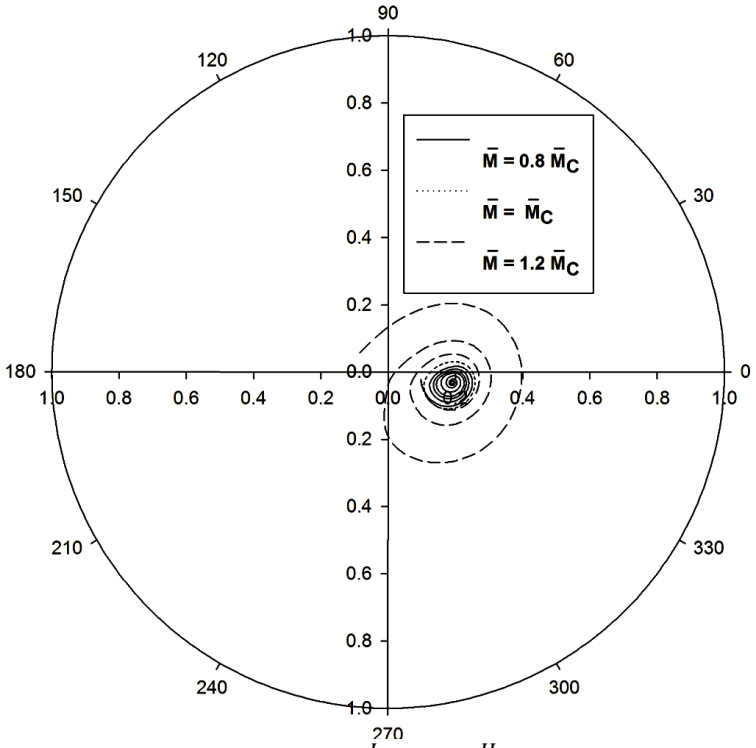

Figure 5.18 Trajectory of Journal center at $\frac{L}{D} = 1.0, \frac{H}{R} = 0.3, \nu = 0.4, F = 0.3, \varepsilon_0 = 0.1,$ $l_m = 20.0, N^2 = 0.5.$

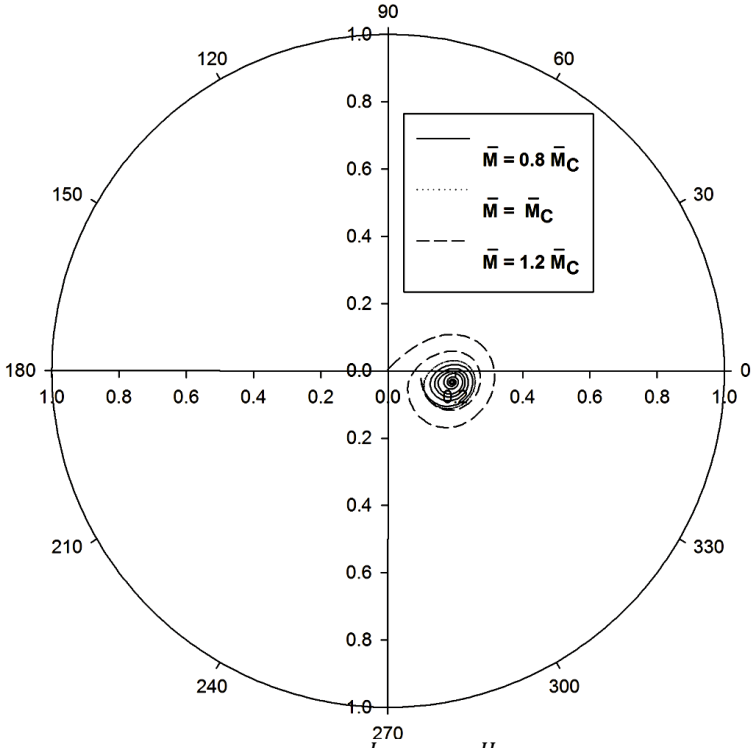

Figure 5.19 Trajectory of Journal center at $\frac{L}{D} = 1.0, \frac{H}{R} = 0.3, \nu = 0.4, F = 0.3, \varepsilon_0 = 0.1,$ $l_m = 40.0, N^2 = 0.5.$

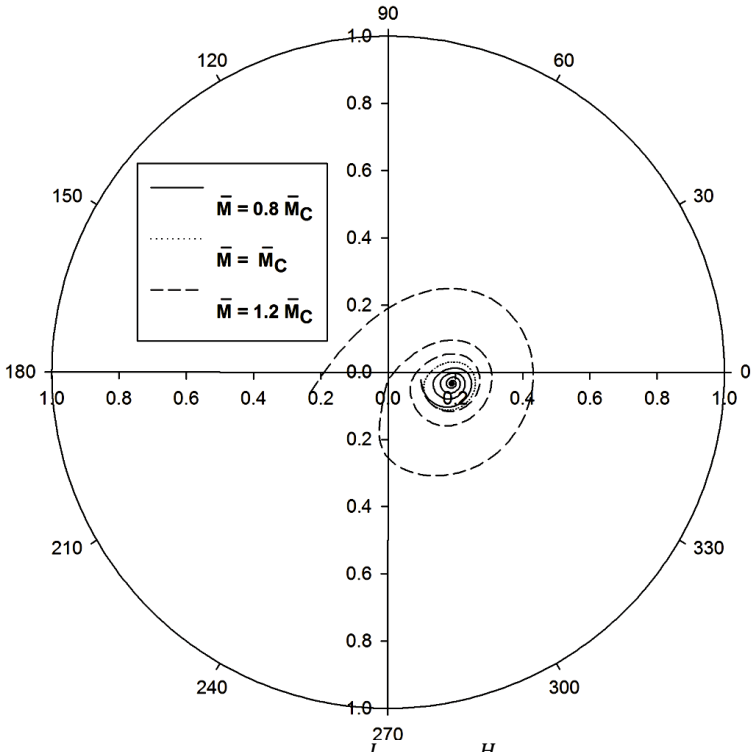

Figure 5.20 Trajectory of Journal center at $\frac{L}{D} = 1.0, \frac{H}{R} = 0.3, \nu = 0.4, F = 0.3, \varepsilon_0 = 0.1,$ $l_m = 50.0, N^2 = 0.5.$

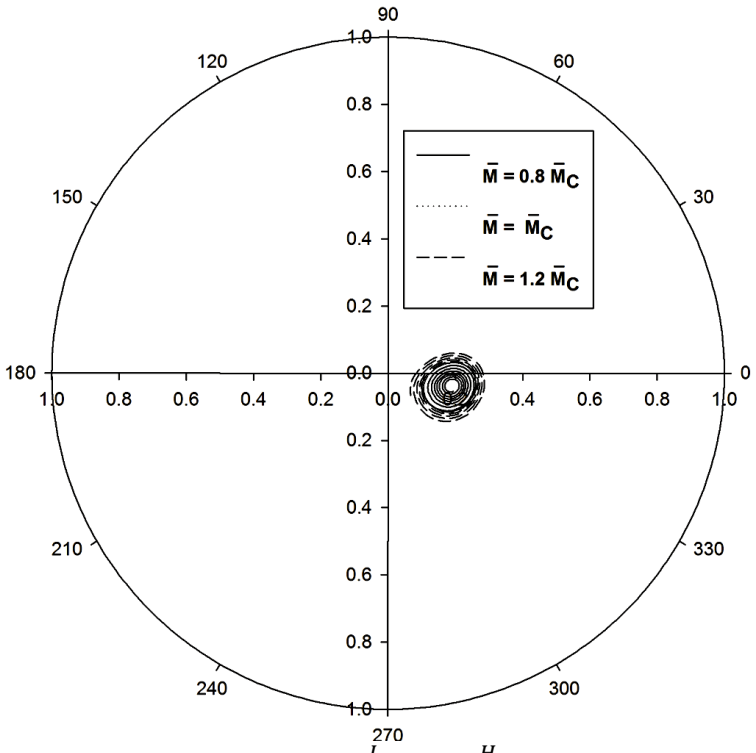

Figure 5.21 Trajectory of Journal center at $\frac{L}{D} = 1.0, \frac{H}{R} = 0.3, \nu = 0.4, F = 0.3, \varepsilon_0 = 0.1,$ $l_m = 30.0, N^2 = 0.1.$

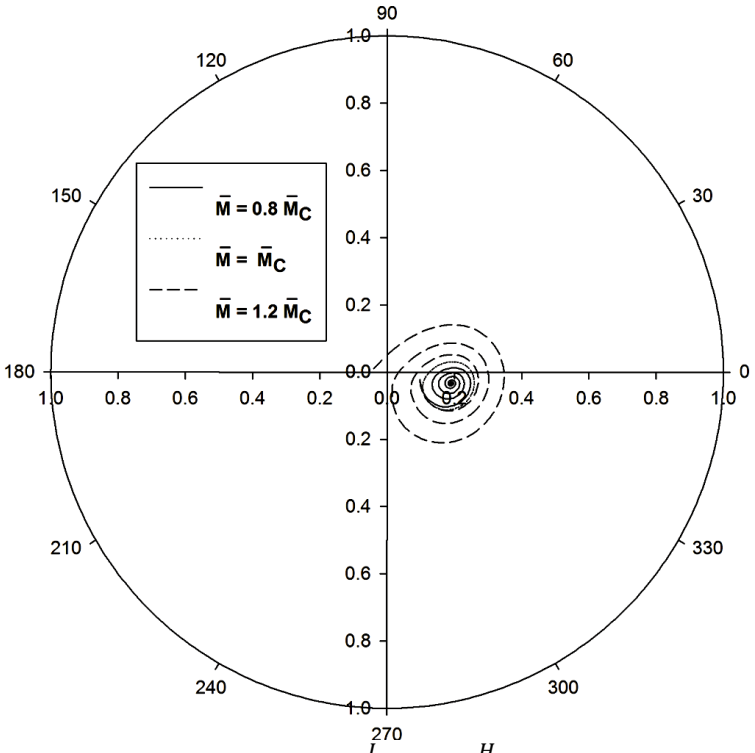

Figure 5.22 Trajectory of Journal center at $\frac{L}{D} = 1.0, \frac{H}{R} = 0.3, \nu = 0.4, F = 0.3, \varepsilon_0 = 0.1,$ $l_m = 30.0, N^2 = 0.3.$

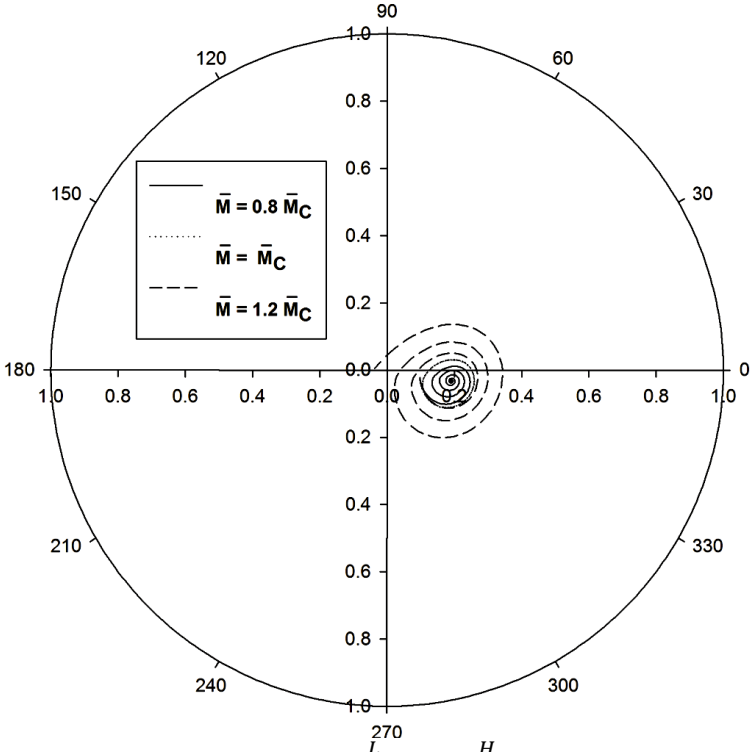

Figure 5.23 Trajectory of Journal center at $\frac{L}{D} = 1.0, \frac{H}{R} = 0.3, \nu = 0.4, F = 0.3, \varepsilon_0 = 0.1,$ $l_m = 30.0, N^2 = 0.7.$

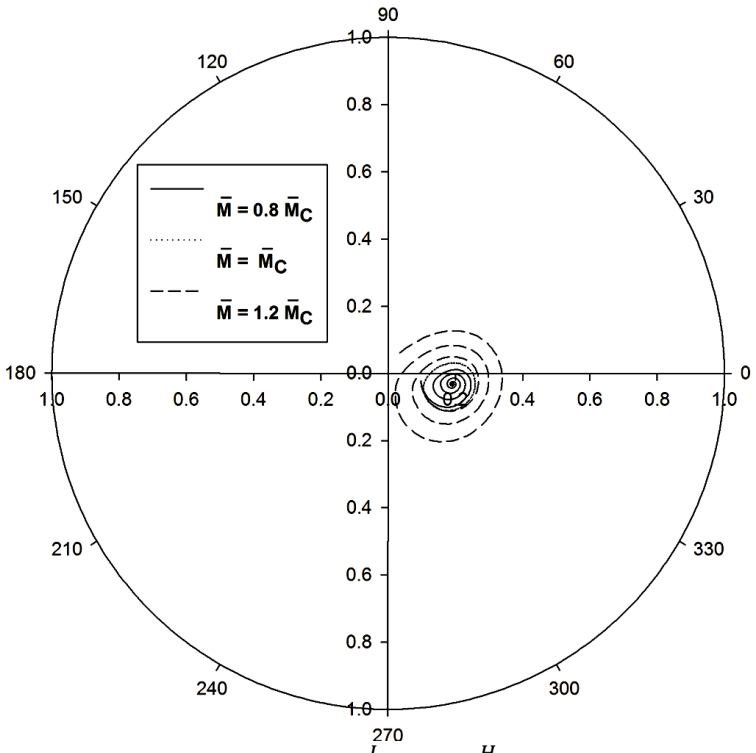

Figure 5.24 Trajectory of Journal center at $\frac{L}{D} = 1.0, \frac{H}{R} = 0.3, \nu = 0.4, F = 0.3, \varepsilon_0 = 0.1,$ $l_m = 30.0, N^2 = 0.9.$

5.3.1 Limit cycle

5.3.1.1 Effect of slenderness ratio ($\frac{L}{D}$)

Comparison of limit cycle for various slenderness ratio at $F = 0.3, \frac{H}{R} = 0.3, \nu = 0.4, \varepsilon_0 = 0.1, l_m = 30.0$ and $N^2 = 0.5$ is shown in figure 5.25. Limit cycle shifts towards right as value of slenderness ratio increases and also journal traces smaller orbit.

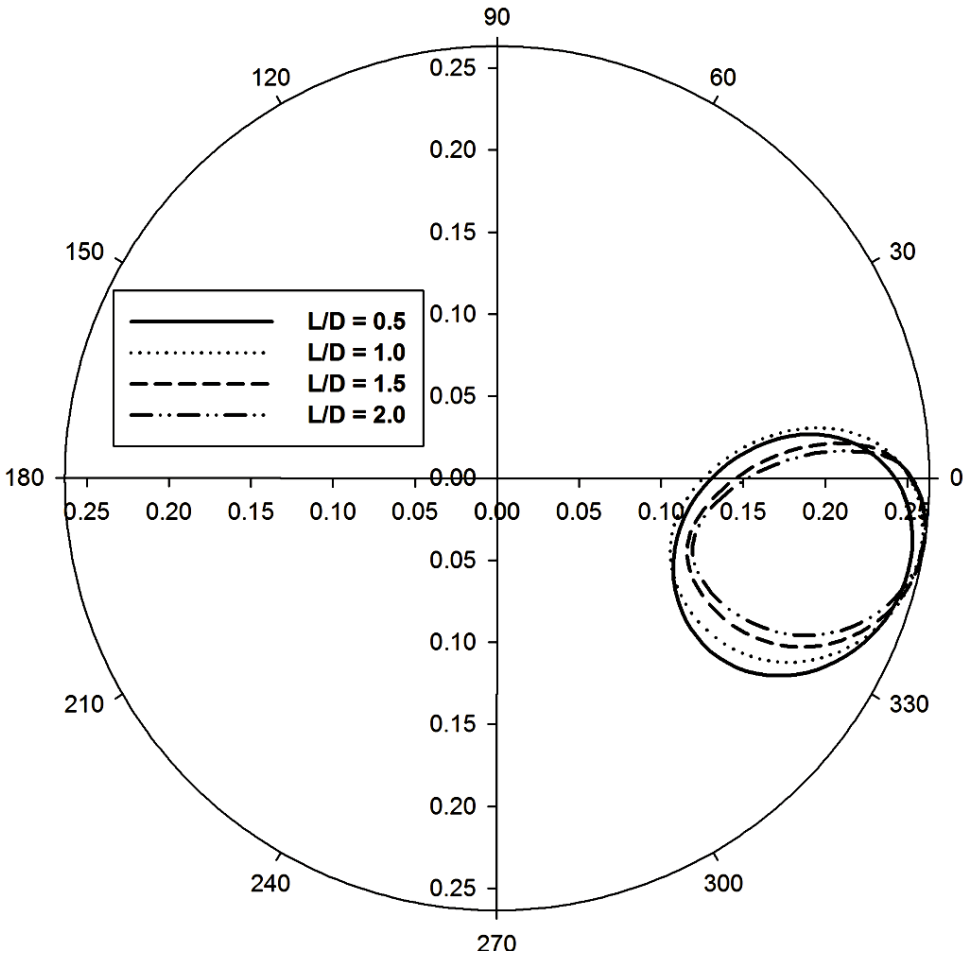

Figure 5.25 Comparison of limit cycle for various $\frac{L}{D}$ at $\frac{H}{R} = 0.3, \nu = 0.4, F = 0.3, \varepsilon_0 = 0.1, l_m = 30.0, N^2 = 0.5$.

5.3.1.2 Effect of deformation factor (F)

Limit cycles for various deformation factor at $\frac{L}{D} = 1.0, \frac{H}{R} = 0.3, \nu = 0.4, \varepsilon_0 = 0.1, l_m = 30.0$ and $N^2 = 0.5$ is shown in figure 5.26. Observations from figure predict that limit cycle shrinks in area as value of deformation factor is increased.

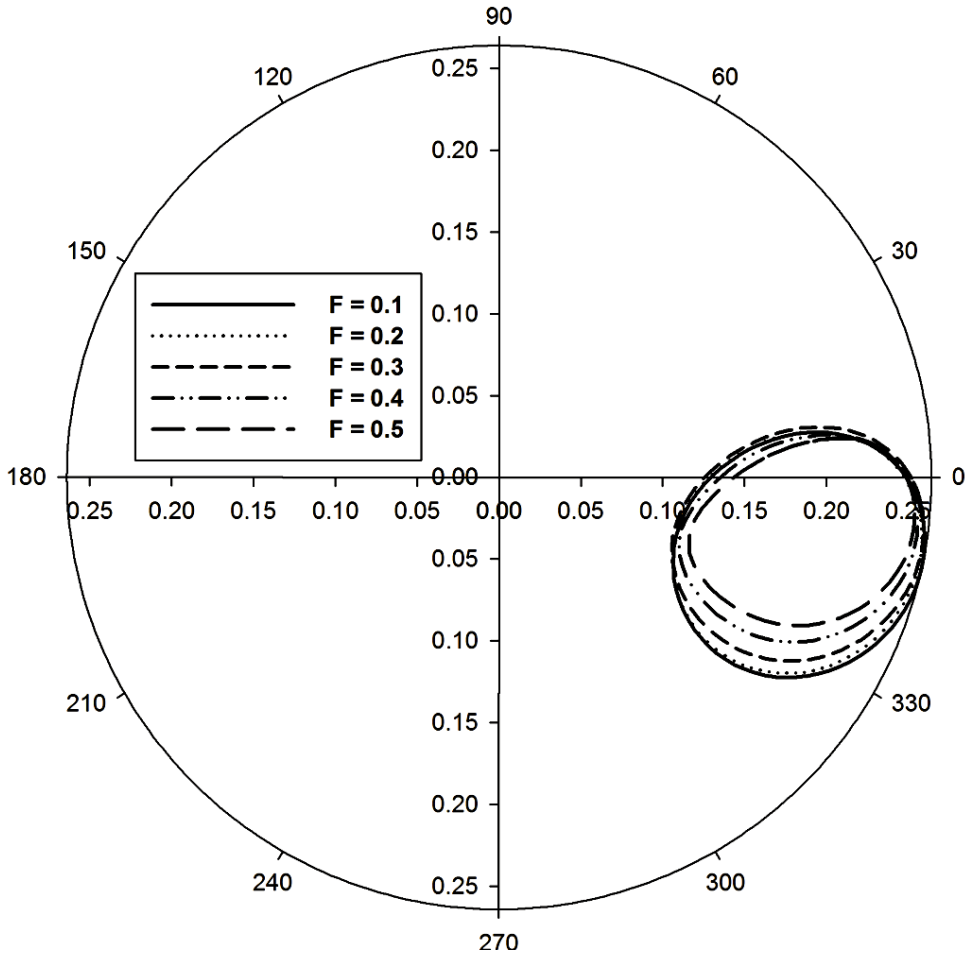

Figure 5.26 Comparison of limit cycle for various F at $\frac{L}{D} = 1.0, \frac{H}{R} = 0.3, \nu = 0.4, \varepsilon_0 = 0.1,$ $l_m = 30.0, N^2 = 0.5.$

5.3.1.3 Effect of Poisson's ratio (ν)

Figure 5.27 shows comparison of limit cycle for various values of Poisson's ratio at $\frac{L}{D} = 1.0,$ $\frac{H}{R} = 0.3, F = 0.3, \varepsilon_0 = 0.1, l_m = 30.0$ and $N^2 = 0.5.$ Study of figure shows that journal traces larger orbit as value of Poisson's ratio is increased.

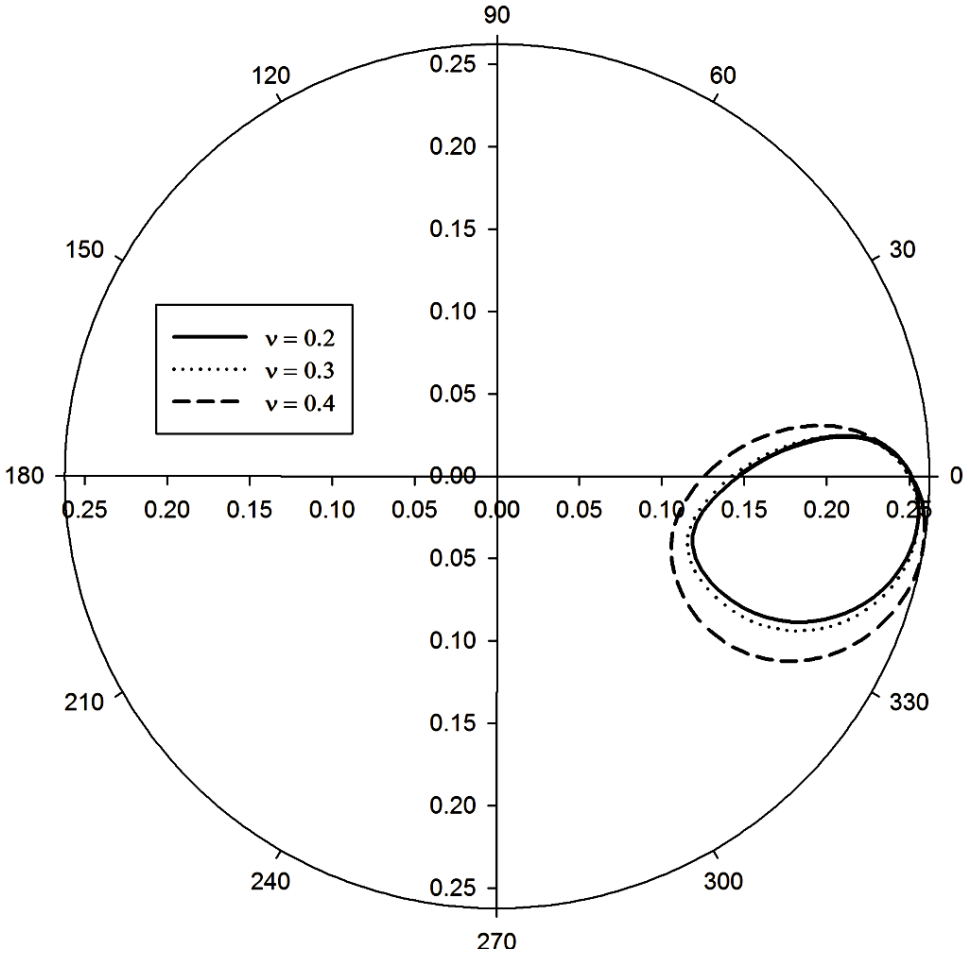

Figure 5.27 Comparison of limit cycle for various ν at $\frac{L}{D} = 1.0, \frac{H}{R} = 0.3, F = 0.3, \varepsilon_0 = 0.1,$ $l_m = 30.0, N^2 = 0.5.$

5.3.1.4 Effect of H/R ratio

Effect of variation of bearing H/R ratio on limit cycle at $\frac{L}{D} = 1.0, F = 0.3, \nu = 0.4, \varepsilon_0 = 0.1,$ $l_m = 30.0$ and $N^2 = 0.5$ is shown in figure 5.28. It is observed from figure that as value of liner thickness to bearing radius is increased journal traces a smaller orbit.

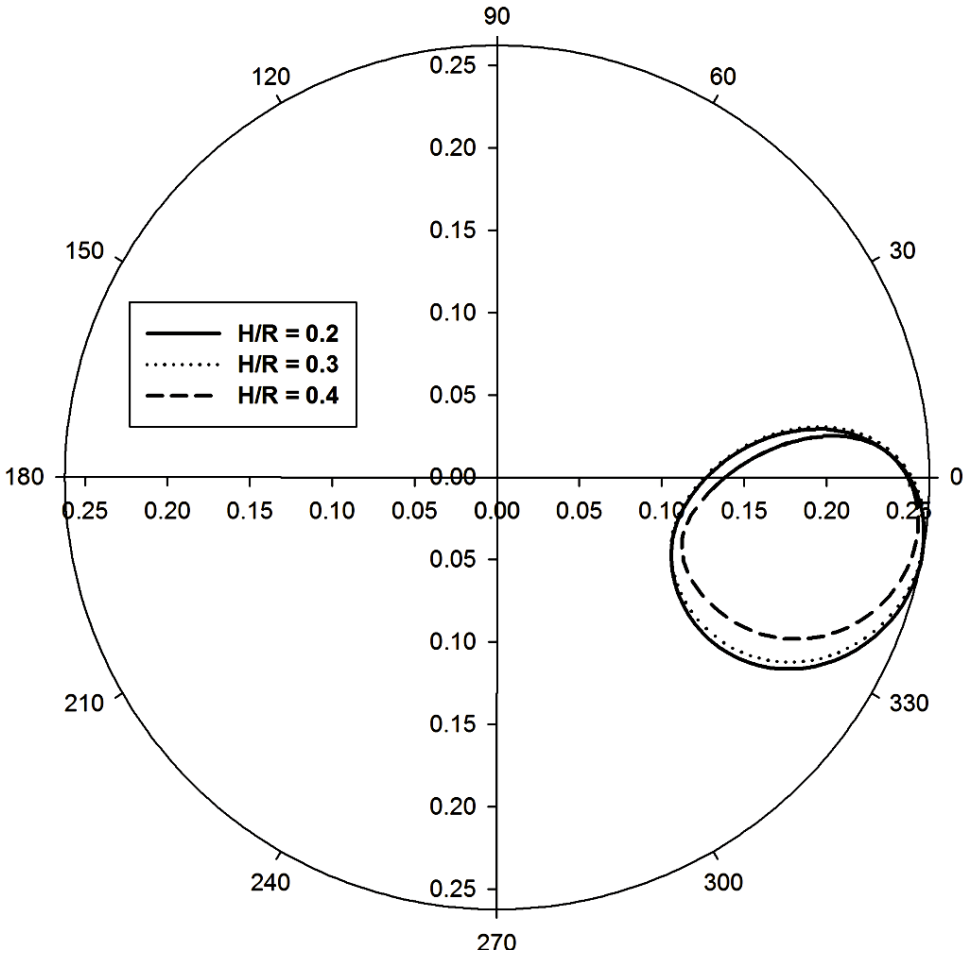

Figure 5.28 Comparison of limit cycle for various $\frac{H}{R}$ at $\frac{L}{D} = 1.0, \nu = 0.4, F = 0.3, \varepsilon_0 = 0.1,$ $l_m = 30.0, N^2 = 0.5.$

5.3.1.5 Effect of characteristic length (l_m)

Figure 5.29 depicts effect of variation of characteristic length when other parameters are kept constant on size of limit cycle at $\frac{L}{D} = 1.0, F = 0.3, \nu = 0.4, \varepsilon_0 = 0.1, \frac{H}{R} = 0.3$ and $N^2 = 0.5$. Size of limit cycle increases in area as value of characteristic length is increased.

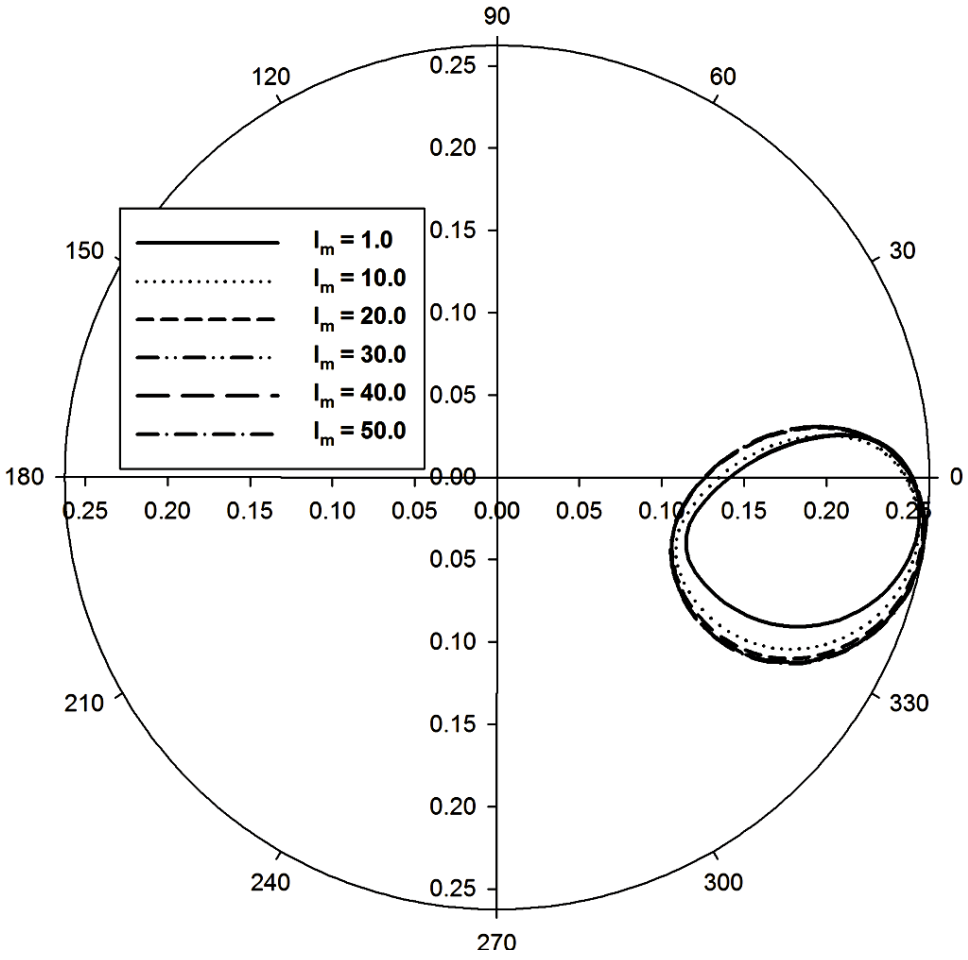

Figure 5.29 Comparison of limit cycle for various l_m at $\frac{L}{D} = 1.0, \frac{H}{R} = 0.3, \nu = 0.4, F = 0.3, \varepsilon_0 = 0.1, N^2 = 0.5$.

5.3.1.6 Effect of coupling number (N)

Comparison of limit cycle for journal center for various coupling numbers at $\frac{L}{D} = 1.0, \nu = 0.4, F = 0.3, \varepsilon_0 = 0.1, \frac{H}{R} = 0.3$ and $l_m = 30.0$ is shown in figure 5.30. Journal center traces smaller orbit as value of coupling number is increased.

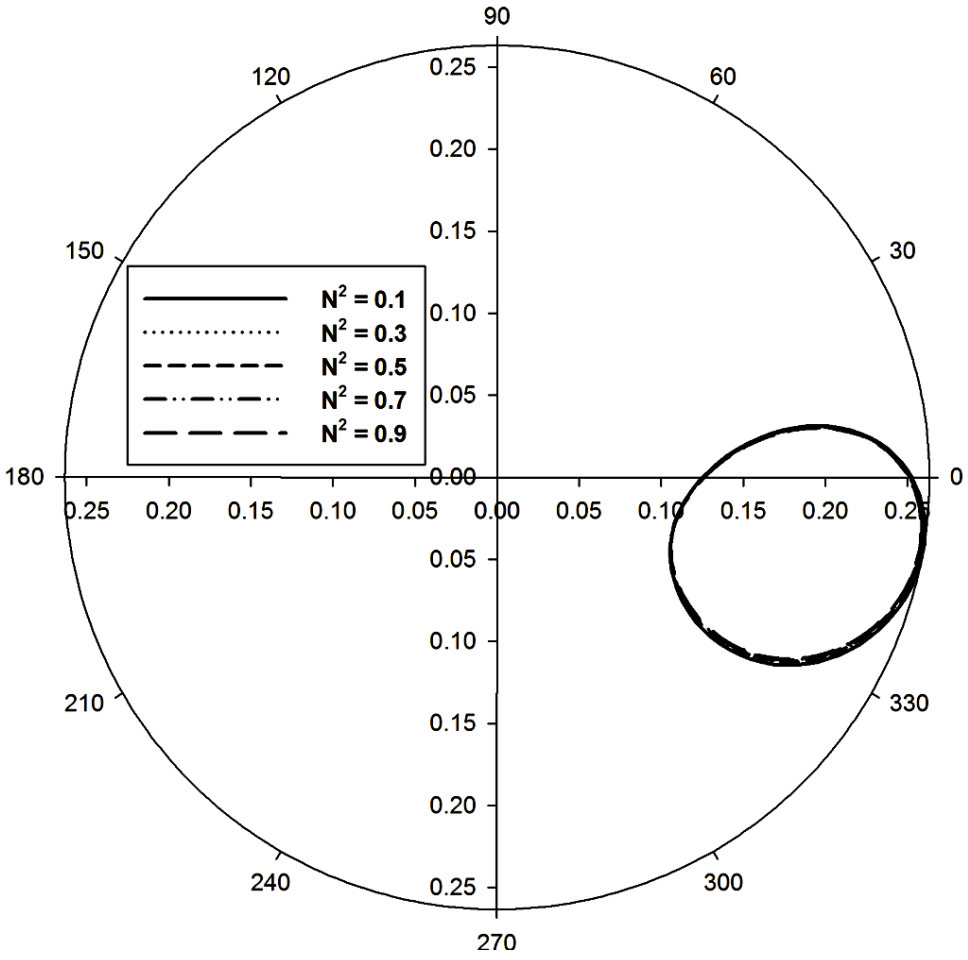

Figure 5.30 Comparison of limit cycle for various N^2 at $\frac{L}{D} = 1.0, \frac{H}{R} = 0.3, \nu = 0.4, F = 0.3,$ $\varepsilon_0 = 0.1, l_m = 30.0.$

5.3.2 Critical mass parameter

5.3.2.1 Effect of deformation factor (F)

Figure 5.31 shows comparison of critical mass parameter obtained by nonlinear analysis and linear dynamic analysis carried out in earlier chapter. Critical mass parameter versus Sommerfeld number is plotted for various deformation factor at $\frac{L}{D} = 1.0, \nu = 0.4, l_m = 30.0,$ $\frac{H}{R} = 0.3$ and $N^2 = 0.5$. It can be observed that critical mass parameter decreases with increase in deformation factor and also decreases with increase in Sommerfeld number. Linear analysis predicts better stability at higher Sommerfeld number. Non-linear analysis gives better stability at lower Sommerfeld number.

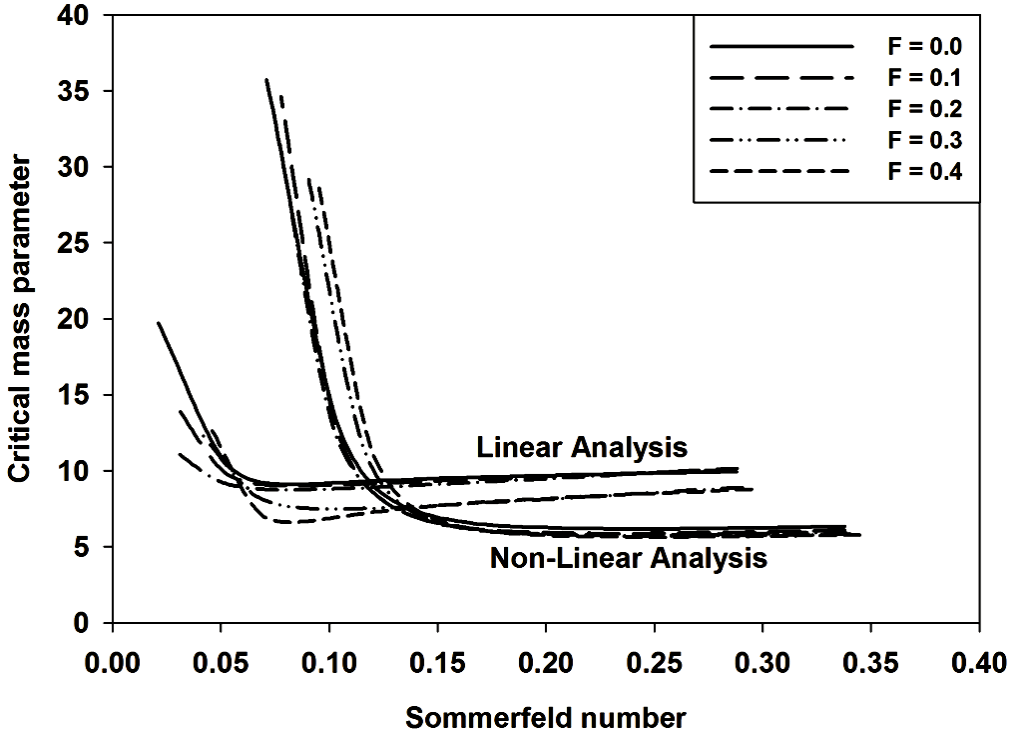

Figure 5.31 $\bar{M}_C$ Vs. Sommerfeld number for various F at $\frac{L}{D} = 1.0, \frac{H}{R} = 0.3, \nu = 0.4,$ $l_m = 30.0, N^2 = 0.5.$

5.3.2.2 Effect of coupling number (N)

Critical mass parameter versus Sommerfeld number for values of coupling number at $\frac{L}{D} = 1.0, \nu = 0.4, \varepsilon_0 = 0.1, \frac{H}{R} = 0.3$ and $F = 0.3$ is shown in figure 5.32. Critical mass parameter increases with increase in coupling number. Linear dynamic analysis predicts higher stability that non-linear analysis. Results are in line with results predicted by Das et al. [142] that at lower eccentricity ratio linear dynamic analysis predicts higher stability in comparison to non-linear dynamic analysis.

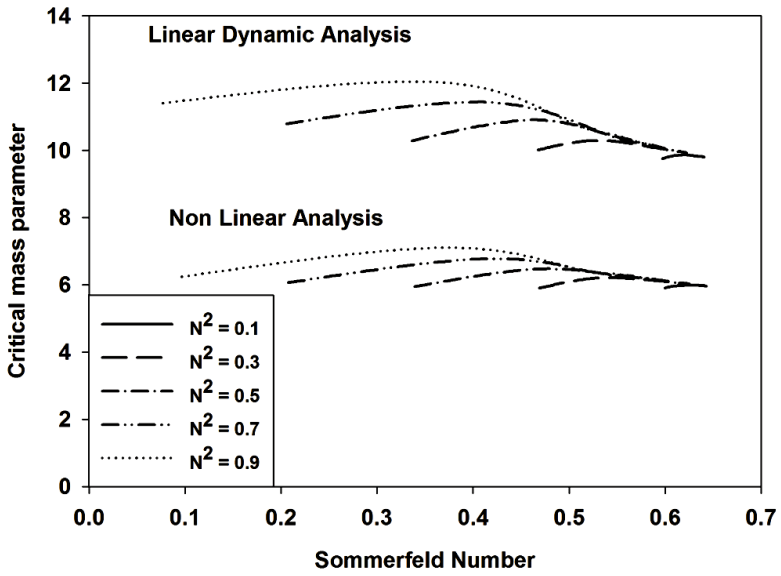

Figure 5.32 $\bar{M}_C$ Vs. Sommerfeld number for various N^2 at $\frac{L}{D} = 1.0, \frac{H}{R} = 0.3, \nu = 0.4,$ $l_m = 30.0, F = 0.3.$

5.3.2.3 Effect of slenderness ratio ($\frac{L}{D}$)

Critical mass parameter versus deformation factor for values of slenderness ratio is shown in figure 5.33. Variation in graph shows that stability of journal bearing decreases with increase in slenderness ratio. It can also be observed that linear dynamic analysis predicts better stability in comparison to non-linear dynamic analysis.

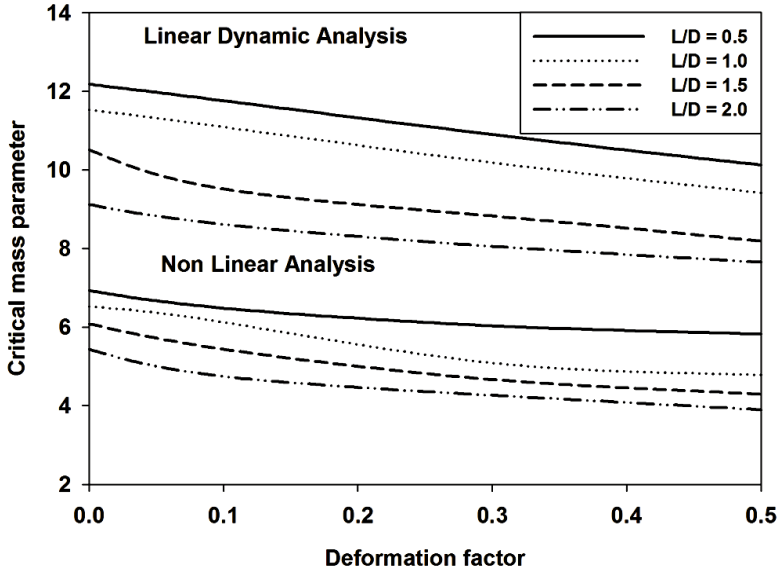

Figure 5.33 $\bar{M}_C$ Vs. F for various $\frac{L}{D}$ at $\varepsilon_0 = 0.1, \frac{H}{R} = 0.3, \nu = 0.4,$ $l_m = 30.0, N^2 = 0.5, F = 0.3.$

5.3.2.4 Effect of Poisson's ratio (ν)

Effect of Poisson's ratio on critical mass parameter for linear dynamic analysis and non-linear dynamic analysis at $\frac{L}{D} = 1.0, l_m = 30.0, \varepsilon_0 = 0.1, \frac{H}{R} = 0.3, N^2 = 0.5$ and $F = 0.3$ is shown in figure 5.34. $\bar{M}_C$ increases as Poisson's ratio increases. $\bar{M}_C$ decreases with increase in deformation factor.

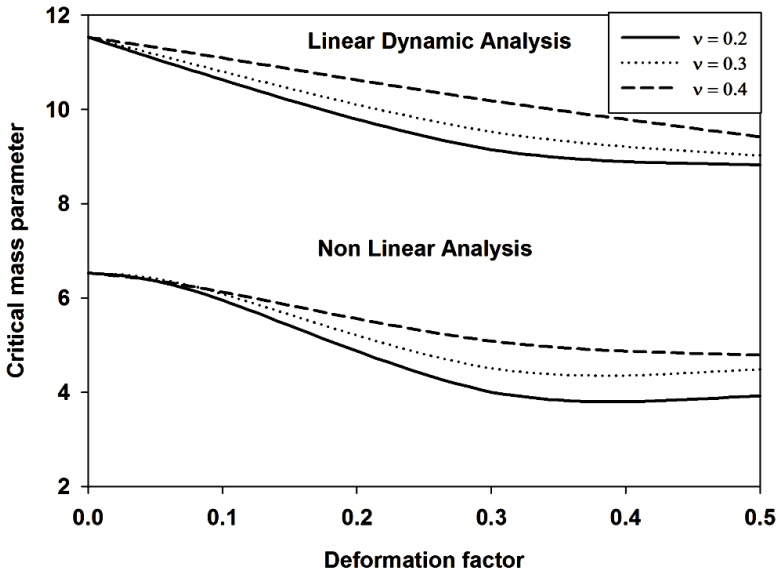

Figure 5.34 $\bar{M}_C$ Vs. F for various ν at $\varepsilon_0 = 0.1, \frac{H}{R} = 0.3, \frac{L}{D} = 0.1, l_m = 30.0, N^2 = 0.5, F = 0.3.$

5.3.2.5 Effect of $\frac{H}{R}$ ratio

Critical mass parameter versus deformation factor for various values of Poisson's ratio at $\frac{L}{D} = 1.0, l_m = 30.0, \varepsilon_0 = 0.1, \frac{H}{R} = 0.3, N^2 = 0.5, \nu = 0.4$ and $F = 0.3$ is shown in figure 5.35. Study of graph shows that $\bar{M}_C$ decreases with increase in H/R ratio.

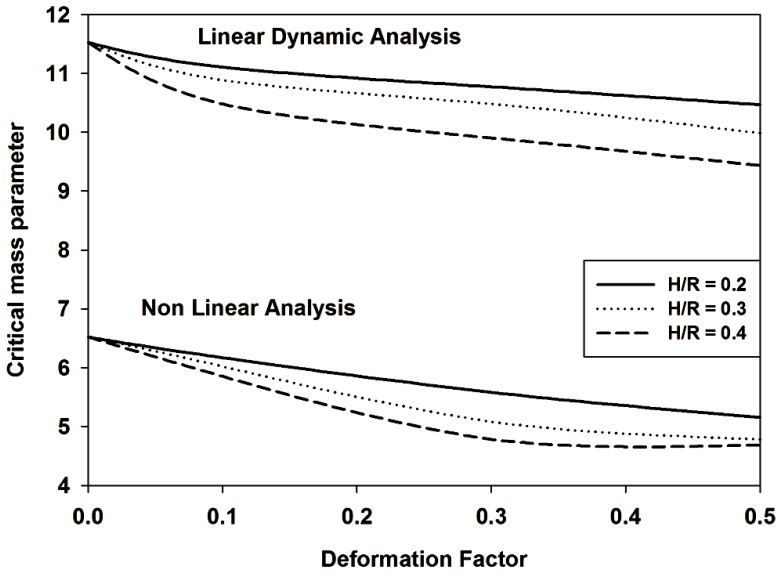

Figure 5.35 $\bar{M}_C$ Vs. F for various $\frac{H}{R}$ at $\varepsilon_0 = 0.1, \nu = 0.4, \frac{L}{D} = 0.1,$ $l_m = 30.0, N^2 = 0.5, F = 0.3.$

Chapter 6 Conclusion and Scope for Future Work

6.1 Conclusions

In this dissertation, theoretical analysis of hydrodynamic journal bearings under micropolar lubrication considering effect of flexibility of bearing liner is conducted. Parametric study is conducted which enables us to use every possible value of various parameters.

From studies and results presented in above chapters, following conclusions may be drawn.

6.1.1 Conclusions for steady state analysis.

1. Load carrying capacity is enhanced with increase in eccentricity ratio. However, at very high eccentricity ratio's 0.85, load parameter decreases from that at ε_0 = 0.8 beyond F=0.15. This is due to effect of flexibility of liner which is more pronounced at higher eccentricity ratio. From this observation it can be concluded that while designing bearings effect of flexibility of bearing liner can't be neglected for applications where eccentricity ratio is high.

2. The load carrying capacity of the bearing decreases as we increase value of deformation factor F. Also, deformation factor is inversely proportional to Young's modulus of elasticity for a particular bearing configuration. So, it can be interpreted from the results that load carrying capacity is directly proportional to young's modulus of elasticity of bearing liner material.

3. Non-dimensional load carrying capacity is more for higher slenderness ratio for particular deformation factor, eccentricity ratio and micropolar parameters.

4. As value of Poisson's ratio is increased steady state non-dimensional load parameters decreases when all other parameters are kept constant. Steady state load parameter decreases with increase in H/R ratio.

5. Increase in characteristic length leads to decrease in load carrying capacity. Enhanced effective viscosity leads to higher load carrying capacity due to increase in coupling

effect between linear and angular momentum as coupling number increases. Load parameter converges to Newtonian values as $l_m \to \infty$ and $N^2 \to 0$.

6. Attitude angle decreases as eccentricity ratio is increased and it is also concluded that attitude angle remains constant with deformation factor for a particular value of eccentricity for $\varepsilon_0 \leq 0.6$. Attitude angle increases with increase in deformation factor for higher values of eccentricity ratio.

7. Attitude angle increases with increase in slenderness ratio. With an increase in Poisson's ratio keeping all other micropolar as well as bearing parameters constant there is increase in attitude angle. Attitude angle is more at higher H/R ratio.

8. Attitude angle initially decreases as l_m increases reaching a minimum value near $l_m \to 10.0$ and then trend is reversed. Attitude angle decreases as coupling number is increased.

9. Friction parameter decreases as deformation factor increases at lower values of eccentricity ratio. But friction parameter increases as deformation factor increases at higher values of eccentricity ratio.

10. Friction parameter decreases as L/D and H/R increases. Friction parameter increases as Poisson's ratio increases.

11. Friction parameter decreases as l_m increases from 0-20.0 and as l_m is increased further there is increase in friction parameter. Friction parameter decreases as coupling number increases.

12. Value of end flow remains almost constant at low eccentricity ratio, but at $\varepsilon_0 \geq 0.7$ $\bar{Q}_Z$ increases as deformation factor increases.

13. $\bar{Q}_Z$ increases as L/D and H/R increases. $\bar{Q}_Z$ decreases as Poisson's ratio increases.

14. $\bar{Q}_Z$ reaches minimum as $l_m \rightarrow 10.0$ and as l_m is increased beyond 10.0 $\bar{Q}_Z$ increases with increase in l_m. $\bar{Q}_Z$ decreases with increase in coupling number.

6.1.2 Conclusions for stability characteristics obtained by linear dynamic analysis.

1. Direct and cross components of stiffness increase with increase in eccentricity ratio and decrease with increase in deformation factor. Similar trends are noted for direct and cross components of damping.

2. Other parameters remaining constant, damping and stiffness coefficients increase as ν increases, decreases as H/R increases, increases with increase in L/D.

3. Stiffness and damping coefficients decrease with increase in non-dimensional characteristic length and increase with increase in coupling number.

4. Increase in deformation factor results in decrease of non-dimensional mass parameter and it decreases sharply for curves with higher eccentricity ratio such that curve with ε_0=0.85 comes below curve with ε_0=0.8. Further decrease in curve is sharp when deformation factor increases from 0.0 to 0.1.

5. Keeping other parameters unaltered, stability of the bearing decreases with increase in deformation factor (F). Deformation factor is inversely proportional to Young's modulus of elasticity. Therefore, while designing bearing with liner designer should choose a liner material with a high Young's modulus to achieve better stability, especially when the bearing is operating at high eccentricity ratio (i.e. $\varepsilon_0 \geq 0.8$).

6. An increase in the micropolar characteristics of a fluid increases stability while an increase in the deformation factor of the liner reduces stability. An optimized solution may be created when designing a journal bearing with a flexible liner.

7. $\bar{M}_C$ decreases with increase in slenderness ratio, increases with increase in ν and decreases as H/R increases.

8. An increase in l_m increases $\bar{M}_C$. This increase is sharp as characteristic length increases from 0.0 to 10.0 and when value of characteristic length increases beyond 10.0 value of critical mass parameter remains relatively constant.

9. Whirl ratio decreases with increase in eccentricity ratio but as eccentricity ratio increases beyond 0.8 and at higher deformation factor reversed trends are observed.

10. As slenderness ratio increases whirl ratio also increases. Whirl ratio increases with increase in H/R.

11. Whirl ratio decreases with increase in Poisson's ratio. Whirl ratio decreases with increase in l_m and this decrease is sharp as value of l_m increases from 01 to 10.0. Whirl ratio decreases as N^2 increases.

6.1.3 Conclusions for stability characteristics obtained by Non-linear dynamic analysis.

1. Journal center traces smaller orbit as value of slenderness ratio is increased. Limit cycle shrinks in area as deformation factor is increased.

2. When all other factors are kept constant, limit cycle traces a smaller orbit as value of H/R is increased. Journal traces a larger orbit as Poisson's ratio is increased.

3. Size of limit cycle increases in area as value of non-dimensional characteristic length is increased. Journal center traces a smaller orbit as value of coupling number is increased.

4. Critical mass parameter decreases with increase in Sommerfeld number. At higher Sommerfeld number linear dynamic analysis gives slightly better stability, whereas at lower Sommerfeld number non-linear analysis predicts much better stability.

5. Critical mass parameter is more for higher coupling number. Stability of journal bearings decreases as slenderness ratio increases.

6. Stability of journal bearing increases as Poisson's ratio increases. Stability decreases at higher deformation factor.

7. Stability of journal bearings decreases with increase in H/R ratio.

6.2 Scope for future work

Following are some suggested areas, which are related to present work and deserve to be explored:

1. A suitable experimentation to validate theoretical results of present analysis.

2. Thermal analysis of hydrodynamic flexible oil journal bearings under micropolar lubrication.

3. Theoretical and experimental study of flexible oil hydrodynamic journal bearings considering roughness under micropolar lubrication.

APPENDIX – I

Fourier series of pressure distribution

Oil film pressure can be expressed in double Fourier series form as

$$p = \sum_{m}^{|} \sum_{n}^{|} p_{m,n} \cos\left(\frac{2m\pi z}{L}\right) \cos(n\theta + \beta_{m,n}) \tag{A 1.1}$$

where $\sum^{|}$ indicates that first term of series is halved

$$p = \frac{p_{0,0}}{2} + \sum_{m=0}^{\infty} \sum_{n=0}^{\infty} p_{m,n} \cos\left(\frac{2m\pi z}{L}\right) \cos(n\theta + \beta_{m,n}) \quad (m,n) \neq (0,0) \tag{A 1.2}$$

$$p = \frac{p_{0,0}}{2} + \sum_{\substack{m=0 \\ (m,n)\neq(0,0)}}^{\infty} \sum_{n=0}^{\infty} p_{m,n} \cos\left(\frac{2m\pi z}{L}\right) \cos n\theta \cos\beta_{m,n} - \sum_{\substack{m=0 \\ (m,n)\neq(0,0)}}^{\infty} \sum_{n=0}^{\infty} p_{m,n} \cos\left(\frac{2m\pi z}{L}\right) \sin n\theta \sin\beta_{m,n}$$

$$\int_0^{2\pi} \int_0^{\frac{L}{2}} p \cos\left(\frac{2m\pi z}{L}\right) \cos n\theta \, dz d\theta = \frac{p_{0,0}}{2} \int_0^{2\pi} \int_0^{\frac{L}{2}} \cos\left(\frac{2m\pi z}{L}\right) \cos n\theta \, dz d\theta +$$

$$\int_0^{2\pi} \int_0^{\frac{L}{2}} \left[\sum_{\substack{m=0 \\ (m,n)\neq(0,0)}}^{\infty} \sum_{n=0}^{\infty} p_{m,n} \cos\left(\frac{2m\pi z}{L}\right) \cos n\theta \cos\beta_{m,n} \right] \cos\left(\frac{2m\pi z}{L}\right) \cos n\theta \, dz d\theta$$

$$- \int_0^{2\pi} \int_0^{\frac{L}{2}} \left[\sum_{\substack{m=0 \\ (m,n)\neq(0,0)}}^{\infty} \sum_{n=0}^{\infty} p_{m,n} \cos\left(\frac{2m\pi z}{L}\right) \sin n\theta \sin\beta_{m,n} \right] \cos\left(\frac{2m\pi z}{L}\right) \cos n\theta \, dz d\theta \tag{A 1.3}$$

1st term of R.H.S. of equation (A 1.2)

$$I_1 = \frac{p_{0,0}}{2} \int_0^{2\pi} \left[\int_0^{\frac{L}{2}} \cos\left(\frac{2m\pi z}{L}\right) dz \right] \cos n\theta \, d\theta$$

$$= \frac{p_{0,0}}{2} \int_0^{2\pi} \left[\frac{L}{2m\pi} \sin\left(\frac{2m\pi z}{L}\right) \right]_0^{\frac{L}{2}} \cos n\theta \, d\theta$$

Where m = 1, 2, 3

$$= 0$$

2nd term of R.H.S. of equation (A 1.3)

$$I_2 = \left(p_{m,n}\cos\beta_{m,n}\right)\int_0^{2\pi}\int_0^{\frac{L}{2}}\cos^2\left(\frac{2m\pi z}{L}\right)\cos^2 n\theta\, dzd\theta$$

$$= \left(p_{m,n}\cos\beta_{m,n}\right)\int_0^{2\pi}\left[\int_0^{\frac{L}{2}}\frac{1}{2}\left\{1+\cos\left(\frac{4m\pi z}{L}\right)\right\}dz\right]\cos^2 n\theta\, d\theta$$

$$= \left(p_{m,n}\cos\beta_{m,n}\right)\left(\frac{L}{4}\right)\int_0^{2\pi}\frac{1}{2}(1+\cos 2n\theta)d\theta$$

$$= \left(p_{m,n}\cos\beta_{m,n}\right)\left(\frac{\pi L}{4}\right)$$

3rd term of R.H.S. of equation (A 1.3)

$$I_3 = -\left(p_{m,n}\sin\beta_{m,n}\right)\int_0^{2\pi}\int_0^{\frac{L}{2}}\cos^2\left(\frac{2m\pi z}{L}\right)\cos n\theta\,\sin n\theta\, dzd\theta$$

$$= -\left(p_{m,n}\sin\beta_{m,n}\right)\int_0^{2\pi}\frac{1}{2}\left[\int_0^{\frac{L}{2}}\left[\frac{1}{2}\left\{1+\cos\left(\frac{4m\pi z}{L}\right)\right\}\right]dz\right]\sin 2n\theta\, d\theta$$

$$= -\left(p_{m,n}\sin\beta_{m,n}\right)\left(\frac{L}{4}\right)\int_0^{2\pi}\frac{1}{2}\sin 2n\theta\, d\theta$$

$$= -\left(p_{m,n}\sin\beta_{m,n}\right)\left(\frac{L}{4}\right)\frac{1}{2}\left[-\frac{\cos 2n\theta}{2n}\right]_0^{2\pi}$$

$$= 0$$

therefore, $$I = I_1 + I_2 + I_3$$

$$\int_0^{2\pi}\int_0^{\frac{L}{2}} p\cos\left(\frac{2m\pi z}{L}\right)\cos n\theta\, dzd\theta = \left(p_{m,n}\cos\beta_{m,n}\right)\left(\frac{\pi L}{4}\right)$$

$$\left(p_{m,n}\cos\beta_{m,n}\right) = \frac{4}{\pi L}\int_0^{2\pi}\int_0^{\frac{L}{2}} p\cos\left(\frac{2m\pi z}{L}\right)\cos n\theta\, dzd\theta \qquad \text{(A 1.4)}$$

$$\int_0^{2\pi}\int_0^{\frac{L}{2}} p\cos\left(\frac{2m\pi z}{L}\right)\sin n\theta\, dzd\theta = \frac{p_{0,0}}{2}\int_0^{2\pi}\int_0^{\frac{L}{2}} \cos\left(\frac{2m\pi z}{L}\right)\sin n\theta\, dzd\theta +$$
$$\int_0^{2\pi}\int_0^{\frac{L}{2}}\left[\sum_{m=0}^{\infty}\sum_{n=0}^{\infty} p_{m,n}\cos\left(\frac{2m\pi z}{L}\right)\cos n\theta\cos\beta_{m,n}\right]_{(m,n)\neq(0,0)}\cos\left(\frac{2m\pi z}{L}\right)\sin n\theta\, dzd\theta$$
$$-\int_0^{2\pi}\int_0^{\frac{L}{2}}\left[\sum_{m=0}^{\infty}\sum_{n=0}^{\infty} p_{m,n}\cos\left(\frac{2m\pi z}{L}\right)\sin n\theta\sin\beta_{m,n}\right]_{(m,n)\neq(0,0)}\cos\left(\frac{2m\pi z}{L}\right)\sin n\theta\, dzd\theta \quad \text{(A 1.5)}$$

1st and 2nd term of R.H.S. of equation (A 1.5) are zero and 3rd term of R.H.S. of equation (A 1.5) will be

$$I_3 = -\left(p_{m,n}\sin\beta_{m,n}\right)\int_0^{2\pi}\int_0^{\frac{L}{2}}\cos^2\left(\frac{2m\pi z}{L}\right)\sin^2 n\theta\, dzd\theta$$
$$= -\left(p_{m,n}\sin\beta_{m,n}\right)\int_0^{2\pi}\frac{1}{2}\left[\int_0^{\frac{L}{2}}\frac{1}{2}\left\{1+\cos\left(\frac{4m\pi z}{L}\right)\right\}dz\right](1-\cos 2n\theta)d\theta$$
$$= -\left(p_{m,n}\sin\beta_{m,n}\right)\left(\frac{L}{4}\right)\int_0^{2\pi}\frac{1}{2}(1-\cos 2n\theta)d\theta$$
$$= -\left(p_{m,n}\sin\beta_{m,n}\right)\left(\frac{\pi L}{4}\right)$$

therefore,

$$\int_0^{2\pi}\int_0^{\frac{L}{2}} p\cos\left(\frac{2m\pi z}{L}\right)\sin n\theta\, dzd\theta = -\left(p_{m,n}\sin\beta_{m,n}\right)\left(\frac{\pi L}{4}\right)$$
$$-\left(p_{m,n}\sin\beta_{m,n}\right) = \frac{4}{\pi L}\int_0^{2\pi}\int_0^{\frac{L}{2}} p\cos\left(\frac{2m\pi z}{L}\right)\sin n\theta\, dzd\theta \quad \text{(A 1.6)}$$

From relation (A 1.4) & (A 1.6) we get $p_{m,n}$ and $\beta_{m,n}$ as follows,

$$p_{m,n} = \frac{4}{\pi L}\left[\left\{\int_0^{2\pi}\int_0^{\frac{L}{2}} p\cos\left(\frac{2m\pi z}{L}\right)\cos n\theta\, dzd\theta\right\}^2 + \left\{\int_0^{2\pi}\int_0^{\frac{L}{2}} p\cos\left(\frac{2m\pi z}{L}\right)\sin n\theta\, dzd\theta\right\}^2\right]^{\frac{1}{2}} \quad \text{(A 1.7)}$$

$$\beta_{m,n} = \tan^{-1}\left[\frac{-\int_0^{2\pi}\int_0^{\frac{L}{2}} p\cos\left(\frac{2m\pi z}{L}\right)\sin n\theta\, dz d\theta}{\int_0^{2\pi}\int_0^{\frac{L}{2}} p\cos\left(\frac{2m\pi z}{L}\right)\cos n\theta\, dz d\theta}\right] \tag{A 1.8}$$

$$p_{0,0} = \frac{2}{\pi L}\int_0^{2\pi}\int_0^{\frac{L}{2}} p\, d\theta\, dz \tag{A 1.9}$$

Using end conditions of bearing (i.e. $p = 0$ at $= \frac{L}{2}$) we can obtain $p_{0,0}$. This term does not contribute any deformation at $z = \frac{L}{2}$. Its effect for other values of z is included in total deformation. After non-dimensionalisation, equation (A 1.7), (A 1.8) and (A 1.9) becomes

$$\bar{p}_{m,n} = \frac{2}{\pi}\left[\left\{\int_0^{2\pi}\int_0^{1} \bar{p}\cos(m\pi\bar{z})\cos n\theta\, d\bar{z} d\theta\right\}^2 + \left\{\int_0^{2\pi}\int_0^{1} \bar{p}\cos(m\pi\bar{z})\sin n\theta\, d\bar{z} d\theta\right\}^2\right]^{\frac{1}{2}} \tag{A 1.10}$$

$$\beta_{m,n} = \tan^{-1}\left[\frac{-\int_0^{2\pi}\int_0^{1} \bar{p}\cos(m\pi\bar{z})\sin n\theta\, d\bar{z} d\theta}{\int_0^{2\pi}\int_0^{1} \bar{p}\cos(m\pi\bar{z})\cos n\theta\, d\bar{z} d\theta}\right] \tag{A 1.11}$$

$$\bar{p}_{0,0} = \frac{1}{\pi}\int_0^{2\pi}\int_0^{1} \bar{p}\, d\theta\, d\bar{z} \tag{A 1.12}$$

where

$$\bar{p}_{m,n} = \frac{p_{m,n}C^2}{\mu\omega R^2}, \bar{p} = \frac{pC^2}{\mu\omega R^2}, \bar{z} = \frac{2z}{L}$$

and equation (A 1.2) will be reduced to

$$\bar{p} = \frac{\bar{p}_{0,0}}{2} + \sum_{m=0}^{\infty}\sum_{n=0}^{\infty} \bar{p}_{m,n}\cos\left(\frac{2m\pi\bar{z}}{L}\right)\cos\left(n\theta + \beta_{m,n}\right)$$
$$(m,n) \neq (0,0)$$

APPENDIX –II

Elastic displacement equation

Displacement components in r, θ and z directions are found from pressure distribution, which has been expressed in Fourier series. It is apparent that displacements will also be harmonic functions.

Displacement components in r, θ and z directions can be assumed are as follows:

$$u_r = u' r_0 \cos\left(n\theta + \beta_{m,n}\right) \cos\left(\frac{2m\pi z}{L}\right) \tag{A 2.1}$$

$$u_\theta = v' r_0 \cos\left(n\theta + \beta_{m,n}\right) \cos\left(\frac{2m\pi z}{L}\right) \tag{A 2.2}$$

$$u_z = w' r_0 \cos\left(n\theta + \beta_{m,n}\right) \cos\left(\frac{2m\pi z}{L}\right) \tag{A 2.3}$$

where $u', v' \; and \; w'$ are dependent on r only and r_0 is inside radius of bearing.

These displacements are substituted in stress-strain relationships using Lame's constants. Six components of stresses are then used in equations of equilibrium to obtain three displacement equations. Therefore, displacement equations are constituted from fundamentals of theory of elasticity and are reproduced below.

From stress displacement relationship we get,

$$\tau_{rr} = \lambda\left[\frac{1}{r}\frac{\partial(ru_r)}{\partial r} + \frac{1}{r}\frac{\partial u_\theta}{\partial \theta} + \frac{\partial u_z}{\partial z}\right] + 2G\frac{\partial u_r}{\partial r} \tag{A 2.4}$$

$$\tau_{\theta\theta} = \lambda\left[\frac{1}{r}\frac{\partial(ru_r)}{\partial r} + \frac{1}{r}\frac{\partial u_\theta}{\partial \theta} + \frac{\partial u_z}{\partial z}\right] + 2\frac{G}{r}\left(\frac{\partial u_\theta}{\partial \theta} + u_r\right) \tag{A 2.5}$$

$$\tau_{zz} = \lambda\left[\frac{1}{r}\frac{\partial(ru_r)}{\partial r} + \frac{1}{r}\frac{\partial u_\theta}{\partial \theta} + \frac{\partial u_z}{\partial z}\right] + 2G\frac{\partial u_z}{\partial z} \tag{A 2.6}$$

$$\tau_{r\theta} = G\left[\frac{1}{r}\frac{\partial u_\theta}{\partial \theta} + r\frac{\partial}{\partial r}\left(\frac{u_\theta}{r}\right)\right] \tag{A 2.7}$$

$$\tau_{\theta z} = G\left[\frac{\partial u_\theta}{\partial z} + \frac{1}{r}\frac{\partial u_z}{\partial \theta}\right] \tag{A 2.8}$$

$$\tau_{zr} = G\left[\frac{\partial u_z}{\partial r} + \frac{\partial u_r}{\partial z}\right] \tag{A 2.9}$$

$$\frac{\partial \tau_{rr}}{\partial r} + \frac{1}{r}\frac{\partial \tau_{r\theta}}{\partial \theta} + \frac{\partial \tau_{rz}}{\partial z} + \frac{\tau_{rr} - \tau_{\theta\theta}}{r} = 0 \tag{A 2.10}$$

$$\frac{\partial \tau_{r\theta}}{\partial r} + \frac{1}{r}\frac{\partial \tau_{\theta\theta}}{\partial \theta} + \frac{\partial \tau_{\theta z}}{\partial z} + 2\frac{\tau_{r\theta}}{r} = 0 \tag{A 2.11}$$

$$\frac{\partial \tau_{rz}}{\partial r} + \frac{1}{r}\frac{\partial \tau_{\theta z}}{\partial \theta} + \frac{\partial \tau_{zz}}{\partial z} + \frac{\tau_{rz}}{r} = 0 \tag{A 2.12}$$

$\lambda = \frac{E\nu}{(1+\nu)(1-2\nu)}$ and $G = \frac{E}{2(1+\nu)}$. Terms λ and G are called Lame's constant.

Substituting values of $u_r, u_\theta \; and \; u_z$ in stress displacement equation (A 2.4) and putting $\bar{y} = \frac{r}{r_0}$, $\frac{2m\pi}{L} = m_1$, $k = r_0 m_1$ and $r_0 d\bar{y} = dr$ we get

$$\tau_{rr} = \lambda\left[\frac{1}{r}\left\{r\frac{\partial u_r}{\partial r} + u_r\right\} + \frac{1}{r}\frac{\partial u_\theta}{\partial \theta} + \frac{\partial u_z}{\partial z}\right] + 2G\frac{\partial u_r}{\partial r}$$

$$= \lambda\left[\frac{1}{r}\left\{r\frac{du'}{dr}r_0\cos\left(n\theta + \beta_{m,n}\right)\cos m_1 z + u' r_0\cos\left(n\theta + \beta_{m,n}\right)\cos m_1 z\right\}\right.$$
$$\left. + \frac{1}{r}v' r_0 n\cos\left(n\theta + \beta_{m,n}\right)\cos m_1 z + w' r_0 m_1\cos\left(n\theta + \beta_{m,n}\right)\cos m_1 z\right]$$
$$+ 2G\left[\frac{du'}{dr}r_0\cos\left(n\theta + \beta_{m,n}\right)\cos m_1 z\right]$$

$$= \lambda\left[\frac{du'}{d\bar{y}}\cos\left(n\theta + \beta_{m,n}\right)\cos m_1 z + \frac{u'}{\bar{y}}\cos\left(n\theta + \beta_{m,n}\right)\cos m_1 z + \frac{nv'}{\bar{y}}\cos\left(n\theta + \beta_{m,n}\right)\cos m_1 z\right.$$
$$\left. + w' r_0 m_1\cos\left(n\theta + \beta_{m,n}\right)\cos m_1 z\right] + 2G\left[\frac{du'}{d\bar{y}}\cos\left(n\theta + \beta_{m,n}\right)\cos m_1 z\right]$$

$$\tau_{rr} = \lambda\left[\frac{du'}{d\bar{y}} + \frac{u'}{\bar{y}} + \frac{nv'}{\bar{y}} + w'k\right]\cos\left(n\theta + \beta_{m,n}\right)\cos m_1 z + 2G\frac{du'}{d\bar{y}}\cos\left(n\theta + \beta_{m,n}\right)\cos m_1 z \tag{A 2.13}$$

Similarly substituting values of $u_r, u_\theta \; and \; u_z$ in stress displacement equation (A 2.5) and putting $\bar{y} = \frac{r}{r_0}$, $\frac{2m\pi}{L} = m_1$, $k = r_0 m_1$ and $r_0 d\bar{y} = dr$ we get

$$\tau_{\theta\theta}$$
$$= \lambda\left[\frac{du'}{d\bar{y}} + \frac{u'}{\bar{y}} + \frac{nv'}{\bar{y}} + w'k\right]\cos\left(n\theta + \beta_{m,n}\right)\cos m_1 z + 2G\left[\frac{nv'}{\bar{y}} + \frac{u'}{\bar{y}}\right]\cos\left(n\theta + \beta_{m,n}\right)\cos m_1 z \tag{A 2.14}$$

$$\tau_{zz} = \lambda\left[\frac{du'}{d\bar{y}} + \frac{u'}{\bar{y}} + \frac{nv'}{\bar{y}} + w'k\right]\cos\left(n\theta + \beta_{m,n}\right)\cos m_1 z + 2Gw'k\cos\left(n\theta + \beta_{m,n}\right)\cos m_1 z \quad \text{(A 2.15)}$$

Similarly substituting values of $u_r, u_\theta \; and \; u_z$ in stress displacement equation (A 2.7), (A 2.8) & (A 2.9) and putting $\bar{y} = \frac{r}{r_0}$, $\frac{2m\pi}{L} = m_1$, $k = r_0 m_1$ and $r_0 d\bar{y} = dr$ we get

$$\tau_{r\theta} = G\left[-\frac{nu'}{\bar{y}} + \frac{dv'}{d\bar{y}} - \frac{v'}{\bar{y}}\right]\sin\left(n\theta + \beta_{m,n}\right)\cos m_1 z \quad \text{(A 2.16)}$$

$$\tau_{\theta z} = -G\left[v'k + \frac{nw'}{\bar{y}}\right]\sin\left(n\theta + \beta_{m,n}\right)\sin m_1 z \quad \text{(A 2.17)}$$

$$\tau_{zr} = G\left[\frac{dw'}{d\bar{y}} - u'k\right]\cos\left(n\theta + \beta_{m,n}\right)\sin m_1 z \quad \text{(A 2.18)}$$

Substituting values of $\tau_{rr},\ \tau_{\theta\theta},\ \tau_{zz},\ \tau_{r\theta},\ \tau_{\theta z} \; and \; \tau_{zr}$ in equation (A 2.10) and putting $\bar{y} = \frac{r}{r_0}$ we have,

$$\frac{\partial \tau_{rr}}{r_0 \partial \bar{y}} + \frac{1}{r_0 \bar{y}}\frac{\partial \tau_{r\theta}}{\partial \theta} + \frac{\partial \tau_{rz}}{\partial z} + \frac{\tau_{rr} - \tau_{\theta\theta}}{r_0 \bar{y}} = 0$$

$$\frac{\partial \tau_{rr}}{\partial \bar{y}} + \frac{1}{\bar{y}}\frac{\partial \tau_{r\theta}}{\partial \theta} + r_0\frac{\partial \tau_{rz}}{\partial z} + \frac{\tau_{rr} - \tau_{\theta\theta}}{\bar{y}} = 0$$

$$\lambda\left[\frac{d^2u'}{d\bar{y}^2} + \left\{\frac{1}{\bar{y}}\frac{du'}{d\bar{y}} - \frac{u'}{\bar{y}^2}\right\} + n\left\{\frac{1}{\bar{y}}\frac{dv'}{d\bar{y}} - \frac{v'}{\bar{y}^2}\right\} + k\frac{dw'}{d\bar{y}}\right]\cos\left(n\theta + \beta_{m,n}\right)\cos m_1 z +$$

$$2G\frac{d^2u'}{d\bar{y}^2}\cos\left(n\theta + \beta_{m,n}\right)\cos m_1 z + \frac{nG}{\bar{y}}\left[-\frac{nu'}{\bar{y}} + \frac{dv'}{d\bar{y}} - \frac{v'}{\bar{y}}\right]\cos\left(n\theta + \beta_{m,n}\right)\cos m_1 z +$$

$$Gr_0 m_1\left[\frac{dw'}{d\bar{y}} - u'k\right]\cos\left(n\theta + \beta_{m,n}\right)\cos m_1 z$$

$$+\frac{1}{\bar{y}}\left[\lambda\left\{\frac{du'}{d\bar{y}} + \frac{u'}{\bar{y}} + \frac{nv'}{\bar{y}} + w'k\right\}\cos\left(n\theta + \beta_{m,n}\right)\cos m_1 z\right]$$

$$+\frac{2}{\bar{y}}G\frac{du'}{d\bar{y}}\cos\left(n\theta + \beta_{m,n}\right)\cos m_1 z - \lambda\frac{1}{\bar{y}}\left[\frac{du'}{d\bar{y}} + \frac{u'}{\bar{y}} + \frac{nv'}{\bar{y}} + w'k\right]\cos\left(n\theta + \beta_{m,n}\right)\cos m_1 z$$

$$-\frac{2}{\bar{y}}G\left[\frac{nv'}{\bar{y}} + \frac{u'}{\bar{y}}\right]\cos\left(n\theta + \beta_{m,n}\right)\cos m_1 z = 0$$

$$\lambda\left[\frac{d^2u'}{d\bar{y}^2} + \left\{\frac{1}{\bar{y}}\frac{du'}{d\bar{y}} - \frac{u'}{\bar{y}^2}\right\} + n\left\{\frac{1}{\bar{y}}\frac{dv'}{d\bar{y}} - \frac{v'}{\bar{y}^2}\right\} + k\frac{dw'}{d\bar{y}}\right] + 2G\frac{d^2u'}{d\bar{y}^2} + \frac{nG}{\bar{y}}\left[-\frac{nu'}{\bar{y}} + \frac{dv'}{d\bar{y}} - \frac{v'}{\bar{y}}\right] +$$

$$Gr_0 m_1\left[\frac{dw'}{d\bar{y}} - u'k\right] + \frac{2}{\bar{y}}G\frac{du'}{d\bar{y}} - \frac{2}{\bar{y}}G\left[\frac{nv'}{\bar{y}} + \frac{u'}{\bar{y}}\right] = 0$$

or

$$(\lambda+2G)\frac{d^2u'}{d\bar{y}^2}+\frac{du'}{d\bar{y}}\frac{(\lambda+2G)}{\bar{y}}+\frac{dv'}{d\bar{y}}\frac{n(\lambda+G)}{\bar{y}}+\frac{dw'}{d\bar{y}}k(\lambda+G)-$$
$$\frac{u'}{\bar{y}^2}(\lambda+n^2G+2G)-Gk^2u'-\frac{v'}{\bar{y}^2}[n(\lambda+3G)]=0$$

(A 2.19)

Substituting $C'=2+\frac{\lambda}{G}$ in equation (A 2.19) we have,

$$C'\frac{d^2u'}{d\bar{y}^2}+\frac{C'}{\bar{y}}\frac{du'}{d\bar{y}}-(C'+n^2)\frac{u'}{\bar{y}^2}+(C'-1)\frac{n}{\bar{y}}\frac{dv'}{d\bar{y}}-(C'+1)\frac{n}{\bar{y}^2}v'-k^2u'$$
$$+(C'-1)k\frac{dw'}{d\bar{y}}=0$$

(A 2.20)

Substituting values of $\tau_{rr},\ \tau_{\theta\theta},\ \tau_{zz},\ \tau_{r\theta},\ \tau_{\theta z}\ and\ \tau_{zr}$ in equation (A 2.11) and (A 2.22) and putting $\bar{y}=\frac{r}{r_0}$ and $C'=2+\frac{\lambda}{G}$ we have,

$$\frac{d^2v'}{d\bar{y}^2}+\frac{1}{\bar{y}}\frac{dv'}{d\bar{y}}-(1+C'n^2)\frac{v'}{\bar{y}^2}-(C'-1)\frac{n}{\bar{y}}\frac{du'}{d\bar{y}}-(C'+1)\frac{n}{\bar{y}^2}u'-k^2v'-nk(C'-1)\frac{w'}{\bar{y}}$$
$$=0$$

(A 2.21)

$$\frac{d^2w'}{d\bar{y}^2}+\frac{1}{\bar{y}}\frac{dw'}{d\bar{y}}-\frac{n^2}{\bar{y}^2}w'-C'k^2w'-k(C'-1)\frac{du'}{d\bar{y}}-k(C'-1)\frac{u'}{\bar{y}}-nk(C'-1)\frac{v'}{\bar{y}}=0$$

(A 2.22)

Outer surface is rigidly enclosed by housing making displacement of outer surface zero. Ends of bearing are prevented from expanding axially, but are free to move circumferentially or radially.

Boundary conditions of inner radius are

$$\tau_{rr}=-p,\ \tau_{r\theta}=0,\tau_{rz}=0$$

(A 2.23)

Boundary conditions are,

at $\bar{y}=1$,

$$C'\frac{du'}{d\bar{y}}=-\frac{1}{G}p_{m,n}-(C'-2)\left(\frac{u'}{\bar{y}}+\frac{nv'}{\bar{y}}+w'k\right)$$

(A 2.24)

$$\frac{dv'}{d\bar{y}}=\frac{nu'}{\bar{y}}+\frac{v'}{\bar{y}}$$

(A 2.25)

$$\frac{dw'}{d\bar{y}}=u'k$$

(A 2.26)

and at $\bar{y}=\frac{b}{a}$

$$u'=v'=w'=0$$

(A 2.27)

Equations (A 2.20), (A 2.21) and (A 2.22) are solved satisfying boundary conditions (A 2.23), (A 2.24), (A 2.25), (A 2.26) and (A 2.27) for unit pressure, G to find out displacement components by FDM (Gauss-Siedel iteration) with SOR scheme. For this purpose equations are written in finite difference form. Numerical solution these equations, satisfying boundary conditions, is obtained.

Second order and first order derivatives of displacement components are approximated by central differences as:

$$\frac{\partial^2 u'}{\partial \bar{y}^2} = \frac{u'_{i+1} - 2u'_i + u'_{i-1}}{\Delta \bar{y}^2}$$
$$\frac{\partial^2 v'}{\partial \bar{y}^2} = \frac{v'_{i+1} - 2v'_i + v'_{i-1}}{\Delta \bar{y}^2}$$
$$\frac{\partial^2 w'}{\partial \bar{y}^2} = \frac{w'_{i+1} - 2w'_i + w'_{i-1}}{\Delta \bar{y}^2}$$
$$\frac{\partial u'}{\partial \bar{y}} = \frac{u'_{i+1} - u'_{i-1}}{2(\Delta \bar{y})}$$
$$\frac{\partial v'}{\partial \bar{y}} = \frac{v'_{i+1} - v'_{i-1}}{2(\Delta \bar{y})}$$
$$\frac{\partial w'}{\partial \bar{y}} = \frac{w'_{i+1} - w'_{i-1}}{2(\Delta \bar{y})}$$

Using above representation equation (A 2.20), (A 2.21) and (A 2.22) can be expressed in finite difference form as:

$$u'_i = A_i u'_{i+1} + B_i u'_{i-1} + C_i v'_{i+1} + D_i v'_{i-1} + E_i v'_i + F_i w'_{i+1} + G_i w'_{i-1} \quad \text{(A 2.28)}$$

$$v'_i = H_i v'_{i+1} + K_i v'_{i-1} + L_i u'_{i+1} + M_i u'_{i-1} + N_i u'_i + Q_i w'_i \quad \text{(A 2.29)}$$

$$w'_i = R_i w'_{i+1} + S_i w'_{i-1} + X_i u'_{i+1} + Y_i u'_{i-1} + Z_i v'_i + P_i u'_i \quad \text{(A 2.30)}$$

where

$$AA = 2[2C'\bar{y}_i^2 + (C' + n^2)(\Delta \bar{y}_i)^2 + k^2(\Delta \bar{y})^2(\bar{y}_i)^2]$$
$$BB = 2[2\bar{y}_i^2 + (1 + C'n^2)(\Delta \bar{y}_i)^2 + k^2(\Delta \bar{y})^2(\bar{y}_i)^2]$$
$$CC = 2[2\bar{y}_i^2 + n^2(\Delta \bar{y})^2 + C'k^2(\Delta \bar{y})^2(\bar{y}_i)^2]$$
$$A_i = \frac{C'\bar{y}_i(2\bar{y}_i + \Delta \bar{y})}{AA}$$
$$B_i = \frac{C'\bar{y}_i(2\bar{y}_i - \Delta \bar{y})}{AA}$$
$$C_i = \frac{n(C' - 1)\Delta \bar{y}\bar{y}_i}{AA}$$
$$D_i = \frac{-n(C' - 1)\Delta \bar{y}\bar{y}_i}{AA}$$

$$E_i = \frac{-n(C'+1)(\Delta\bar{y})^2}{AA}$$

$$F_i = \frac{k(C'-1)\Delta\bar{y}(\bar{y}_i)^2}{AA}$$

$$G_i = \frac{-k(C'-1)\Delta\bar{y}(\bar{y}_i)^2}{AA}$$

$$H_i = \frac{\bar{y}_i(2\bar{y}_i + \Delta\bar{y})}{BB}$$

$$K_i = \frac{\bar{y}_i(2\bar{y}_i - \Delta\bar{y})}{BB}$$

$$M_i = -L_i = \frac{n(C'-1)\Delta\bar{y}\bar{y}_i}{BB}$$

$$N_i = \frac{-2n(C'+1)(\Delta\bar{y})^2}{BB}$$

$$Q_i = \frac{-2nk(C'-1)(\Delta\bar{y})^2\bar{y}_i}{BB}$$

$$R_i = \frac{\bar{y}_i(2\bar{y}_i + \Delta\bar{y})}{CC}$$

$$S_i = \frac{\bar{y}_i(2\bar{y}_i - \Delta\bar{y})}{CC}$$

$$X_i = -Y_i = \frac{-k(C'-1)\Delta\bar{y}(\bar{y})^2}{CC}$$

$$P_i = \frac{-2k\bar{y}(C'-1)(\Delta\bar{y})^2}{CC}$$

$$Z_i = \frac{-2nk\bar{y}(C'-1)(\Delta\bar{y})^2}{CC}$$

$$C' = 2 + \frac{\lambda}{G} = 2 + \frac{2\nu}{1-2\nu} = \frac{2(1-\nu)}{1-2\nu},$$

$$k = \frac{2m\pi r_0}{L}$$

In finite difference form, boundary conditions given by equations (A 2.23) to (A 2.27) can be written as:

$$u_i' = \frac{\bar{y}_i}{[2\Delta\bar{y}(C'-2) - 3C'\bar{y}_i]}\left[C'u_{i+2}' - 4C'u_{i+1}' - 2\Delta\bar{y} - 2\Delta\bar{y}(C'-2)\left\{\frac{nv_i'}{\bar{y}_i} + kw_i'\right\}\right] \quad \text{(A 2.31)}$$

$$v_i' = \frac{\bar{y}_i}{(3\bar{y}_i + 2\Delta\bar{y})}\left[4v_{i+1}' - v_{i+2}' - 2\Delta\bar{y}\left(\frac{nu_i'}{\bar{y}_i}\right)\right] \quad \text{(A 2.32)}$$

$$w_i' = \frac{1}{3}[4w_{i+1}' - w_{i+2}' - 2\Delta\bar{y}ku_i'] \quad \text{(A 2.33)}$$

Above three equation give boundary conditions when n, m or k is not equal to zero. Three cases can arise.

CASE – I

When n = 0 and m = 0 (i.e. k = 0), equations (A 2.20), (A 2.21) and (A 2.22) will take form

$$\frac{d^2u'}{d\bar{y}^2}+\frac{1}{\bar{y}}\frac{du'}{d\bar{y}}-\frac{u'}{\bar{y}^2}=0 \tag{A 2.34}$$

$$\frac{d^2v'}{d\bar{y}^2}+\frac{1}{\bar{y}}\frac{dv'}{d\bar{y}}-\frac{v'}{\bar{y}^2}=0 \tag{A 2.35}$$

$$\frac{d^2w'}{d\bar{y}^2}+\frac{1}{\bar{y}}\frac{dw'}{d\bar{y}}=0 \tag{A 2.36}$$

from equation (A 2.34) we get,

$$\bar{y}^2\frac{d^2u'}{d\bar{y}^2}+\bar{y}\frac{du'}{d\bar{y}}-u'=0 \tag{A 2.37}$$

Substituting $\bar{y}=e^z$or, $z=\ln\bar{y}$ therefore $\frac{du'}{d\bar{y}}=\frac{du'}{dz}\times\frac{dz}{d\bar{y}}=\frac{1}{\bar{y}}\frac{du'}{dz}$

$$\bar{y}\frac{du'}{d\bar{y}}=\frac{du'}{dz}$$

$$\frac{d^2u'}{d\bar{y}^2}=\frac{d}{d\bar{y}}\left(\frac{du'}{d\bar{y}}\right)=\frac{d}{d\bar{y}}\left(\frac{1}{\bar{y}}\frac{du'}{dz}\right)=\frac{d}{dz}\left(e^{-z}\frac{du'}{dz}\right)\times\frac{dz}{d\bar{y}}=\left[e^{-z}\frac{d^2u'}{dz^2}-e^{-z}\frac{du'}{dz}\right]\times\frac{1}{\bar{y}}$$

$$\bar{y}^2\frac{d^2u'}{d\bar{y}^2}=\left[\frac{d^2u'}{dz^2}-\frac{du'}{dz}\right]$$

Substituting above relation in equation (A 2.37) reduces to,

$$\frac{d^2u'}{dz^2}-u'=0 \tag{A 2.38}$$

Solution of equation (A 2.38) is $u'=K_1e^z+K_1e^{-z}$

$$u'=K_1\bar{y}+K_2\frac{1}{\bar{y}}$$

(Where K_1 and K_2 are constants) (A 2.39)

from boundary conditions we get,

at $\bar{y} = 1$,

$$C' \frac{du'}{d\bar{y}} = -1 - (C' - 2)\frac{u'}{\bar{y}}$$

$$\left.\frac{du'}{d\bar{y}}\right|_{\bar{y}=1} = -\frac{1}{C'} - (C' - 2)\frac{1}{C'}\left.\frac{u'}{\bar{y}}\right|_{\bar{y}=1} \quad \text{(A 2.40)}$$

at $\bar{y} = \frac{b}{a}$

$$u' = 0 \quad \text{(A 2.41)}$$

from equation (A 2.39) we get,

$$\frac{du'}{d\bar{y}} = K_1 - \frac{K_2}{\bar{y}^2} \quad \text{(A 2.42)}$$

from equation (A 2.40) and (A 2.42) we get,

$$K_1 - K_2 = -\frac{1}{C'}[1 + (C' - 2)(K_1 + K_2)] \quad \text{(A 2.43)}$$

from equation (A 2.39) and (A 2.41) we get,

$$K_1\left(\frac{b}{a}\right) + K_2\left(\frac{b}{a}\right) = 0$$

$$K_2 = -K_1\left(\frac{b}{a}\right)^2 \quad \text{(A 2.44)}$$

Equation (A 2.43) can be written as

$$K_2 = -K_1\left(1 + \frac{b-a}{a}\right)^2 \quad \text{(A 2.45)}$$

where b = outer radius of bearing. a = r_0 = inner radius of bearing.

Since clearance between bearing and journal is very small therefore relation (A 2.45) can be written as:

$$K_2 = -K_1\left(1 + \frac{b-a}{a}\right)^2 = -K_1\left(1 + \frac{H}{R}\right)^2 \quad \text{(A 2.46)}$$

H = b-a= thickness of bearing.

Substituting relation in equation (A 2.43) we have,

$$K_1\left[1 + \left(1 + \frac{H}{R}\right)^2\right] = -\frac{1}{C'}\left[1 + K_1(C' - 2)\left\{1 - \left(1 + \frac{H}{R}\right)^2\right\}\right]$$

$$K_1 C'\left[1 + \left(1 + \frac{H}{R}\right)^2\right] + \left[K_1(C' - 2)\left\{1 - \left(1 + \frac{H}{R}\right)^2\right\}\right] = -1$$

$$K_1\left[C' + C'\left(1+\frac{H}{R}\right)^2 + (C'-2) - (C'-2)\left(1+\frac{H}{R}\right)^2\right] = -1$$

(A 2.47)

$$K_1 = \frac{1}{2\left[1 - C' - \left(1+\frac{H}{R}\right)^2\right]}$$

Substituting value of K_1 in equation (A 2.46) we get,

$$K_2 = \frac{\left(1+\frac{H}{R}\right)^2}{2\left[1 - C' - \left(1+\frac{H}{R}\right)^2\right]}$$

(A 2.48)

Substituting value of K_1 and K_2 in equation (A 2.39) we get,

$$u' = \frac{\bar{y}^2 - \left(1+\frac{H}{R}\right)^2}{2\bar{y}\left[1 - C' - \left(1+\frac{H}{R}\right)^2\right]}$$

(A 2.49)

CASE – II

When $n \neq 0$ and m = 0 (i.e k = 0), equation (A 2.20), (A 2.21) and (A 2.22) will take form

$$u_i' = \frac{1}{2[2C'\bar{y}_i^2 + (C'+n^2)(\Delta\bar{y})^2]}[C'\bar{y}_i(2\bar{y}_i + \Delta\bar{y})u_{i+1}' + C'\bar{y}_i(2\bar{y}_i - \Delta\bar{y})u_{i-1}' + n(C'-1)(\Delta\bar{y})\bar{y}_i v_{i+1}' - n(C'-1)(\Delta\bar{y})\bar{y}_i v_{i-1}' - n(C'+1)(\Delta\bar{y})^2 v_i']$$

(A 2.50)

$$v_i' = \frac{1}{2[2\bar{y}_i^2 + (1+C'n^2)(\Delta\bar{y})^2]}[\bar{y}_i(2\bar{y}_i + \Delta\bar{y})v_{i+1}' + \bar{y}_i(2\bar{y}_i - \Delta\bar{y})v_{i-1}' - n(C'-1)(\Delta\bar{y})\bar{y}_i u_{i+1}' + n(C'-1)(\Delta\bar{y})\bar{y}_i u_{i-1}' - 2n(C'+1)(\Delta\bar{y})^2 u_i']$$

(A 2.51)

$$w_i' = \frac{1}{2[2\bar{y}_i^2 + n^2(\Delta\bar{y})^2]}[\bar{y}_i(2\bar{y}_i + \Delta\bar{y})w_{i+1}' + \bar{y}_i(2\bar{y}_i - \Delta\bar{y})w_{i-1}']$$

(A 2.52)

Solving above displacement equations we get,

$$u_i' = \frac{\bar{y}_i}{[2\Delta\bar{y}(C'-2) - 3C'\bar{y}_i]} \times \left[C'u_{i+2}' - 4C'u_{i+1}' - 2\Delta\bar{y} - 2\Delta\bar{y}(C'-2)\left\{\frac{nv_i'}{\bar{y}_i}\right\}\right]$$

(A 2.53)

$$v_i' = \frac{\bar{y}_i}{[3\bar{y}_i + 2\Delta\bar{y}]}\left[4v_{i+1}' - v_{i+2}' - 2\Delta\bar{y}\left(\frac{nu_i'}{\bar{y}_i}\right)\right]$$

(A 2.54)

$$w_i' = \frac{1}{3}[4w_{i+1}' - w_{i+2}']$$

(A 2.55)

CASE – III

When n = 0, and $m \neq 0$ (i.e. $k \neq 0$), equations (A 2.20), (A 2.21) and (A 2.22) will take for

$$u_i' = \frac{1}{2\left[2C'\bar{y}_i^2 + C'(\Delta\bar{y})^2 + k^2(\Delta\bar{y})^2(\bar{y}_i)^2\right]}\left[C'\bar{y}_i(2\bar{y}_i + \Delta\bar{y})u_{i+1}' + C'\bar{y}_i(2\bar{y}_i - \Delta\bar{y})u_{i-1}'\right.$$

$$\left. + k(C'-1)(\Delta\bar{y})(\bar{y}_i)^2 w_{i+1}' - k(C'-1)(\Delta\bar{y})(\bar{y}_i)^2 w_{i-1}'\right] \quad \text{(A 2.56)}$$

$$v_i' = \frac{1}{2\left[2\bar{y}_i^2 + (\Delta\bar{y})^2 + k^2(\Delta\bar{y})^2(\bar{y}_i)^2\right]} \times \left[\bar{y}_i(2\bar{y}_i + \Delta\bar{y})v_{i+1}' + \bar{y}_i(2\bar{y}_i - \Delta\bar{y})v_{i-1}'\right] \quad \text{(A 2.57)}$$

$$w_i' = \frac{1}{2\left[2\bar{y}_i^2 + C'k^2(\Delta\bar{y})^2(\bar{y}_i)^2\right]}\left[\bar{y}_i(2\bar{y}_i + \Delta\bar{y})w_{i+1}' + \bar{y}_i(2\bar{y}_i - \Delta\bar{y})w_{i-1}' - k(C'-1)(\Delta\bar{y})(\bar{y}_i)^2 u_{i+1}'\right.$$

$$\left. + k(C'-1)(\Delta\bar{y})(\bar{y}_i)^2 u_{i-1}' - 2k\bar{y}_i(C'-1)(\Delta\bar{y})^2 u_i'\right] \quad \text{(A 2.58)}$$

Solving above displacement equations we get,

$$u_i' = \frac{\bar{y}_i}{[2\Delta\bar{y}(C'-2) - 3C'\bar{y}_i]} \times \left[C'u_{i+2}' - 4C'u_{i+1}' - 2\Delta\bar{y} - 2\Delta\bar{y}(C'-2)kw_i'\right] \quad \text{(A 2.59)}$$

$$v_i' = \frac{\bar{y}_i}{[3\bar{y}_i + 2\Delta\bar{y}]}\left[4v_{i+1}' - v_{i+2}'\right] \quad \text{(A 2.60)}$$

$$w_i' = \frac{1}{3}\left[4w_{i+1}' - w_{i+2}' - 2\Delta\bar{y}ku_i'\right] \quad \text{(A 2.61)}$$

Solving displacement equations values of distortion coefficient $d_{m,n}$ were obtained and expressed as,

$$d_{m,n} = \frac{Gu'}{p} \quad \text{(A 2.62)}$$

Radial distortion δ of bearing surface will be

$$\delta = u_r$$

$$\delta = d_{m,n}\frac{p}{G}r_0\cos\left(n\theta + \beta_{m,n}\right)\cos\left(\frac{2m\pi z}{L}\right)$$

Considering bearing clearance is very small in comparison to diameter of journal, total radial deformation will be

$$\delta = \frac{Rp_{0,0}d_{0,0}}{2G} + \sum_{m=0}^{\infty}\sum_{n=0}^{\infty} d_{m,n}\frac{R}{G}p_{m,n}\cos\left(n\theta + \beta_{m,n}\right)\cos\left(\frac{2m\pi z}{L}\right)$$

$$(m,n) \neq (0,0)$$

Using $\bar{p} = \frac{pC^2}{\mu\omega R^2}$, $\bar{z} = \frac{2z}{L}$ and G is replaced by $\frac{E}{2(1+\nu)}$, radial deformation in inner surface will be in form,

$$\bar{\delta} = 2(1+\nu)F\left[\bar{p}_{0,0}d_{0,0} + \sum_{m=0}^{\infty}\sum_{n=0}^{\infty}{}_{(m,n)\neq(0,0)}\bar{p}_{m,n}\, d_{m,n}\cos\left(n\theta + \beta_{m,n}\right)\cos\left(\frac{2m\pi\bar{z}}{L}\right)\right] \quad \text{(A 2.63)}$$

where $\bar{\delta} = \frac{\delta}{c}$ and $F = \frac{\mu\omega R^3}{Ec^3}$

REFERENCES

[1]. I. Newton, "Mathematical Principles of Natural Philosophy", London, 1668, Cajori's revision of Motte's translation, Univ. of California Press, 1946.

[2]. N. Petroff, "Friction in Machines and the Effect of Lubricant", (In Russian) Engng. J. St. Petersburg, Vol.1-4, 1883, pp.71-140, 228-274, 377-436.

[3]. B. Tower, "First Report on Friction Experiments", Proc. Inst. Mech. Engrs., London, Vol.34, 1883, pp.632-659; "Second Report on Friction Experiments", Proc. Inst. Mech. Engrs., London, Vol.36, 1885, pp.58-70; "Third Report on Friction Experiments", Proc. Inst. Mech. Engrs., London, 1888, pp.173-205; "Fourth Report on Friction Experiments", Proc. Inst. Mech. Engrs., London, 1891, pp.111-140.

[4]. O. Reynolds, "On the Theory of Lubrication and Its Application to Mr. Beuchamp Tower's Experiments, including An Experimental Determination of the Viscosity of Olive Oil", Phil. Trans. Roy. Soc., London, Vol.177(1), 1886, pp. 157-234.

[5]. A. Kingsbury, "Experiments with an Air Lubricated Journal", J. American Soc. Naval Engrs., Vol.9(2), 1897, pp.267-292.

[6]. A. Sommerfeld, "Zur Hydrodynamischen Theorie der Schmiermittelneibung", Z. Maths. u. Physik, Vol.50, 1904, pp.97-155.

[7]. W.J. Harrison, "The Hydrodynamical Theory of Lubrication with Special Reference to Air as a Lubricant", Trans. Cambridge. Phil. Soc., Vol.22(3), 1913, pp.39-54.

[8]. L. Rayleigh, "Notes on the Theory of Lubrication", Phil. Mag., Vol.35(1), 1918, pp.1-12.

[9]. D.G. Christopherson, "A New Mathematical Method for the Solution of Film Lubrication Problems", Proc. Inst. Mech. Engrs., London, Vol.146, 1941, pp.126-135.

[10]. A. Cameron and (Mrs.) L. Wood, "The Full Journal Bearing", Proc. Inst. Mech. Engrs., London, Vol.161, 1949, pp.59-64.

[11]. G. Vogelpohl, "Zur Integration der Reynoldschen Gleichung fur des Zapfenlager Endlicher Breite", Ingenieur Archiv., Vol.14(3), 1943, pp.192-212.

[12]. F.W. Ocvirk, "Short Bearing Approximation for Full Journal Bearings", NACA TN 2808.

[13]. W.J. Harrison, "The Hydrodynamic Theory of Lubrication of Cylindrical Bearings under Variable Load", Trans. Cambridge. Phil. Soc., Vol.22, 1913, p.373.

[14]. W. Kahlert, “Der Einfluß der Trägheitskräfte bei der hydrodynamischen Schmiermitteltheorie”, Ingenieur Archiv., Vol.16(5), 1948, pp.321-342.

[15]. F. Osterle and E. Saibel, “On the Effect of Lubricant Inertia in Hydrodynamic Lubrication”, Z. angew. Maths. u. Physik, Vol.6, 1955, pp.334-339.

[16]. J.A. Coles and C.J. Hughes, “Oil Flow and Film extend in Complete Journal Bearings”, Proc. Inst. Mech. Engrs., Vol.170, 1956, pp.499-510.

[17]. B. Jacobson and L. Floberg, “The Finite Journal Bearing considering Vaporization”, Trans. Chalmers Univ. Tech. Gothenburg, Vol.190, 1957, pp.1-116.

[18]. O. Pinkus, “Solution of Reynolds Equation for Finite Journal Bearings”, Trans. ASME, Vol.80, 1958, pp.858-864.

[19]. A.A. Raimondi and J. Boyd, “A Solution for the Finite Journal Bearing and Its Application to Analysis and Design, I, II and III”, Trans. ASLE, Vol.1(1), 1958, pp.159-209.

[20]. G.R. Hinggison, “The Theoretical Effects of Elastic Deformation of the Bearing Liner on Journal Bearing Performance”, Proc. of the symp. on Elastohydrodynamic Lubrication, IMechE, London (UK), Vol.180(3), 1965-66, pp. 31-37.

[21]. R. Holmes, “Instability Phenomena due to Circular Bearing Oil Films”, J. of Mech. Engg. Sci., Vol.8, 1966, pp. 419-425.

[22]. J. O’Donoghue, D.K. Brighton and C.J.K. Hooke, “The Effect of Elastic Distortions on Journal Bearing Performance”, J. Lubr. Tech., Vol.89(4), 1967, pp. 409-415.

[23]. D.K. Brighton, C.J.K. Hooke and J. O’Donoghue, “Theoretical and Experimental Investigation of the Effect of Elastic Distortions on the Performance of Journal Bearing”, Tribology Convention, Proc of IMechE, Vol.182(3), 1968, pp. 192-200.

[24]. M.K. Benjamin, V. Castelli, “A Theoretical Investigation of Complaint Surface Journal Bearings”, ASME J. Lubr. Tech., Vol.93(1), 1971, pp. 191-201.

[25]. K.P. Oh and K.H. Huebner, “Solution of the Elastohydrodynamic Finite Journal Bearing Problem”, ASME J. Lubr. Tech., Vol.95(3), 1973, pp. 342-351.

[26]. H.D. Conway and H.C. Lee, “The Analysis of the Lubrication of a Flexible Journal Bearing”, ASME J. Lubr. Tech., Vol.97(4), 1975, pp. 599-604.

[27]. S.C. Jain, R. Sinhasan and D.V. Singh, “Elastohydrodynamic Analysis of a Cylindrical Journal Bearing with a Flexible Bearing Shell”, Wear, Vol.78, 1982, pp. 325-335.

[28]. S.C. Jain, R. Sinhasan and D.V. Singh, “The Performance Characteristics of Thin Compliant Shell Journal Bearings”, Wear, Vol.81, 1982, pp. 251-261.

[29]. B.C. Majumdar, D.E. Brewe and M.M. Khonsari, “Stability of a Rigid Rotor Supported on Flexible Oil Journal Bearing”, Tribol. Trans., Vol.110, 1988, pp. 181-187.

[30]. H.N. Chandrawat and R.A. Sinhasan, “Study of Steady state and Transient Performance Characteristics of a Flexible Shell Journal Bearing”, Tribol. Int., Vol.21, 1988, pp. 137-148.

[31]. M.J. Braun and J.D. Dougherty, “Hydrodynamic Analysis and Fluid-Solid Interaction Effects on the Behavior of a Compliant Wall (Thick) Journal Bearing. Part 1: Theory”, J. Tribol., Vol.111(1), 1989, pp. 70-79.

[32]. M.J. Braun and J.D. Dougherty, “Hydrodynamic Analysis and Fluid-Solid Interaction Effects on the Behavior of a Compliant Wall (Thick) Journal Bearing. Part 2: Results”, J. Tribol., Vol.111(1), 1989, pp. 80-86.

[33]. M. Lahmar, “Elastohydrodynamic Analysis of Double-Layered Journal Bearing Lubricated With Couple-Stress Fluids”, Proc. IMechE, Part J: J. Engg. Tribol., Vol.219, 2005, pp. 145-171.

[34]. H. Boucherit, M. Lahmar and B. Bou-Saïd, “Misalignment Effects on Steady-State and Dynamic Behavior of Complaint Journal Bearings Lubricated With Couple Stress Fluids”, Lubr. Sci., Wiley Inter-Science, Vol.20, 2008, pp. 241-268.

[35]. M. Lahmar, S. Ellagoune and B. Bou-Saïd, “Elastohydrodynamic Lubrication Analysis of a Compliant Journal Bearing Considering Static and Dynamic Deformations of the Bearing Liner”, Tribol. Trans., Vol.53(3), 2010, pp. 349-368.

[36]. E. Kuznetsov, S. Glavatskih, “Dynamic characteristics of compliant journal bearings considering thermal effects”, Tribol. Int., Vol.94, 2016, pp. 288-305.

[37]. B.L. Newkirk, “Shaft Whipping”, Gen. Elec. Rev., Vol.27, 1924, p.169-178.

[38]. B.L. Newkirk and H.D. Taylor, “Shaft Whipping due to Oil Action in Journal Bearings”, Gen. Elec. Rev., Vol.28, 1925, p.559-568.

[39]. A.C. Hagg, “The Influence of Oil-film Journal Bearings on the Stability of RotatingMachines”, J. Appl. Mech., Vol.13, 1946, p.211.

[40]. H. Poritsky, “Contribution to the Theory of Oil Whip”, Trans. ASME, Vol.75, 1953, pp.1153-1161.

[41]. A.C. Hagg and P.C. Warner, “Oil Whip of Flexible Rotors”, Trans. ASME, Vol.75, pp.1339-1344.

[42]. B.L. Newkirk and J.F. Lewis, “Oil Film Whirl— An Investigation of Disturbances due to Oil Films in Journal Bearings”, Trans. ASME, Vol.78, 1956, p. 21-27.

[43]. O. Pinkus, “Experimental Investigation of Resonant Whip”, Trans. ASME, Vol.78, 1956, p. 975-983.

[44]. V.N. Constantinescu, “Stability of the Motion of Circular Bearings lubricated with Gas”, Studii Si Cercetari Mecania Applicata, Vol.10(1), 1959, pp.117-140.

[45]. B. Sternlicht, H. Poritsky and E. Arwas, “Dynamic Stability Aspects of Cylindrical Journal Bearings using Compressible and Incompressible Fluids”, First Int. Symp. On Gas-lubricated Bearings, ONR Deptt. of Navy ACR-49, Oct.1959, pp.119-160.

[46]. J. Hori, “A Theory of Whirl Whip”, ASME J. Appl. Mech., Vol.26, 1959, pp.189-198.

[47]. V. Castelli and H.G. Elrod, “Perturbation Analysis of the Stability of Self-acting Gas Lubricated Journal Bearings”, Franklin Inst. Report No. I-A 2049-11, Feb., 1960.

[48]. G.M. Rentzepis and B. Sternlicht, “On the Stability of Rotors in Cylindrical Journal Bearings”, ONR Tech. Report, May 15, 1961, Contract No. NONR 28440(00), Task No. NR 097-348 and Trans. ASME Paper No. 61-WA-196.

[49]. W.A. Gross, “Investigation of Whirl in Externally Pressurised Air-lubricated Journal Bearings”, ASME J. Basic Engng., Vol.84(1), 1962, pp. 132-138.

[50]. C.H.T. Pan and B. Sternlicht, “On the Translatory Whirl Motion of a Vertical Rotor in Plain Cylindrical Gas Dynamic Journal Bearings”, ASME J. Basic Engng., Vol.84(1), 1962, pp. 152-158.

[51]. D. Morrison, “Influence of Plain Journal Bearings on Whirling of an Elastic Rotor”, Proc. Inst. Mech. Engrs., Vol.176, 1962, p. 542-553.

[52]. D.B. Reynolds, and W.A. Gross, “Experimental Investigation of Whirl in Self-acting Airlubricated Journal Bearings”, ASLE Tribol. Trans., Vol.5(2), 1962, pp. 392-403.

[53]. J.W. Lund and B. Sternlicht, “Rotor Bearing Dynamics with Emphasis on Attenuation”, ASME J. Basic Engng., Vol.84(4), 1962, p.491.

[54]. B. Sternlicht and L.W. Winn, “On the Load Capacity and Stability of Rotors in Self-acting Gas-lubricated Plain Cylindrical Journal Bearings”, ASME J. Basic Engng., Vol.85(4), 1963, pp.503-512.

[55]. R. Holmes, “The Role of Oil-film Bearings in Promoting Shaft Instability and the Remedial Effect of Damping”, Tribol. Int., Vol.13(5), 1980, pp.243-248.

[56]. H. Marsh, “The Stability of Aerodynamic Gas Bearings”, Ph.D. Dissertation, Cambridge Univ. 1963.

[57]. J.S. Ausman, “Linearised ph Stability Theory for Translatory Half-speed Whirl of Long, Selfacting Gas-lubricated Journal bearings”, ASME J. Basic Engng., Vol.85(4), 1963, pp.611-618.

[58]. R. Holmes, “Instability Phenomenon due to Circular Bearing Oil Films”, J. Mech. Engng. Sci., Vol.8(4), 1966, p.419-425.

[59]. D.M. Smith, “Dynamic Characteristics of Turbine Journal Bearings”, Proc. Lub. Wear Conv. (I. Mech. E., London), 1963, p.72-86.

[60]. R.H. Badgley, “Turborotor Instability, Dynamic Unbalance, Gyroscopic and Variable Speed Effects with Finite Length, Cavitated Fluid Film Bearings”, Ph. D. Dissertation, Connel Univ., N.Y. June, 1967.

[61]. R.H. Badgley and J.F. Booker, “Turborotor Instability Effect of Initial Transients on Plane Motion”, ASME J. Lub. Technol., Vol.91(4), 1969, p.625-630.

[62]. A. Akers, S. Michaelson and A. Cameron, “Stability Contours for a Whirling Finite Journal Bearing”, ASME J. Lub. Technol., Vol.93(1), 1971, pp.177-189.

[63]. E. Capone, “Oil Whirl in Journal Bearings under No Load Conditions”, Wear, Vol.26, 1973, pp.207-217.

[64]. D.V. Singh and R. Sinhasan, “Stability and Relative Stability of Porous Journal Bearing System with Axes Skewed”, ASME J. Lub. Technol., Vol.96(4), 1974, pp.621-630.

[65]. T. Yoshihiro, I. Junkichi, T. Hideyuki and S. Atsuo, “On the Stability of A Rotating Elastic Shaft supported by Journal Bearings”, Bull. JSME, Vol.25, 1982, pp. 856-861.

[66]. S.K. Guha, “Study of Conical Whirl Instability of Hydrodynamic Porous Oil Journal Bearings with Tangential Velocity Slip”, Tribol. Int., Vol.19(2), 1986, pp.72-78.

[67]. S.K. Guha, “Study of Conical Whirl Instability of Externally Pressurized Porous Oil Journal Bearings with Tangential Velocity Slip”, ASME J. Tribol., Vol.108(2), 1986, pp.256-261.

[68]. S.K. Guha, “Study of Conical Whirl Instability of Self-Acting Porous Gas Journal Bearings considering Tangential Velocity Slip”, ASME J. Tribol., Vol.110(1), 1988, pp.139-143.

[69]. J. Ramesh, B.C. Majumdar, “Stability of Journal Bearings using Nonlinear Transient Method”, ASME J. Tribol., Vol.117(4), 1995, 691-695.

[70]. A. Kingsbury, “A New Oil Testing Machine and Some of Its Results”, Trans. ASME, Vol.24, 1903, p.143-160.

[71]. E. Cosserat and F. Cosserat, “Theory of Deformable Bodies”, translated by D.H. Delphenich, Scientific Library A. Hermann & Sons, Paris, 1909.

[72]. G.B. Jeffery, “The Motion of Ellipsoidal Particles Immersed in A Viscous Fluid”, Proc. Roy. Soc., London, Ser. A., Vol.102, 1922, pp.171-179.

[73]. W. Hardy and M. Nottage, “Studies in Adhesion – I”, Proc. Roy. Soc., London, Ser. A., Vol.112, 1926, p.62-75.

[74]. S.J. Needs, “Boundary Film Investigations”, Trans. ASME, Vol.62(4), 1940, pp.331-345.

[75]. R. Buckley, “Viscous Flow and Surface Films”, Nat. Bur. Standards Washington, J. Research, Vol.6, 1931, p.89-112.

[76]. A. Anzelius, “About the movement of Anisotropic liquid”, Dissertation at Univ. of Uppsala, 1931.

[77]. J.C. Henniker, “The depth of the Surface Zone of a Liquid”, Revs. Mod. Phys., Vol.21, 1949, pp.322-341.

[78]. G.I. Fuks, “The Properties of Solutions of Organic Acids in Liquid Hydrocarbons at Solid Surfaces”, Research in Surface Forces, ed. B. V. Deryagin, Vol.1, 1960, p.79.

[79]. G.I. Fuks, “The Polymolecular Component of the Lubricating Boundary Layer”, ibid, Vol.2, 1964, p.159.

[80]. J.W. Hoyt and A.G. Fabula, “The Effect of Additives on Fluid Friction”, U.S. Naval Ordnance Test Station Report, 1964.

[81]. W.M. Vogel and A.M. Patterson, “An Experimental Investigation of the Effect of Additives Injected into the Boundary Layer of A Underwater Body”, Pacific Naval Lab., Defence Research Board of Canada, Report 1964.

[82]. T.C. Askwith, A. Cameron and R.F. Crouch, “Chain Length of Additives in Relation to Lubricant in Thin Film and Boundary Lubrication”, Proc. Roy. Soc., London, Ser. A., Vol.291, 1966, p.500-519.

[83]. A. Cameron and R. Gohar, “Theoretical and Experimental Studies of the Oil Film in Lubricated Point Contact”, Proc. Roy. Soc., London, Ser. A., Vol.291, 1966, p.520-536.

[84]. J.W. Kannel, J.C. Bell, J.A.B. Walowit and C.M. Allen, “A Study of the Influence of Lubricants on High Speed Rolling Contact Bearing Performance”, Part IV, Tech.

Rep. No. ASD-TDR-61-643, Air Force Aero Propulsion Laboratory, Dayton, Ohio, 1964.

[85]. R.J. Parker and J.W. Kannel, "Elastohydrodynamic Film Thickness between Rolling Disks with a Synthetic Paraffinic Oil to 589K", NASA TN D-6411, July 1971.

[86]. E. Drauglis, et al. "Thin Film Rheology of Boundary Lubricating Surface Films, Part-I", Battelle Memorial Institute Report, 1970.

[87]. J.L. Ericksen and C. Truesdell, "Exact theory of stress and strain in rods and shell", Archive for Rational Mechanics and Analysis, Vol.1(1), 1957, p.295-323.

[88]. J.L. Ericksen, "Anisotropic fluids", Archive for Rational Mechanics and Analysis, Vol.4, 1960, p.231-237.

[89]. J.L. Ericksen, "Transvesely Isotropic Fluids", Springer Colloid and Polymer Science, Vol.173, 1960, p.117-122.

[90]. H. Grad, "Statistical Mechanics, Thermodynamics, and Fluid Dynamics of Systems with an Arbitrary Number of Integers", Communication for Pure Applied Mathematics, Vol.5(4), 1952, p.455-494.

[91]. J.S. Dahler and L.E. Scriven, "Theory of Structured Continua. I. General Consideration of Angular Momentum and Polarization", Proc. Roy. Soc., London, Ser. A., Vol.275, 1963, p.504-527.

[92]. G.L. Hand, "A theory of Anisotropic Fluids", J. Fluid Mech., Vol.13, 1962, p.33-46.

[93]. J.L. Ericksen, "Continuum Theory of Liquid Crystals", Appl. Mech. Review, Vol.20, 1967, pp.1029-1032.

[94]. D.W. Condiff, and J.S. Dahler, "Fluid Mechanical Aspects of Antisymmetric Stress", J. Phy. Fluids, Vol.7(6), 1964, pp.842-854.

[95]. S.J. Allen, C.N. DeSilva and K.A. Kline, "Theory of Simple Deformable Directed Fluids", J. Phy. Fluids, Vol.10(12), 1967, pp.2551-2555.

[96]. P.N. Kaloni and C.N. DeSilva, "Oriented Fluids and the Rheology of Suspensions", J. Phy. Fluids, Vol.12(5), 1969, pp.994-999.

[97]. K.A. Kline and S.J. Allen, "Nonsteady Flows of Fluids with Microstructure", J. Phy. Fluids, Vol.13(2), 1970, pp.263-270.

[98]. K.A. Kline and S.J. Allen, "A Thermodynamical Theory of Fluid Suspensions", J. Phy. Fluids, Vol.14(9), 1971, pp.1863-1869.

[99]. A.C. Eringen and E.S. Suhubi, "Non-linear Theory of Simple Micro-Elastic Solids - I", Int. J. Engng. Sci., Vol.2, 1964, pp.189-203.

[100]. E.S. Suhubi and A.C. Eringen, “Non-linear Theory of Micro-Elastic Solids - II”, Int. J. Engng. Sci., Vol.2, 1964, pp.389-404.

[101]. A.C. Eringen, “Simple Microfluids”, Int. J. Engng. Sci., Vol.2, 1964, pp.205-217.

[102]. A.C. Eringen, “Mechanics of Micromorphic Materials”, Proc. XI Int. Cong. of Appl. Mech., Munich (Germany), 1964, pp.131-138.

[103]. A.C. Eringen, “Theory of Micropolar Continua”, Dev. in Mech., Vol.3(1), 1965, pp.23-40.

[104]. A.C. Eringen, “Linear Theory of Micropolar Elasticity”, J. Math. Mech., Vol.15(1), 1965, pp.909-923.

[105]. A.C. Eringen, “Theory of Micropolar Fluids”, J. Math. Mech., Vol.16(1), 1966, pp.1-18.

[106]. T. Ariman and A.S. Cakmak, “Couple Stresses in Fluids”, J. Phy. Fluids, Vol.10(11), 1967, pp.2497-2499.

[107]. T. Ariman, A.S. Cakmak, and L.R. Hill, “Flow of Micropolar Fluids between Two Concentric Cylinders”, J. Phy. Fluids, Vol.10(12), 1967, pp.2545-2550.

[108]. S.J. Allen and K.A. Kline, “Lubrication Theory for Micropolar Fluids”, ASME J. Appl. Mech., Vol.38(3), 1971, pp.646-650.

[109]. A.B. Datta, “Pivoted Slider Bearing with Convex Pad Surface in Micropolar Fluid”, Jap. J Appl. Phys., Vol.11(1), 1972, pp.98-102.

[110]. M. Balaram and V.U.K. Sastri, “Micropolar Lubrication”, ASME J. Appl. Mech., Vol.39(3), 1972, pp.834-836.

[111]. V.K. Agrawal, K.L. Ganju and S.C. Jethi, “Squeeze Film and Externally Pressurized Bearings Micropolar Fluid Lubricated”, Wear, Vol.19, 1972, pp.259-265.

[112]. M.S. Khader, and R.I. Vachon, “Theoretical Effects of Solid Particles in Hydrostatic Bearing Lubricant”, ASME J. Lub. Technol., Vol.95(1), 1973, pp.104-106.

[113]. G. Maiti, “Composite and Step Slider Bearings in Micropolar Fluid”, Jap. J. Appl. Phys., Vol.12(7), 1973, pp.1058-1064.

[114]. A. Indrasena, “Some Properties of Micropolar Fluid Flows”, Jap. J. Appl. Phys., Vol.12(12), 1973, pp.1941-1943.

[115]. G. Maiti, “Micropolar Squeeze Film Bearing”, Jap. J. Appl. Phys., Vol.13(9), 1974, pp.1440-1442.

[116]. J.B. Shukla and Md. Isa, “Externally Pressurised Optimum Bearing with Micropolar Fluid as Lubricant”, Jap. J. Appl. Phys., Vol.14(2), 1975, pp.275-279.

[117]. M. Balaram, “Micropolar Squeeze Films”, ASME J. Lub. Technol., Vol.97(4), 1975, pp.635-637.

[118]. J. Prakash and H. Christensen, “Rheological Anomalies in Thin Hydrodynamic Films — A Microcontinuum View”, Symposium on Lubricant Properties in Thin Lubricating Films, American Chem. Soc., NY Meet., Apr. 4-9, 1976, pp.79-90.

[119]. J. Prakash and P. Sinha, “Lubrication Theory for Micropolar Fluids and Its Application to a Journal Bearing”, Int. J. Engng. Sci., Vol.13, 1975, pp.217-232.

[120]. J. Prakash and P. Sinha, “Squeeze Film Theory for Micropolar Fluids”, ASME J. Lub. Technol. Trans., Vol.98(1), 1976, pp.139-144.

[121]. J. Prakash and P. Sinha, “A Study of Squeezing Flow in Micropolar Fluid Lubricated Journal Bearings”, Wear, Vol.38, 1976, pp.17-28.

[122]. J. Prakash and P. Sinha, “Cyclic Squeeze Films in Micropolar Fluid Lubricated Journal Bearings”, ASME J. Lub. Technol., Vol.98(3), 1976, 412-417.

[123]. A.C. Mahanti and G. Ramanaiah, “Inertia Effect of Micropolar Fluid in Squeeze Bearings and Thrust Bearings”, Wear, Vol.39, 1976, pp.227-238.

[124]. J. Prakash and H. Christensen, “A Microcontinuum Theory for the Elastohydrodynamic Inlet Zone”, ASME J. Lub. Technol., Vol.99(1), 1977, pp.24-29.

[125]. Md. Isa and Kh. Zaheeruddin, “Hydrostatic Step Seal and Externally Pressurized Conical Step Bearing with Micropolar Lubricant”, Jap. J. Appl. Phys., Vol.16(9), 1977, pp.1577-1582.

[126]. Kh. Zaheeruddin and Md. Isa, “Micropolar Fluid Lubrication of One-Dimensional Journal Bearings”, Wear, Vol.50, 1978, pp.211-220.

[127]. N. Tipei, “Lubrication with Micropolar Liquids and Its Application to Short Bearings”, ASME J. Lub. Technol., Vol.101(3), 1979, pp.356-363.

[128]. Md. Isa and Kh. Zaheeruddin, “Characteristics of Squeeze Film Porous Journal Bearings with Micropolar Lubricant”, Trans. CSME, Vol.6(3), 1982, pp.146-150.

[129]. Kh. Zaheeruddin, “The Dynamic Behaviour of Squeeze Films in One-Dimensional Porous Journal Bearings Lubricated by a Micropolar Fluid”, Wear, Vol.71, 1981, pp.139-152.

[130]. C. Singh and P. Sinha, “The Three-Dimensional Reynolds Equation for Micropolar Fluid Lubricated Bearings”, Wear, Vol.76(2), 1982, pp.199-209.

[131]. T-W. Huang, C-I Weng and C-K. Chen, “Analysis of Finite Width Journal Bearings with Micropolar Fluids”, Wear, Vol.123, 1988, pp.1-12.

[132]. M. M. Khonsari and D. E. Brewe, “On the Performance of Finite Journal Bearings Lubricated with Micropolar Fluids”, STLE Tribology Trans., Vol.32(2), 1989, pp.155-160.

[133]. T-W. Huang and C-I. Weng, “Dynamic Characteristics of Finite-Width Journal Bearings with Micropolar Fluids”, Wear, Vol.141(1), 1990, pp.23-33.

[134]. P. Chaturani and S. Narasimman, “Numerical Solution of a Micropolar Fluid Flow between Two Rotating Coaxial Disks”, Acta Mech., Vol.89(1), 1991, pp.133-145.

[135]. H.A. Hogan, “Finite Element Formulation for Laminar Flow of a Fluid with Microstructure”, Int. J. Numer. Methods Fluids, Vol.13(10), 1991, pp.1267-1287.

[136]. N.M. Bessonov, “A new Generalization of the Reynolds Equation for Micropolar Fluid Its Application to Bearing theory”, Tribol. Int., Vo1.27, 1994, pp.105-108.

[137]. A.C. Eringen and K. Okada, “A Lubrication Theory for Fluids with Microstructure”, Int. J. Engng. Sci., Vol.33(15), 1995, pp.2297-2308.

[138]. T.R. Lin, “Hydrodynamic Lubrication of Journal Bearings Including Micropolar Lubricants and Three Dimensional Irregularities”, Wear, Vol.192, 1996, pp. 21-28.

[139]. S. Das, S.K. Guha and A.K. Chattopadhyay, “On the Conical Whirl Instability of Hydrodynamic Journal Bearings Lubricated with Micropolar Fluids”, Proc. I. Mech. E.-Par J., J. Eng. Tribol., Vol.215(5), 2001, pp.431-439.

[140]. S. Das, S.K. Guha and A.K. Chattopadhyay, “On Steady State Performance of Misaligned Hydrodynamic Journal Bearings Lubricated with Micropolar Fluids”, Tribol. Int., Vol.35, 2002, pp.201-210.

[141]. X.L. Wang and K.Q. Zhu, “A Study of the Lubricating Effectiveness of Micropolar Fluids in a Dynamically Loaded Journal Bearings”, Tribol. Int., Vol.37, 2004, pp.481-490.

[142]. S. Das, S.K. Guha and A.K. Chattopadhyay, “Theoretical Analysis of Stability Characteristics of Hydrodynamic Journal Bearings Lubricated with Micropolar Fluids”, Proc. I. Mech. E.-Part J., J. Eng. Tribol., Vol.218(1), 2004, pp.45-56.

[143]. S. Das, S.K. Guha and A.K. Chattopadhyay, “Linear Stability of Hydrodynamic Journal Bearings under Micropolar Lubrication”, Tribol. Int., Vol.38, 2005, pp.500-507.

[144]. X.L. Wang and K.Q. Zhu, “Numerical Analysis of Journal Bearings Lubricated with Micropolar Fluids including Thermal and Cavitating Effects”, Tribol. Int., Vol.39, 2006, pp.227-237.

[145]. K.P. Nair, V.P.S. Nair and N.H. Jayadas, "Static and Dynamic Analysis of Elastohydrodynamic Elliptical Journal Bearing with Micropolar Lubricant", Tribol. Int. Vol.40, 2007, pp.297-305.

[146]. S. Verma, V. Kumar, K.D. Gupta, "Analysis of Multirecess Hydrostatic Journal Bearings operating with Micropolar Lubricant", J. Tribol., Vol.131(2), 2009, pp.021103-1-9.

[147]. E.R. Nicodemus and S.C. Sharma, "Influence of Wear on the Performance of Multirecess Hydrostatic Journal Bearing operating with Micropolar Lubricant", J. Tribol., Vol.132(2), 2010, pp.021703-1-11.

[148]. A.D. Rahmatabadi, M. Nekoeimehr and R. Rashidi, "Micropolar Lubricant Effects on the Performance of Noncircular Lobed Bearings", Tribol. Int., Vol.43, 2010, pp.404-413

[149]. N.B. Naduvinamani and S. Santosh, "Micropolar Fluid Squeeze Film Lubrication of Finite Porous Journal Bearing", Tribol. Int., Vol.44, 2011, pp.409-416.

[150]. E.R. Nicodemus and S.C. Sharma, "Performance Characteristics of Micropolar Lubricated Membrane-Compensated Worn Hybrid Journal Bearings", Tribol. Trans., Vol.55(1), 2012, pp.59-70.

[151]. J.R. Lin, T.L. Chou, L.J., Liang and T.C. Hung, "Non-Newtonian Dynamic Characteristics of Parabolic-Film Slider Bearings: Micropolar Fluid Model", Tribol. Int., Vol.48, 2012, pp.226-231.

[152]. S.C. Sharma and A.K. Rajput, "Effect of Geometric Imperfections of Journal on the Performance of Micropolar Lubricated 4-Pocket Hybrid Journal Bearing", Tribol. Int. Vol.60, 2013, pp.156-168.

[153]. R. Dhawan, S. Verma, "Analyzing Micropolar Lubrication in Noncircuar Hybrid Journal Bearings", Tribol.Trans., Vol.57(2), 2014, pp.182-189.

[154]. M.Z. Mehrjardi, A.D. Rahmatabadi, R.R. Meybodi, "A study on the Stability Performance of Noncircular Lobed Journal Bearings with Micropolar Lubricant", Proc. I. Mech. E.-Par J., J. Eng. Tribol., Vol.230(1), 2016, pp.14-30.

[155]. R. Kumar, S.Verma, "Analysis of Noncircular Hole-Entry Capillary-Compensated Hybrid Journal Bearing with Micropolar Lubrication", Tribol. Trans., Vol.59(1), 2016, pp.33-43.

[156]. P. Khatak, H.C. Garg, "Thermohydrostatic Analysis of Hybrid Journl Bearing Compensated by Constant Flow Valve Operating with Micropolar Lubricant", Proc. I. Mech. E.-Par J., J. Eng. Tribol., Published online before print, Dec. 2015.

BIBLIOGRAPHY

[1]. A. Cameron, “The principles of Lubrication”, Longman Group Ltd., 1970.

[2]. G. Lakaszewicz, “Micropolar Fluids- Theory and Applications”, Birkhauser, 1999.

[3]. A.E.H. Love, “Mathematical Theory of Elasticity”, Cambridge: At the University Press, 1893.

[4]. A.C. Eringen, “Microcontinuum Field Theories Vol-I&II”, Springer-Verlag New York Inc., 2001.

[5]. O. Pinkus, B. Sternlicht, “Theory of Hydrodynamic Lubrication”, McGraw Hill, NY, 1961.

[6]. F.M. White, “Fluid Mechanics”, McGraw Hill, NY, 2010.

[7]. J.H. Ferziger, M.Peric, “Computational Methods for Fluid Dynamics”, Springer-Verlag Berlin Heidelberg.